

HD-R137 710

INVESTIGATION OF OPERATIONAL AND DESIGN FACTORS
RESULTING FROM MAIN ROTOR. (U) BOEING VERTOL CO
PHILADELPHIA PA P F SHERIDAN ET AL. JAN 84

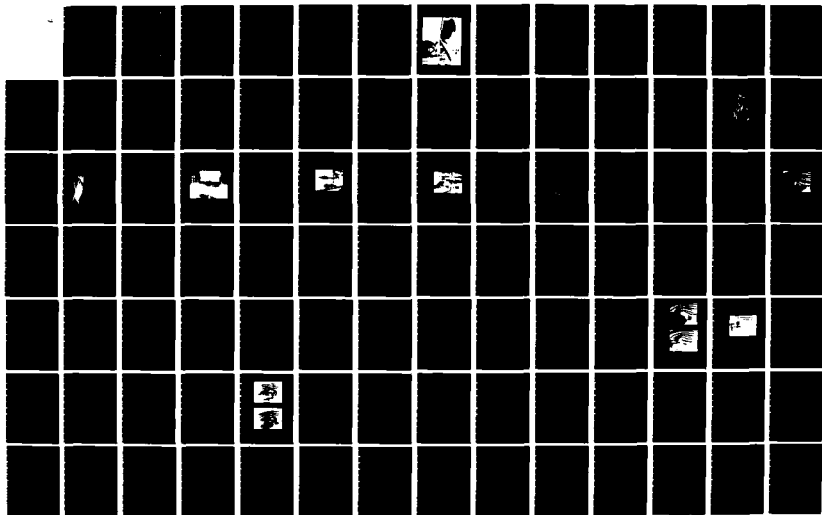
1/2

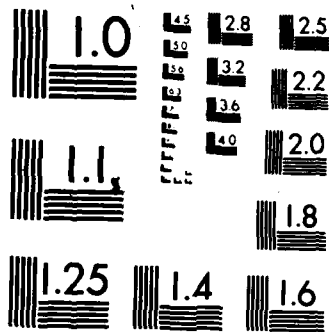
UNCLASSIFIED

USAAVRADCOM-TR-82-D-40 DAAK51-80-C-0025

F/G 20/4

NL





MICROCOPY RESOLUTION TEST CHART
NATIONAL BUREAU OF STANDARDS-1963-A

USAAVRADCOM-TR-82-D-40

AD A137710



12

**INVESTIGATION OF OPERATIONAL AND DESIGN FACTORS
RESULTING FROM MAIN ROTOR AND TAIL ROTOR INTERACTIONS**

Philip F. Sheridan, Edward J. Hanker, Jr., Bruce B. Blake
BOEING VERTOL COMPANY
P.O. Box 16858
Philadelphia, Penn. 19142

January 1984

Final Report for Period 8 July 1980 - 8 November 1982

Approved for public release;
distribution unlimited.

DTIC
ELECTE
FEB 9 1984
S B D

Prepared for
APPLIED TECHNOLOGY LABORATORY
U. S. ARMY RESEARCH AND TECHNOLOGY LABORATORIES (AVRADCOM)
Fort Eustis, Va. 23604

DTIC FILE COPY

84 02 00 046

APPLIED TECHNOLOGY LABORATORY POSITION STATEMENT

Helicopters have encountered a number of aerodynamic and dynamic problems in hover, rearward flight, sideward flight, low-speed forward and transition flight while operating in ground effect (nap-of-the-earth environment). A major cause of these problems is the aerodynamic flow interactions that are generated between components of the helicopter and the associated environment (ground, wind and obstacles).

This contractual research and development effort has resulted in conducting an investigation in the Boeing Vertol V/STOL Wind Tunnel to understand the aerodynamic flow interaction effect of a vertical fin on main rotor/tail rotor interactions, and develop an extensive data base that would enable upgrading of the Tail Rotor Design Guide, particularly for the larger fin sizes currently in use. Powered wind model test data were obtained and analyzed to obtain a better understanding of the aerodynamic mechanisms and their effects.

Robert P. Smith of the Aeronautical Technology Division served as project engineer for this effort.

DISCLAIMERS

The findings in this report are not to be construed as an official Department of the Army position unless so designated by other authorized documents.

When Government drawings, specifications, or other data are used for any purpose other than in connection with a definitely related Government procurement operation, the United States Government thereby incurs no responsibility nor any obligation whatsoever; and the fact that the Government may have formulated, furnished, or in any way supplied the said drawings, specifications, or other data is not to be regarded by implication or otherwise as in any manner licensing the holder or any other person or corporation, or conveying any rights or permission, to manufacture, use, or sell any patented invention that may in any way be related thereto.

Trade names cited in this report do not constitute an official endorsement or approval of the use of such commercial hardware or software.

DISPOSITION INSTRUCTIONS

Destroy this report when no longer needed. Do not return it to the originator.

Unclassified

SECURITY CLASSIFICATION OF THIS PAGE (When Data Entered)

REPORT DOCUMENTATION PAGE		READ INSTRUCTIONS BEFORE COMPLETING FORM
1. REPORT NUMBER USAAVRADCOM TR-82-D-40	2. GOVT ACCESSION NO.	3. RECIPIENT'S CATALOG NUMBER
4. TITLE (and Subtitle) INVESTIGATION OF OPERATIONAL AND DESIGN FACTORS RESULTING FROM MAIN ROTOR AND TAIL ROTOR INTERACTIONS	5. TYPE OF REPORT & PERIOD COVERED Final Report 8 July 1980-8 Nov. 1982	
	6. PERFORMING ORG. REPORT NUMBER	
7. AUTHOR(s) Philip F. Sheridan Edward J. Hanker, Jr. Bruce B. Blake	8. CONTRACT OR GRANT NUMBER(s) DAAK51-80-C-0025	
9. PERFORMING ORGANIZATION NAME AND ADDRESS Boeing Vertol Company P. O. Box 16858 Philadelphia, Pennsylvania 19142	10. PROGRAM ELEMENT, PROJECT, TASK AREA & WORK UNIT NUMBERS 62209A 1L162209AH76 H76A 043	
11. CONTROLLING OFFICE NAME AND ADDRESS Applied Technology Laboratory U.S. Army Research & Technology Labora- tories (AVRADCOM), Fort Eustis, Va. 23604	12. REPORT DATE January 1984	
	13. NUMBER OF PAGES 161	
14. MONITORING AGENCY NAME & ADDRESS (if different from Controlling Office)	15. SECURITY CLASS. (of this report) Unclassified	
	15a. DECLASSIFICATION/DOWNGRADING SCHEDULE	
16. DISTRIBUTION STATEMENT (of this Report) Approved for public release; distribution unlimited.		
17. DISTRIBUTION STATEMENT (of the abstract entered in Block 20, if different from Report)		
18. SUPPLEMENTARY NOTES		
19. KEY WORDS (Continue on reverse side if necessary and identify by block number) Aerodynamic interaction Ground effect Nap of the earth Configuration aerodynamics Ground vortex Powered model Configuration Helicopter Rotor Downwash Interaction Vortex Empennage Interference Wind tunnel		
20. ABSTRACT (Continue on reverse side if necessary and identify by block number) An experimental investigation was conducted at the Boeing 20-ft. x 20-ft. VSTOL wind tunnel to study the aerodynamic interactions of the main rotor and tail rotor of a single rotor helicopter in ground effect. The model employed for this test was the YUH-61A UTTAS at a scale of 1/4.85 with both rotors operated at full scale tip speed. A comprehensive array of parametric data was obtained to examine the interactions between main rotor/tail rotor/fin, and main rotor/fin for various wind azimuths and airspeeds.		

DD FORM 1 JAN 73 1473 EDITION OF 1 NOV 65 IS OBSOLETE

Unclassified

SECURITY CLASSIFICATION OF THIS PAGE (When Data Entered)

Unclassified

SECURITY CLASSIFICATION OF THIS PAGE(When Data Entered)

Extensive flow visualization records were taken to define the flow mechanisms involved. In addition, quantitative data of the flow characteristics were provided by hot film measurements.

Tests were conducted at the four principal wind azimuths of 0, +90, 180, -90 degrees. Parametric sweeps of airspeed, main rotor thrust, and tail rotor thrust were studied at each yaw condition. The baseline configuration for these parametric studies was the 1/4.85th scale UTTAS model with a 35-percent blockage fin. The model height-to-diameter ratio was fixed to 0.35 for the majority of the test. Limited investigations of the effects of varying fin size and height above the ground supplemented the parametric sweeps for the right sideward and rearward flight conditions. Furthermore, the effects of tail rotor placement were investigated for the tail rotor power critical flight condition of 35 knots sideward to the right.

A fine grain yaw sweep from -90 to +225 degrees was conducted at a wind speed of 30 knots in ground effect ($h/d = 0.35$). Tail rotor thrust was varied at each yaw condition to study the effects of tail rotor thrust on adverse fin force. The detailed yaw sweep also provided data for the effects of main rotor wake on the tail rotor/fin interactions, particularly the effects of the main rotor tip vortices and the ground vortex phenomenon. For conditions of high interactivity, as indicated by the flow visualization records and model loads data, flow velocity and orientation measurements were obtained using a hot film probe to further understand the flow mechanisms at work.

This test program succeeded in exercising many of the key parameters that affect interactional aerodynamics of the single rotor helicopter. This provided a comprehensive and consistent database that allows presentation of a broad range of data useful to support design selection trade studies. Presented herein are the generalized experimental results along with descriptions of the associated physical processes.

Unclassified

SECURITY CLASSIFICATION OF THIS PAGE(When Data Entered)

PREFACE

This report is the culmination of four years of work which began with the preliminary stages of the proposal, progressed through model fabrication and wind tunnel testing, and finally resulted in the data reduction and presentation found in this document. Applied Technology Laboratory technical direction was provided by Mr. Robert P. Smith. Boeing Vertol program management was provided by Mr. Bruce B. Blake, Chief of Flying Qualities.

The principal investigators for this study were Messrs. Philip F. Sheridan, Project Engineer, and John Shaw, Project Engineer. Additional contributions have been made by Edward Hanker, Jr., Carl Robinson, Research Engineers, John Munzenrider, Jesse Achey, Bernard Borek, Leslie Holland, Bob Endriss, and James McLaughlin, Research Technicians.

Supplemental work was conducted under a separate contract funded by the Army Research Office, Contract Number DAAG29-78-C-0021, entitled, "A Study of the Aerodynamic Interactions of the Tail Rotor and Fin". Technical direction for that contract was provided by Dr. Robert Singleton, ARO, Durham, North Carolina.

Accession For

NTIS GRA&I	<input checked="" type="checkbox"/>
DTIC TAB	<input type="checkbox"/>
Unannounced	<input type="checkbox"/>
Justification	

By _____

Distribution/ _____

Availability Codes

Dist	Avail and/or	
A-1	Special	

SEARCHED
SERIALIZED
INDEXED



FIGURE 1. PHILIP F. SHERIDAN (1823-1881).

TRIBUTE TO PHIL SHERIDAN

Phil dedicated many years of his life to the study of configurational aerodynamics. His involvement in this sub-discipline of aerodynamics began during the UTTAS program where several operational and design problems evolved from the aerodynamic interactions of the main rotor wake, the fuselage, and the ground. Subsequent to the UTTAS competition, Phil began a program to gain additional insight into these phenomena. His findings were documented in the following publications.

"Interactional Aerodynamics - A New Challenge to Helicopter Technology", P. F. Sheridan and R. P. Smith, Preprint No. 79-59, Presented at the 35th Annual National Forum of the American Helicopter Society, Washington, D.C., May 1979.

"Interactional Aerodynamics of the Single Rotor Helicopter Configuration, Volume I, Final Report", USARTL Technical Report 78-23A, Applied Technology Laboratory, (AVRADCOM), Fort Eustis, Virginia, September 1978, AD A060389.

"Aerodynamics of Helicopter Flight Near the Ground", Preprint No. 77.33-04, Presented at the 33rd Annual National Forum of the American Helicopter Society, Washington, D.C., May 1977.

His dedication and commitment to the study of the complex aerodynamic interactions of the single rotor helicopter, particularly in flight near the ground, has provided a significant data base for others to use.

Phil's name has been included on this report to acknowledge the years that he spent directing the proposal effort, the model fabrication, and the wind tunnel test. He died suddenly after completing the experimental effort. Phil will be sorely missed by his colleagues at Boeing Vertol and the helicopter community as a whole.

TABLE OF CONTENTS

	<u>Page</u>
PREFACE	3
TRIBUTE TO PHIL SHERIDAN.	5
LIST OF ILLUSTRATIONS	9
LIST OF TABLES.	16
INTRODUCTION.	17
Interactional Aerodynamics	17
Background	19
TEST FACILITIES	23
Wind Tunnel Description.	23
Tunnel Configuration.	25
Fixed Ground Plane.	25
Model Description.	28
Instrumentation and Flow Visualization	36
Model Loads Data.	36
Flow Characteristics.	36
MODEL CONFIGURATIONS AND TEST CONDITIONS.	41
MAIN ROTOR/TAIL ROTOR INTERACTIONS.	55
Main Rotor on Tail Rotor Interactions.	55
Effects of Wind Azimuth	56
Effects of Airspeed and Main Rotor Thrust	61
Effects of Height Above the Ground.	81
Tail Rotor on Main Rotor Interactions.	81
Effects of Wind Azimuth	81
Effects of Airspeed and Tail Rotor Thrust	83
TAIL ROTOR/FIN INTERACTIONS	101
Tail Rotor-on-Fin Interactions	102
Effects of Wind Azimuth and Tail Rotor Thrust	102
Effects of Airspeed and Tail Rotor Thrust	107
Effects of Airspeed and Fin Size.	122
Effects of Rotor Height Above the Ground.	122
Effects of Tail Rotor Placement	126
Fin on Tail Rotor Interactions	133
Effects of Airspeed and Fin Size.	133
Effects of Tail Rotor Placement	133



	<u>Page</u>
MAIN ROTOR/FIN INTERACTIONS.	139
Main Rotor on Fin Interactions.	139
Effects of Wind Azimuth and Main Rotor Thrust.	139
Effects of Airspeed and Main Rotor Thrust.	142
Fin-on-Main Rotor Interactions.	146
CONCLUSIONS.	157
RECOMMENDATIONS.	158
REFERENCES	159
LIST OF SYMBOLS.	160

LIST OF ILLUSTRATIONS

<u>Figure</u>		<u>Page</u>
1	Philip F. Sheridan (1923 - 1981)	4
2	Boeing V/STOL Wind Tunnel	24
3	Spatial Relationship of the Model, Fixed Ground Plane, and Test Section Boundaries	26
4	Detailed Perspective View of Fixed Ground Plane	27
5	Front View of SRH Model in YUH-61A Configuration with External Tail Rotor Drive Mechanism	29
6	Rear View of SRH Model in YUH-61A Configuration	31
7	Close-Up of External Tail Rotor Mechanism	33
8	SRH Empennage with Interchangeable Fins and Removable Stabilizer	34
9	Interchangeable Vertical Fin	35
10	Detailed Diagram of the Model, Balances, and Power Pod	37
11	Balance Orientations	38
12	Flow Visualization	39
13	Schematic of Hot Film Probe Locations (Top View) and Associated Flight Conditions	53
14	Variation of Tail Rotor Power to Thrust Ratio as a Function of Wind Azimuth	57
15	Variation of Tail Rotor Collective Required to Maintain Thrust as a Function of Wind Azimuth	58
16	Main Rotor Wake Near the Empennage in Yawed Flight - Alpha Component.	59
17	Main Rotor Wake Near the Empennage in Yawed Flight - Beta Component	60

LIST OF ILLUSTRATIONS

<u>Figure</u>	<u>Page</u>
18 Variation of Tail Rotor Power to Thrust Ratio as a Function of Airspeed and Main Rotor Thrust at $\psi = -90^\circ$	62
19 Variation in Tail Rotor Collective Required to Maintain Constant Thrust as a Function of Airspeed and Main Rotor Thrust at $\psi = -90^\circ$. . .	63
20 Flow Visualization Near the Empennage in Right Sideward Flight	64
21 Variation of Main Rotor Wake Near the Empennage as a Function of Airspeed in Right Sideward Flight - Alpha Component.	65
22 Variation of Main Rotor Wake Near the Empennage as a Function of Airspeed in Right Sideward Flight - Beta Component	68
23 Variation of Tail Rotor Power to Thrust Ratio as a Function of Airspeed and Main Rotor Thrust in Rearward Flight.	70
24 Variation of Tail Rotor Collective Required to Maintain Constant Thrust as a Function of Airspeed and Main Rotor Thrust in Rearward Flight.	71
25 Variation in Main Rotor Wake in Ground Effect as a Function of Main Rotor Thrust at $\psi = 180^\circ$	72
26 Variation of Tail Rotor Power to Thrust Ratio as a Function of Airspeed and Wind Azimuth	73
27 Variation of Tail Rotor Collective Required to Maintain Constant Thrust as a Function of Airspeed and Wind Azimuth	74
28 Variation of Tail Rotor Collective Required to Maintain Constant Thrust as a Function of Airspeed and Height Above Ground (Low Main Rotor Thrust)	75
29 Variation of Tail Rotor Power to Thrust Ratio as a Function of Airspeed and Height Above Ground (Low Main Rotor Thrust)	76

LIST OF ILLUSTRATIONS

<u>Figure</u>	<u>Page</u>
30	Variation of Tail Rotor Collective Required to Maintain Constant Thrust as a Function of Airspeed and Height Above Ground (Nominal Main Rotor Thrust) 77
31	Variation of Tail Rotor Power to Thrust Ratio as a Function of Airspeed and Height Above Ground (Nominal Main Rotor Thrust) 78
32	Variation of Tail Rotor Collective Required to Maintain Constant Thrust as a Function of Airspeed and Height Above Ground (High Main Rotor Thrust) 79
33	Variation of Tail Rotor Power to Thrust Ratio as a Function of Airspeed and Height Above Ground (High Main Rotor Thrust). 80
34	Variation of Main Rotor Power Coefficient as a Function of Wind Azimuth and Tail Rotor Thrust 82
35	Variation of Lateral Cyclic Pitch Required for Zero Hub Moment as a Function of Wind Azimuth and Tail Rotor Thrust 84
36	Variation of Longitudinal Cyclic Pitch Required for Zero Hub Moment as a Function of Wind Azimuth and Tail Rotor Thrust 85
37	Variation of Main Rotor Power Coefficient as a Function of Airspeed and Tail Rotor Thrust ($\psi = 0^\circ$). 86
38	Variation of Lateral Cyclic Required for Zero Hub Moment as a Function of Airspeed and Tail Rotor Thrust ($\psi = 0^\circ$). 87
39	Variation of Longitudinal Cyclic Required for Zero Hub Moment as a Function of Airspeed and Tail Rotor Thrust ($\psi = 0^\circ$). 88
40	Variation of Main Rotor Power Coefficient as a Function of Airspeed and Tail Rotor Thrust ($\psi = -90^\circ$). 90

LIST OF ILLUSTRATIONS

<u>Figure</u>	<u>Page</u>
41 Variation of Lateral Cyclic Required for Zero Hub Moment as a Function of Airspeed and Tail Rotor Thrust ($\psi = -90^\circ$)	91
42 Variation of Longitudinal Cyclic Required for Zero Hub Moment as a Function of Airspeed and Tail Rotor Thrust ($\psi = -90^\circ$)	92
43 Variation of Main Rotor Power Coefficient as a Function of Airspeed and Tail Rotor Thrust ($\psi = 180^\circ$)	93
44 Variation of Lateral Cyclic Required for Zero Hub Moment as a Function of Airspeed and Tail Rotor Thrust ($\psi = 180^\circ$)	94
45 Variation of Longitudinal Cyclic Required for Zero Hub Moment as a Function of Airspeed and Tail Rotor Thrust ($\psi = 180^\circ$)	95
46 Variation of Main Rotor Power Coefficient as a Function of Airspeed and Tail Rotor Thrust ($\psi = 90^\circ$)	96
47 Variation of Lateral Cyclic Required for Zero Hub Moment as a Function of Airspeed and Tail Rotor Thrust ($\psi = 90^\circ$)	97
48 Variation of Longitudinal Cyclic Required for Zero Hub Moment as a Function of Airspeed and Tail Rotor Thrust ($\psi = 90^\circ$)	98
49 Variation of Main Rotor Power Coefficient as a Function of Airspeed and Wind Azimuth	100
50 Effects of Wind Azimuth and Tail Rotor Thrust on Fin Side Force Coefficient	103
51 Effects of Tail Rotor Thrust on Fin Tuft Pattern at $\psi = 40^\circ$, $V = 30$ Knots.	104
52 Effects of Wind Azimuth and Tail Rotor Thrust on Boom Side Force Coefficient	105
53 Effects of Wind Azimuth and Tail Rotor Thrust on Nondimensional Empennage Lift.	108

LIST OF ILLUSTRATIONS

<u>Figure</u>		<u>Page</u>
54	Effects of Airspeed and Tail Rotor Thrust on Fin Side Force Coefficient for $\psi = 0^\circ$	109
55	Effects of Airspeed and Tail Rotor Thrust on Nondimensional Empennage Lift at $\psi = 0^\circ$	110
56	Effects of Airspeed and Tail Rotor Thrust on Fin Side Force Coefficient for $\psi = -90^\circ$	112
57	Effects of Airspeed and Tail Rotor Thrust on Nondimensional Empennage Lift at $\psi = -90^\circ$	113
58	Effects of Airspeed and Tail Rotor Thrust on Fin Side Force Coefficient for $\psi = 180^\circ$	114
59	Effects of Airspeed and Tail Rotor Thrust on Nondimensional Empennage Lift at $\psi = 180^\circ$	115
60	Fin Tuft Patterns at $\psi = 170^\circ$, $V = 30$ Knots	117
61	Effects of Airspeed and Tail Rotor Thrust on Fin Side Force Coefficient for $\psi = 90^\circ$	118
62	Effects of Airspeed and Tail Rotor Thrust on Nondimensional Empennage Lift at $\psi = 90^\circ$	119
63	Effects of Airspeed and Wind Azimuth on Fin Side Force Coefficient.	120
64	Effects of Airspeed and Wind Azimuth on Nondimensional Empennage Lift	121
65	Effects of Airspeed and Fin Size on Fin Side Force Coefficient for $\psi = -90^\circ$	123
66	Effects of Airspeed and Fin Size on Non- dimensional Fuselage Lift for $\psi = -90^\circ$	124
67	Effects of Airspeed and Height Above the Ground on Fin Side Force Coefficient for $\psi = 0^\circ$	125
68	Effects of Airspeed and Height Above the Ground on Fin Side Force Coefficient for $\psi = -90^\circ$	127

LIST OF ILLUSTRATIONS

<u>Figure</u>		<u>Page</u>
69	Effect of Tail Rotor Longitudinal Placement on Fin Side Force Coefficient in Right Sideward Flight	129
70	Effect of Tail Rotor Lateral Placement on Fin Side Force Coefficient in Right Sideward Flight.	130
71	Effect of Tail Rotor Vertical Placement on Fin Side Force Coefficient in Right Sideward Flight.	132
72	Effects of Airspeed and Fin Size on Tail Rotor Power Coefficient at $\psi = -90^\circ$	134
73	Effect of Tail Rotor Longitudinal Placement on Tail Rotor Power Coefficient in Right Sideward Flight.	135
74	Effect of Tail Rotor Lateral Placement on Tail Rotor Power Coefficient in Right Sideward Flight.	136
75	Effect of Tail Rotor Vertical Placement on Tail Rotor Power Coefficient in Right Sideward Flight.	137
76	Fin Side Force as a Function of Wind Azimuth and Main Rotor Thrust	140
77	Fin Side Force as a Function of Wind Azimuth and Main Rotor Thrust	141
78	Fin Side Force as a Function of Wind Azimuth and Tail Rotor Thrust	143
79	Fin Side Force Coefficient as a Function of Airspeed and Main Rotor Thrust in Right Sideward Flight	144
80	Nondimensional Empennage Lift as a Function of Airspeed and Main Rotor Thrust in Right Sideward Flight	145
81	Fin Force Coefficient as a Function of Airspeed and Main Rotor Thrust in Rearward Flight.	147

LIST OF ILLUSTRATIONS

<u>Figure</u>	<u>Page</u>
82 Nondimensional Empennage Lift as a Function of Airspeed and Main Rotor Thrust in Rearward Flight.	148
83 Main Rotor Power Coefficient as a Function of Airspeed and Fin Size in Right Sideward Flight.	150
84 Lateral Cyclic Required for Zero Hub Moment as a Function of Airspeed and Fin Size in Right Sideward Flight	151
85 Longitudinal Cyclic Required for Zero Hub Moment as a Function of Airspeed and Fin Size in Right Sideward Flight.	152
86 Main Rotor Power Coefficient as a Function of Airspeed and Fin Size in Rearward Flight	153
87 Lateral Cyclic Required for Zero Hub Moment as a Function of Airspeed and Fin Size in Rearward Flight	154
88 Longitudinal Cyclic Required for Zero Hub Moment as a Function of Airspeed and Fin Size in Rearward Flight.	155

LIST OF TABLES

<u>TABLE</u>		<u>PAGE</u>
1	Specific Aerodynamic Interactions Analyzed in this Report	20
2	Model Parameters	30
3	Run Log for $h/d = 0.8$ Configuration	42
4	Run Log for 35% Blockage Fin	43
5	Run Log for 25% Blockage Fin	46
6	Run Log for Fin-Off Configuration	47
7	Run Log for Tail Rotor Placement Investigation	47
8	Run Log for Hot Film Flow Measurement Investigation	48
9	Configuration Code Definitions	49
10	Flag Note Summary	50

INTRODUCTION

INTERACTIONAL AERODYNAMICS

A renewed interest in helicopter operations near the ground has been precipitated in recent years by the emergence of the Army's nap-of-the-earth (NOE) concept. The capability for sustained operation in the NOE will be required for any military helicopter operating in the high-threat, detection-critical forward battle zone. This includes all helicopter missions from attack and surveillance to utility and logistics when supporting the forward areas. It is thus a universal concern of all involved in helicopter manufacture and operational deployment.

Helicopters have always operated within the NOE. It is their natural regime, and indeed that capability is their main reason for existence. In the past, however, helicopters have passed through the NOE envelope quickly as they transitioned from hover to forward flight. Only with the development of the NOE tactical doctrine has the possibility of sustained flight in this "transition" regime been realized. Future NOE operations will require flying low to avoid detection and operating slowly to avoid collisions with foliage, obstacles, and other aircraft.

Within the NOE flight regime the tail rotor is exercised to its fullest. The tail rotor is required to provide directional trim in winds up to 35 knots from any direction in varying degrees of ground effect. It will encounter its highest thrust loading coefficient at hover ceiling where maximum and minimum collective control limits of the tail rotor may be encountered. Maneuvering in close quarters at high thrust requirements close to rotor stall results in highest drive system torque. This is aggravated by the control activity occasioned by turbulent air conditions associated with hovering in winds. The turbulence seems to be caused largely by the flow interactions at low speeds. These interactions between the main rotor wake, the tail rotor wake, and the ground flow make the NOE regime the most complex operational environment of any aircraft.

The complex aerodynamics manifests itself in an array of problems. Some of these NOE related problems are presented in Reference 1. Both military and civilian helicopters have

1. Sheridan, Philip, F., and Smith, Robert P., "Interactional Aerodynamics - A New Challenge to Helicopter Technology", Presented at the 35th Annual National Forum of the American Helicopter Society, Washington, D.C., May 1979.

experienced NOE problems in hover, and in forward, rearward, and sideward flight while operating in ground effect. Their occurrence is partly due to a basic difficulty in accommodating a wide variety of inflow conditions which are attributable to such factors as the wide range of azimuths that may be encountered at varying speeds, the main rotor wake impinging on the tail rotor/empennage, and conversely, the tail rotor wake interfering with the main rotor flow. All of these conditions can occur well away from the ground boundary and can cause problems at any height in the NOE regime. The effect of ground proximity, however, is to make flow conditions more complex, especially with the formation of the ground vortex.

The occurrence of these problems is also strongly influenced by the relative placement of components of the helicopter configuration, i.e., the tail rotor with respect to the main rotor, the fin in close proximity to the tail rotor, and others. There is a general requirement for the helicopters today to be more compact in design arrangement for transportability, for low profile, and for weight/cost benefits. This leads to a closer proximity of components with more critical aerodynamic interfacing, resulting in more severe problems for contemporary aircraft.

Other aspects of modern helicopters that make them more susceptible to severe aerodynamic interactions are the general increase in disk loadings over the years and the requirement for directional trim after complete tail rotor failure. The average disk loading of the new generation of Army helicopters operating in the mid-80's will be nearly twice that prevailing in 1965. This causes much higher energy levels in the rotor wake to which the interaction strengths seem to be proportional. In addition, current helicopter specifications require that the vertical fin be able to provide directional trim in the event of a tail rotor failure. This results in very large tail surfaces relative to the tail rotor disk area. Tail rotor/fin interactions can only be aggravated by such an arrangement.

As the helicopter assumes a more prominent role in the combat forward battle zones, the proliferation of the NOE tactical doctrine is inevitable. Compounded by the more stringent demands on today's helicopters in terms of compactness and directional control requirements, the NOE flight regime is the most complex and interactional of any flight regime. The interactions found in this regime cause problems over the whole range of disciplines, including performance, flying qualities, noise, and structural loads. Many such problems have emerged in the past, and a significant number have occurred during the UTTAS and AAH programs. Comprehensive test

programs like the one reported herein are required to thoroughly understand the design and operational problems of the NOE environment. Such a comprehensive data base will foster the development of a math model based on fundamental parameters such as airspeed, main rotor thrust, and tail rotor thrust and will aid in analyzing various fuselage, fin, and rotor configurations. More sophisticated methodology will help in predicting loads and stability and thus save the costs of corrective design and flight test.

BACKGROUND

A detailed experimental investigation of main rotor and tail rotor interactions of a single rotor helicopter model was conducted at Boeing Vertol in 1981. Wind tunnel test results are presented that quantify the effects of variations in fundamental parameters such as wind azimuth and airspeed, main rotor thrust, tail rotor thrust, and height above the ground. The effects of changes in model configuration were also studied. The baseline model was a 1/4.85 scale model of the YUH-61A UTTAS with a 35% blockage vertical fin. Model variations included 25% blockage fin and fin-removed configurations. An external tail rotor mount provided for a limited study of the effects of tail rotor placement for the baseline fin.

The specific aerodynamic interactions that were investigated under this contract included the mutual effects of

- Main rotor/tail rotor
- Tail rotor/fin
- Main rotor/fin

The influence of fuselage aerodynamics was not considered in this study, yet a scaled fuselage model was incorporated in the test program to properly simulate the general flow field about the helicopter.

The specific interactions and related problems discussed in this report are summarized in Table 1. The key parameters affecting each of these interactions are also listed in the table.

The entire test program was conducted in ground effect ($h/d < 1.0$) where ground proximity clearly makes the flow conditions more complex and the operational problems more severe. To aid in the study of the flow mechanisms involved in these little-understood interactional phenomena and the associated problems, flow visualization techniques were used extensively throughout the test program. Further details of the flow characteristics were provided by hot film flow measurements

for conditions of particularly high interactions. Correlation of the loads data with these special data provided a very comprehensive data base regarding the structure of the flow field near the helicopter and the resulting variations in aircraft loads and control requirements.

TABLE 1. SPECIFIC AERODYNAMIC INTERACTIONS ANALYZED IN THIS REPORT

<u>Interaction</u>	<u>Problems or Phenomena</u>	<u>Key Parameters</u>
Main Rotor/ Tail Rotor	Tail rotor proximity to main rotor tip vortices in sideslip.	Airspeed for various wind azimuths (V, ψ), main rotor thrust (CT_{MR}), and tail rotor thrust (CT_{TR})
	Tail rotor interactions with ground vortex in rearward flight.	height above ground (h/d)
	Main rotor inflow variations due to tail rotor flow in rearward flight.	
Tail Rotor/Fin	Adverse fin load due to tail rotor pressurization of fin surface.	(V, ψ), CT_{TR} , fin blockage ratio \bar{A} , (h/d)
	Tail rotor performance for various inflow conditions determined by fin size.	
Main Rotor/Fin	Main rotor wake effects on adverse fin loads.	(V, ψ), CT_{MR} , \bar{A} , h/d
	Main rotor trim variations due to fin flow field for various fin configurations.	

This investigation represents another milestone in the study of the complex interactional flows of the single rotor helicopter. The entire test program was dedicated solely to gaining a fundamental understanding of the interrelationship of main rotor, tail rotor, and free stream flows. The broad outlines of the NOE problem areas are well developed (see

References 2, 3, 4 and 5). Developing design solutions and resolving operational questions, however, are difficult because of the lack of a comprehensive data base. This lack is due to the large number of pertinent variables in the rotor operating conditions, the geometry and relative positions of the aircraft components, and the flight envelope. The recent experimental test program at Boeing succeeded in exercising many of the key parameters known to be significant. This provided a comprehensive and consistent data base that allows presentation of a broad range of data useful for support of design selection trade studies. Presented herein are the generalized experimental results along with descriptions of the associated physical processes.

The comprehensive nature of these tests results now make it even more possible to begin developing a mathematical model that would approximate the performance of conventional main rotor/tail rotor/fin designs with respect to interactional aerodynamics and provide the basis for more sophisticated math models that would predict the efficiency of more radical

-
2. Sheridan, Philip F., "Interactional Aerodynamics of the Single Rotor Helicopter Configuration, Volume I, Final Report", USARTL Technical Report 78-23A, Applied Technology Laboratory, U.S. Army Research and Technology Laboratories (AVRADCOM), Fort Eustis, Virginia, September 1978, ADA060389.
 3. Wiesner, W., and Kohler, Gary, "Tail Rotor Design Guide", Boeing Vertol Company, USAAMRDL Technical Report 73-99, Eustis Directorate, U.S. Army Air Mobility Research and Development Laboratory, Fort Eustis, Virginia, January 1974, AD775391.
 4. Huston, Robert J., and Morris, Charles E.K., Jr., "A Wind Tunnel Investigation of Helicopter Directional Control in Rearward Flight in Ground Effect", NASA Technical Note D-6118, National Aeronautics and Space Administration, Langley Research Center, Hampton, Virginia, March 1971.
 5. Yeager, William T., Jr., Young, Warren H., Jr., and Mantay, Wayne R., "A Wind Tunnel Investigation of Parameters Affecting Helicopter Directional Control at Low Speeds in Ground Effect", NASA Technical Note D-7694, Langley Directorate, U.S. Army Air Mobility Research and Development Laboratory, Langley Research Center, Hampton, Virginia, November 1974.

directional control schemes of the future. Analytical work has already begun at Princeton University (see Reference 6) where data for an isolated main rotor in ground effect in the presence of the ground vortex are being compared to simple theories to develop a first approximation of the conditions leading to the formation of the ground vortex and its corresponding influence on rotor loads as functions of fundamental parameters such as airspeed, collective pitch, and height above the ground. The data obtained in the recent wind tunnel test under this contract provide the baseline for developing a simplified model of a complete single rotor helicopter in ground effect. Further research work is clearly needed to provide a complete data base of the mutual interactions between the primary components - the fuselage, main and tail rotors, engines and ground plane - but the foundation has been laid for the beginning stages.

-
6. Sheridan, Philip F., Hanker, Edward J., Jr., and Blake, Bruce B., "A Study of the Aerodynamic Interactions of the Tail Rotor and Fin", ARO, June 1983.

TEST FACILITIES

WIND TUNNEL DESCRIPTION

The experimental investigation was conducted at the Boeing Vertol V/STOL Wind Tunnel during August 1981. A schematic of the tunnel and its associated support facilities is seen in Figure 2. The tunnel circuit includes a test section that has a 20-foot by 20-foot cross section and is 45 feet long. Also shown in Figure 2 are the control room, the model shop, the model assembly area, and the engineering offices. With all of these dedicated facilities, the Boeing V/STOL tunnel can design, fabricate, instrument, and test a model with precision and reliability.

Among the many key features of this tunnel, which were highlighted in Reference 2, one particularly significant feature is a new set of computers - a VAX 11/780 and a PDP 11/34 - which is located adjacent to the control room. The new computer system has been specially tailored to real-time data acquisition and processing. The system also provides for multi-user and multi-tasking capabilities in real time. On-line features include two "function control panels" that give a digital readout of 60 different parameters to verify that the tunnel and model are "on condition". The function control panels can also be used in concert with an array of oscilloscopes to display strain and temperature gage data that is used to continuously monitor the model integrity. This provides an early warning system that helps prevent severe damage to the model in the event of subsystem failures. Finally, there is a capability for linking up six x-y plotters that can plot data seconds after a test point is obtained.

Off-line data processing has been greatly enhanced with acquisition of a new General Graphics Package. This computer graphics program provides versatile manipulations of large amounts of data such as cross plotting between runs, sum and difference of curves, curve-fitting options, and interpolation routines. Most of the data presented in this report was reduced and presented through the use of this package.

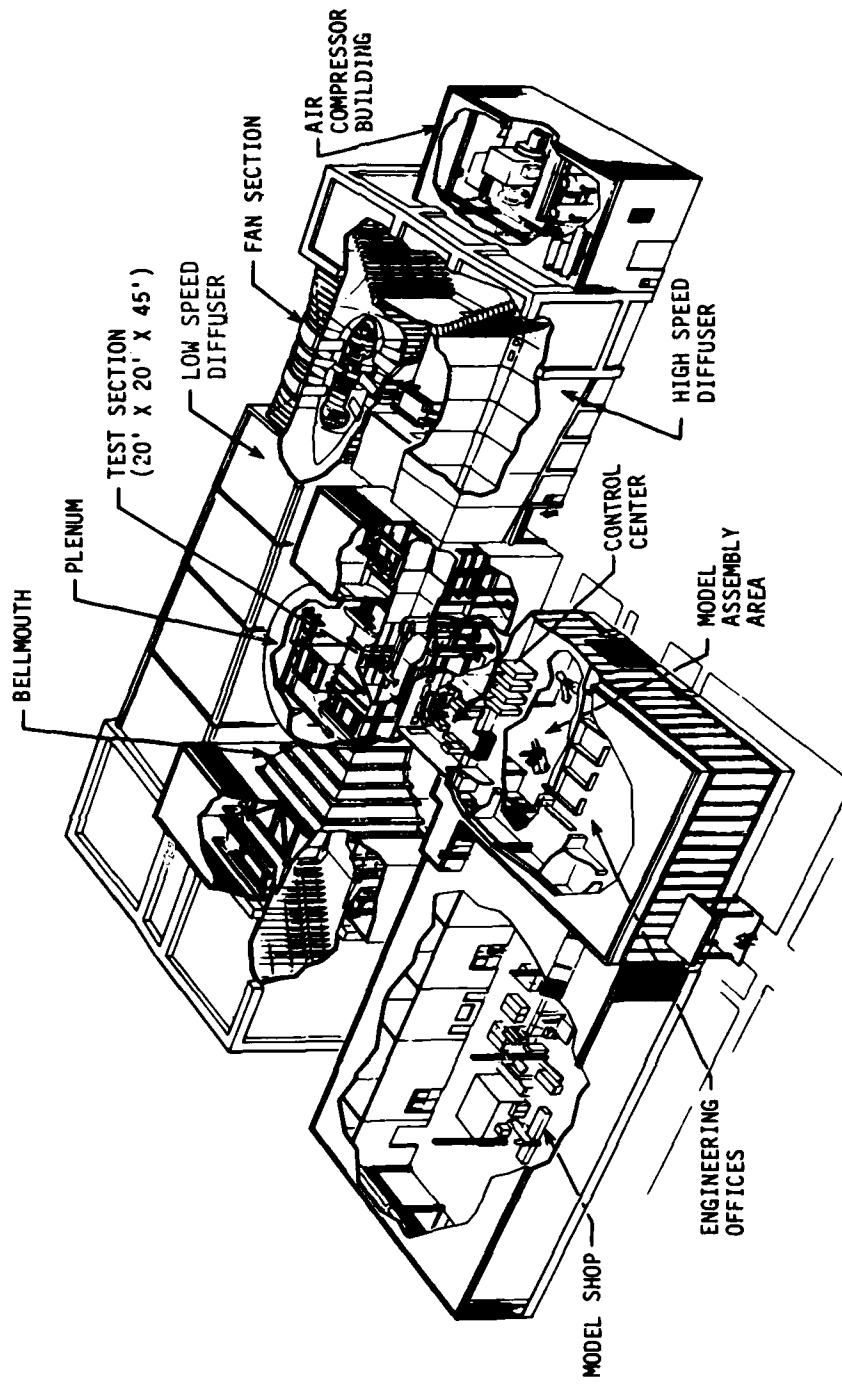


FIGURE 2. BOEING V/STOL WIND TUNNEL.

Due to the comprehensive nature of the experimental investigation, such a versatile capability was integral to the data analysis process.

Tunnel Configuration

Although the maximum capability of the tunnel is 235 knots, testing was limited to the NOE operating range between hover and 45 knots. When testing at these low speeds, a 28-foot section of the tunnel walls and ceiling is removed. In this open throat configuration no boundary correction factors were applied to the data. A diagram of the relative positions of the model to the fixed ground plane and the open throat of the tunnel is shown in Figure 3. To simulate IGE flight, a fixed ground plane was installed on the tunnel floor which can be raised or lowered on the lift platform shown in Figure 3.

Inspection of Figure 3 shows that the fixed ground plane was positioned flush with the tunnel floor. This positioned the model further below the upper jet boundary to prevent any possible flow breakaway. At the beginning of the test, observations of smoke flow at the upper boundary indicated that there was no problem with flow instability.

Flow visualization, tufts and smoke, was a significant feature of this test program, and permanent records were taken in the form of still photos and motion pictures. In Figure 3, the position of the top view cameras is noted. A TV camera was also located at the top of the top section for a real-time check on the model and the flow visualization. Not shown in Figure 3 are the locations of the still and movie cameras positioned on the opposite side of the tunnel (in the perspective of Figure 3) for side views of tuft and smoke patterns.

Fixed Ground Plane

The majority of the test was conducted in ground effect at a height to diameter ratio of 0.35. A detailed cutaway of the model, the ground plane, and associated support mechanisms is shown in Figure 4. Two features of this test configuration are important to note. First, the fixed ground plane has been modified to include a turntable insert that permits testing IGE over the full range (360°) of wind azimuth. This feature was added to accommodate the second feature which is the external tail rotor support and drive mechanism that affords 5 degrees of motion of the tail rotor relative to the fin. During this test, however, only 3 of those degrees of freedom were exercised. The longitudinal, lateral, and vertical positions of the tail rotor relative to the empennage

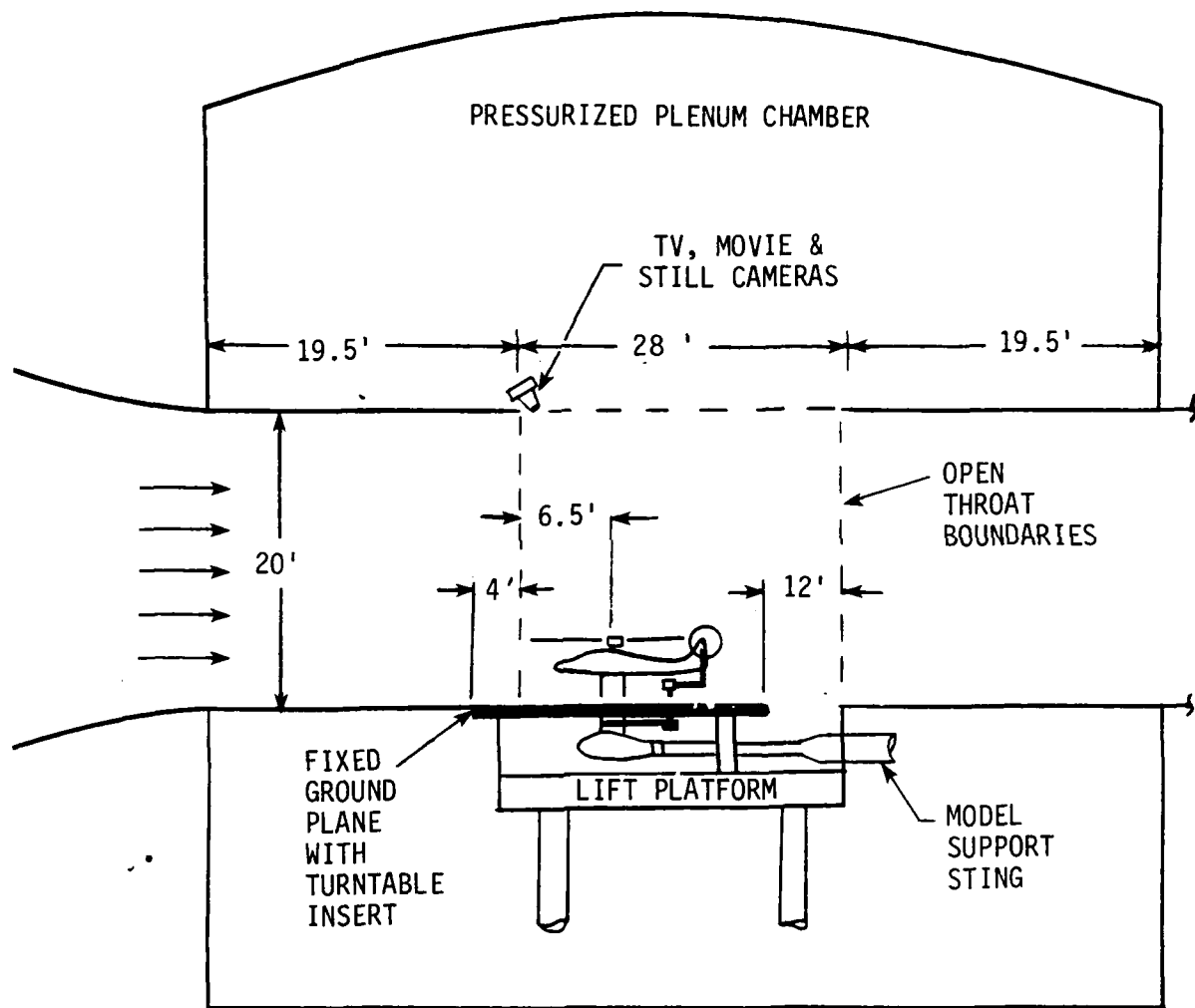


FIGURE 3. SPATIAL RELATIONSHIP OF THE MODEL, FIXED GROUND PLANE, AND TEST SECTION BOUNDARIES.

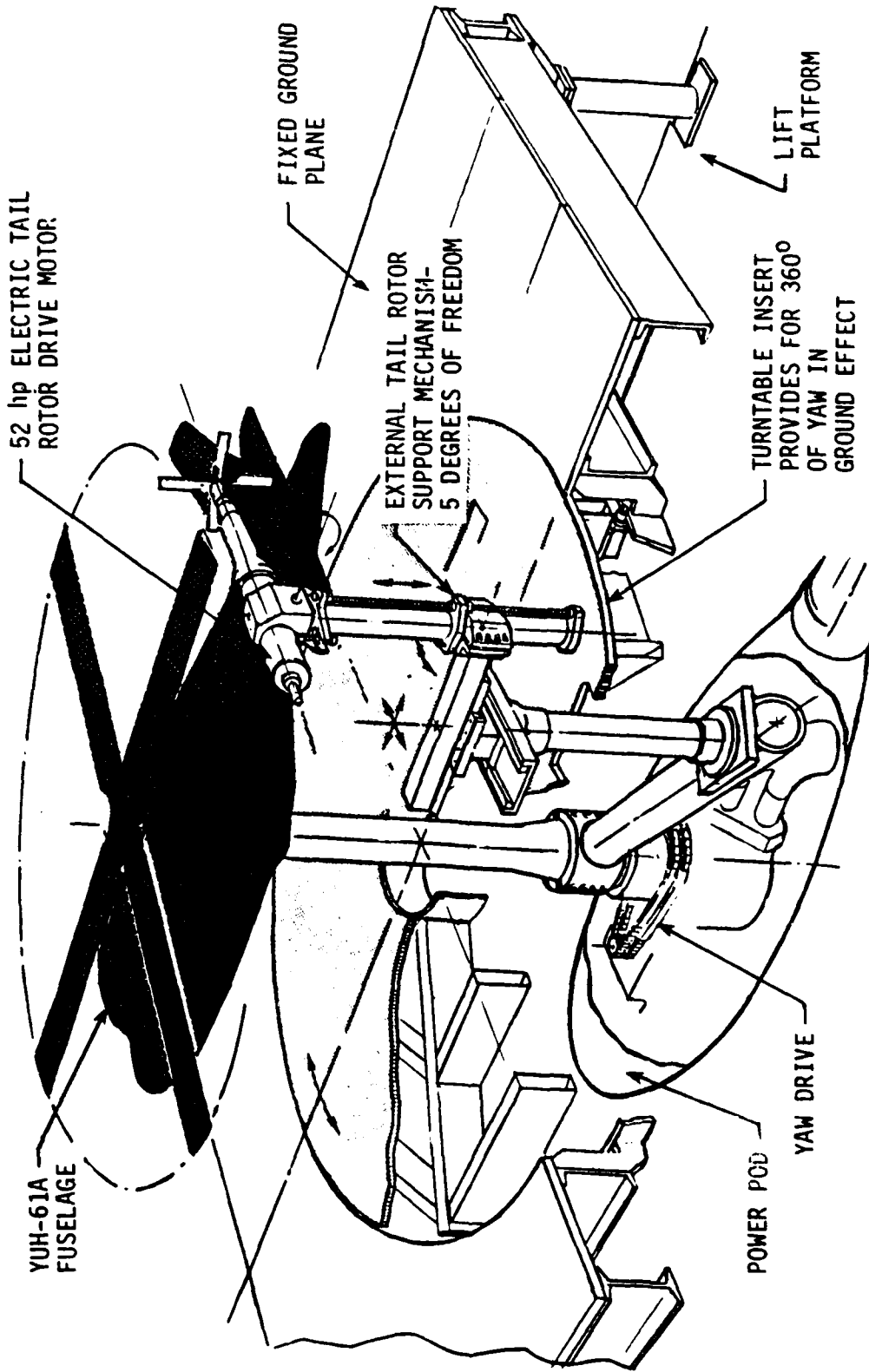


FIGURE 4. SKETCH OF MODEL AND TEST STAND ARRANGEMENT.

were varied while the cant and yaw angles of the tail rotor remained fixed, keeping the disk plane parallel to the plane of symmetry of the model.

Underneath the turntable is the sting boom and power pod that both support the model and provide power and other services to the main rotor, the tail rotor and the instrumentation. The main rotor is powered by three air motors with a total capability of providing 400 horsepower. These air motors are located below the floor so that the exhaust does not interfere with the main rotor and tail rotor flows in close ground proximity. The tail rotor is driven by a compact 52-horsepower electric motor that is water cooled. During the test, the model yaw angle was set by the yaw drive mechanism, shown in Figure 4, that rotates the entire model and turntable.

MODEL DESCRIPTION

The model employed for this experimental investigation was the YUH-61A at a scale of 1/4.85 (see Figure 5). The model was mounted on the single rotor helicopter (SRH) model system which includes a package of five strain gage balances for measuring main rotor, fuselage, empennage, fin and total aircraft forces and moments. The main rotor, operating at full scale tip speed, was fully articulated to allow large variations in tip path plane (TPP) tilt through cyclic pitch variations without experiencing the large hub moments associated with hingeless rotor systems (which was the original configuration of the YUH-61A model). The SRH provides full remote control over main rotor and model parameters such as collective pitch, longitudinal and lateral cyclics, RPM and aircraft yaw angle. Key model parameters are listed in Table 2.

One of the significant features of this test was the external tail rotor mechanism. The tail rotor was mounted on a separate support in much the same manner as the models used in the tail rotor placement tests reported in References 3 and 5. The test results presented in Reference 3 did not include a fuselage but did include a fin. Reference 5, however, presents the results of tail rotor placement tests with a fuselage but with the fin removed. The objective here was to study the effects of tail rotor placement for the complete helicopter model (rear view shown in Figure 6) at specific flight conditions. This will be discussed later in the report. The external tail rotor rig not only has 5 degrees of freedom but can also be adapted to operate as a pusher or a tractor. In this investigation only the pusher configuration was studied.

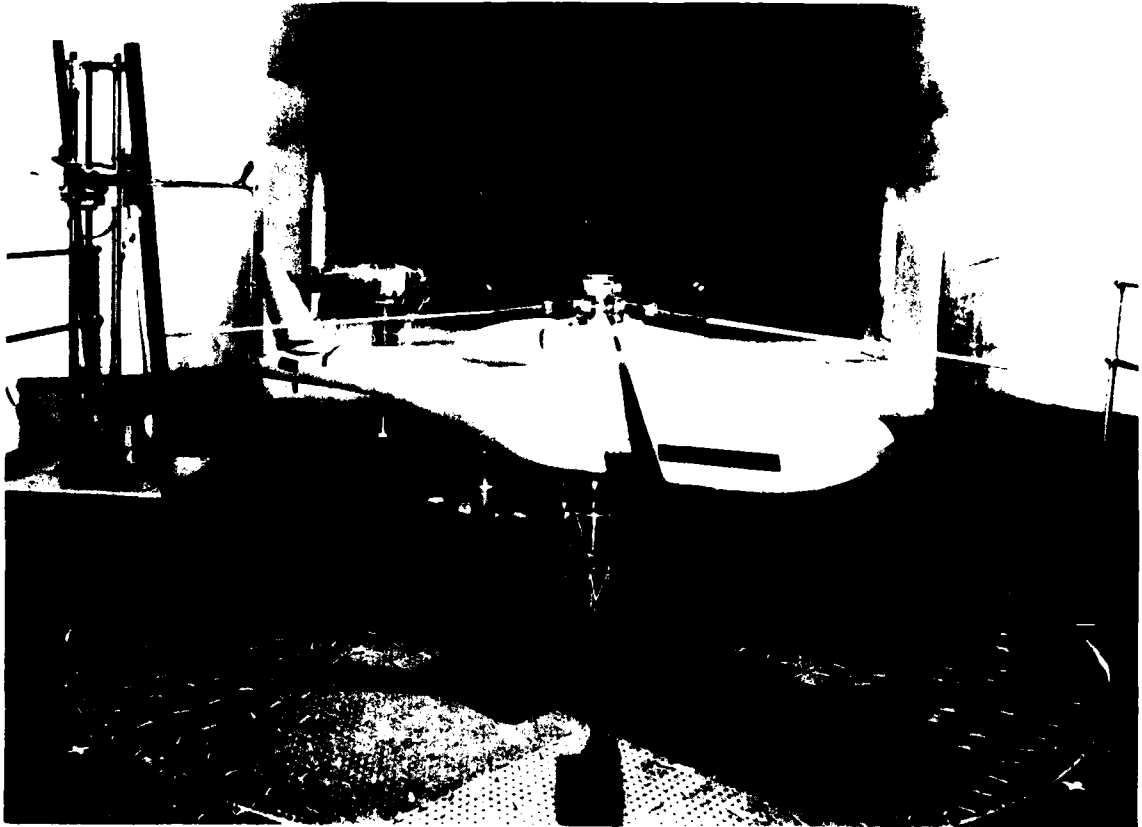


FIGURE 5. FRONT VIEW OF SRH MODEL IN YUH-61A CONFIGURATION WITH EXTERNAL TAIL ROTOR DRIVE MECHANISM.

TABLE 2. MODEL PARAMETERS

Main/Tail Rotors

Airfoil Cross-Section	VR7 .75R VR8 .91R VR9 _{TIP} /VR7
Rotor Radius - Main/Tail	60.62/12.50 inches
Reference Chord - Main/Tail	4.74/1.812 inches
Blade Number - Main/Tail	4/4
RPM - Main/Tail	1390/6000
Tip Speed - Main/Tail	735/648 fps
Main Rotor Shaft Incidence to WL	4 degrees forward
Main Rotor Center Station/ Waterline	41.6/43.6 inches
Tail Rotor Center Station/ Waterline	116.1/48.6 inches
Solidity - Main/Tail	0.0883/0.0943
Twist - Main/Tail	12.0°/0.0 degrees
Hinge Offset - Main/Tail	4.5%/0.0 (effective)

Horizontal Stabilizer

Airfoil Cross-Section	NACA 0012
Span	40.20 inches
Mean Aerodynamic Chord (MAC)	6.87 inches
Root Chord (Extended)	8.25 inches
Tip Chord	5.15 inches
1/4 - Chord Sweep	6.8 degrees
Tail Arm (25% MAC to STA 44.3)	63 inches
Incidence	45 degrees

Vertical Tail

Airfoil Cross-Section	NACA 63 ₄ - 421
Blockage Ratio	35% / 25%
Height (Tip to WL 37.5) - 35/25%	17.37/14.85 inches
Root Chord - 35/25%	15.2/13.46 inches
Tip Chord - 35/25%	6.4/5.41 inches
Mean Aerodynamic Chord (MAC)	11.4/10.4 inches
1/4 - Chord Sweep - 35/25%	37.5/37.5 degrees
Tail Arm (25% MAC to STA 44.3) - 35/25%	66.9/65.9 inches
Incidence - 35/25%	0/0 degrees

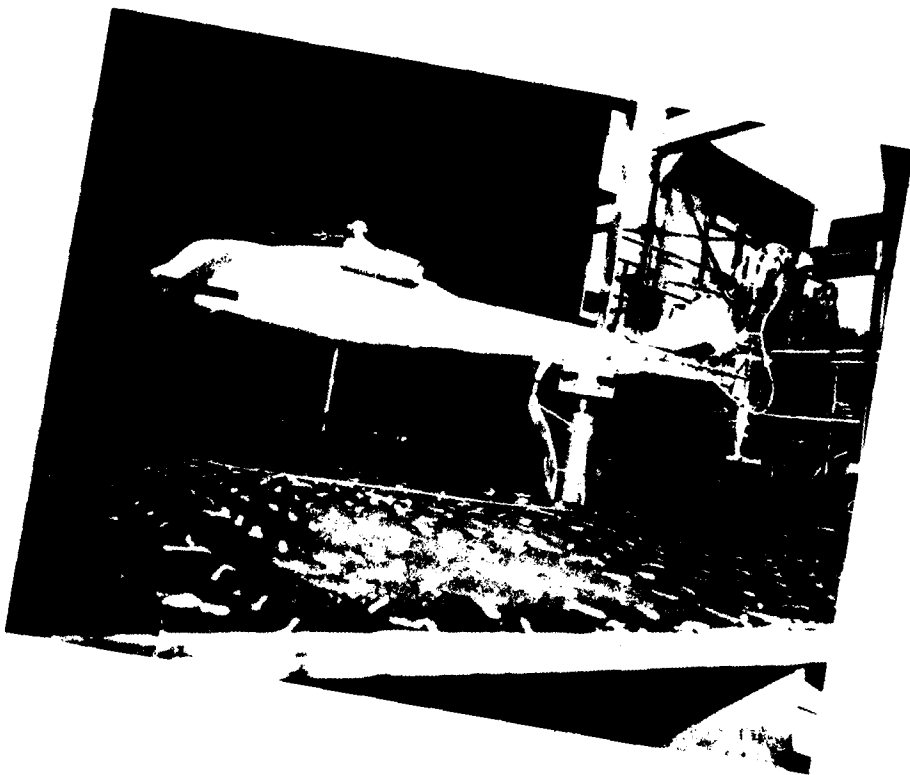


FIGURE 6. REAR VIEW OF SRH MODEL IN YUH-61A CONFIGURATION.

The tail rotor, like the main rotor, was controlled remotely with collective pitch to maintain the desired thrust levels and RPM to maintain full scale tip speed. Figure 7 shows a close-up of the four-bladed flex-strap tail rotor and the 52-horsepower electric drive motor employed in this test. Being a flex-strap rotor made it susceptible to a flap-lag instability. This prevented testing at high tail rotor thrust at certain conditions of wind azimuth and airspeed. This means that the variations in tail rotor thrust presented herein do not include tail rotor stall. Future tests in the area of tail rotor stall effects should incorporate a more rigid tail rotor.

With the complexity of the tail rotor drive mechanism and control system removed from the fin and boom structures, fin size and shape were varied more readily. Furthermore, the SRH assembly was modified to accommodate a separate fin balance to measure adverse fin force directly. The fin balance was mounted on the empennage spar as seen in Figure 8 which is a schematic of the subassembly for both tail surfaces. To study the influence of fin size on main rotor and tail rotor interactions, two new fins were fabricated and tested. Both fins have symmetrical airfoils and are shown in Figure 9. The larger of the two fins had a blockage ratio of 35% while the smaller fin blocks only 25% of the tail rotor swept area. The fins were positioned so that the 1/4-chord lines were coincident.

A third fin configuration was tested as part of a complementary contract funded by the Army Research Office. The ARO fin was a constant chord symmetrical airfoil with rounded trailing and leading edges. A variable fin incidence mechanism (see Figure 9) was developed to provide remote control over a range of fin incidences from $+90^\circ$ to -90° . The analysis of these data and related interactional effects was presented in Reference 6.

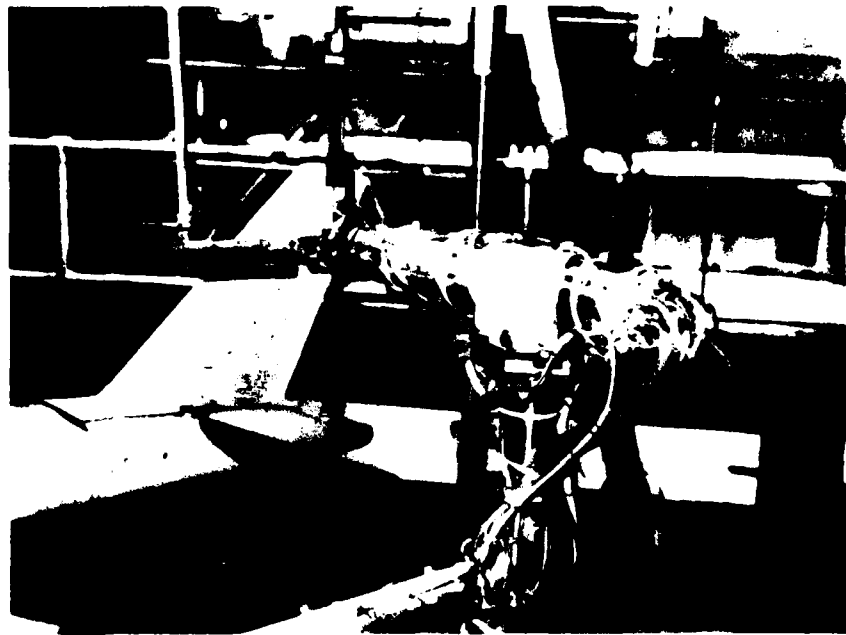


FIGURE 7. CLOSE-UP OF EXTERNAL TAIL ROTOR MECHANISM.

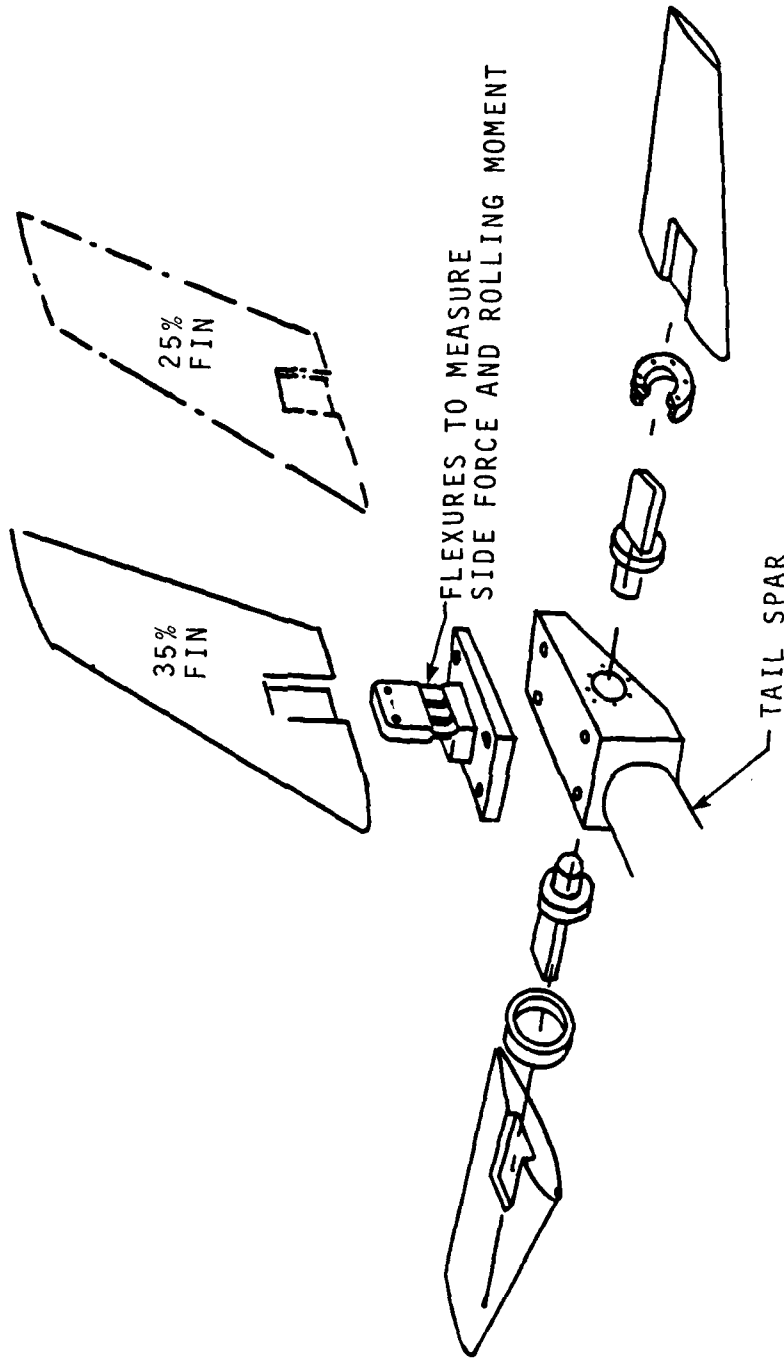


FIGURE 8. SRH EMPENNAGE WITH INTERCHANGEABLE FINS AND REMOVABLE STABILIZER.

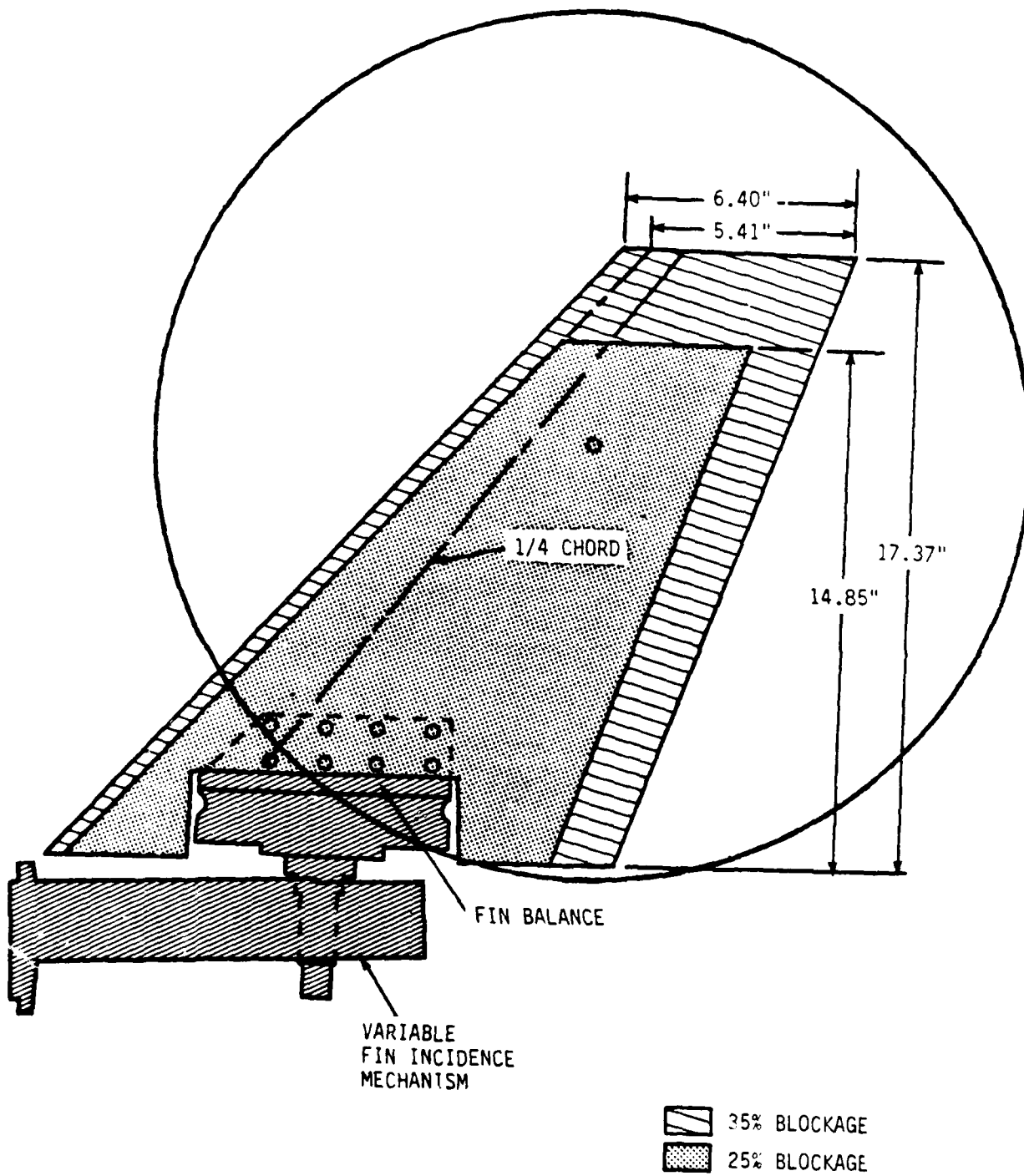


FIGURE 9. INTERCHANGEABLE VERTICAL FIN.

INSTRUMENTATION AND FLOW VISUALIZATION

Model Loads Data

Figure 10 gives a schematic of the model and power pod. The primary data for this investigation was provided by the complement of six strain gauge balances and the control systems for the main and tail rotors shown in Figure 10. The five balances that are integral to the SRH test assembly include the total loads, fuselage, empennage, fin and main rotor. The tail rotor balance is obviously included on the external tail rotor support. The empennage and fin balances do not measure the complete set of six forces and moments. The empennage balance measures all but axial force. The fin balance measures only fin side force and rolling moment. The remaining four balances measure the complete set of three forces and three moments each. The orientation of all six balances and the associated sign convention of the forces and moments is given in Figure 11.

Additional data is provided by transducers on the vertical fin and horizontal stabilizer that measure their respective incidence angles. The yaw and pitch drive systems are instrumented to provide the model orientation angles. Finally, approximately 20 temperature gauges, blade stress gauges, and other safety-of-flight parameters are also continuously monitored to check model integrity.

Flow Characteristics

Flow visualization was employed extensively during the test program. The flow characteristics on the ground plane and vertical fin surfaces were of particular interest. Tufts were placed on the fixed ground plane to track the position of the main rotor wake, particularly the ground vortex, as flight condition was varied. The vertical fin was also covered with tufts on the side nearest the tail rotor to visualize the effects of tail rotor thrust and flight condition on the flow over the tail plane (see Figure 7).

Main rotor and tail rotor flow characteristics and their interactions were also the focus of this investigation. For this a vertical smoke rake with eight probes was designed and fabricated. For most of the test the rake was positioned in the plane of symmetry of the model for forward flight. This provided a cross-sectional view of the flow for a given set of conditions. An example of the resulting flow patterns is given in Figure 12.

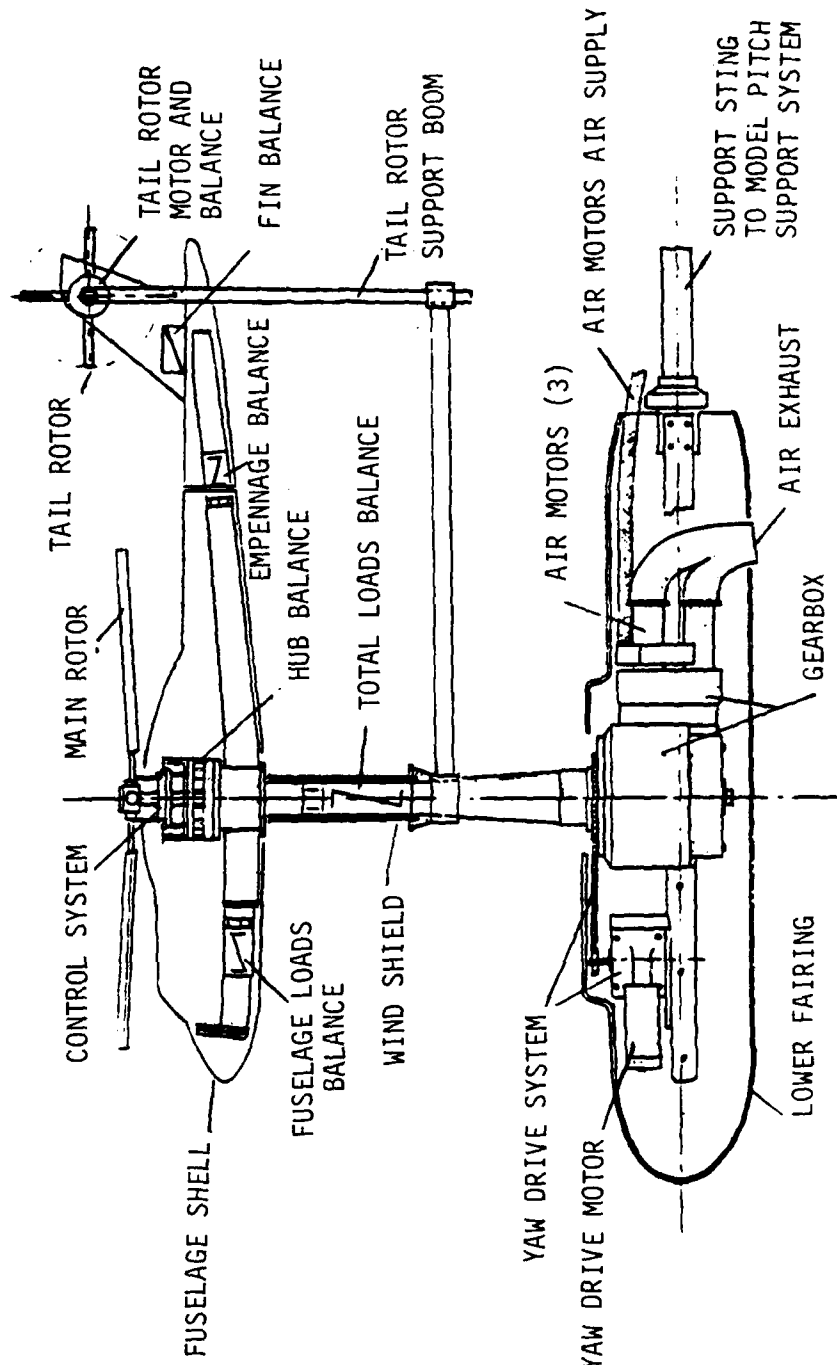


FIGURE 10. DETAILED DIAGRAM OF THE MODEL, BALANCES, AND POWER POD.

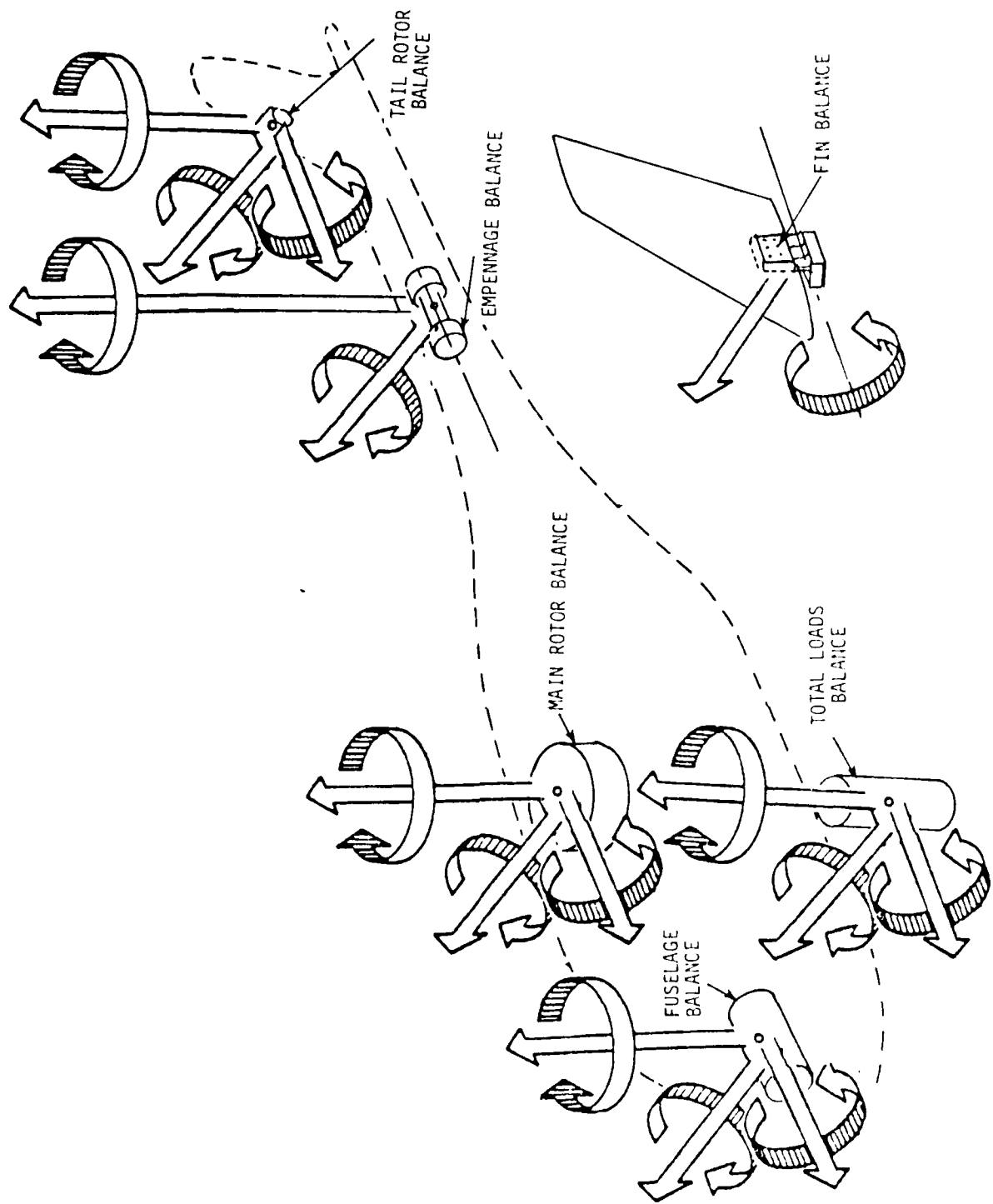


FIGURE 11. BALANCE ORIENTATIONS.



$\alpha = -90^\circ$ $V = 30 \text{ KTS}$

$C_{T_{MR}} = .0031$ $h/D = .35$

FIGURE 12. FLOW VISUALIZATION.

At conditions where the interactions of the principal flows are severe, distributional wake measurements were obtained through the use of a hot film probe. The sensor was mounted on a remotely actuated traversing mechanism to allow vertical sweeps of the probe. The traversing mechanism can be seen in the background of Figure 5 on the left side of the test section. The probe employed two hot film sensors that were oriented perpendicular to each other to provide both longitudinal (alpha) and lateral (beta) flow angles and the associated velocities. The hot film data runs and their respective probe locations are summarized in the next section.

MODEL CONFIGURATIONS AND TEST CONDITIONS

The next three sections of this report present the interaction of the main rotor, tail rotor, and free stream flows for various model configurations and flight conditions. The data that provided the basis for this discussion is summarized by run number in Tables 3 through 8. The configuration codes listed in the second column indicate which model configuration was tested, and are defined in Table 9. Tables 3 through 8 also list the flight conditions for each run. For most of the runs all parameters were held constant except one. Parametric sweeps are denoted by the flags and are summarized in Table 10.

In general, each table is a summary of runs that form a logical group. For example, Table 3 presents all of the data obtained at the high h/d condition ($h/d = 0.8$) with the 35% blockage fin. The runs for the three fin configurations at the low h/d condition ($h/d = 0.35$) are summarized in Tables 4, 5 and 6 for the 35% blockage, 25% blockage, and fin-removed configurations, respectively. The runs for the tail rotor placement study with the 35% fin are given in Table 7. The flight conditions where the flow measurement tests were conducted are summarized in Table 8.

The fundamental parameters involved in the study of interactional aerodynamics include airspeed and wind azimuth for various loading conditions of the main rotor and tail rotor. These parameters were varied individually from run to run as well as during each run for each of the configurations in Tables 3 through 8. In general, the test procedure was to stabilize at a given airspeed and wind azimuth, then set the main and tail rotor thrusts to prespecified levels. The nominal loading conditions were $C_{TMR} = 0.0062$ and $C_{TTR} = 0.012$ for the two rotors, respectively. Throughout the entire test the main rotor shaft remained perpendicular to the ground plane. For all of the runs except the cyclic pitch sweeps, the hub rolling and pitching moments were trimmed to zero with cyclic pitch controls. Both rotors were operated at a constant RPM throughout the program.

The operating conditions of particular interest included speed sweeps in rearward flight ($\psi=180^\circ$), left and right side-ward flight ($\pm 90^\circ$), and sideslip conditions of ± 45 degrees in yaw. For each of these wind azimuths the main rotor and tail rotor thrusts were varied independently and arbitrarily. That is, the test conditions were not selected to simulate a particular trimmed flight condition but to quantify the effects of the variations in main rotor, tail rotor, and free stream flows on their mutual interactions.

TABLE 3. RUN LOG FOR $h/d = 0.8$ CONFIGURATION

RUN NO.	CONFIGURATION CODE	RUN TYPE	V_{TUN} (KTS)	MR/TR RPM	C_{TMR}	C_{TTR}	AZIMUTH ψ -DEG	H/D
53	$B_1 M_1 V_1 H_1 T_1 HS_1$	MR C_T Sweep	15	1390/ 6000	10	0.012	-90	0.8
54	✓	✓	20	✓	✓	✓	✓	✓
55	✓	✓	25	✓	✓	✓	✓	✓
56	✓	✓	30	✓	✓	✓	✓	✓
57	✓	Airspeed Sweep	11	✓	0.0062	✓	0	✓
58	✓	✓	✓	✓	✓	0	✓	✓
59	✓	MR C_T Sweep	15	✓	10	✓	-90	✓
60	✓	✓	20	✓	✓	✓	✓	✓
61	✓	✓	25	✓	✓	✓	✓	✓
62	✓	✓	30	✓	✓	✓	✓	✓
63	✓	Wind Azimuth Sweep	35	✓	0.0062	0.012	12	✓
64	✓	✓	20	✓	✓	✓	✓	✓
65	✓	✓	25	✓	✓	0.011	✓	✓
66	✓	✓	30	✓	✓	✓	✓	✓
67	✓	Airspeed Sweep	13	✓	✓	0.012	180°	✓

TABLE 4. RUN LOG FOR 35% BLOCKAGE FIN

RUN NO.	CONFIGURATION CODE	RUN TYPE	V _{TUN} (KTS)	MR/TR RPM	C _T MR	C _T TR	ACIMUTH ψ-DEG	H/D
73	B ₁ M ₁ V ₁ H ₁ T ₀ HS ₁	MR C _T Sweep	15	1390/0	10	0.11	-90	0.35
74	✓	✓	20	✓	✓	✓	✓	✓
75	✓	✓	25	✓	✓	✓	✓	✓
76	✓	✓	30	✓	✓	✓	✓	✓
77	✓	Airspeed Sweep	11	✓	0.0062	✓	0	✓
79	✓	MR C _T Sweep	35	✓	13	✓	180	✓
80	✓	✓	✓	✓	✓	✓	135	✓
81	✓	✓	✓	✓	✓	✓	90	✓
82	✓	✓	✓	✓	✓	✓	45	✓
83	✓	✓	✓	✓	✓	✓	0	✓
84	✓	✓	✓	✓	✓	✓	-30	✓
85	✓	✓	✓	✓	✓	✓	-40	✓
87	✓	✓	✓	✓	✓	✓	-50	✓
88	✓	✓	✓	✓	✓	✓	-60	✓
89	✓	✓	✓	✓	✓	✓	-90	✓
90	✓	Airspeed Sweep	15	✓	0.0062	✓	0	✓
91	✓	✓ ①	✓	✓	✓	✓	✓	✓
92	✓	✓	16	✓	✓	✓	✓	✓
93	✓	MR RPM Sweep	②	② /0	✓	✓	✓	✓
95	B ₁ M ₁ V ₁ H ₁ T ₁ HS ₁	MR C _T Sweep	15	1390/ 6000	10	0.012	-90	✓
196	✓	TR C _T Sweep	30	✓	0.0062	17	225	✓
197	✓	✓	✓	✓	✓	✓	200	✓
198	✓	✓	✓	✓	✓	✓	190	✓
200	✓	✓	✓	✓	✓	✓	180	✓
201	✓	✓	✓	✓	✓	✓	170	✓
202	✓	✓	✓	✓	✓	✓	160	✓
203	✓	✓	✓	✓	✓	✓	150	✓
204	✓	✓	✓	✓	✓	✓	135	✓
205	✓	✓	✓	✓	✓	✓	90	✓
206	✓	✓	✓	✓	✓	✓	75	✓
207	✓	✓	✓	✓	✓	✓	60	✓
208	✓	✓	✓	✓	✓	✓	50	✓

- LONGITUDINAL AND LATERAL CYCLICS FIXED AT TRIM VALUES FOR 20 KNOT CONDITION
- TEST CONDITIONS FOR R.P.M. VARIATIONS
 (RPM = 1182, V = 29.7 KNOTS)
 (RPM = 973, V = 24.5 KNOTS)

TABLE 4. (CONTINUED)

RUN NO.	CONFIGURATION CODE	RUN TYPE	V _{TUN} (KTS)	MR/TR RPM	C _T MR	C _T TR	AZIMUTH ψ -DEG	H/D	
209	B ₁ M ₁ V ₁ H ₁ T ₁ HS ₁	TR C _T Sweep	30	1390/ 6000	0.0062	17	40	0.35	
210	✓	✓	✓	✓	✓	✓	30	✓	
211	✓	✓	✓	✓	✓	✓	20	✓	
212	✓	✓	✓	✓	✓	✓	0	✓	
213	✓	✓	✓	✓	✓	✓	-20	✓	
214	✓	✓	✓	✓	✓	✓	-30	✓	
215	✓	✓	✓	✓	✓	✓	-40	✓	
216	✓	✓	✓	✓	✓	✓	-50	✓	
217	✓	✓	✓	✓	✓	✓	-60	✓	
218	✓	✓	✓	✓	✓	✓	-75	✓	
219	✓	✓	✓	✓	✓	✓	-90	✓	
220	✓	Cyclic Pitch Sweep	18	30	1390/ 6000	0.0062	0.011	-90	✓
221	✓	✓	0	✓	✓	✓	0	✓	
222	✓	✓	✓	✓	✓	✓	0	✓	
223	✓	✓	30	✓	✓	✓	-90	✓	
225	✓	MR C _T Sweep	21	1182/ 5100	20	0.012	0	✓	
226	✓	✓	30	✓	✓	✓	✓	✓	
227	✓	✓	18	973/ 4200	✓	✓	✓	✓	
228	✓	✓	25	✓	✓	✓	✓	✓	
229	✓	TR C _T Sweep	0	1390/ 6000	.0062	21	-90	✓	
230	✓	MR C _T Sweep	✓	✓	22	0.012	✓	✓	
231	✓	TR C _T Sweep	15	✓	0.0062	21	✓	✓	
232	✓	MR C _T Sweep	✓	✓	22	0.012	✓	✓	
233	✓	TR C _T Sweep	20	✓	0.0062	21	✓	✓	
234	✓	MR C _T Sweep	✓	✓	22	0.12	✓	✓	
235	✓	TR C _T Sweep	25	✓	0.0062	21	✓	✓	
236	✓	MR C _T Sweep	✓	✓	22	0.12	✓	✓	
237	✓	TR C _T Sweep	30	✓	0.0062	21	✓	✓	
238	✓	MR C _T Sweep	✓	✓	22	0.012	✓	✓	
239	✓	TR C _T Sweep	35	✓	0.0062	21	✓	✓	
240	✓	MR C _T Sweep	✓	✓	22	0.011	✓	✓	
241	✓	✓	45	✓	0.0062	0.0077	✓	✓	

TABLE 4. (CONTINUED)

RUN NO.	CONFIGURATION CODE	RUN TYPE	V _{TUN} (KTS)	MR/TR RPM	C _T MR	C _T TR	AZIMUTH ψ-DEG	H/D
242	B ₁ M ₁ V ₁ H ₁ T ₁ HS ₁	TR C _T Sweep	45	1390/ 6000	.0062	21	180	0.35
243	✓	✓	35	✓	✓	✓	✓	✓
244	✓	✓	30	✓	✓	✓	✓	✓
245	✓	✓	25	✓	✓	✓	✓	✓
247	✓	✓	20	✓	✓	✓	✓	✓
248	✓	✓	15	✓	✓	✓	✓	✓
249	✓	✓	0	✓	✓	✓	✓	✓
250	✓	MR C _T Sweep	✓	✓	22	0.012	✓	✓
251	✓	✓	15	✓	✓	✓	✓	✓
252	✓	✓	20	✓	✓	✓	✓	✓
253	✓	✓	25	✓	✓	✓	✓	✓
254	✓	✓	30	✓	✓	✓	✓	✓
255	✓	✓	35	✓	✓	✓	✓	✓
256	✓	✓	45	✓	✓	✓	✓	✓
257	✓	TR C _T Sweep	0	✓	0.0062	21	90	✓
258	✓	✓	15	✓	✓	✓	✓	✓
279	✓	✓	20	✓	✓	✓	✓	✓
280	✓	✓	25	✓	✓	✓	✓	✓
281	✓	✓	30	✓	✓	✓	✓	✓
282	✓	✓	35	✓	✓	✓	✓	✓
283	✓	✓	45	✓	✓	✓	✓	✓
285	✓	MR C _T Sweep	35	✓	22	0.012	✓	✓
286	✓	✓	✓	✓	✓	✓	0	✓
287	✓	TR C _T Sweep	45	✓	0.0062	21	✓	✓
288	✓	✓	35	✓	✓	✓	✓	✓
289	✓	✓	30	✓	✓	✓	✓	✓
290	✓	✓	25	✓	✓	✓	✓	✓
291	✓	✓	20	✓	✓	✓	✓	✓
292	✓	✓	15	✓	✓	✓	✓	✓
293	✓	✓	0	✓	✓	✓	✓	✓
294	✓	Airspeed Sweep	23	✓	✓	0.012	-90	✓
295	✓	MR C _T Sweep	30	✓	24	✓	✓	✓
296	✓	TR C _T Sweep	✓	✓	0.0062	25	✓	✓

TABLE 5. RUN LOG FOR 25% BLOCKAGE FIN

RUN NO.	CONFIGURATION CODE	RUN TYPE	V _{TUN} (KTS)	MR/TR RPM	C _T MR	C _T TR	AZIMUTH ϕ -DEG	H/D
297	B ₁ M ₁ V ₂ H ₁ T ₁ HS ₁	Yaw Sweep	30	1300/ 6000	0.0062	0.012	26	0.35
298	✓	MR C _T Sweep	0	✓	27	✓	-90	✓
299	✓	✓	20	✓	✓	✓	✓	✓
300	✓	✓	25	✓	✓	✓	✓	✓
301	✓	✓	30	✓	✓	0.010	✓	✓
302	✓	✓	35	✓	✓	✓	✓	✓
303	✓	✓	45	✓	0.0062	0.008	✓	✓
304	✓	TR C _T Sweep	35	✓	✓	28	✓	✓
305	✓	✓	30	✓	✓	✓	✓	✓
306	✓	✓	25	✓	✓	✓	✓	✓
307	✓	✓	20	✓	✓	✓	✓	✓
308	✓	✓	0	✓	✓	✓	✓	✓
309	✓	✓	20	✓	✓	✓	0	✓
310	✓	✓	25	✓	✓	✓	✓	✓
311	✓	✓	30	✓	✓	✓	✓	✓
312	✓	✓	35	✓	✓	✓	✓	✓
313	✓	✓	45	✓	✓	0.008	✓	✓
314	✓	MR C _T Sweep	35	✓	27	0.010	✓	✓
315	✓	✓	30	✓	✓	0.012	✓	✓
316	✓	✓	25	✓	✓	✓	✓	✓
317	✓	✓	20	✓	✓	✓	✓	✓
318	✓	✓	✓	✓	✓	✓	180	✓
319	✓	✓	25	✓	✓	✓	✓	✓
320	✓	✓	30	✓	✓	✓	✓	✓
321	✓	✓	35	✓	✓	0.010	✓	✓
322	✓	✓	45	✓	✓	✓	✓	✓
323	✓	TR C _T Sweep	35	✓	0.0062	28	✓	✓
324	✓	✓	30	✓	✓	✓	✓	✓
325	✓	✓	25	✓	✓	✓	✓	✓
326	✓	✓	20	✓	✓	✓	✓	✓
327	✓	✓	20	✓	✓	0.012	-90	✓
328	✓	✓	25	✓	✓	0.010	✓	✓
329	✓	✓	30	✓	✓	0.008	✓	✓

TABLE 6. RUN LOG FOR FIN-OFF CONFIGURATION

RUN NO.	CONFIGURATION CODE	RUN TYPE	V _{TUN} (KTS)	MR/TR RPM	C _{TMR}	C _{TTR}	AZIMUTH ϕ -DEG	H/D
330	B ₁ M ₁ V ₀ H ₁ T ₁ HS ₁	MR C _T Sweep	35	1390/6000	27	0.006	-90	0.35
331	✓	TR C _T Sweep	✓	✓	0.0062	28	✓	✓
332	✓	✓	30	✓	✓	0.010	✓	✓
333	✓	✓	25	✓	✓	0.012	✓	✓
334	✓	✓	20	✓	✓	✓	✓	✓
335	✓	✓	15	✓	✓	✓	✓	✓
336	✓	TR C _T Sweep	35	✓	0.0062	28	0	✓
337	✓	MR C _T Sweep	✓	✓	27	0.012	✓	✓
338	✓	TR C _T Sweep	✓	✓	0.0062	28	90	✓
339	✓	MR C _T Sweep	✓	✓	27	0.012	✓	✓
340	✓	TR C _T Sweep	✓	✓	0.0062	28	180	✓
341	✓	MR C _T Sweep	✓	✓	27	0.012	✓	✓

TABLE 7. RUN LOG FOR TAIL ROTOR PLACEMENT INVESTIGATION

RUN NO.	CONFIGURATION CODE	RUN TYPE	V _{TUN} (KTS)	C _{TMR}	C _{TTR}	AZIMUTH ϕ -DEG	X _{MS}	Y _{BL}	Z _{WL}
349	B ₁ M ₁ V ₁ H ₁ T ₁ HS ₁	TR C _T Sweep	35	0.0062	29	-90	116.5	-5.6	48.6
350	✓	✓	✓	✓	✓	✓	116.1	-4.33	✓
351	✓	✓	✓	✓	✓	✓	✓	-6.80	✓
352	✓	✓	✓	✓	✓	✓	✓	-5.60	53.72
353	B ₁ M ₁ V ₁ H ₁ T ₁ HS ₀	✓	✓	✓	✓	✓	✓	✓	43.34
354	✓	✓	✓	✓	✓	✓	✓	✓	48.60
355	✓	Yaw Sweep	✓	✓	0	33	✓	✓	✓
356	✓	✓	✓	✓	0.012	✓	✓	✓	✓
357	B ₁ M ₁ V ₁ H ₁ T ₁ HS ₁	TR C _T Sweep	20	✓	29	-90	✓	-11.0	✓

TABLE 8. RUN LOG FOR HOT FILM FLOW MEASUREMENT INVESTIGATION

RUN NO.	CONFIGURATION CODE	RUN TYPE	V _{TUN} (KTS)	MR/TR RPM	C _{TMR}	C _{TTR}	AZIMUTH ψ -DEG	H/D
358	B ₁ M ₁ V ₁ H ₁ T ₁ HS ₂	Hot Film Sweep	25	1390/ 6000	0.0062	0.012	-90	.35
359	✓	✓	30	✓	✓	✓	✓	✓
360	✓	✓	20	✓	✓	✓	✓	✓
361	✓	✓	✓	✓	✓	0	✓	✓
362	✓	✓	✓	✓	✓	0.012	-50	✓
363	✓	✓	25	✓	✓	✓	✓	✓
364	✓	✓	30	✓	✓	✓	✓	✓
365	✓	✓	✓	✓	✓	0	✓	✓
366	✓	✓	20	✓	✓	0.012	170	✓
367	✓	✓	25	✓	✓	✓	✓	✓
368	✓	✓	✓	✓	✓	0	✓	✓
369	✓	✓	✓	✓	0.093	✓	✓	✓
371	✓	✓	✓	✓	✓	.012	✓	✓
372	✓	✓	22.5	✓	✓	✓	✓	✓
373	✓	✓	20	✓	0.0062	0	✓	✓
374	✓	✓	✓	✓	0	✓	0	✓
375	✓	✓	14	✓	0.0043	✓	✓	✓
376	✓	✓	20	✓	✓	✓	✓	✓
377	✓	✓	19	✓	0.0062	✓	✓	✓
378	✓	✓	22	✓	0.0093	✓	✓	✓
379	✓	✓	20	✓	✓	✓	✓	✓
380	✓	✓	15	1182/ 6000	0.0062	✓	✓	✓
381	✓	✓	13	973/ 6000	✓	✓	✓	✓
382	✓	✓	17	1390/ 6000	✓	✓	✓	✓

TABLE 9. CONFIGURATION CODE DEFINITIONS

<u>COMPONENTS</u>	<u>VARIATIONS</u>	<u>CODE</u>
Fuselage	-	B ₁
Main Rotor	Off	M ₀
	On	M ₁
Hub	Off	H ₀
	On	H ₁
	H ₁ Without Pitch Links	H ₂
Horizontal Stabilizer	Off	HS ₀
	On	HS ₁
	Right Side Off	HS ₂
Tail Rotor	Off	T ₀
	Pusher	T ₁
	Tractor	T ₂
	Isolated	T ₃
Fins	Off	V ₀
	35% Blockage Ratio	V ₁
	25% Blockage Ratio	V ₂

TABLE 10. FLAG NOTE SUMMARY

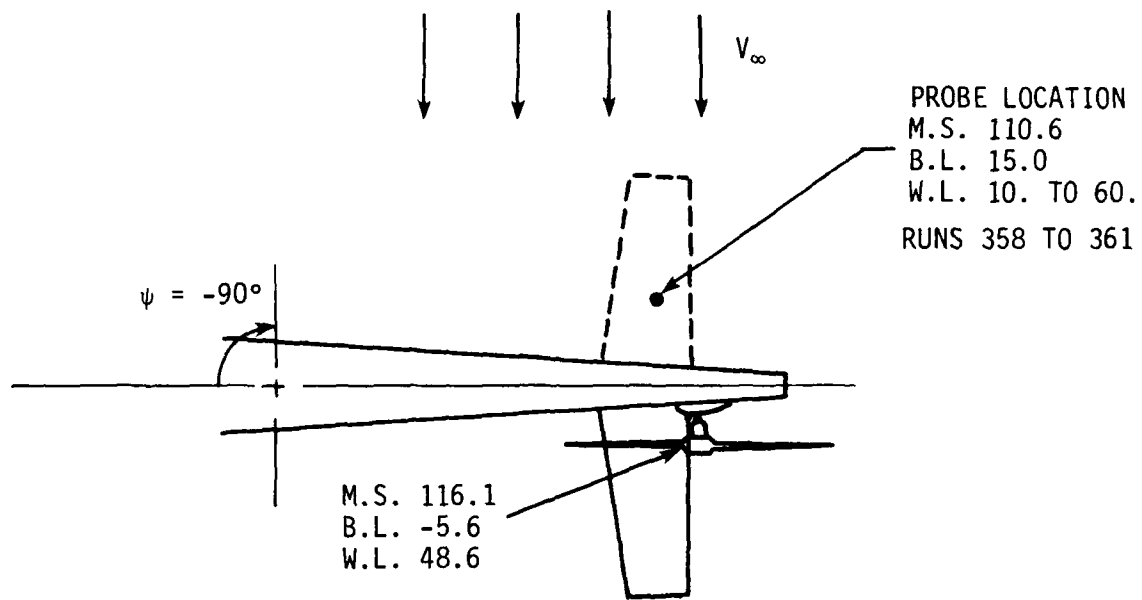
<u>FLAG</u>	<u>PARAMETER VARIATION</u>
1	RPM_{TR} 5000 to 6400 Δ 's = 200
3	$C_{T_{TR}}$ = 0 to 0.028 or MAX.
4	$C_{T_{TR}}$ = 0.006, 0.012, 0.018, 0.024
5	$C_{T_{TR}}$ = 0.006, 0.012, 0.018
6	V_{TUN} = 5 KTS \rightarrow 30 KTS - Continuous
7	h/d = 0.475 \rightarrow 0.80 Continuous
8	i_{fin} = -5, 0, 5, 10, 15°
9	i_{fin} = 0, i_{fin} (for SF = 0)
10	$C_{T_{MR}}$ = 0.0031, 0.0062, 0.0093
11	V = 15, 20, 25, 30 KTS
12	ψ_f' = -30, -40, -50, -60, -70, -90°
13	V = 20, 25, 30, 35 KTS
14	$C_{T_{MR}}$ = 0, 0.0062, 0.0093
15	V = 0, 6, 8, 10, 12, 14, 16, 18, 20, 22, 26, 30 KTS
16	V continuous from 10 to 30 Knots
17	$C_{T_{TR}}$ = 0.006, 0.011
18	B_1 = -9 to +9° by 3's
19	A_1 = -9 to +9° by 3's
20	$C_{T_{MR}}$ = 0, 0.0062
21	$C_{T_{TR}}$ = 0, 0.012, 0.018 or $C_{T_{MAX}}$
22	$C_{T_{MR}}$ = 0.0031, 0.0093
23	V = 8, 12, 17.5, 22.5, 27.5 KTS
24	$C_{T_{MR}}$ = 0.0015, 0.0045, 0.0075
25	$C_{T_{TR}}$ = 0.003, 0.006, 0.009, 0.015, .018 or $C_{T_{MAX}}$
26	ψ_f = 190, 180, 170, 135, 90, 45, 0, -40, -50, -60, -75, -90°
27	$C_{T_{MR}}$ = 0, .0093
28	$C_{T_{TR}}$ = 0, 0.018 or $C_{T_{MAX}}$

TABLE 10. (CONTINUED)

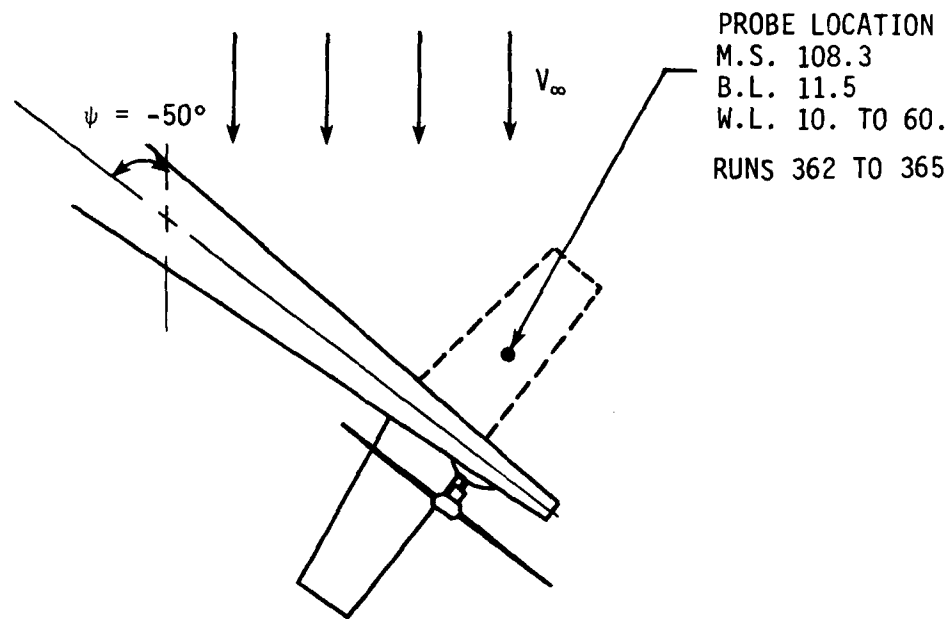
29	$C_{T_{TR}} = 0, 0.006, .012, 0.018$
30	i_{fin} set for sideforce = 0
31	$V = 0, 20, 35$ KTS
32	$C_{T_{TR}} = 0, 0.006, 0.012$
33	$\psi_{f.} = -40, -50, -60^\circ$
34	$i_{fin} = -90, -80, -70, -60 \rightarrow + 60$ by 20° 's, 70, 80
35	$\Delta WL(INS.) = -35, -30, -35, -20 \rightarrow + 10 \times 3''$'s (WRT WL 48.55)

For the tail rotor placement studies (see Table 7), the specified flight condition was 35 knots in right sideward flight. This is the maximum requirement for current military aircraft. The nominal position of the tail rotor was model station +116.1, butt line -5.6, and waterline +48.6. The variations in tail rotor location represent a change of $\pm 19\%$ of tail rotor radius in the longitudinal direction, $\pm 10\%$ of tail rotor radius in the lateral direction, and $\pm 40\%$ of tail rotor radius in the vertical direction.

Distributional flow measurements were also obtained at specific flight conditions. The influence of the main rotor wake near the empennage was measured for the -50 and -90 degree yaw conditions. Effects due to the ground vortex in forward ($\psi = 0^\circ$) and rearward flight ($\psi = 170^\circ$) were also studied. Figure 13 gives a top view of the hot film probe positions relative to the model for the various flight conditions. Hot film data was obtained for the baseline 35% fin configuration. At each azimuth, limited variations in airspeed, main rotor, and tail rotor thrusts were investigated. Refer to Table 8 for specific details. For all of the runs where hot film data was obtained, the probe was aligned with the free stream flow regardless of the model yaw angle.



a. SIDEWARD FLIGHT ($\psi = -90^\circ$)



b. RIGHT SIDESLIP ($\psi = -50^\circ$)

FIGURE 13. SCHEMATIC OF HOT FILM PROBE LOCATIONS (TOP VIEW) AND ASSOCIATED FLIGHT CONDITIONS.

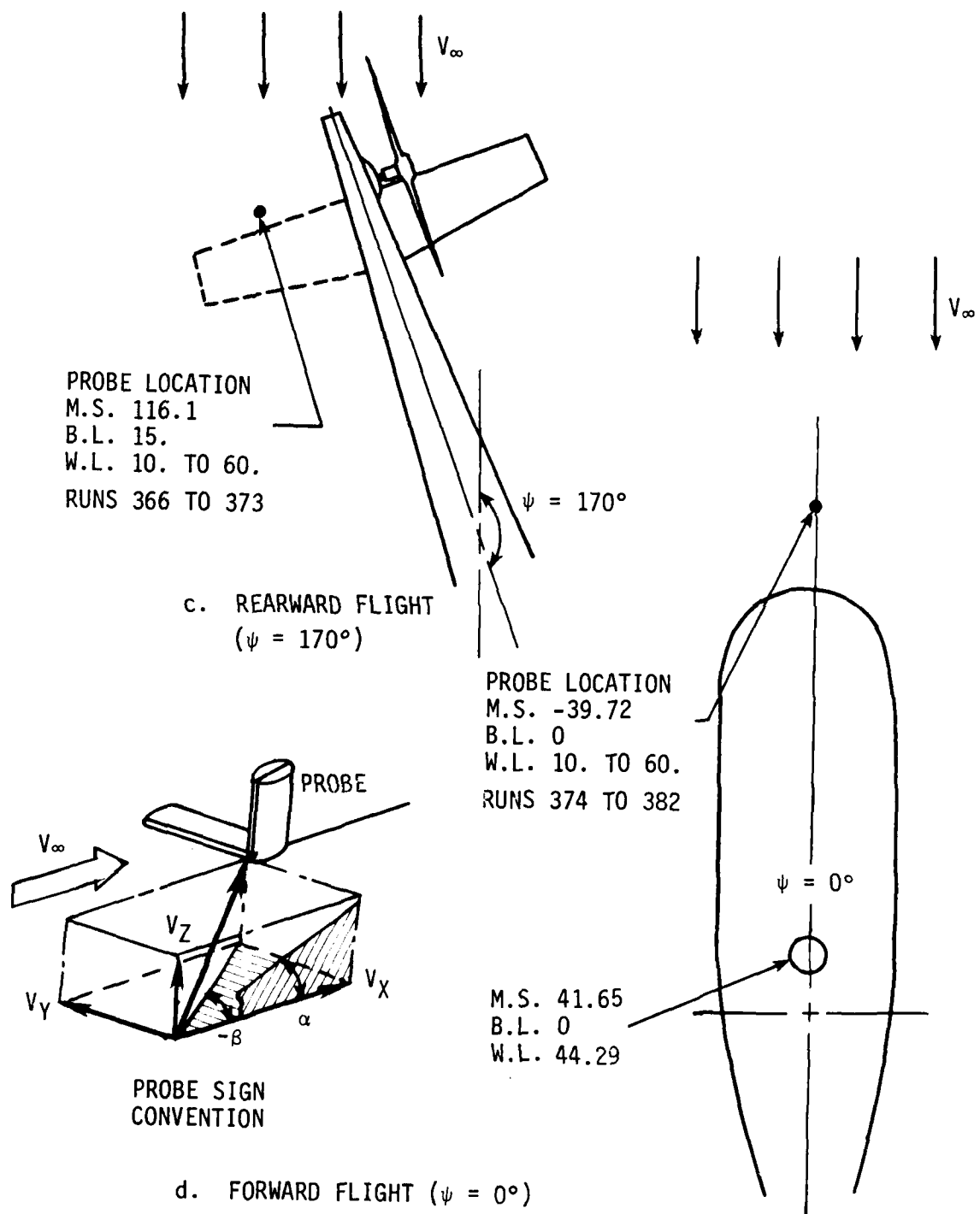


FIGURE 13.(CONTINUED).

MAIN ROTOR/TAIL ROTOR INTERACTIONS

The interaction of the main rotor and tail rotor was investigated at various levels of thrust for both rotors. The variations in main and tail rotor loadings were examined for different airspeeds and specific wind azimuths, thus providing a comprehensive data base regarding main rotor/tail rotor interactions. A novel aspect of the program is that these studies were conducted for the larger fin blockage ratio of 35% which is comparable to many contemporary aircraft due to the tail-rotor-off trim requirements. In this manner the effect of a large fin on main rotor/tail rotor interactions is studied.

The probe into main rotor/tail rotor interactions is important for understanding how helicopter stability and control are affected when these dynamic components and their respective wakes are brought in close proximity to each other and in proximity to the ground. Variations in main as well as tail rotor thrust change the energy level of their wake, thus changing the severity by which the flows interact. The comprehensive investigation presented in this section attempts to quantify those effects. Careful planning of the test conditions for the experiment was required to obtain the necessary parametric variations. The number of variables is so cumbersome that the automatic graphics capability at the Boeing V/STOL tunnel was used extensively to reduce the data.

MAIN ROTOR ON TAIL ROTOR INTERACTIONS

For the study of main rotor wake effects on the tail rotor, two variables are examined to indicate the flow conditions at the tail rotor. These parameters are tail rotor power to thrust ratio (C_P/C_T) and tail rotor collective pitch (θ_{TR}).

The tests concerning main rotor wake effects were all conducted at constant levels of tail rotor thrust; therefore, variations in the tail rotor power to thrust ratio simply reflect variations in tail rotor power required to maintain a constant thrust. Similarly, the variations in tail rotor collective to maintain a constant thrust indicate variations to the inflow through the tail rotor. The tail rotor collective is defined as the blade pitch resulting from an actuator displacement in the static or nonrotating condition. Because the tail rotor is a flex-strap design, the precise definition of tail rotor collective at 3/4 radius while rotating is unknown. However, the variations in tail rotor collective pitch will be indicative of relative effects of main rotor and free-stream flows.

Effects of Wind Azimuth

Wind azimuth is a key parameter in the study of interactional aerodynamics, for it determines the proximity of the tail rotor to such flow anomalies as the main rotor tip vortices and the ground vortex. Tail rotor power to thrust ratio and tail rotor collective required versus wind azimuth at an air-speed of 30 knots are plotted in Figures 14 and 15 respectively. Two levels of tail rotor thrust were tested ($C_{T_{TR}} = 0.006; 0.012$). In Figure 14 the two curves have a somewhat constant delta between them except in the region extending from $\psi = 0$ through $\psi = +60$ degrees. This offset is not attributed to the different levels in tail rotor thrust because the tail rotor power has been normalized by thrust.

Both Figures 14 and 15 show a nonlinearity in the data near wind azimuths of ± 50 degrees. This is clearly the influence of the main rotor tip vortex impinging on the tail rotor. Without the main rotor flow, the variation in tail rotor power and collective pitch would be smooth for the full range of azimuths. At $\psi = -50^\circ$ the main rotor tip vortex adds to the top-blade-aft rotation of the tail rotor, effectively increasing the tail rotor RPM. This results in a reduction in the collective pitch required to maintain a constant thrust. For the left sideslip condition of $+30$ degrees, a similar reduction in tail rotor collective occurs. The main rotor tip vortex again adds to the tail rotor rotational speed, resulting in lower collective pitch settings.

The variations in tail rotor collective pitch shown in Figure 15 due to main rotor wake are much more severe for the left sideslip condition ($\psi = +50^\circ$). However, this is not a major concern with regard to directional control for two reasons. First, in a left sideslip condition the side forces generated by the fuselage and fin build in a sense that aids the tail rotor. The tail rotor would not be required to maintain constant thrust as was done in this test. Second, as seen in Figure 15 the total collective pitch required for constant thrust is highest near $\psi = -90^\circ$. Therefore, the control requirement for the $\psi = +50^\circ$ condition is not critical because it is not approaching a control travel limit. This was probably part of the rationale that was used to determine that the top-blade-aft rotation was the optimum tail rotor design based on test data presented in Reference 3.

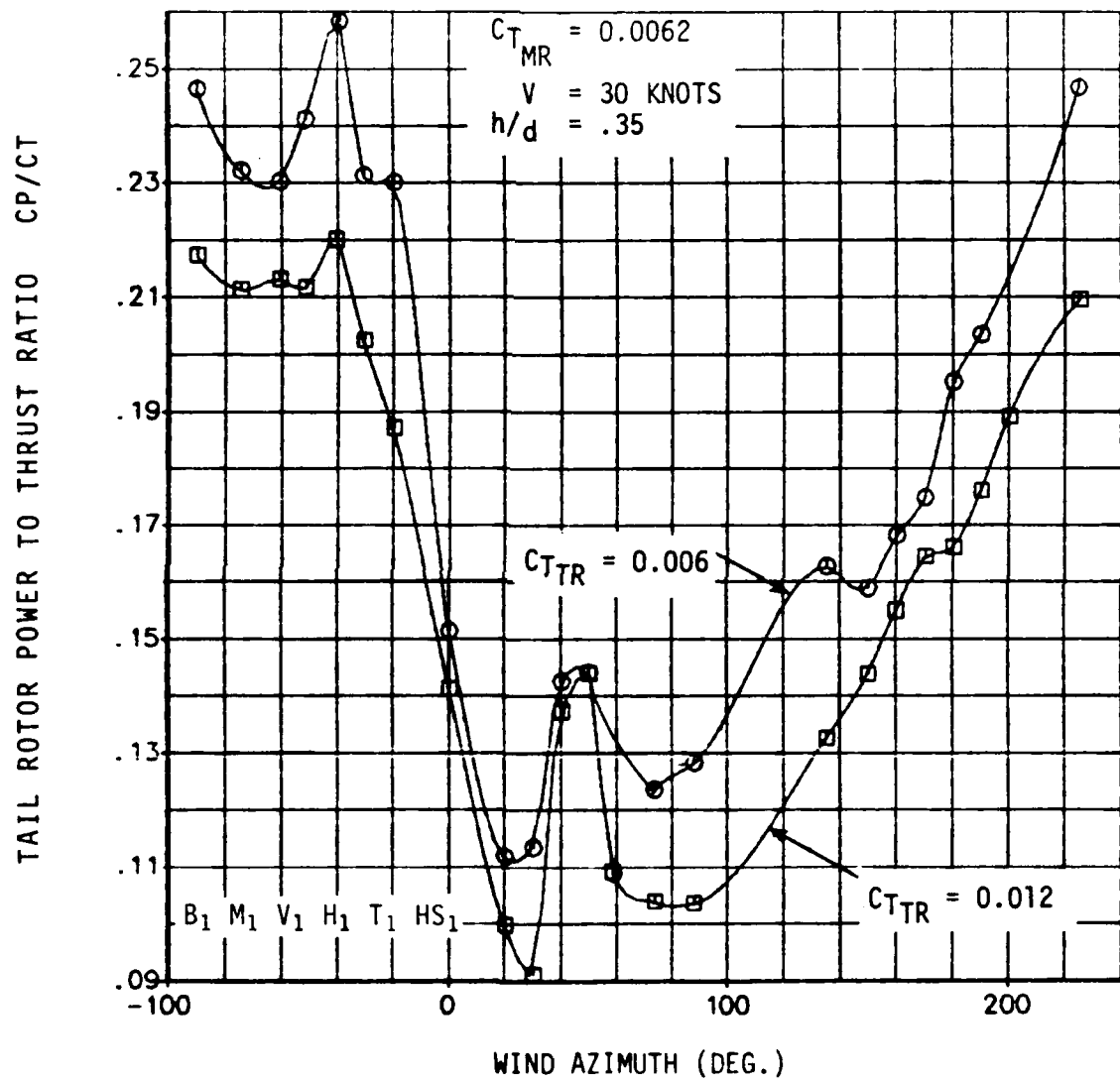


FIGURE 14. VARIATION OF TAIL ROTOR POWER TO THRUST RATIO AS A FUNCTION OF WIND AZIMUTH.

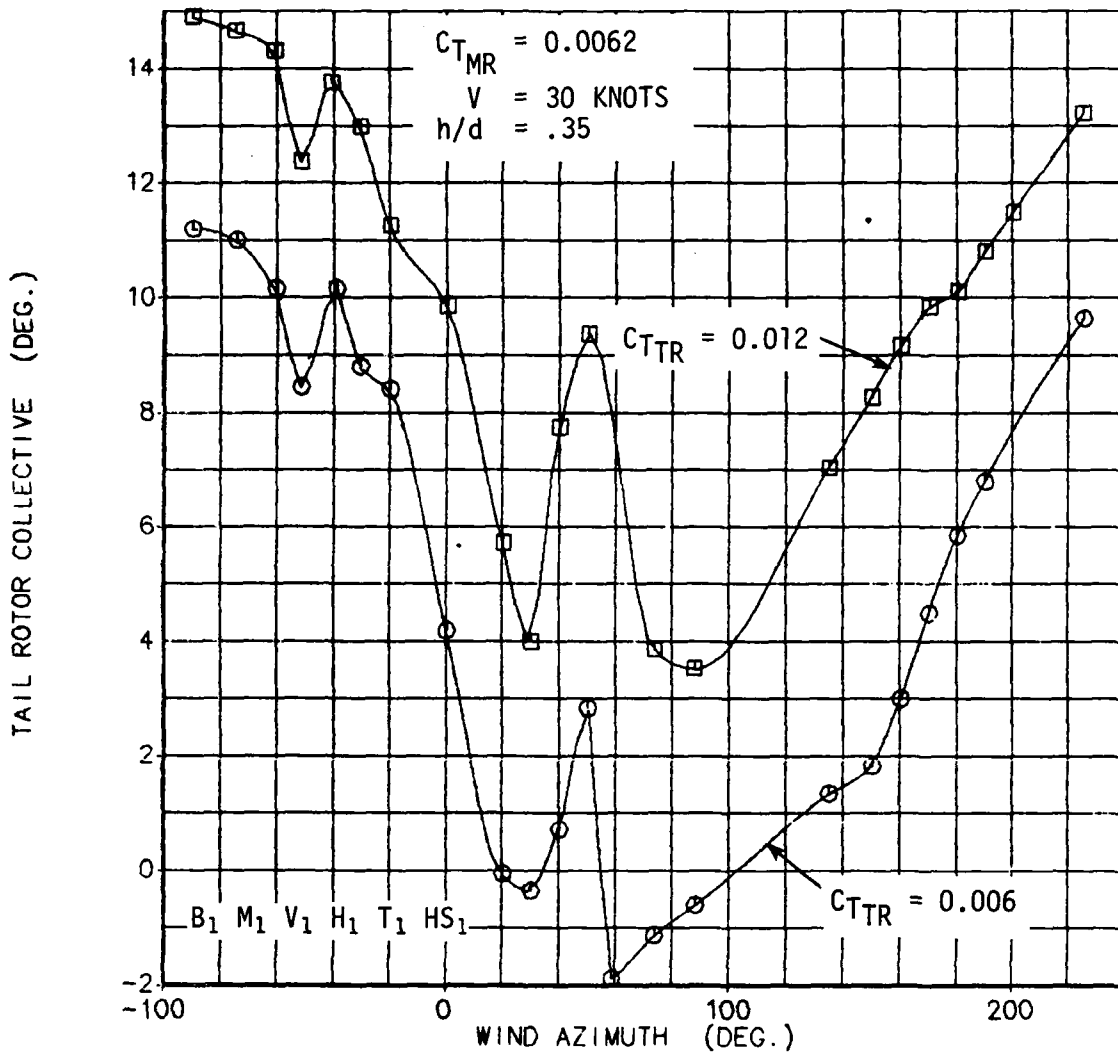


FIGURE 15. VARIATION OF TAIL ROTOR COLLECTIVE REQUIRED TO MAINTAIN THRUST AS A FUNCTION OF WIND AZIMUTH.

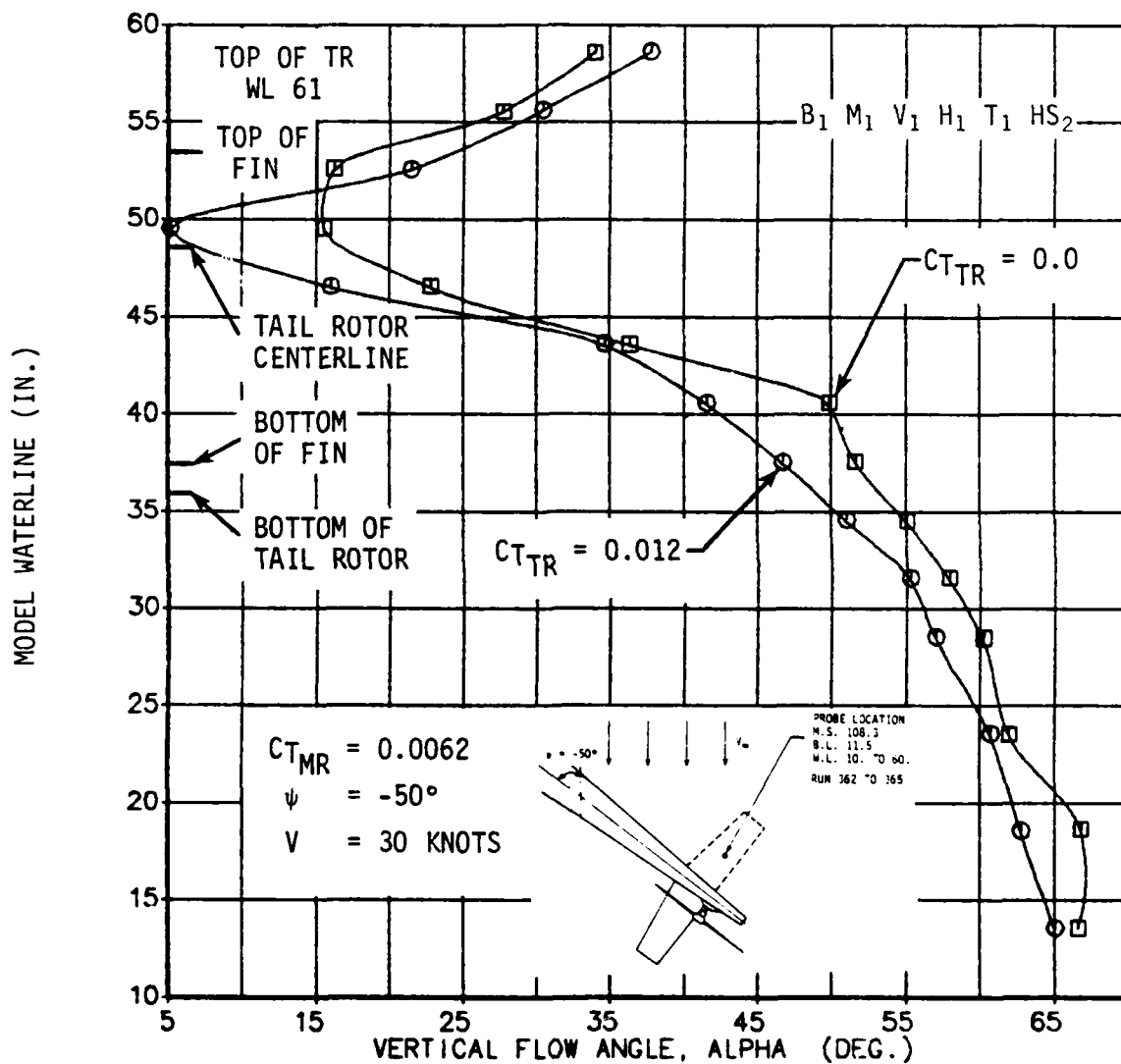


FIGURE 16. MAIN ROTOR WAKE NEAR THE EMPENNAGE IN YAWED FLIGHT - ALPHA COMPONENT.

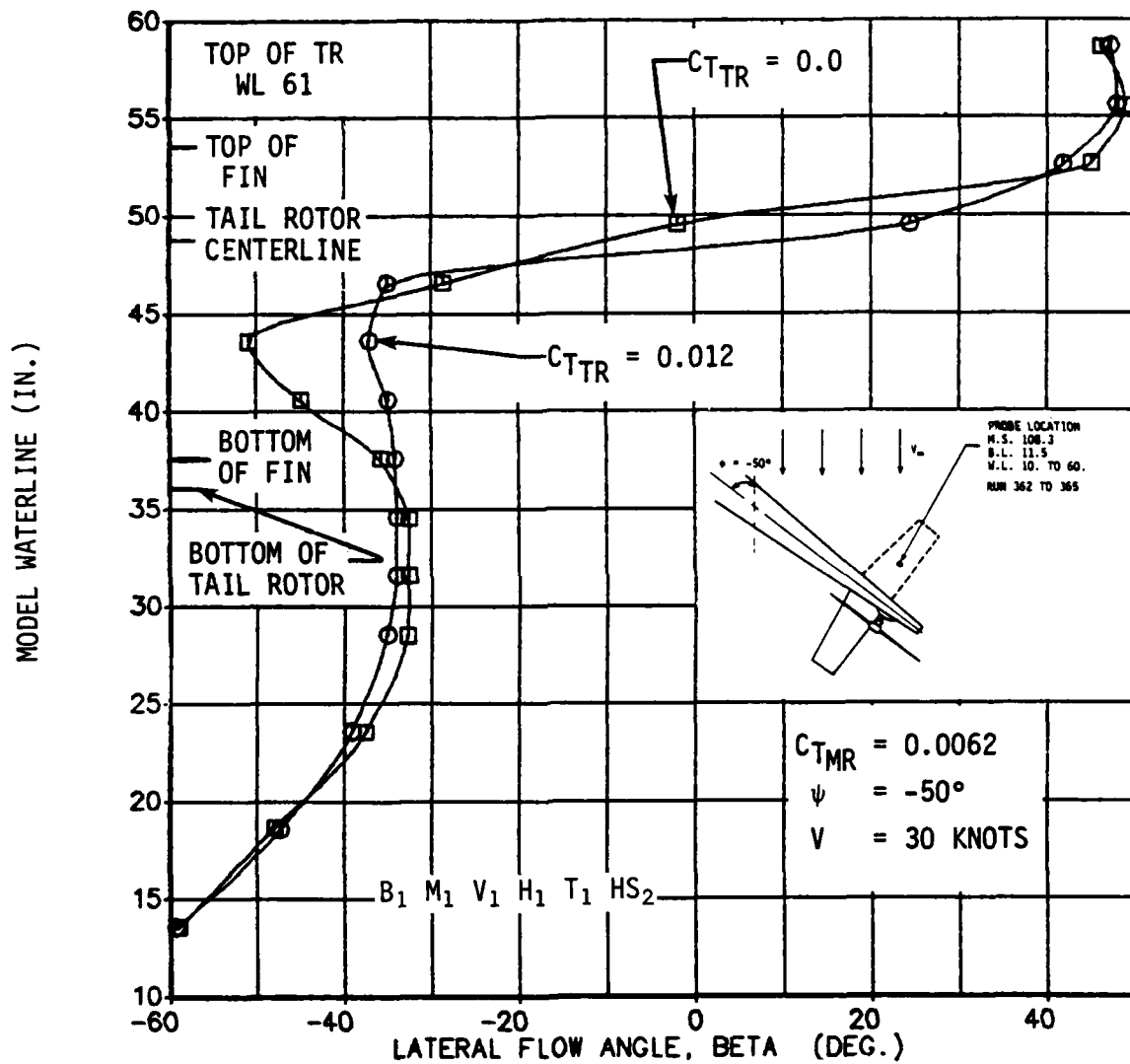


FIGURE 17. MAIN ROTOR WAKE NEAR THE EMPENNAGE IN YAWED FLIGHT - BETA COMPONENT.

The effects displayed in Figures 14 and 15 are due to the interaction of the main rotor wake with the tail rotor. Hot film data are presented in Figures 16 and 17 that indicate how dominant the main rotor wake can be. Figure 16 is a plot of the relative vertical flow angle measured near the empennage for a 30-knot wind from an azimuth $\psi = -50^\circ$. Figure 17 shows the corresponding lateral flow angles for this condition. The probe was aligned with the free stream, and a schematic of the exact probe location relative to the model is given in Figure 13a.

The hot film probe was swept vertically from a point very close to the ground almost up to the top of the tail rotor. The two curves show the resultant flow angles for both tail-rotor-on and tail-rotor-off conditions. The probe virtually passed through the center of the main rotor tip vortex at a model waterline of 50 inches. At this height the alpha component is at its minimum and the beta flow angle is crossing zero. The reversal in the sign of the lateral flow angle about waterline 50 is typical of vortex flow. The difference in the flow structure due to tail rotor loading is insignificant except at a height just below the centerline of the tail rotor. This insensitivity to tail rotor flow is an indication of the strength of the main rotor tip vortices, at least on the advancing side of the rotor.

Effects of Airspeed and Main Rotor Thrust

Airspeed and main rotor thrust are the two key elements that determine the wake skew angle. At very low advance ratios the main rotor downwash dominates and the wake is nearly vertical. For high advance ratios the rotor wake is blown aft and approaches that of a fixed-wing aircraft wake at very high speeds. In transition, however, the trade-off between forward speed and main rotor disk loading has a significant effect on placing the main rotor wake in the vicinity of the tail rotor. In ground effect, the position of the ground vortex is particularly sensitive to these parameters.

$\psi = -90^\circ$: The effects of varying airspeed and main rotor thrust on tail rotor power to thrust ratio and collective pitch are presented in Figures 18 and 19 respectively. The particular flight condition investigated was right sideward flight at a constant tail rotor loading of $C_{T_{TR}} = 0.012$.

For all three levels of main rotor thrust the collective pitch required for constant tail rotor thrust steadily increased over the speed range tested (see Figure 19). This is probably due to the increasing inflow to the tail rotor as the free stream velocity begins to build. Tail rotor power to thrust ratio increased with nondimensional airspeed

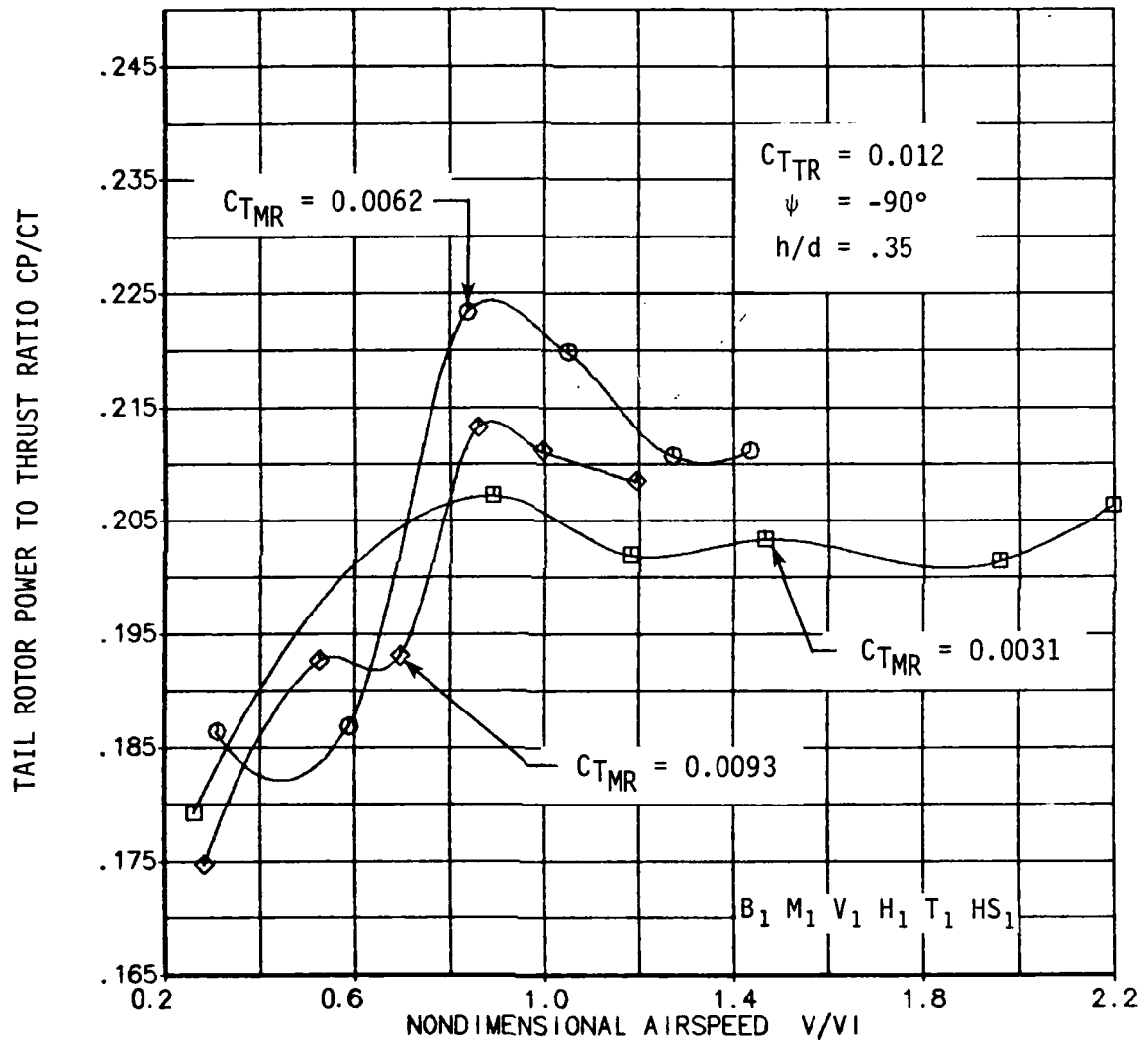


FIGURE 18. VARIATION OF TAIL ROTOR POWER TO THRUST RATIO AS A FUNCTION OF AIRSPEED AND MAIN ROTOR THRUST AT $\psi = -90^\circ$.

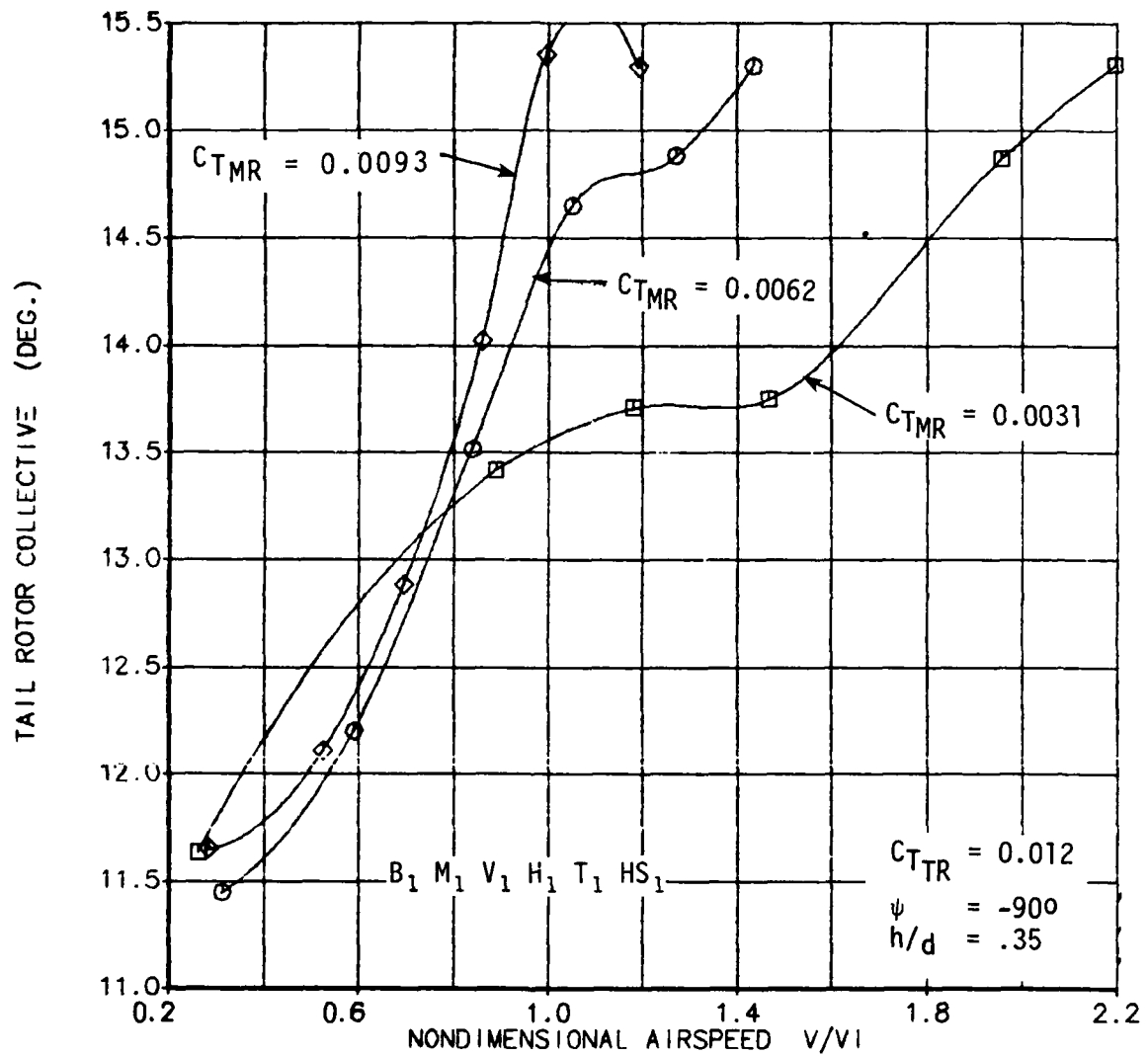


FIGURE 19. VARIATION IN TAIL ROTOR COLLECTIVE REQUIRED TO MAINTAIN CONSTANT THRUST AS A FUNCTION OF AIRSPEED AND MAIN ROTOR THRUST AT $\psi = -90^\circ$.

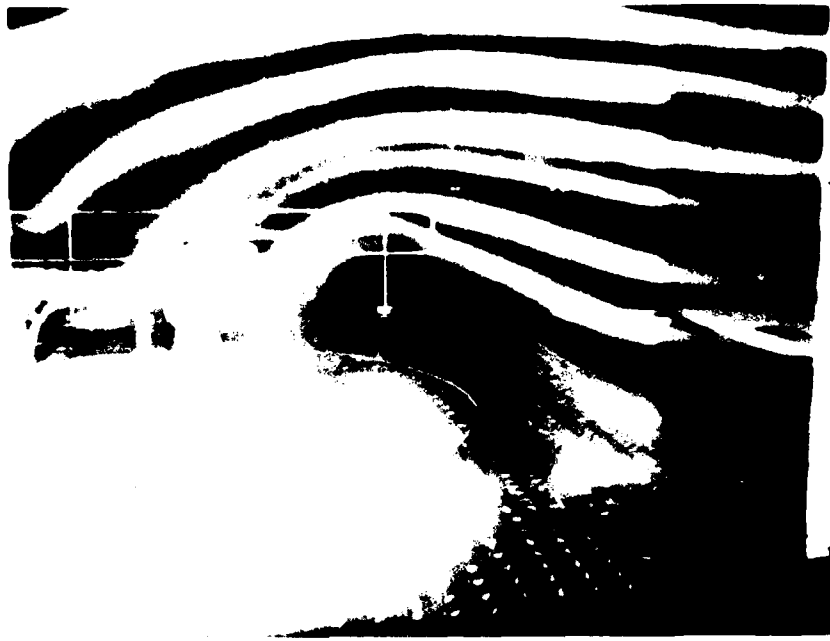
up to a value of approximately 0.9 where the ground vortex passes under the main rotor and moves away from the region of the tail rotor (Figure 18). For airspeeds greater than this the tail rotor power is approximately constant.

Correlation of flow visualization records and hot film data with the load data confirms that the ground vortex moves past the tail rotor at an airspeed of 25 knots for the nominal rotor thrust condition of $C_{TMR} = 0.0062$. Figure 20 is a series of photographs taken at 20, 25 and 30 knots for the -90° flight condition. The smoke used for flow visualization was introduced into the flow in the vertical plane aligned with the near side of the main rotor disk. The tuft patterns on the ground board and the smoke streamlines clearly mark the formation of the ground vortex in Figures 20a and 20b. For the 30-knot condition the ground vortex is apparently gone, since the tufts on the ground board are all aligned with the flow.

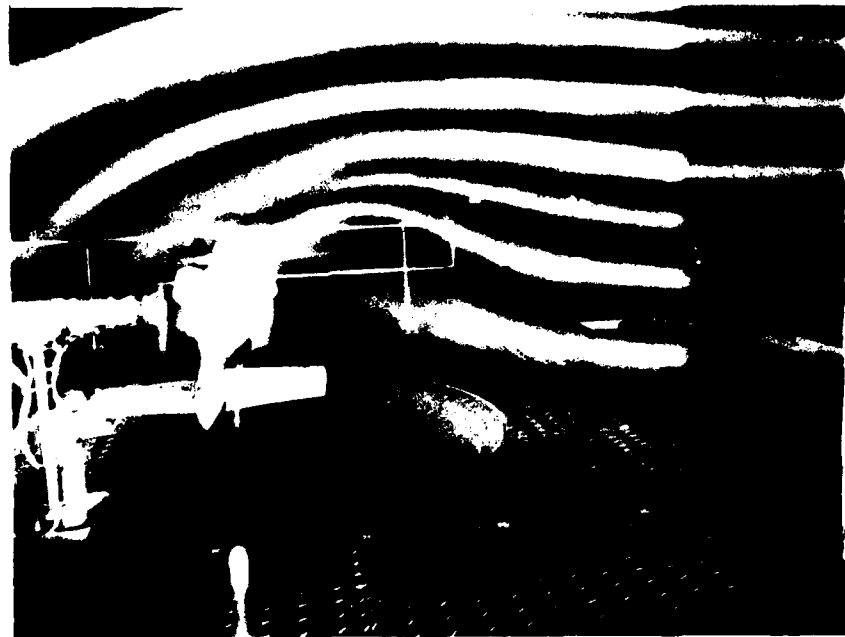
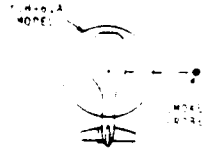
Further evidence of the passage of the ground vortex is given in Figures 21 and 22. Vertical hot film sweeps were again conducted near the empennage in this sideward flight condition. The exact probe position relative to the model is specified in Figure 13d. The vertical and lateral flow angles measured by the hot film probe are presented in Figures 21 and 22 respectively. The data in these figures corresponds exactly with the conditions shown in Figure 20b and 20c.

For the 25-knot case the plot of vertical flow angle, Figure 21, indicates that the probe passed directly through the ground vortex. At a probe height, measured in terms of model waterline, of 18 inches the probe senses a maximum downward flow. This is probably the edge of the ground vortex that is closest to the model. Figure 22 shows a strong lateral flow component at this probe height which is characteristic of the flow in the bow wave formation of the ground vortex.

As the probe height increases, the vertical flow angle becomes less and less negative and crosses zero at a model waterline of 35 inches. This is approximately the upper boundary of the ground vortex. Above this height the vertical flow angle is positive due to the flow that is passing up and over the ground vortex. The lateral flow angle between model waterlines 27 and 47 is approximately constant at a value of -20 degrees. This is probably due to the flow passing around the trailing edge of the vertical fin. At the 47-inch waterline the lateral flow angle breaks in a positive sense and crosses zero at model waterline 52. The top of the fin is located at waterline 55, which implies that the change of sign in lateral flow component is due to the

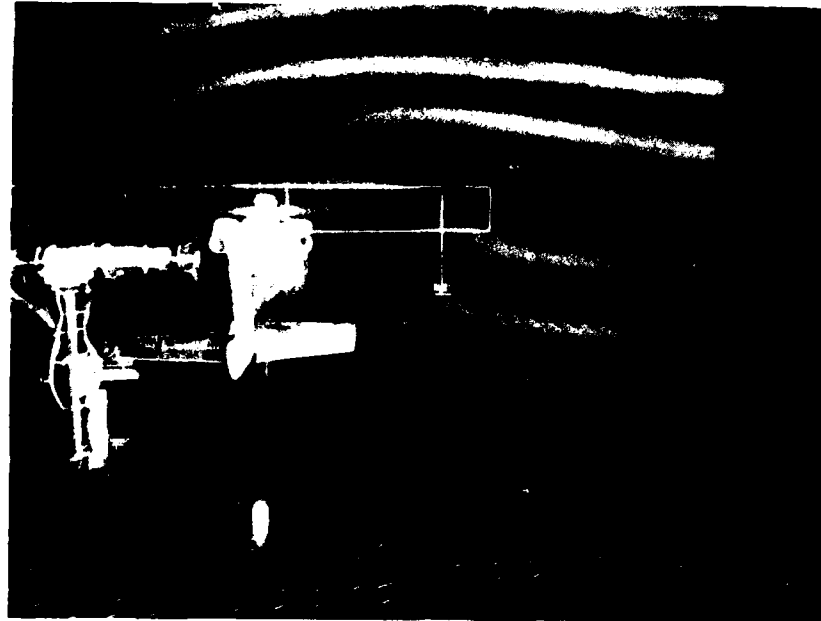


a. FLOW VISUALIZATION AT $V = 20$ KNOTS



b. FLOW VISUALIZATION AT $V = 25$ KNOTS

FIGURE 20. FLOW VISUALIZATION NEAR THE EMPENNAGE IN RIGHT SIDEWARD FLIGHT.



c. FLOW VISUALIZATION AT $V = 30$ KNOTS

$$C_{TMR} = 0.0062$$

$$C_{TR} = 0.012$$

$$\psi = -90^\circ$$

$$h/d = .35$$

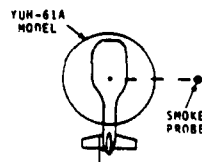


FIGURE 20. (CONTINUED).

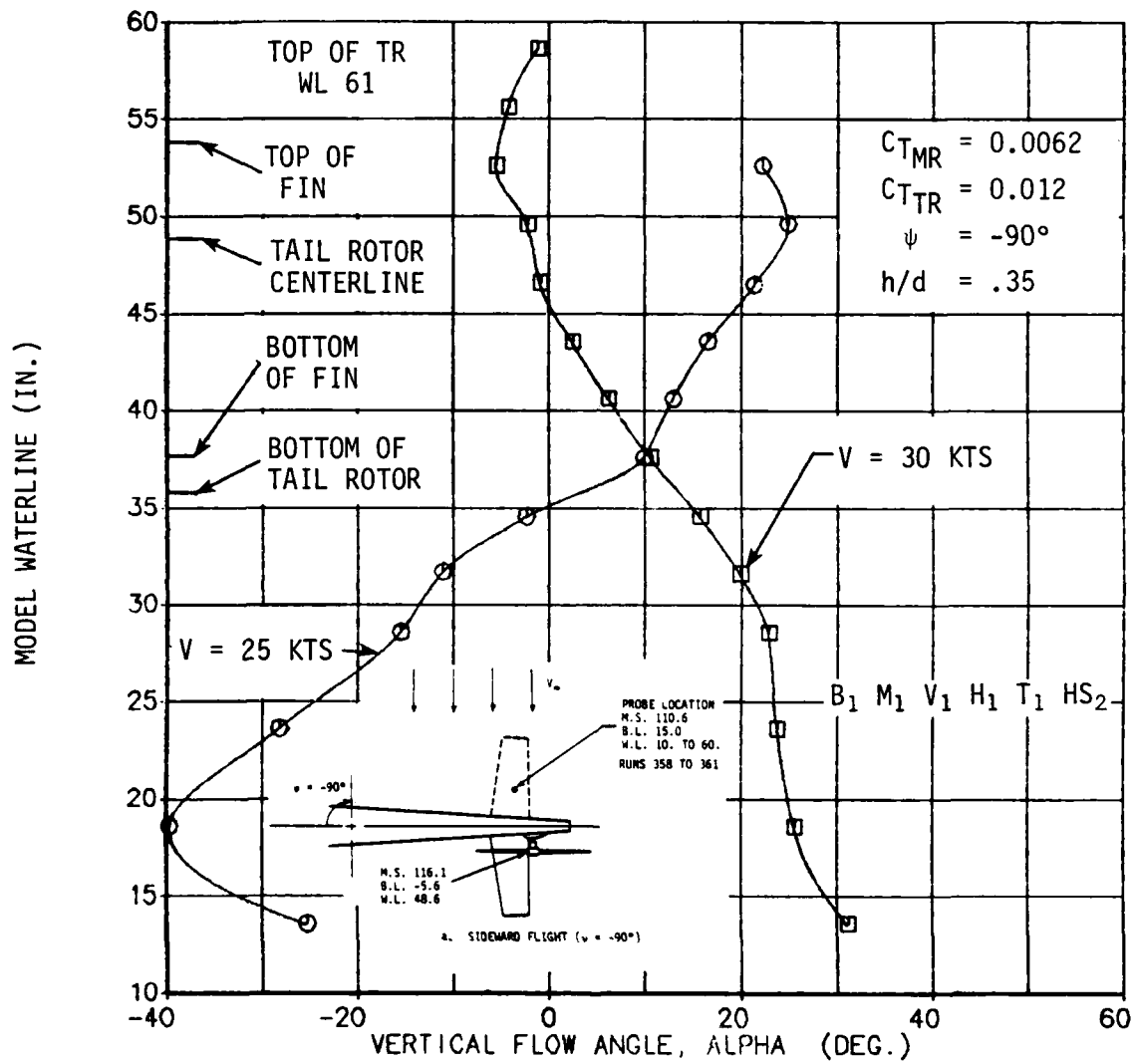


FIGURE 21. VARIATION OF MAIN ROTOR WAKE NEAR THE EMPENNAGE AS A FUNCTION OF AIRSPEED IN RIGHT SIDWARD FLIGHT - ALPHA COMPONENT.

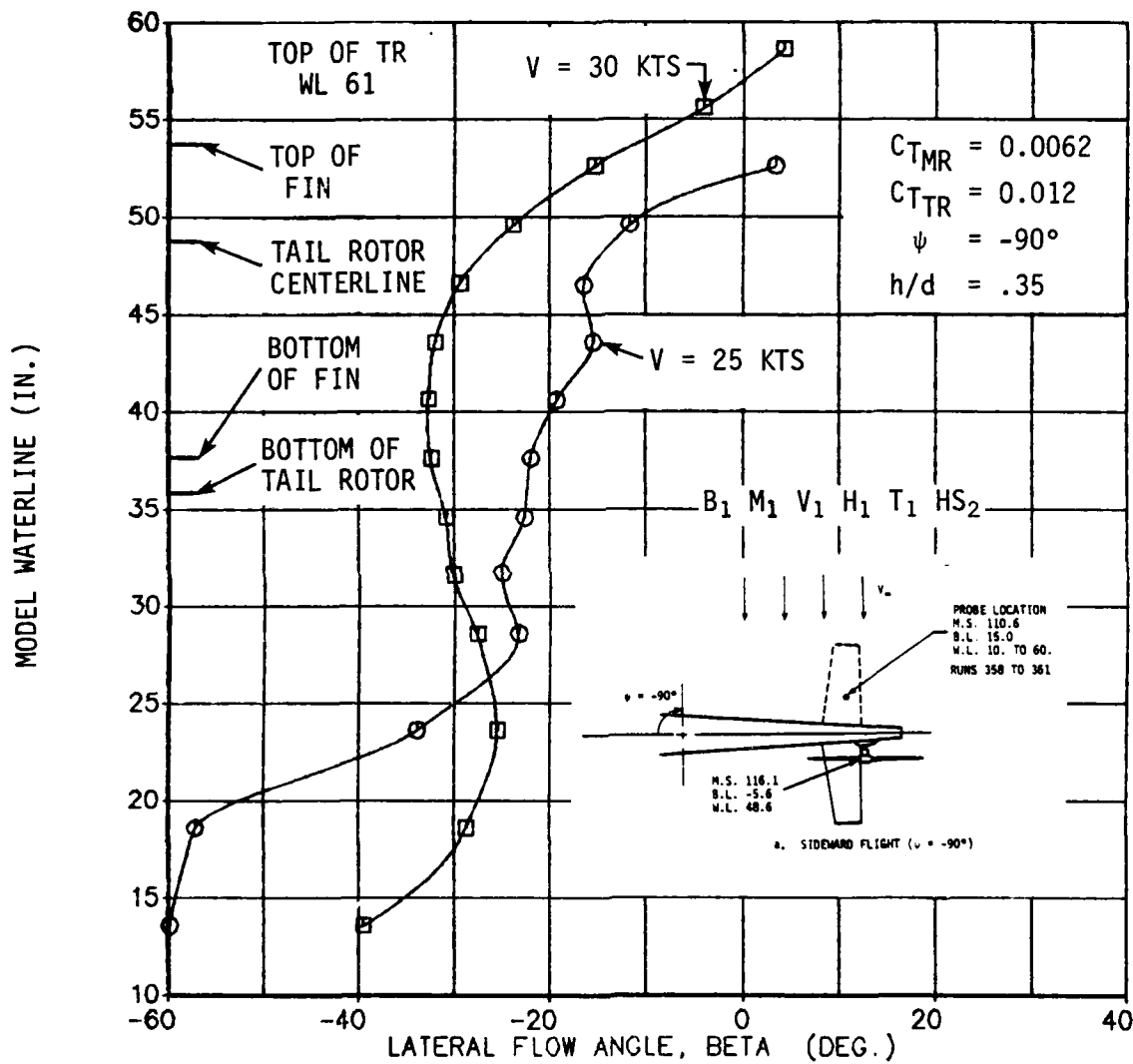


FIGURE 22. VARIATION OF MAIN ROTOR WAKE NEAR THE EMPENNAGE AS A FUNCTION OF AIRSPEED IN RIGHT SIDEMARD FLIGHT - BETA COMPONENT.

flow around the leading edge of the fin and through the tail rotor.

The effects of the ground vortex are completely gone, however, for the 30-knot case. The vertical flow angle shows no variations near the ground like those seen for the 20- and 25-knot cases. In addition, both flow components approach a value of zero at the 55-inch waterline, indicating that the hot film probe is immersed in free stream flow and aligned with the tunnel.

$\psi = 180^\circ$: The effects of the ground vortex on tail rotor performance in rearward flight are shown in Figures 23 and 24. Again the tail rotor power to thrust ratio and collective pitch are plotted against airspeed for three levels of main rotor thrust. The presence of the ground vortex is manifested in nonlinear variations in tail rotor power and collective pitch centered at a nondimensional airspeed of 0.9. The ground vortex rotational sense effectively increases the tail rotor RPM. The relative magnitude of the variations in tail rotor parameters indicates the relative strength of the ground vortex for the different main rotor thrusts.

Correlation of flow visualization records (see Figure 25) with the data presented in Figures 23 and 24 verifies that the ground vortex passes under the main rotor and away from the tail rotor at a nondimensional airspeed of approximately 1.0 for all three thrust levels. Intuitively, it makes sense that the ground vortex should pass under the rotor at the same value of nondimensional airspeed for the three main rotor thrust conditions. The quantity $u/CT/2$ is simply the ratio of forward speed to the average induced velocity through the rotor. For the same ratio of these two quantities, the wake angle should be approximately the same; therefore, the formation of the ground vortex will be approximately the same. This says nothing of the relative strength of the ground vortex for the various rotor loadings. For nondimensional airspeeds greater than 1.1 a general decrease in tail rotor power and collective pitch required results from the change in inflow due to the increase in airspeed.

Figures 26 and 27 present the tail rotor power to thrust ratio and the tail rotor collective as a function of airspeed for the four principal wind azimuth conditions. For the forward flight and left sideward flight conditions the effects of varying main rotor thrust were not investigated; however, data was obtained for the nominal main rotor thrust condition ($C_{TMR} = 0.0062$). For all four wind azimuth conditions the tail rotor thrust was fixed at a value of $C_{TTR} = 0.012$. The right sideward flight condition exhibited the

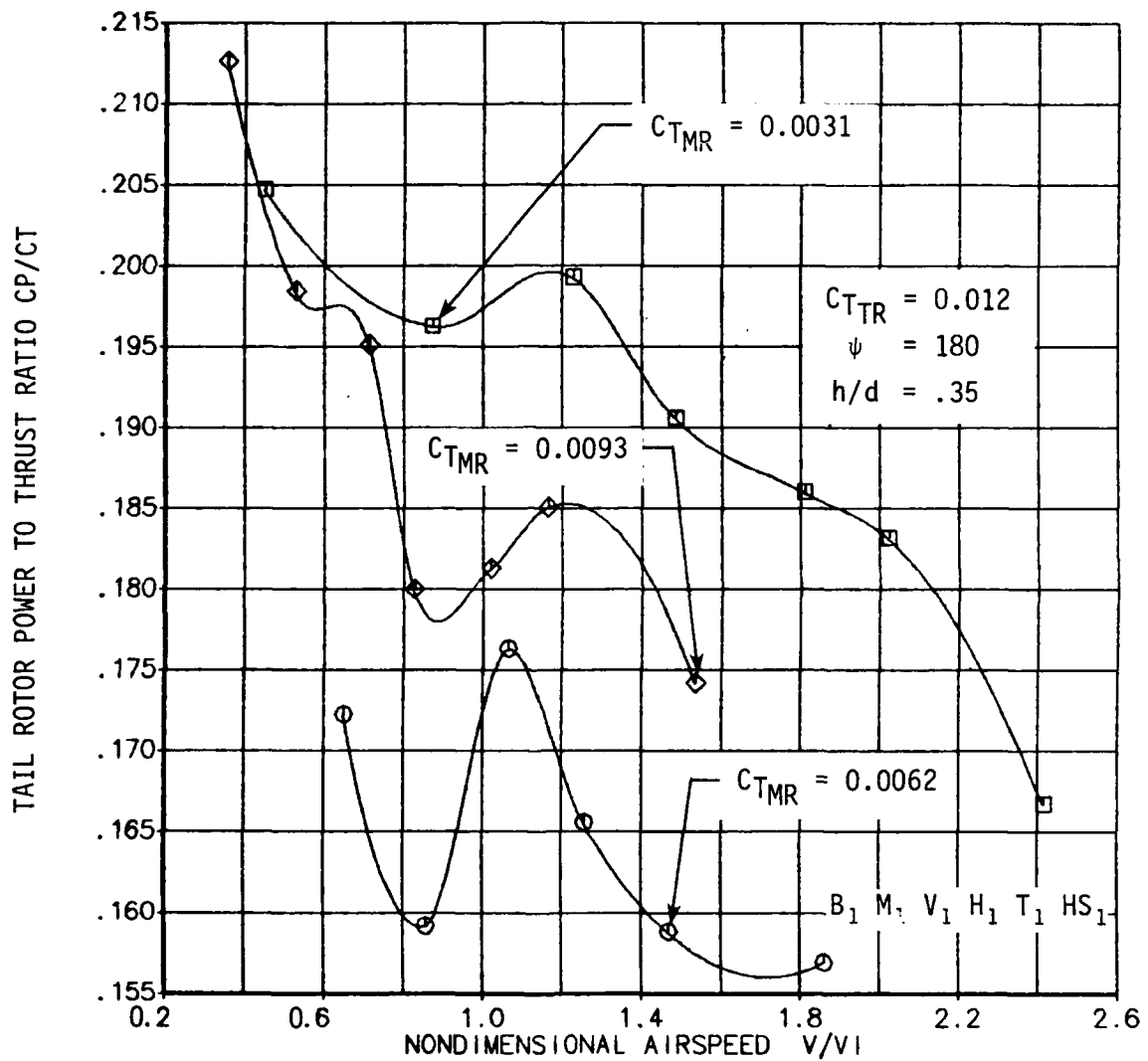


FIGURE 23. VARIATION OF TAIL ROTOR POWER TO THRUST RATIO AS A FUNCTION OF AIRSPEED AND MAIN ROTOR THRUST IN REARWARD FLIGHT.

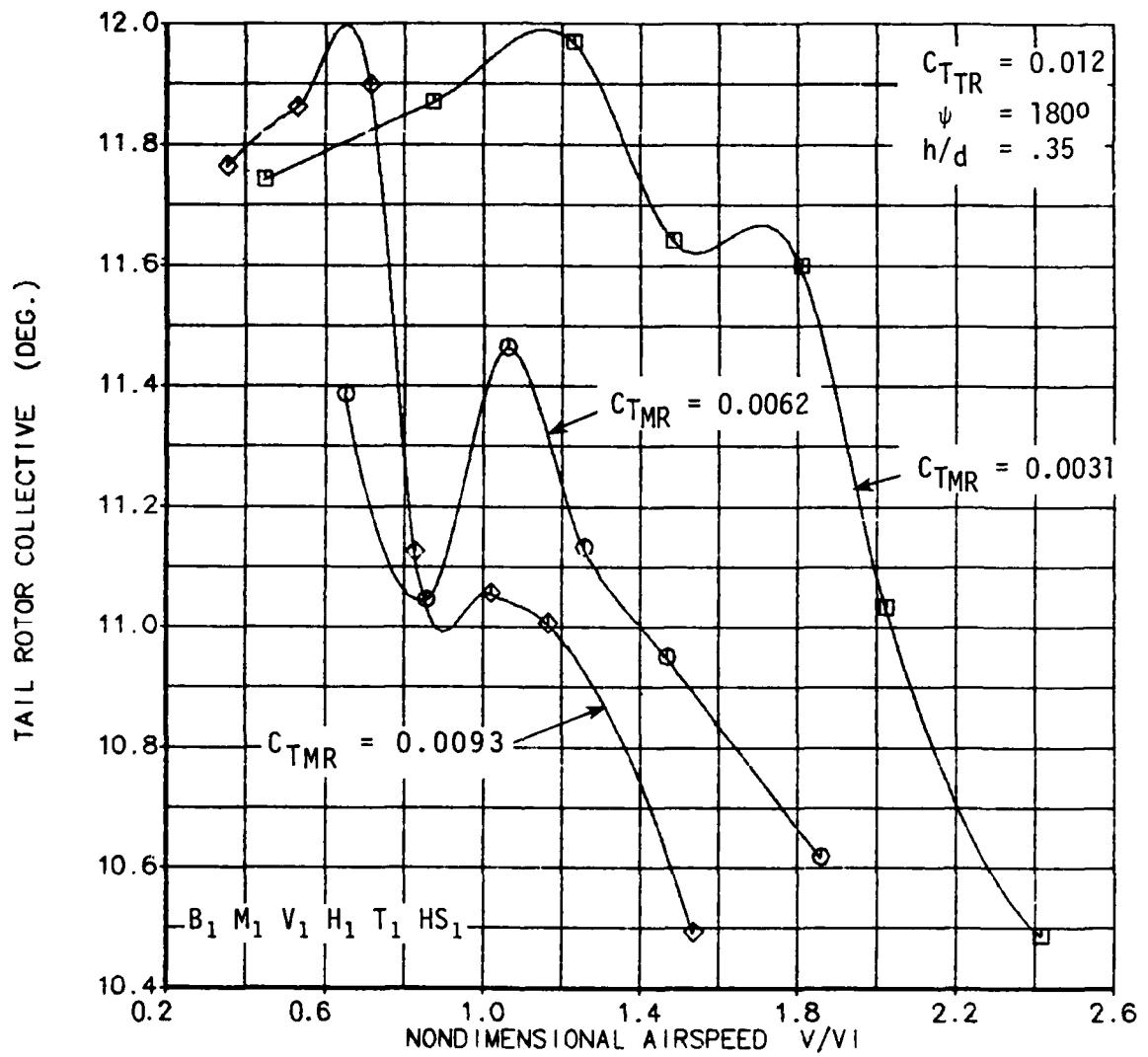
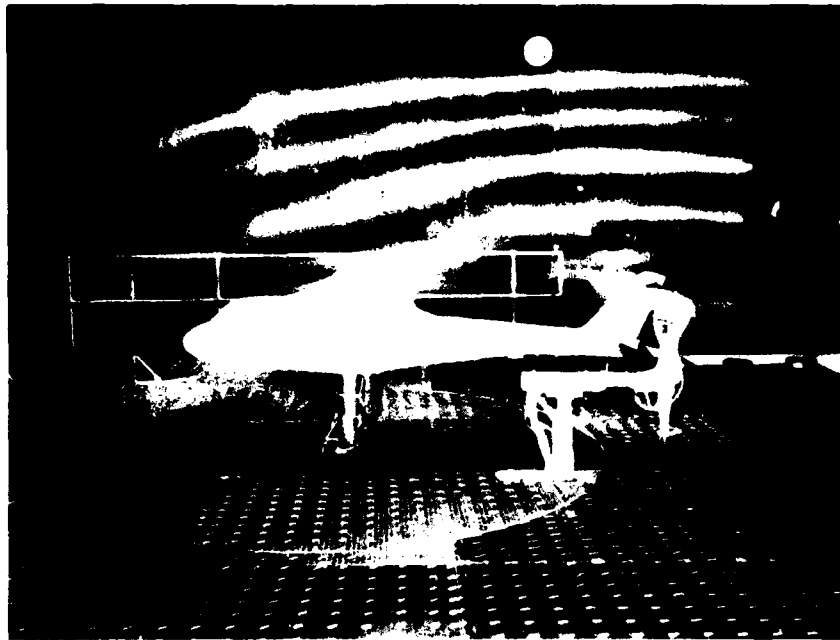
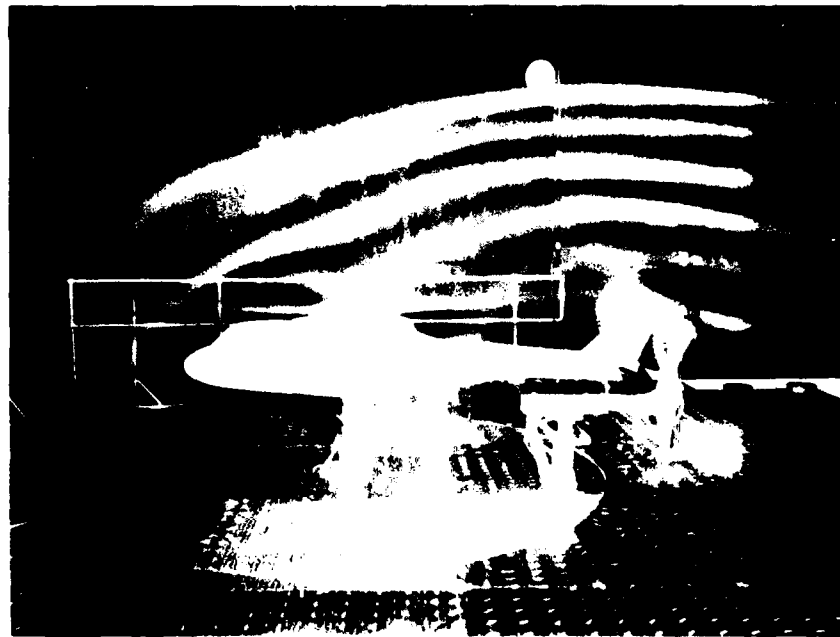
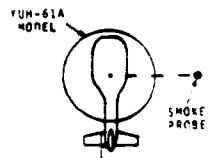


FIGURE 24. VARIATION OF TAIL ROTOR COLLECTIVE REQUIRED TO MAINTAIN CONSTANT THRUST AS A FUNCTION OF AIRSPEED AND MAIN ROTOR THRUST IN REARWARD FLIGHT.



$C_{TMR} = 0.0031$
 $V = 30 \text{ KNOTS}$
 $C_{TTR} = 0.012$



$C_{TMR} = 0.0093$
 $V = 30 \text{ KNOTS}$
 $C_{TTR} = 0.012$

FIGURE 25. VARIATION IN MAIN ROTOR WAKE IN GROUND EFFECT AS A FUNCTION OF MAIN ROTOR THRUST AT $\psi = 180^\circ$.

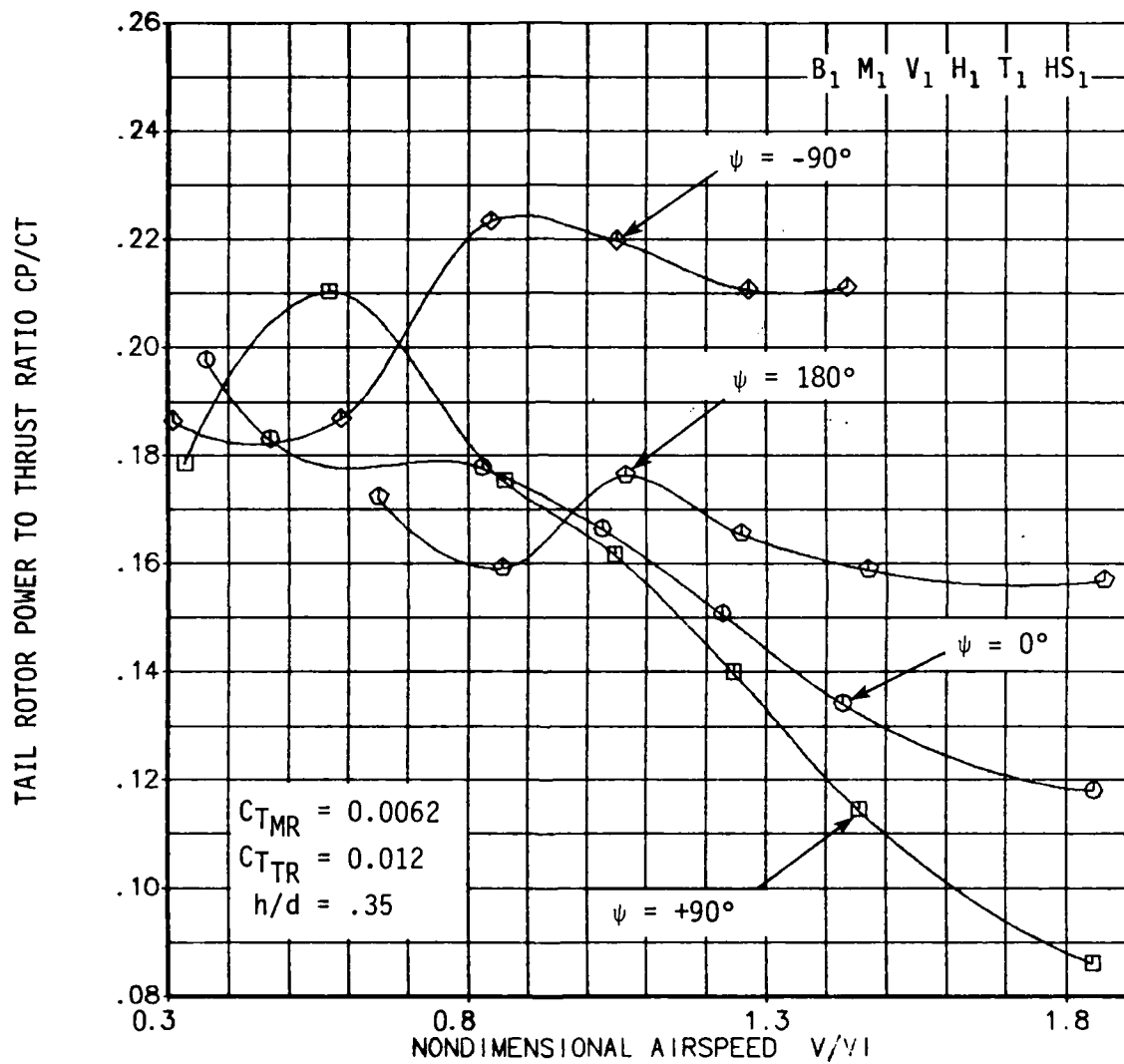


FIGURE 26. VARIATION OF TAIL ROTOR POWER TO THRUST RATIO AS A FUNCTION OF AIRSPEED AND WIND AZIMUTH.

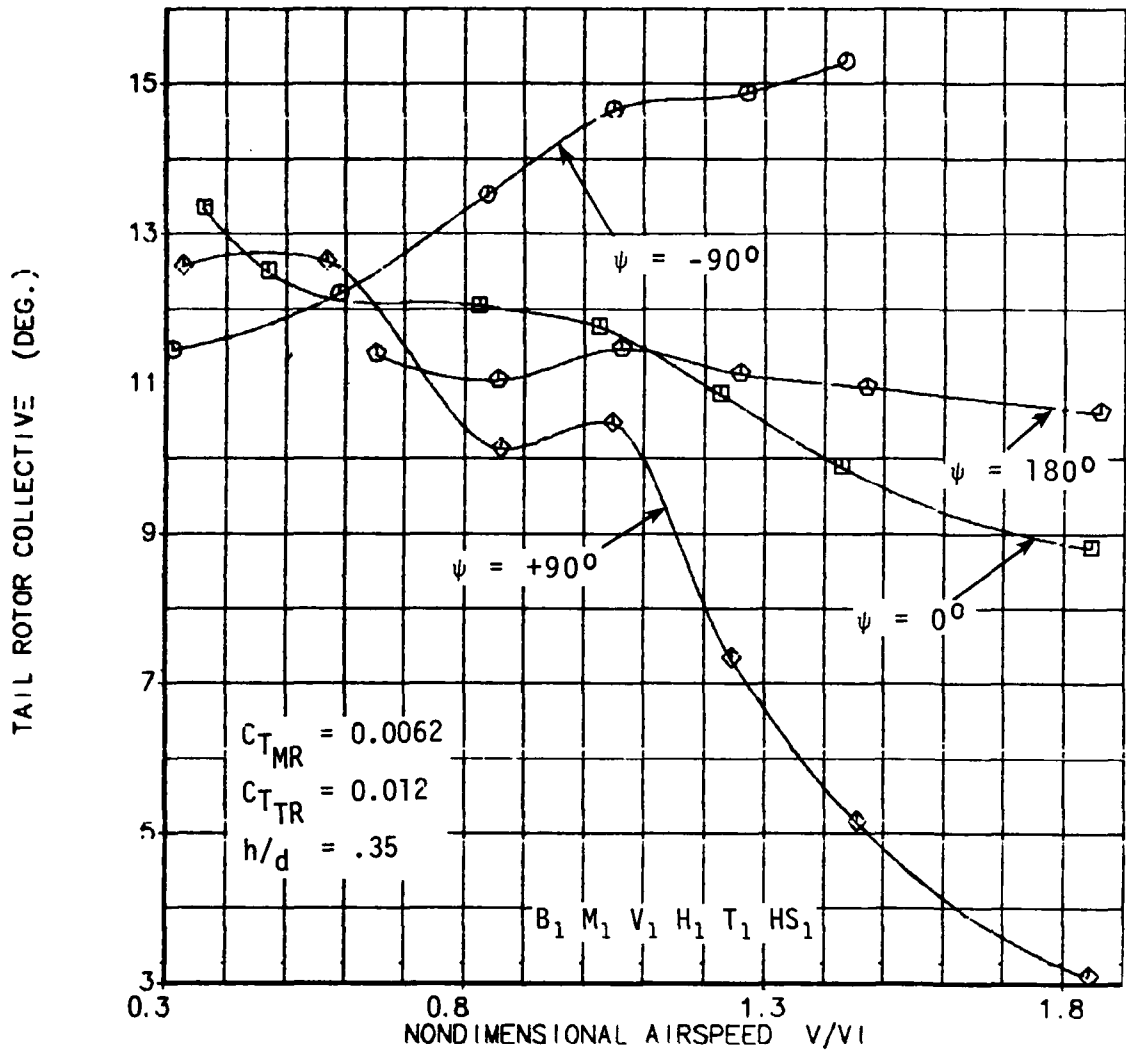


FIGURE 27. VARIATION OF TAIL ROTOR COLLECTIVE REQUIRED TO MAINTAIN CONSTANT THRUST AS A FUNCTION OF AIRSPEED AND WIND AZIMUTH.

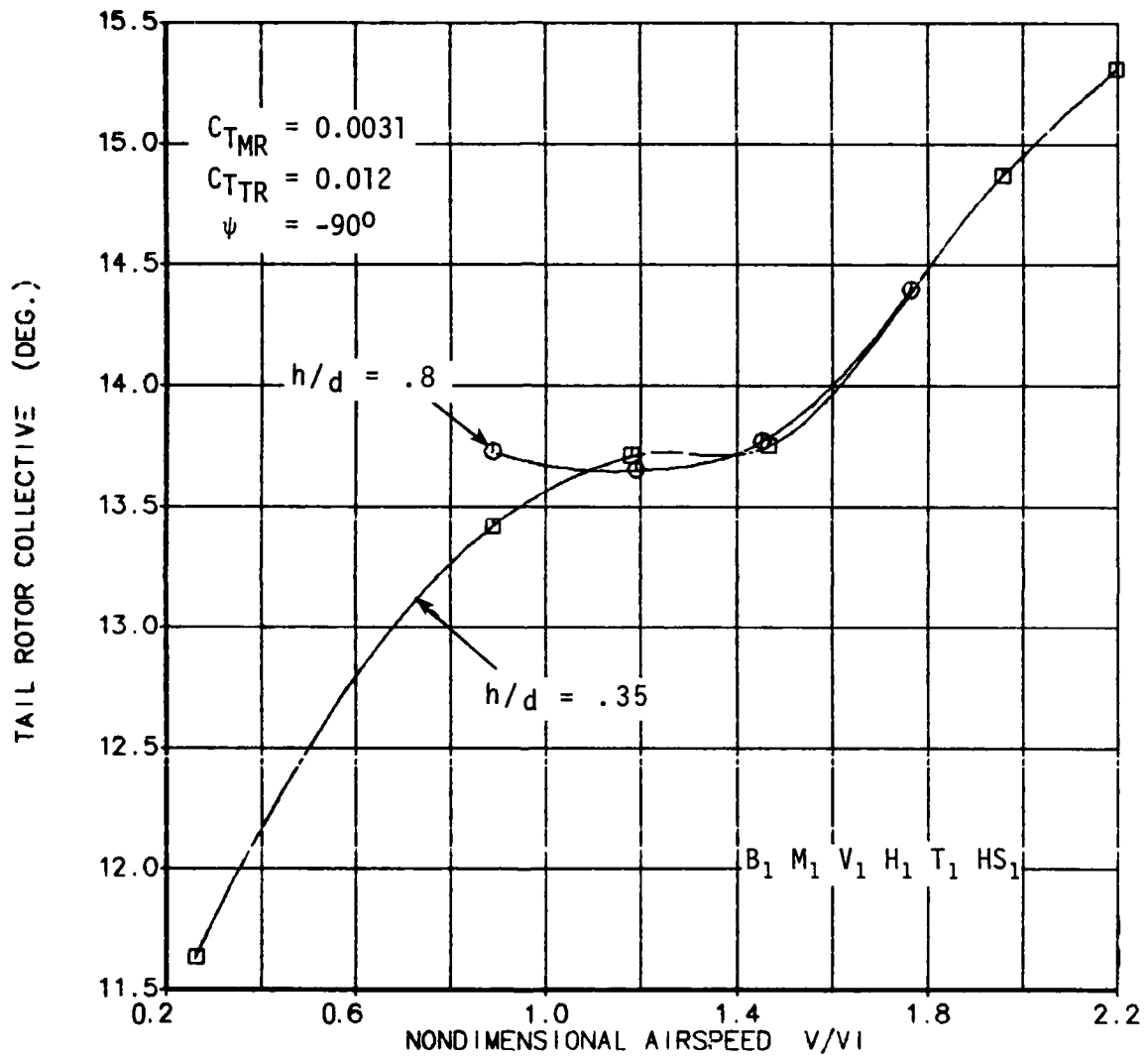


FIGURE 28. VARIATION OF TAIL ROTOR COLLECTIVE REQUIRED TO MAINTAIN CONSTANT THRUST AS A FUNCTION OF AIRSPEED AND HEIGHT ABOVE GROUND (LOW MAIN ROTOR THRUST).

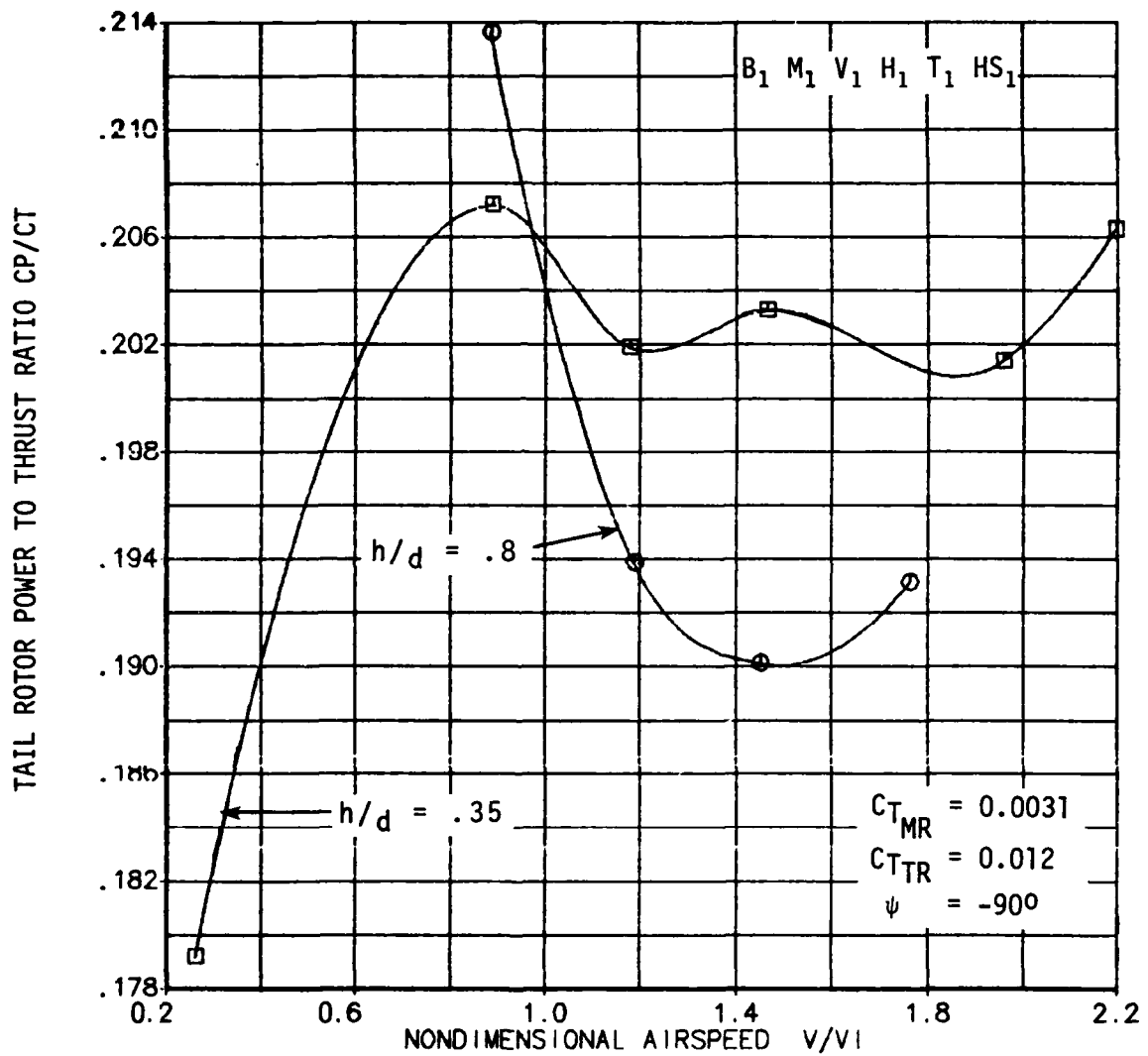


FIGURE 29. VARIATION OF TAIL ROTOR POWER TO THRUST RATIO AS A FUNCTION OF AIRSPEED AND HEIGHT ABOVE GROUND (LOW MAIN ROTOR THRUST).

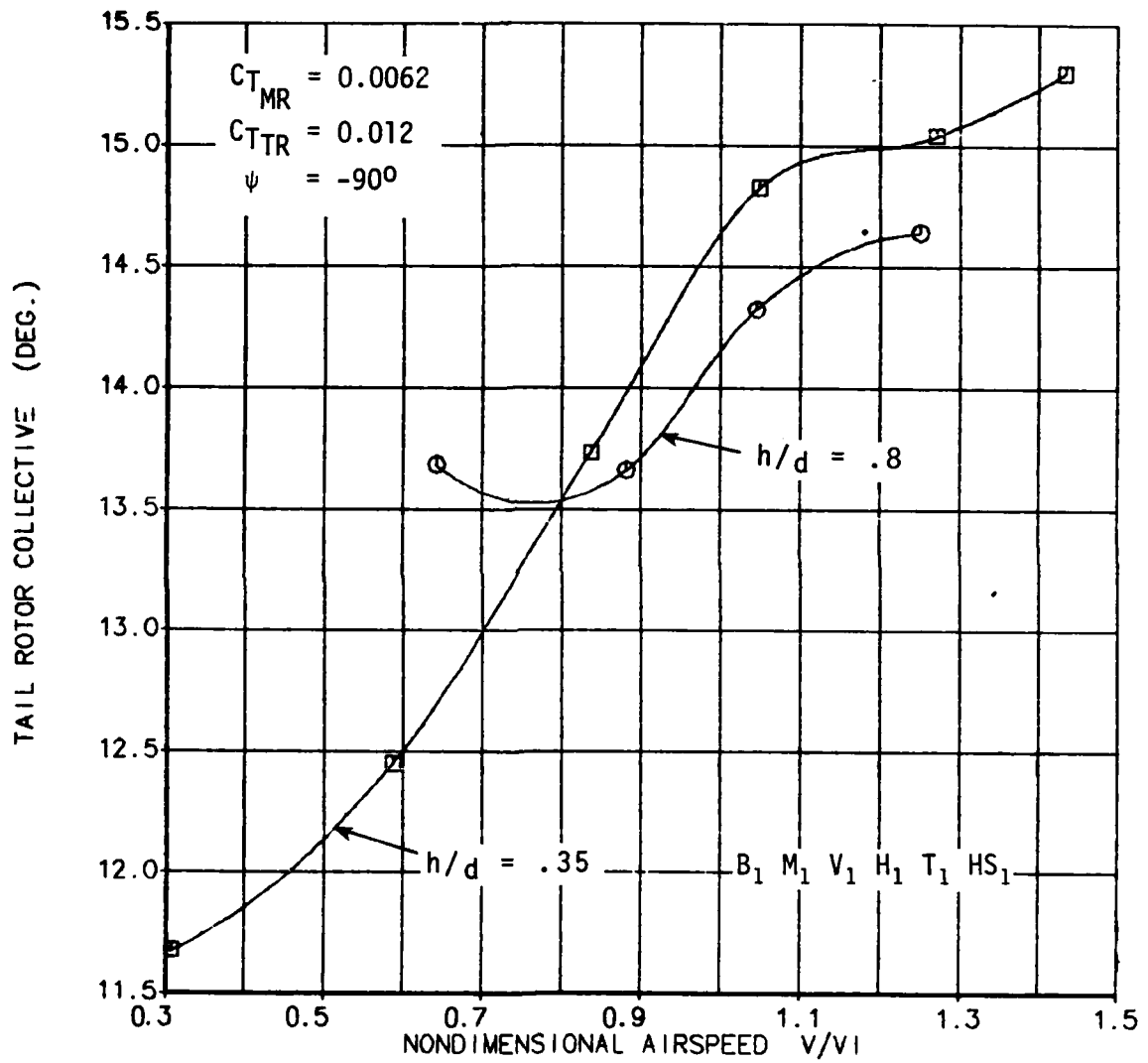


FIGURE 30. VARIATION OF TAIL ROTOR COLLECTIVE REQUIRED TO MAINTAIN CONSTANT THRUST AS A FUNCTION OF AIRSPEED AND HEIGHT ABOVE GROUND (NOMINAL MAIN ROTOR THRUST).

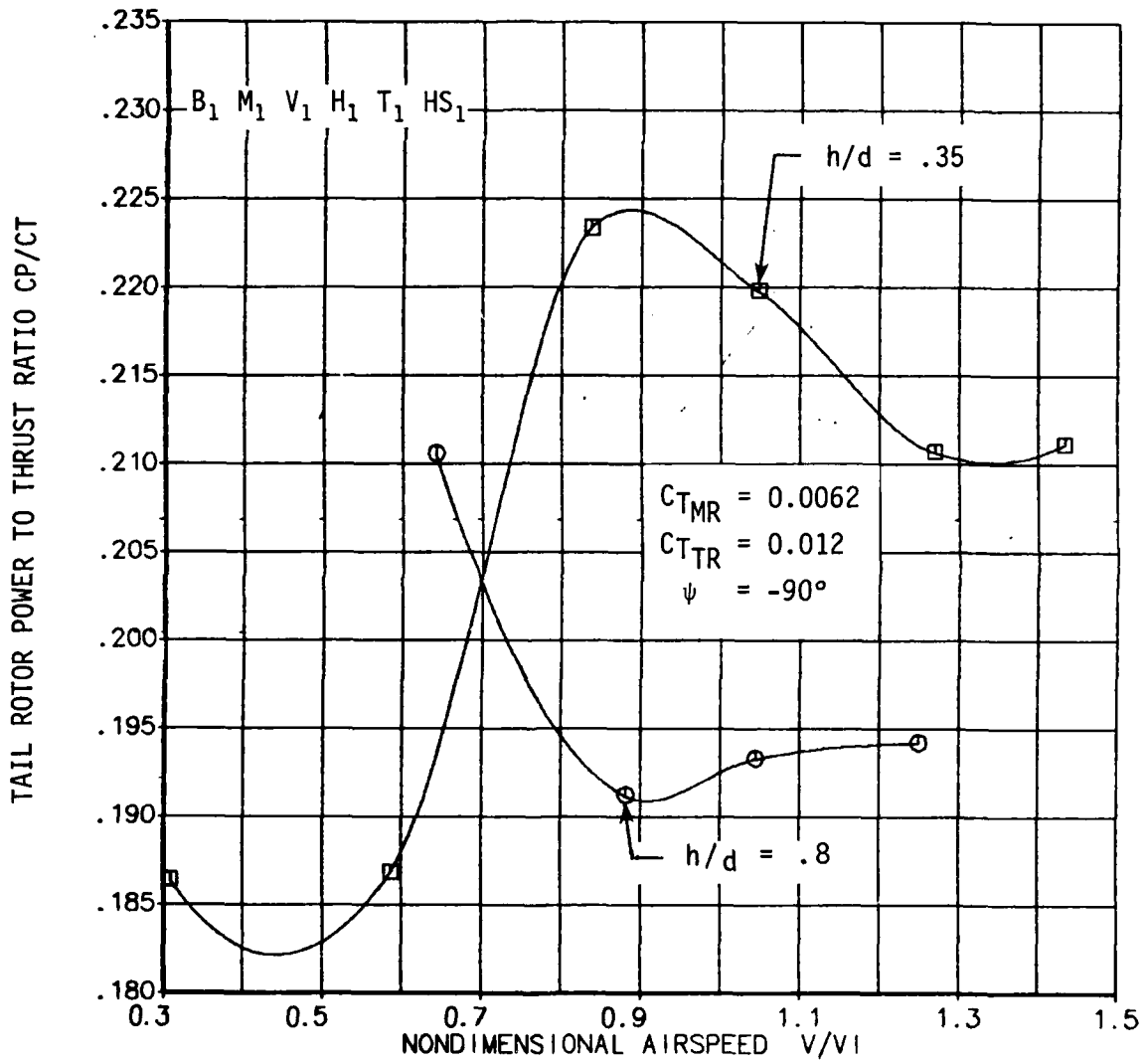


FIGURE 31. VARIATION OF TAIL ROTOR POWER TO THRUST RATIO AS A FUNCTION OF AIRSPEED AND HEIGHT ABOVE GROUND (NOMINAL MAIN ROTOR THRUST).

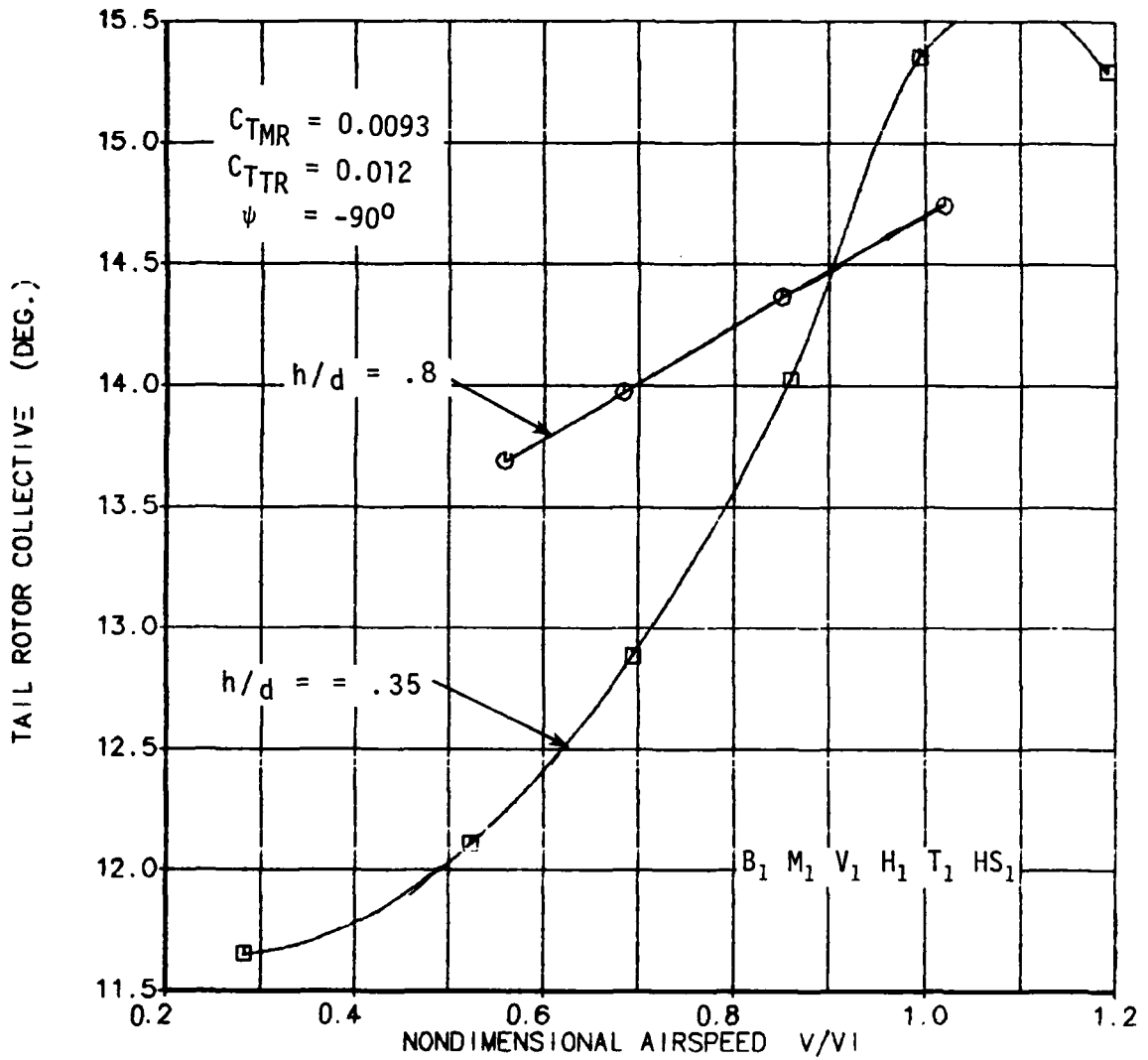


FIGURE 32. VARIATION OF TAIL ROTOR COLLECTIVE REQUIRED TO MAINTAIN CONSTANT THRUST AS A FUNCTION OF AIRSPEED AND HEIGHT ABOVE GROUND (HIGH MAIN ROTOR THRUST).

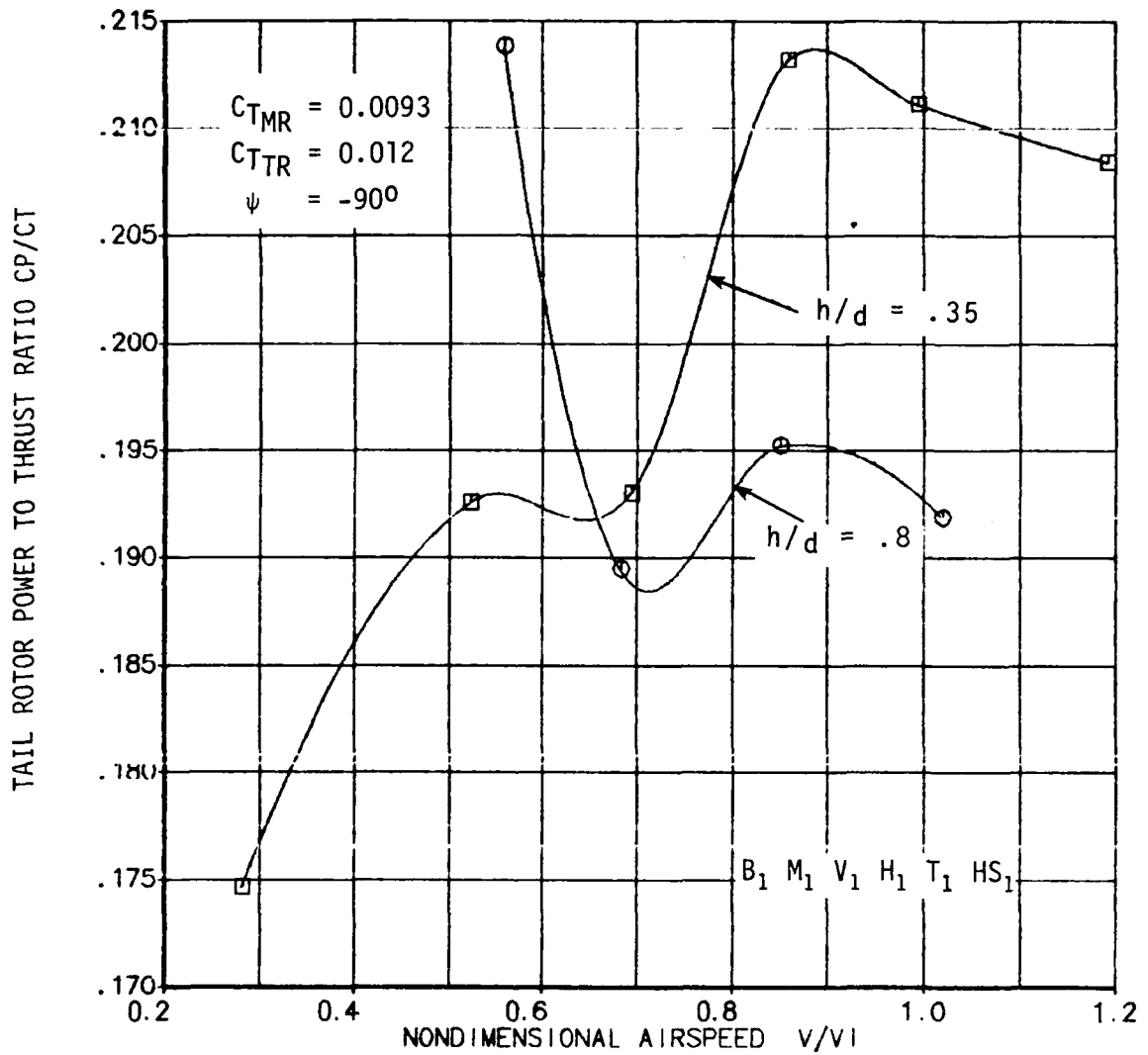


FIGURE 33. VARIATION OF TAIL ROTOR POWER TO THRUST RATIO AS A FUNCTION OF AIRSPEED AND HEIGHT ABOVE GROUND (HIGH MAIN ROTOR THRUST).

highest power required at a constant tail rotor thrust over most of the speed range from 10 to 45 knots. The left sideward flight condition ($\psi = +90^\circ$), except for the point at a nondimensional airspeed of 0.6, showed the lowest power required over most of the speed range. The forward and rearward flight conditions experienced intermediate levels of tail rotor power required for the speeds tested. The corresponding plot of tail rotor collective required to maintain the constant tail rotor thrust is given in Figure 27. The tail rotor collective pitch settings follow trends similar to the tail rotor power to thrust ratio shown in Figure 26.

Effects of Height Above the Ground

Another parameter that has a fundamental influence on the main rotor wake angle is the height of the rotor above the ground. Obviously, the ground vortex phenomenon can occur only in the proximity to the ground plane. Similarly, proximity to the ground tends to raise the rotor wake up, thus moving it closer to the tail rotor/empennage system. A limited amount of data was obtained at a height-to-diameter ratio (h/d) of 0.8 for the right sideward flight condition. Comparisons of tail rotor power required and collective pitch settings for the two rotor heights are presented in Figures 28 through 33. In general, for a nondimensional airspeed greater than 0.8 the tail rotor power and collective pitch settings were lower for the higher altitude condition. Unfortunately, an insufficient number of data points were obtained in the regime where the effects of the ground vortex would be greatest to determine the effects of varying rotor height in any detail. This study will be left for some future test when more data may be obtained.

TAIL ROTOR ON MAIN ROTOR INTERACTIONS

The effects of tail rotor flow on main rotor trim conditions are presented in this section. The variations in main rotor power coefficient, as well as lateral and longitudinal cyclic pitch angles, are presented for various wind azimuth and airspeed conditions. The sensitivity of the main rotor parameters to tail rotor thrust is also investigated. Finally, a brief look at the influence of height-to-diameter ratio on tail rotor/main rotor interactions is reported.

Effects of Wind Azimuth

The effects of tail rotor flow on main rotor power over a wide range of wind azimuths are shown in Figure 34. The wind velocity was held fixed at 30 knots for the two levels of tail rotor thrust shown in the figure. The variations in power reflect the changes needed to maintain a constant main

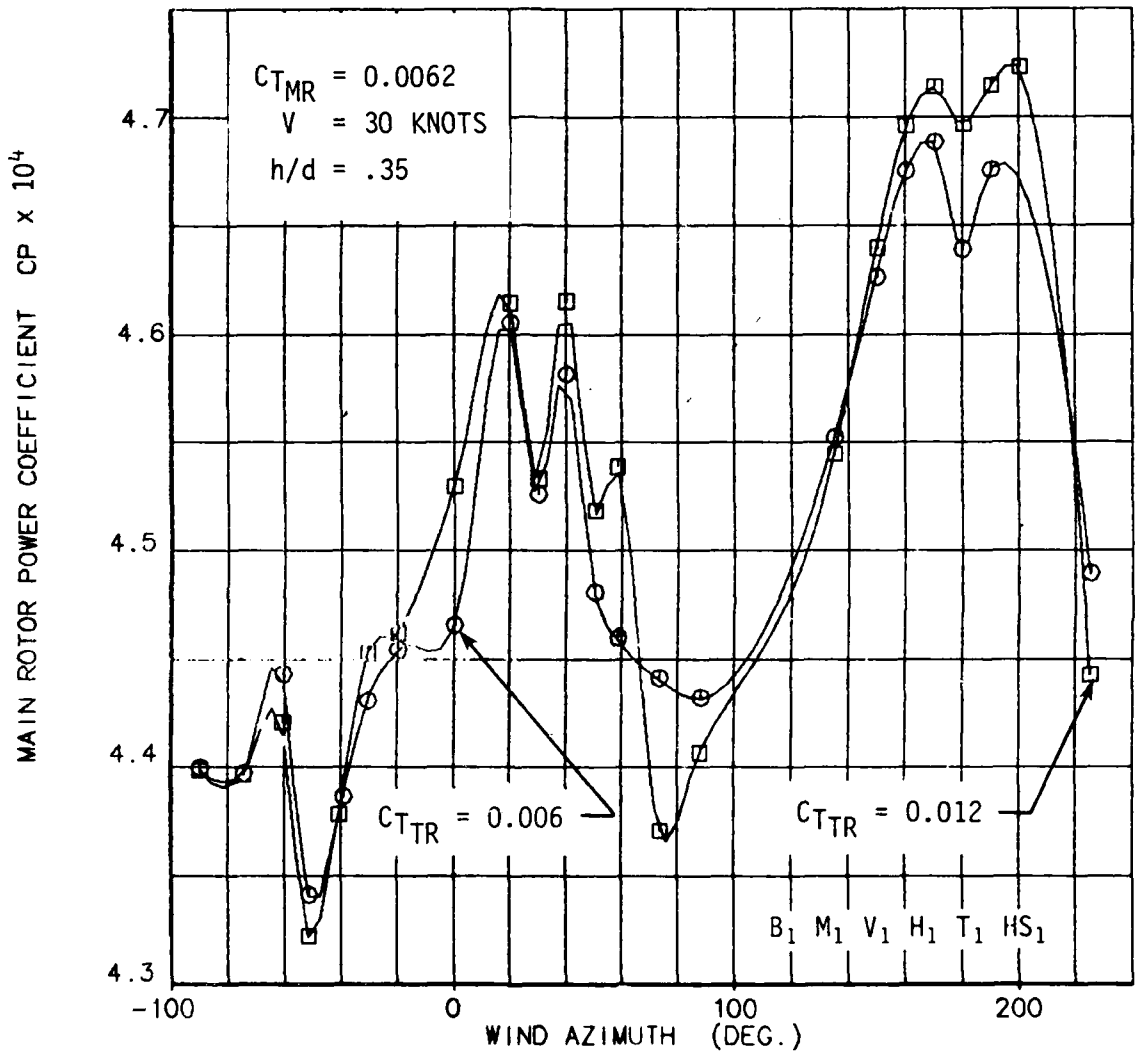


FIGURE 34. VARIATION OF MAIN ROTOR POWER COEFFICIENT AS A FUNCTION OF WIND AZIMUTH AND TAIL ROTOR THRUST.

rotor thrust. Ideally, there would be no variation in main rotor power with azimuth if the tail rotor were not present. Figure 34 indicates, however, that in rearward flight the increase in power due to the tail rotor can be as much as 5% over the forward flight case. In contrast, a slight reduction in main rotor power exists at $\pm 90^\circ$ sideward flight conditions. The greatest reduction in main rotor power required occurs at a wind condition of -50° . This is the condition where the main rotor tip vortex has its greatest influence on tail rotor performance.

The effects of tail rotor flow on main rotor cyclic pitch angles required to trim hub moments to zero are shown in Figures 35 and 36. The overall sinusoidal variation in the control angles is simply due to the change in wind azimuth. The effects of tail rotor flow would be to distort the inflow distribution over the rotor disk in conditions of particularly high interaction, e.g., rearward flight. This would result in higher order variations of main rotor trim cyclics; however, Figure 35 indicates that the tail rotor flow had little effect on main rotor lateral cyclic trim. Similar inconsequential effects on longitudinal cyclic are shown in Figure 36. The apparent insensitivity to tail rotor flow is partly due to the rotor being fully articulated. Typically, hingeless rotors are much more sensitive to variations of the inflow distribution. However, from an operational standpoint the effects of tail rotor flow on main rotor trim have not posed any critical design problems in practice for articulated main rotor systems.

Effects of Airspeed and Tail Rotor Thrust

In the case of the ground vortex, a significant flow anomaly exists in ground effect and is a function of main rotor thrust and forward flight speed. The study of tail rotor effects on main rotor does not involve such a gross flow interaction. The influence of the tail rotor on main rotor inflow distribution is much more subtle than the ground vortex. The effects on main rotor trim due to variations in tail rotor thrust and airspeed for the four principal yaw conditions of $\psi = 0, -90, 180$ and $+90$ degrees are presented in Figures 37 through 48. Variations in main rotor power coefficient, lateral cyclic and longitudinal cyclic are plotted against airspeed for each yaw condition. Curves of constant tail rotor thrust are plotted to illustrate the effects of tail rotor/main rotor interaction.

$\psi = 0^\circ$: Figures 37, 38 and 39 present the data for the forward flight condition. Examination of these figures reveals that the effects of tail rotor thrust are inconsequential

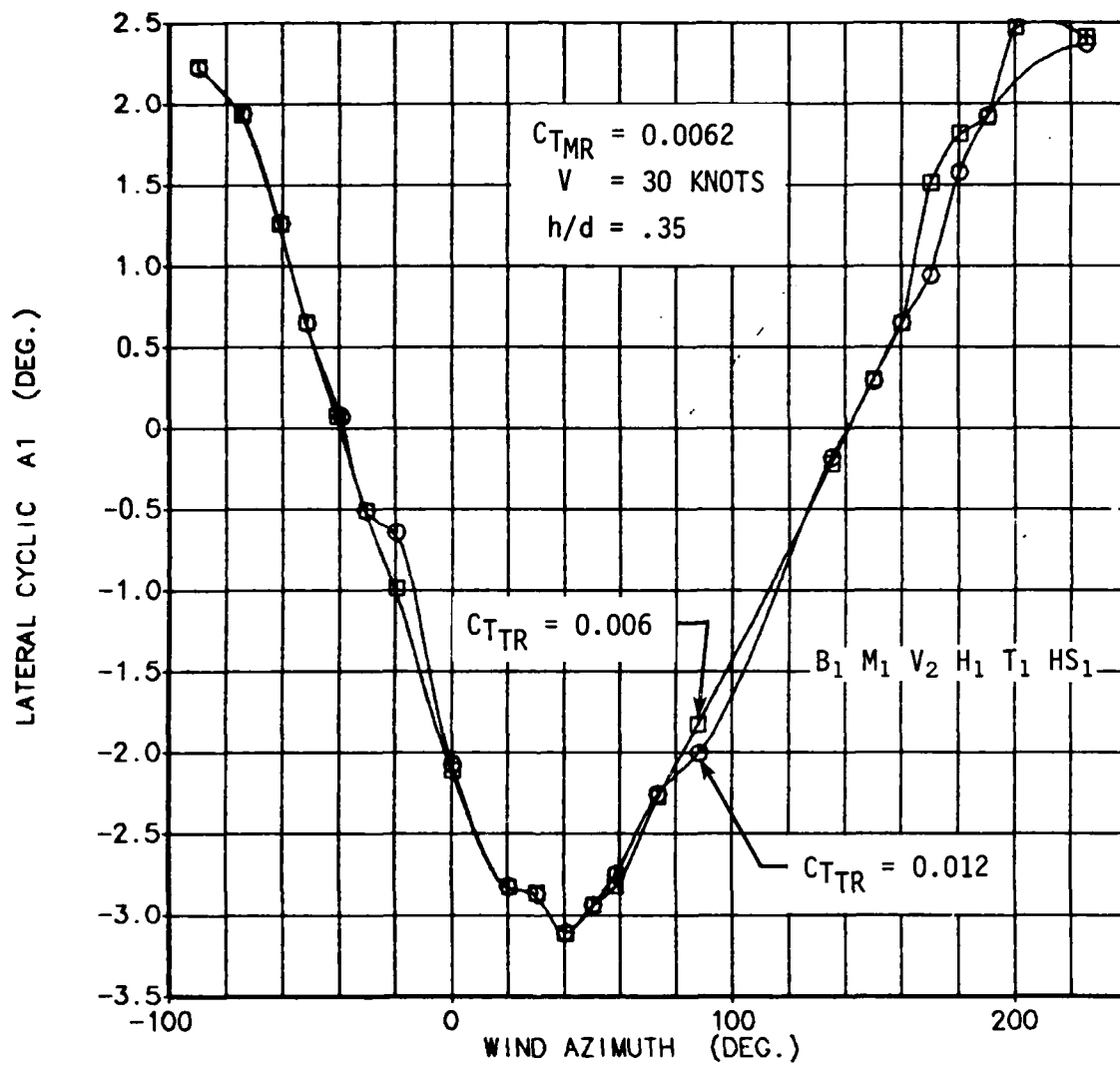


FIGURE 35. VARIATION OF LATERAL CYCLIC PITCH REQUIRED FOR ZERO HUB MOMENT AS A FUNCTION OF WIND AZIMUTH AND TAIL ROTOR THRUST.

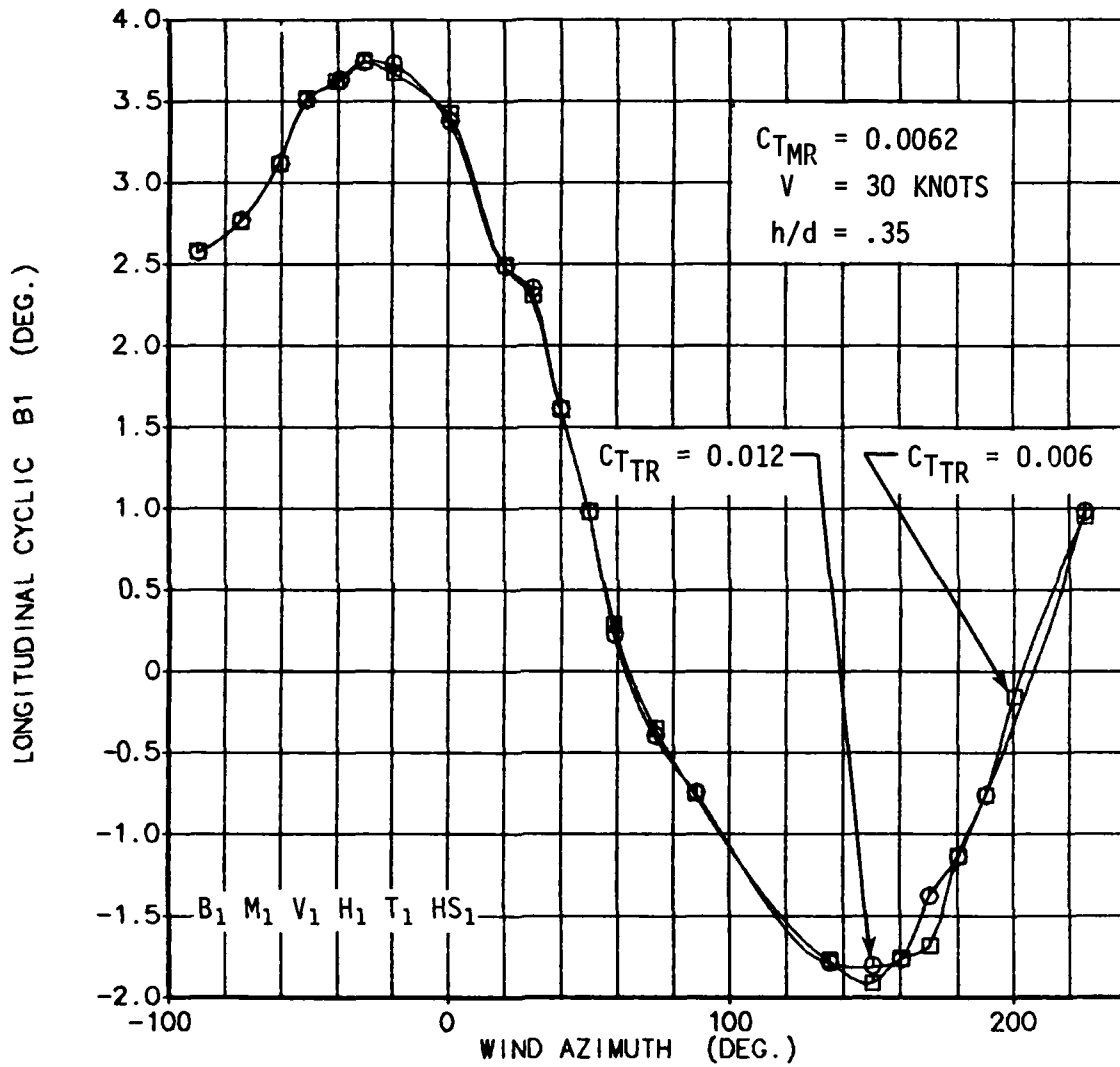


FIGURE 36. VARIATION OF LONGITUDINAL CYCLIC PITCH REQUIRED FOR ZERO HUB MOMENT AS A FUNCTION OF WIND AZIMUTH AND TAIL ROTOR THRUST.

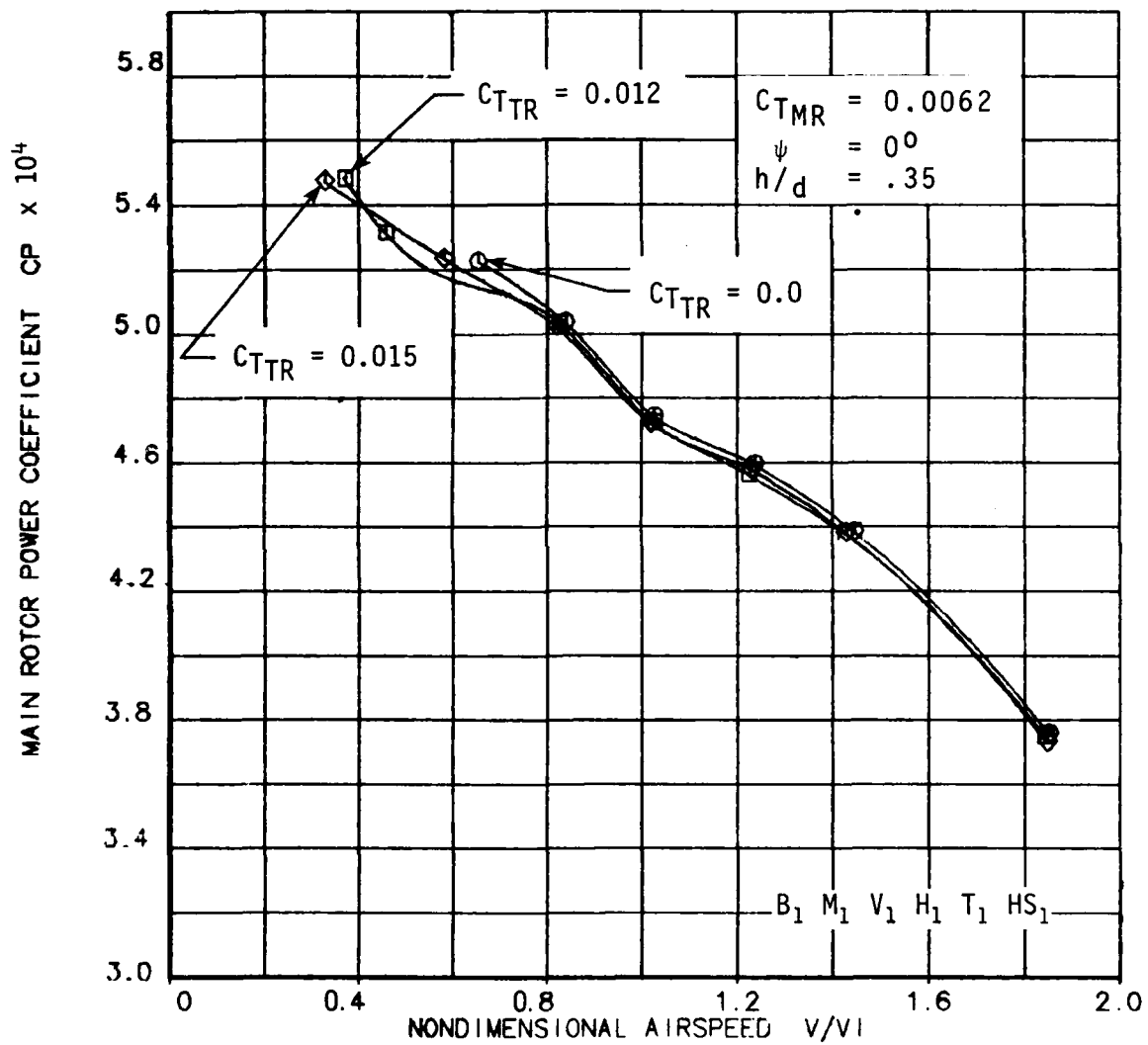


FIGURE 37. VARIATION OF MAIN ROTOR POWER COEFFICIENT AS A FUNCTION OF AIRSPEED AND TAIL ROTOR THRUST ($\psi = 0^\circ$).

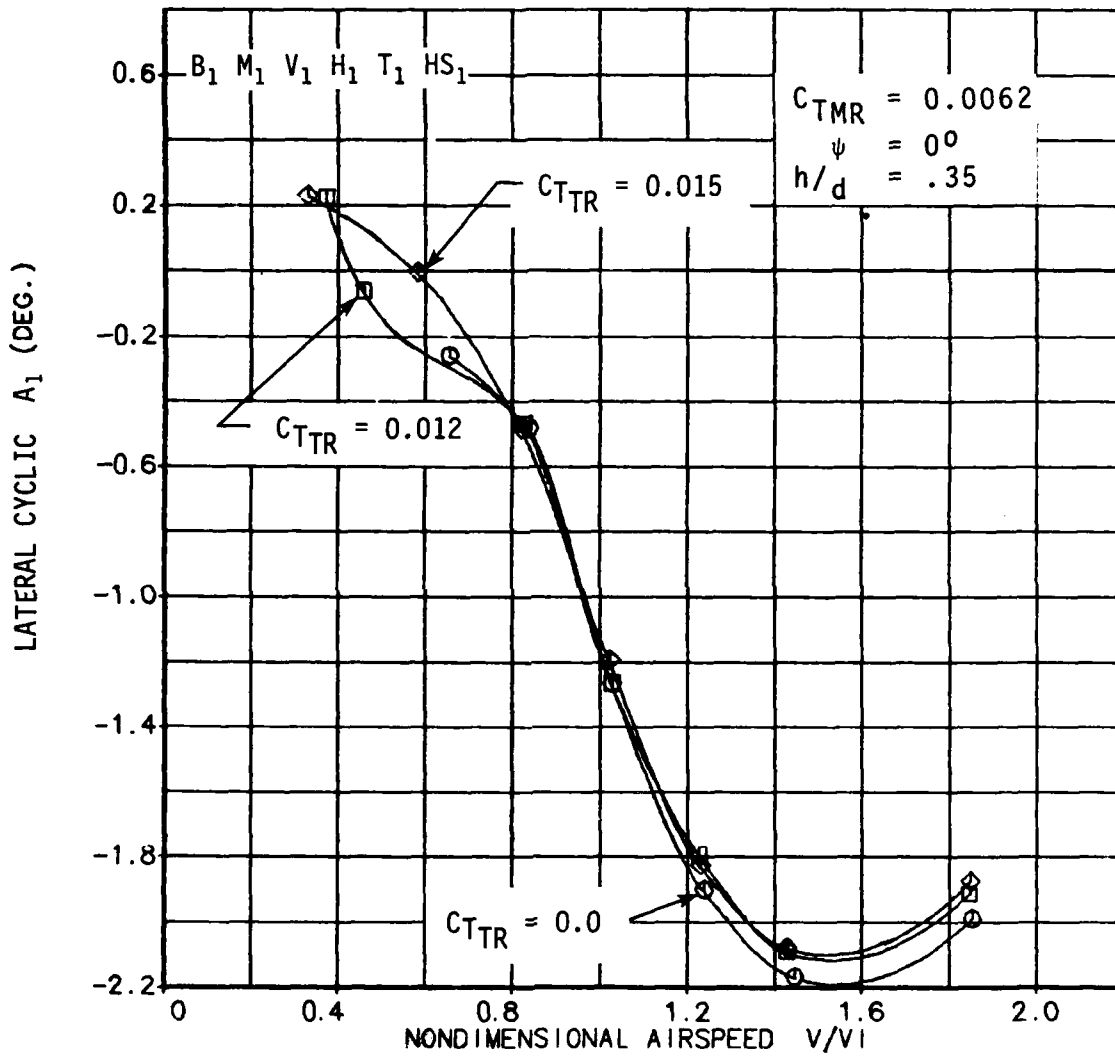


FIGURE 38. VARIATION OF LATERAL CYCLIC REQUIRED FOR ZERO HUB MOMENT AS A FUNCTION OF AIRSPEED AND TAIL ROTOR THRUST ($\psi = 0^\circ$).

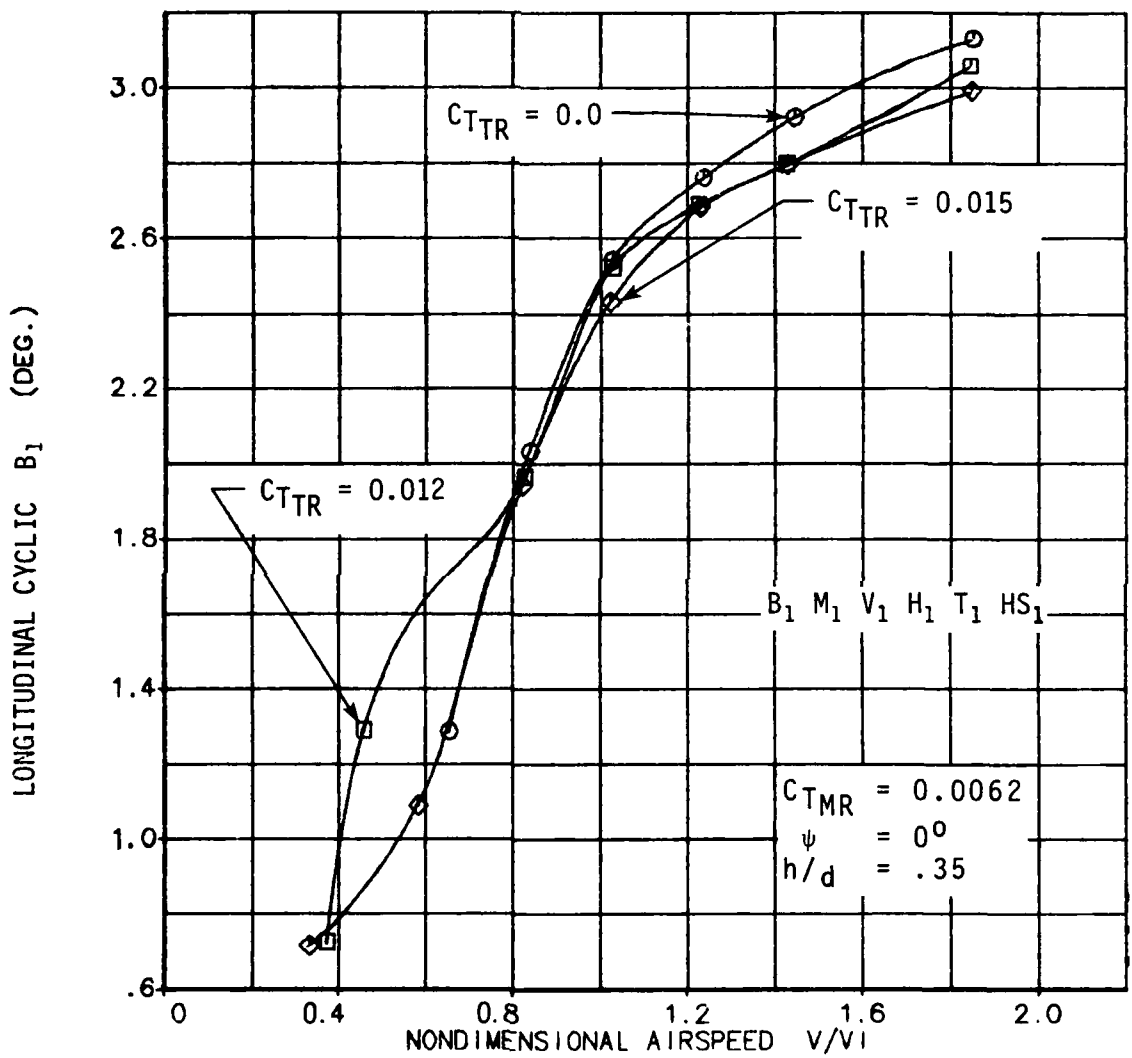


FIGURE 39. VARIATION OF LONGITUDINAL CYCLIC REQUIRED FOR ZERO HUB MOMENT AS A FUNCTION OF AIRSPEED AND TAIL ROTOR THRUST ($\psi = 0^\circ$).

for the three levels of thrust tested. Similar results were presented in Reference 1.

$\psi = -90^\circ$: Figures 40, 41 and 42 present the main rotor trim conditions as a function of airspeed and tail rotor thrust for the right sideward flight condition. The main rotor power varied slightly with tail rotor thrust. For nondimensional airspeeds less than a value of 0.8, the increase in tail rotor loading tends to decrease main rotor power required. Conversely, for airspeeds greater than 0.8, main rotor power increases slightly with tail rotor thrust. The maximum increase of 4% occurs at a nondimensional airspeed of 1.0. The corresponding variations in main rotor trim cyclics are less significant (see Figures 38 and 39).

$\psi = 180^\circ$: For the rearward flight condition, Figures 43, 44 and 45 present the main rotor trim data. The effects of tail rotor thrust are more evident in this condition, as would be expected. The main rotor power required increases almost proportionally with tail rotor thrust over the range of airspeeds tested (Figure 43). Slight variations in trim lateral cyclic pitch are shown in Figure 44. Variations in longitudinal cyclic pitch are more affected by tail rotor presence at low speeds and show virtually no effects at higher speeds (see Figure 45).

$\psi = +90^\circ$: The effects of tail rotor flow on main rotor trim parameters for left sideward flight are shown in Figures 46, 47 and 48. The variations in main rotor power coefficient with changes in tail rotor thrust are given in Figure 46. The data shows that for nondimensional airspeeds lower than 1.0 the main rotor power required increases slightly with increases in tail rotor thrust. For airspeeds greater than 1.0 the main rotor power required appears to decrease slightly with changes in tail rotor loading. At a nondimensional airspeed of 1.25 the decrease in main rotor power is approximately 4 percent.

Figures 47 and 48 show the effects of tail rotor thrust on lateral and longitudinal cyclic pitch requirements for this flight condition. For nondimensional airspeeds lower than a value of 1.0 the main rotor trim is relatively insensitive to changes in tail rotor flow. In this regime the ground vortex has a very large inflow on main rotor inflow distribution that masks the effects of the tail rotor. Above a nondimensional airspeed of 1.0, however, the effect of tail rotor flow on trim cyclic pitch angles is very significant. The lateral trim cyclic pitch is particularly influenced by tail rotor flow (Figure 47). A large decrease in lateral cyclic is experienced when the tail rotor thrust is increased from zero to the nominal value of 0.012 thrust coefficient.

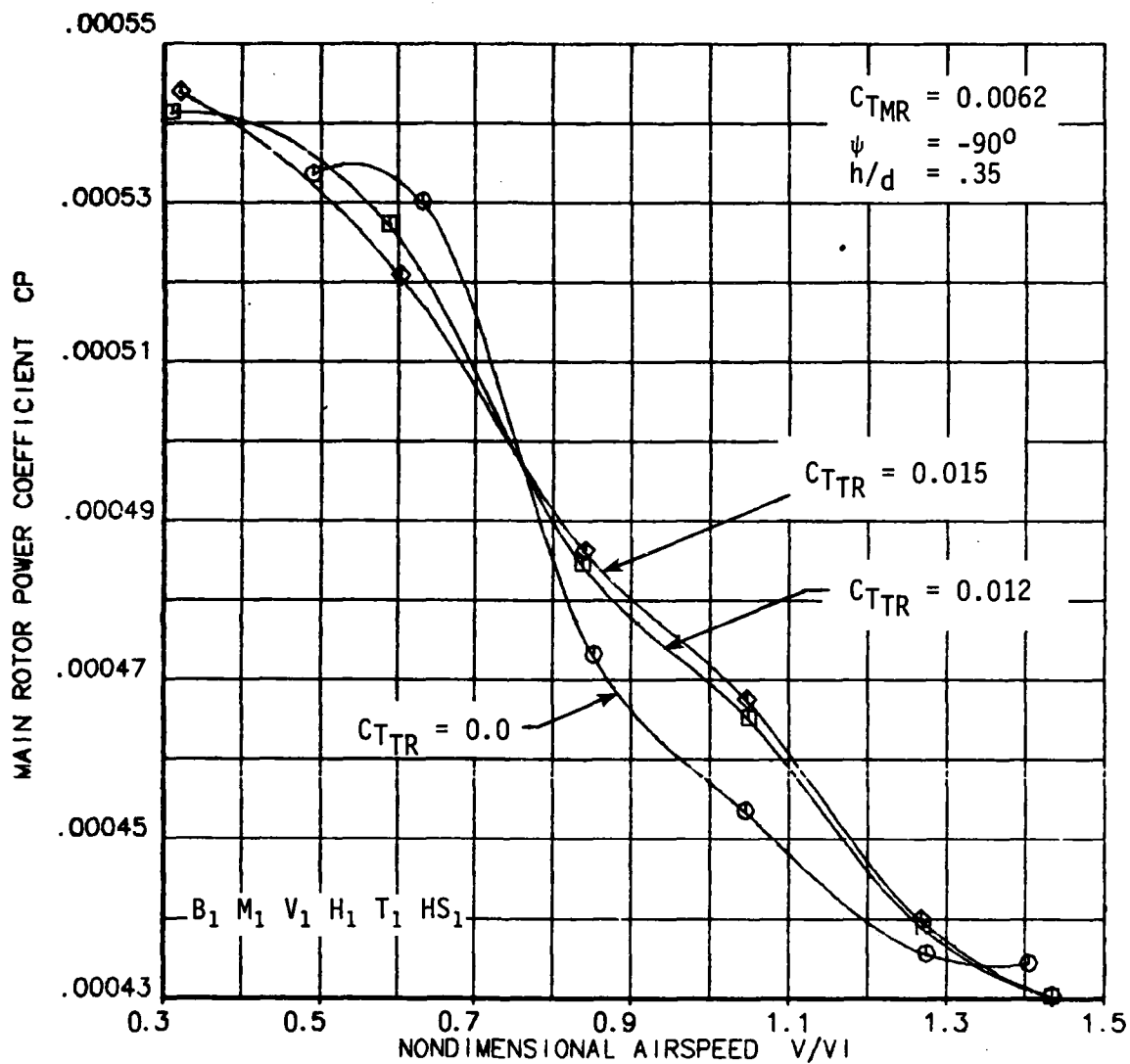


FIGURE 40. VARIATION OF MAIN ROTOR POWER COEFFICIENT AS A FUNCTION OF AIRSPEED AND TAIL ROTOR THRUST ($\psi = -90^\circ$).

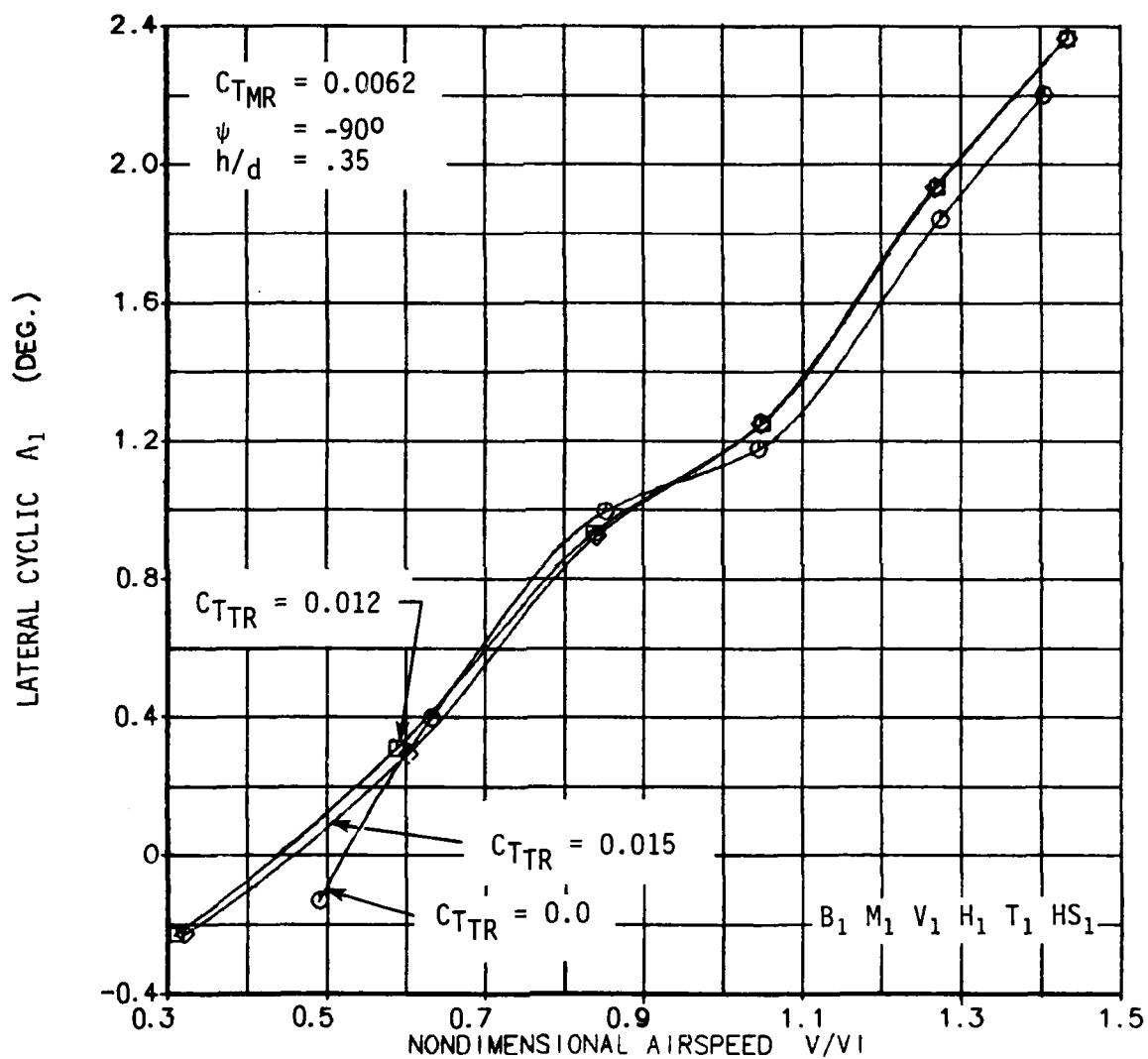


FIGURE 41. VARIATION OF LATERAL CYCLIC REQUIRED FOR ZERO HUB MOMENT AS A FUNCTION OF AIRSPEED AND TAIL ROTOR THRUST ($\psi = -90^\circ$).

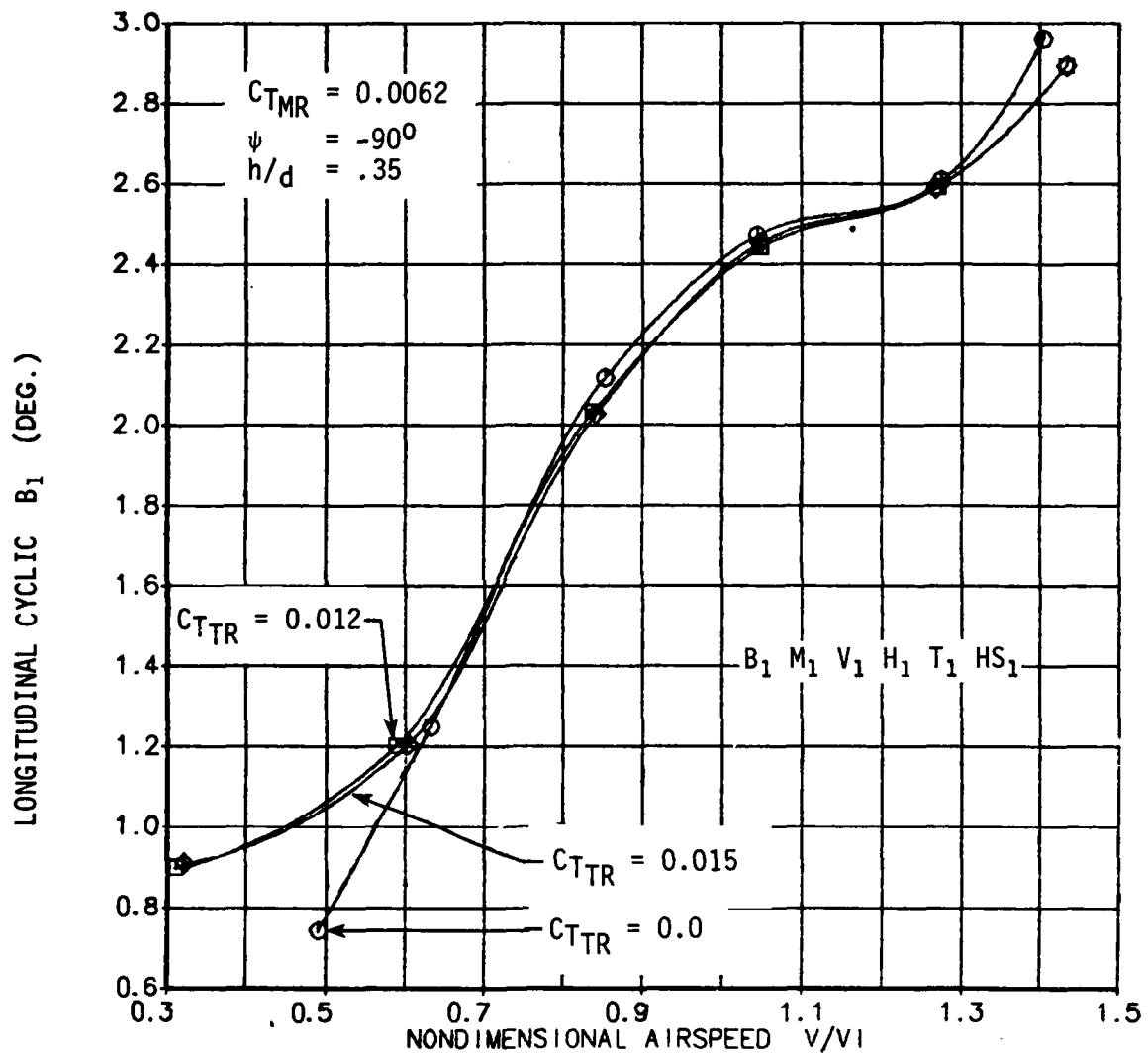


FIGURE 42. VARIATION OF LONGITUDINAL CYCLIC REQUIRED FOR ZERO HUB MOMENT AS A FUNCTION OF AIRSPEED AND TAIL ROTOR THRUST ($\psi = -90^\circ$).

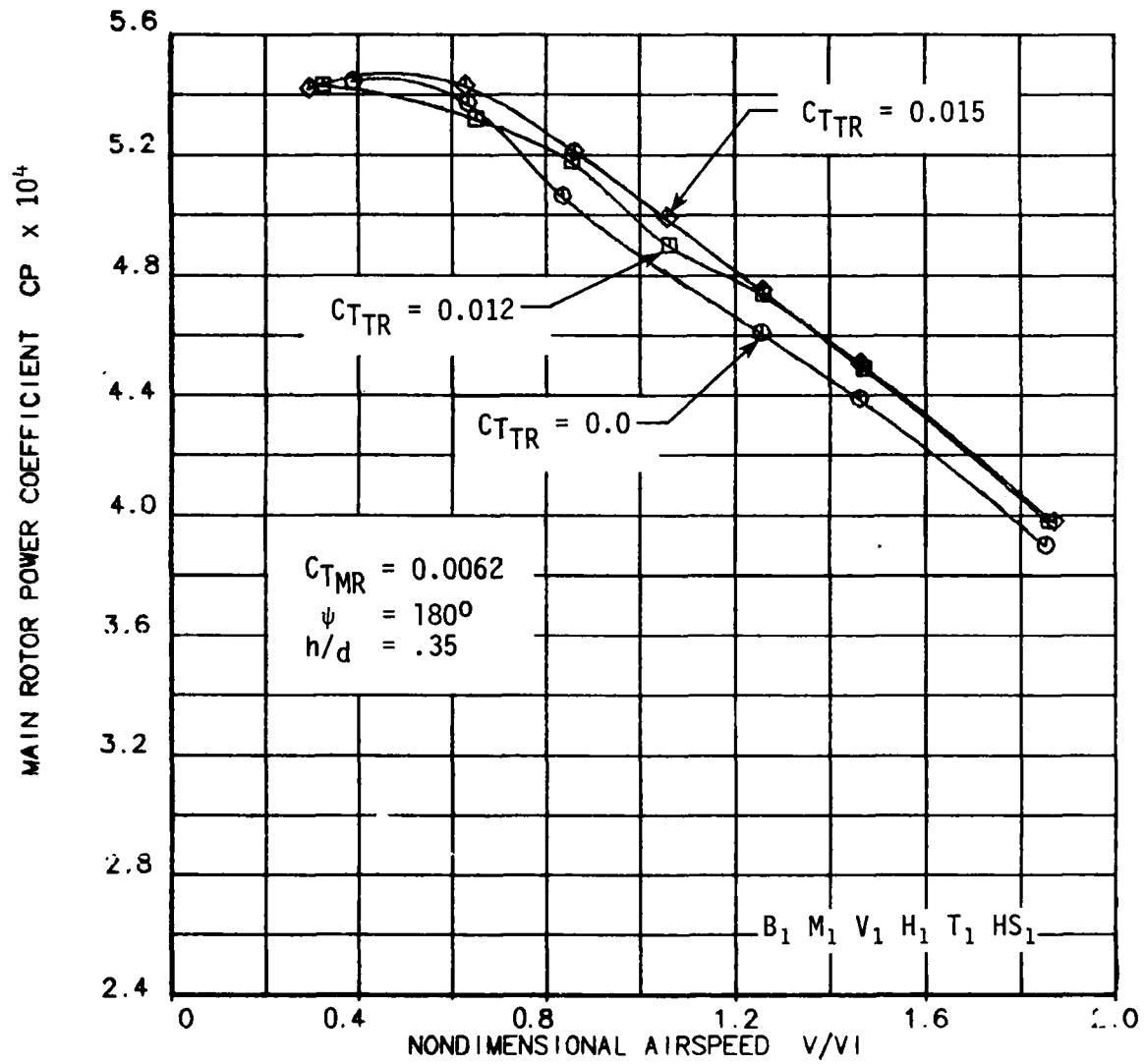


FIGURE 43. VARIATION OF MAIN ROTOR POWER COEFFICIENT AS A FUNCTION OF AIRSPEED AND TAIL ROTOR THRUST ($\psi = 180^\circ$).

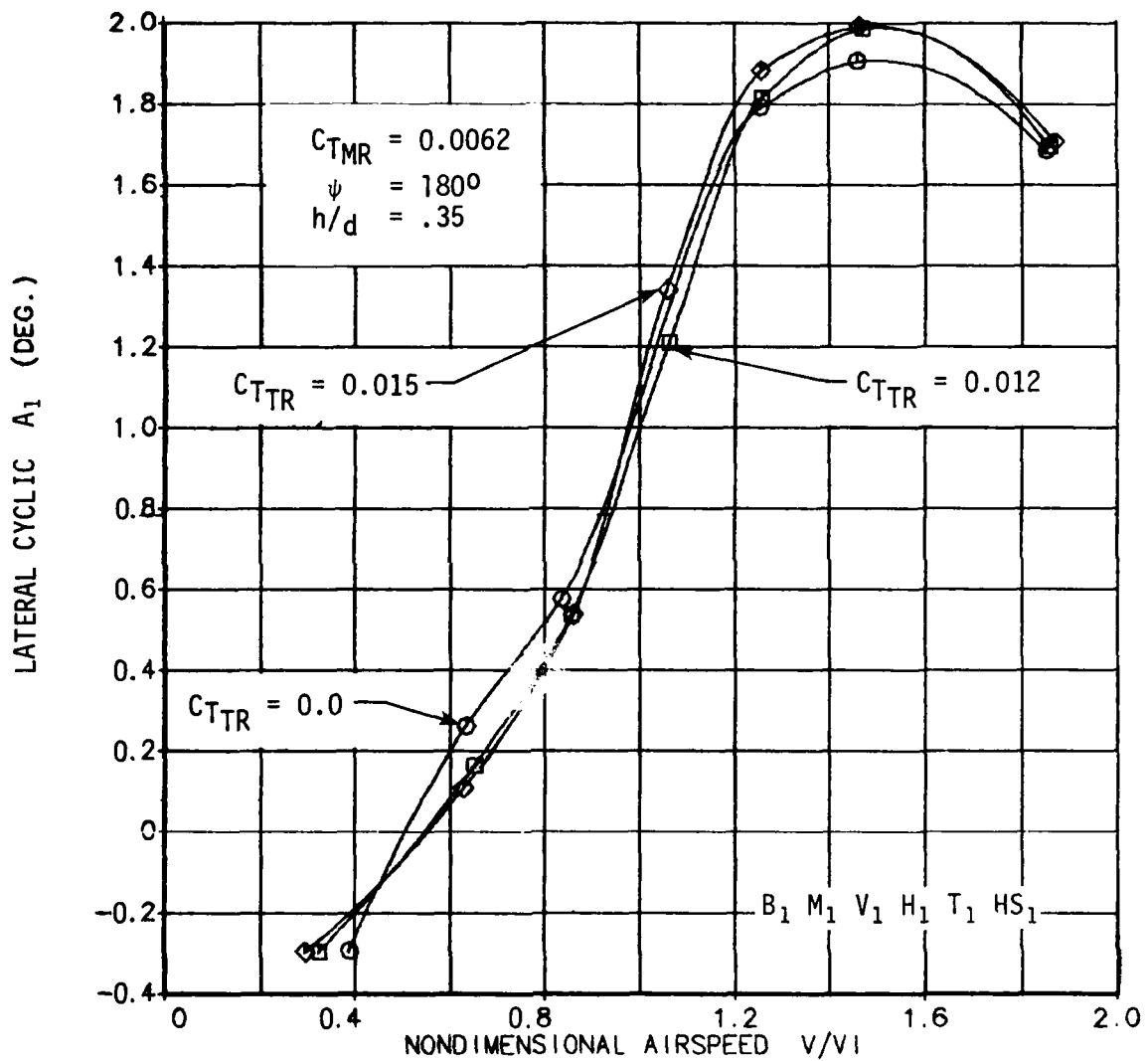


FIGURE 44. VARIATION OF LATERAL CYCLIC REQUIRED FOR ZERO HUB MOMENT AS A FUNCTION OF AIRSPEED AND TAIL ROTOR THRUST ($\psi = 180^\circ$).

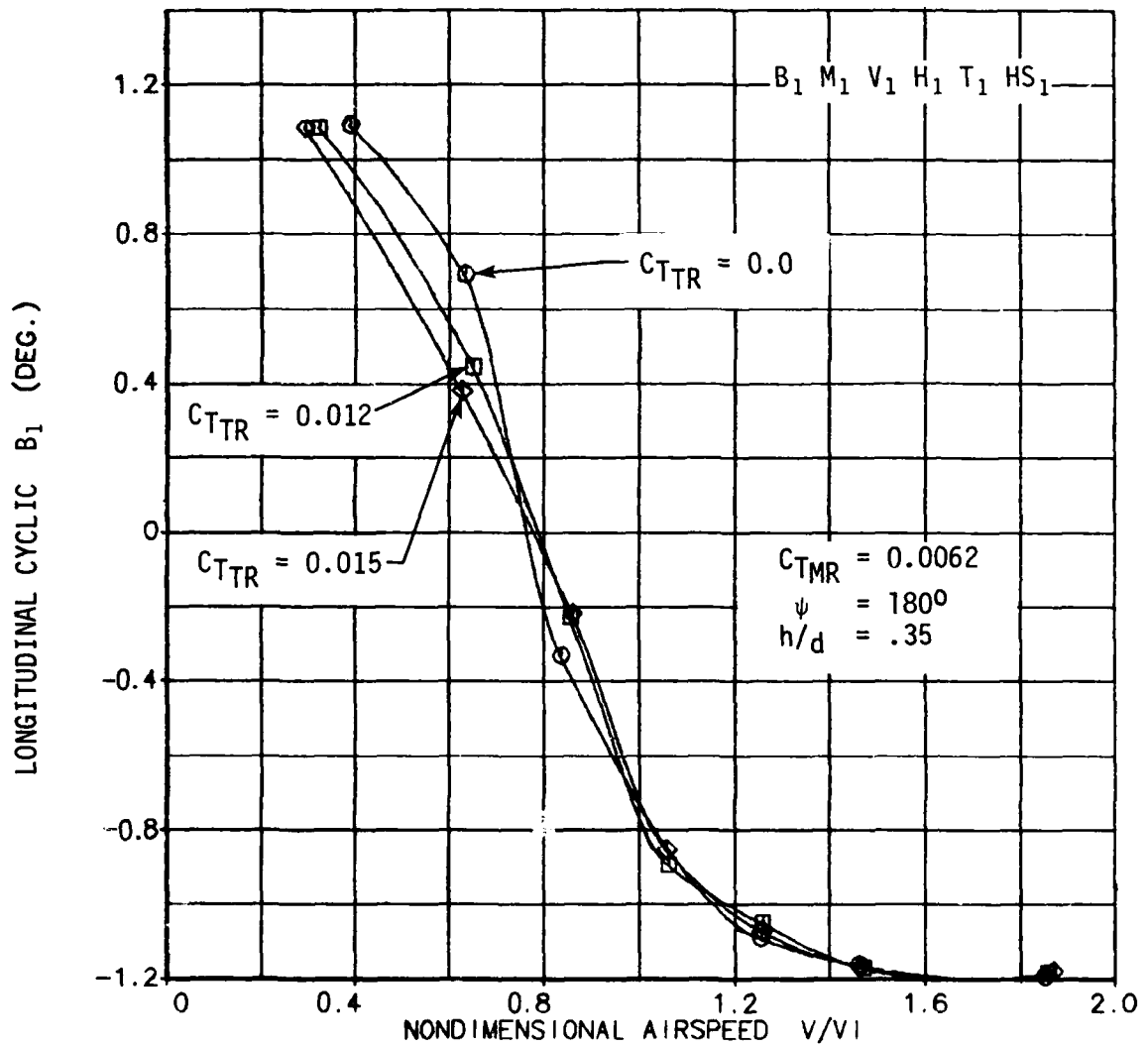
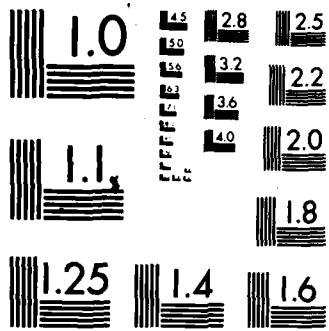


FIGURE 45. VARIATION OF LONGITUDINAL CYCLIC REQUIRED FOR ZERO HUB MOMENT AS A FUNCTION OF AIRSPEED AND TAIL ROTOR THRUST ($\psi = 180^\circ$).



MICROCOPY RESOLUTION TEST CHART
NATIONAL BUREAU OF STANDARDS-1963-A

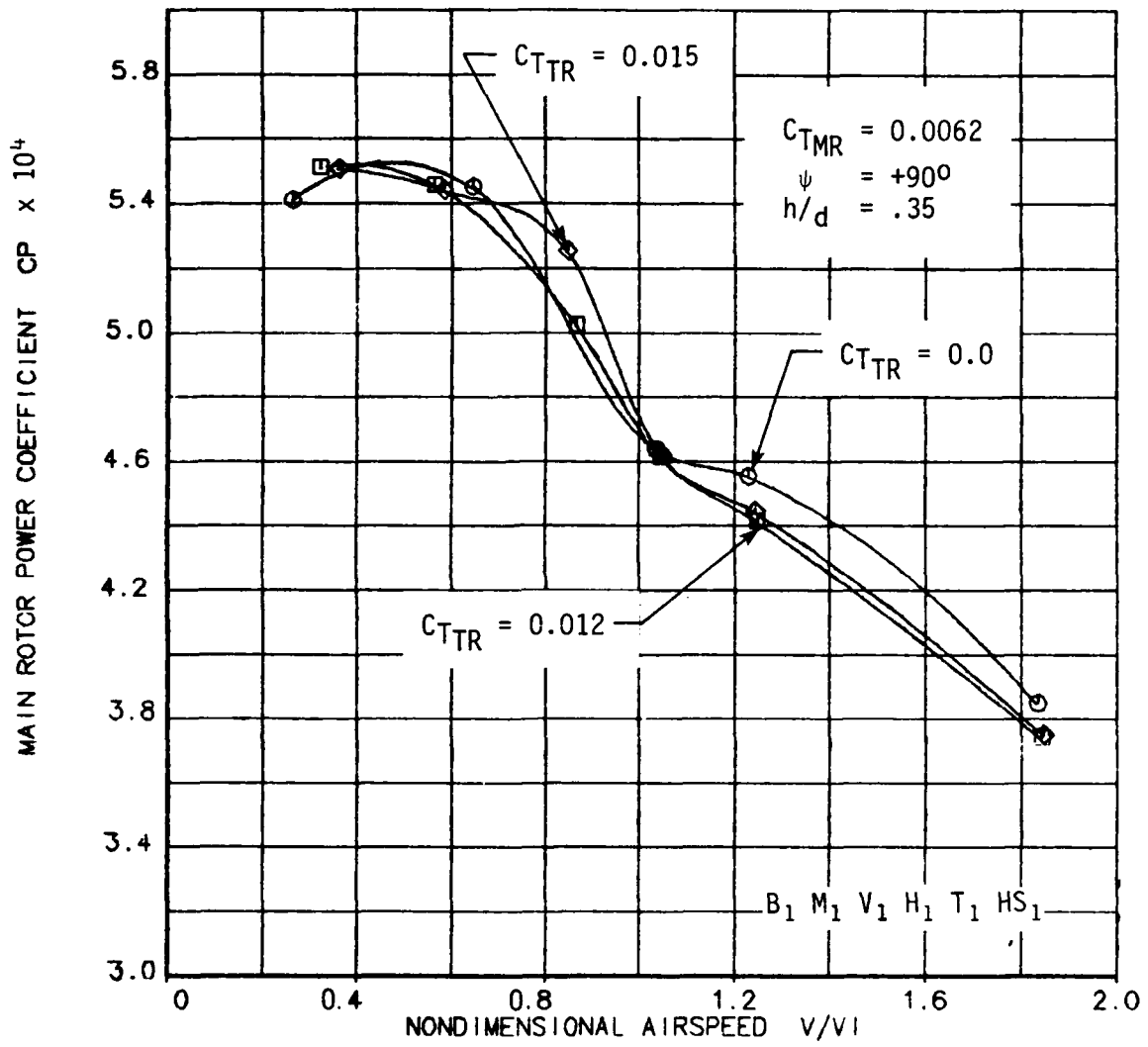


FIGURE 46. VARIATION OF MAIN ROTOR POWER COEFFICIENT AS A FUNCTION OF AIRSPEED AND TAIL ROTOR THRUST ($\psi = 90^\circ$).

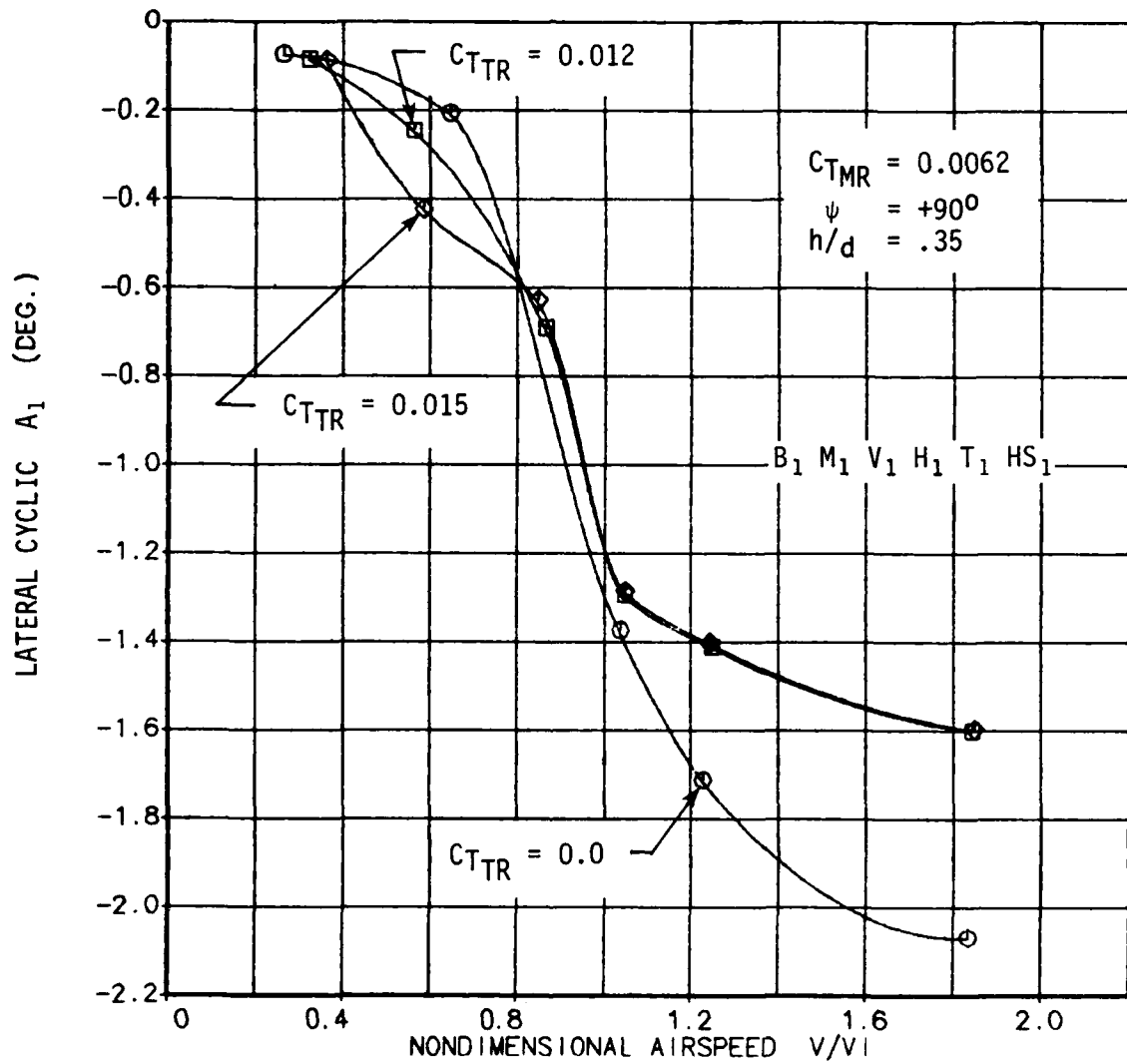


FIGURE 47. VARIATION OF LATERAL CYCLIC REQUIRED FOR ZERO HUB MOMENT AS A FUNCTION OF AIRSPEED AND TAIL ROTOR THRUST ($\psi = 90^\circ$).

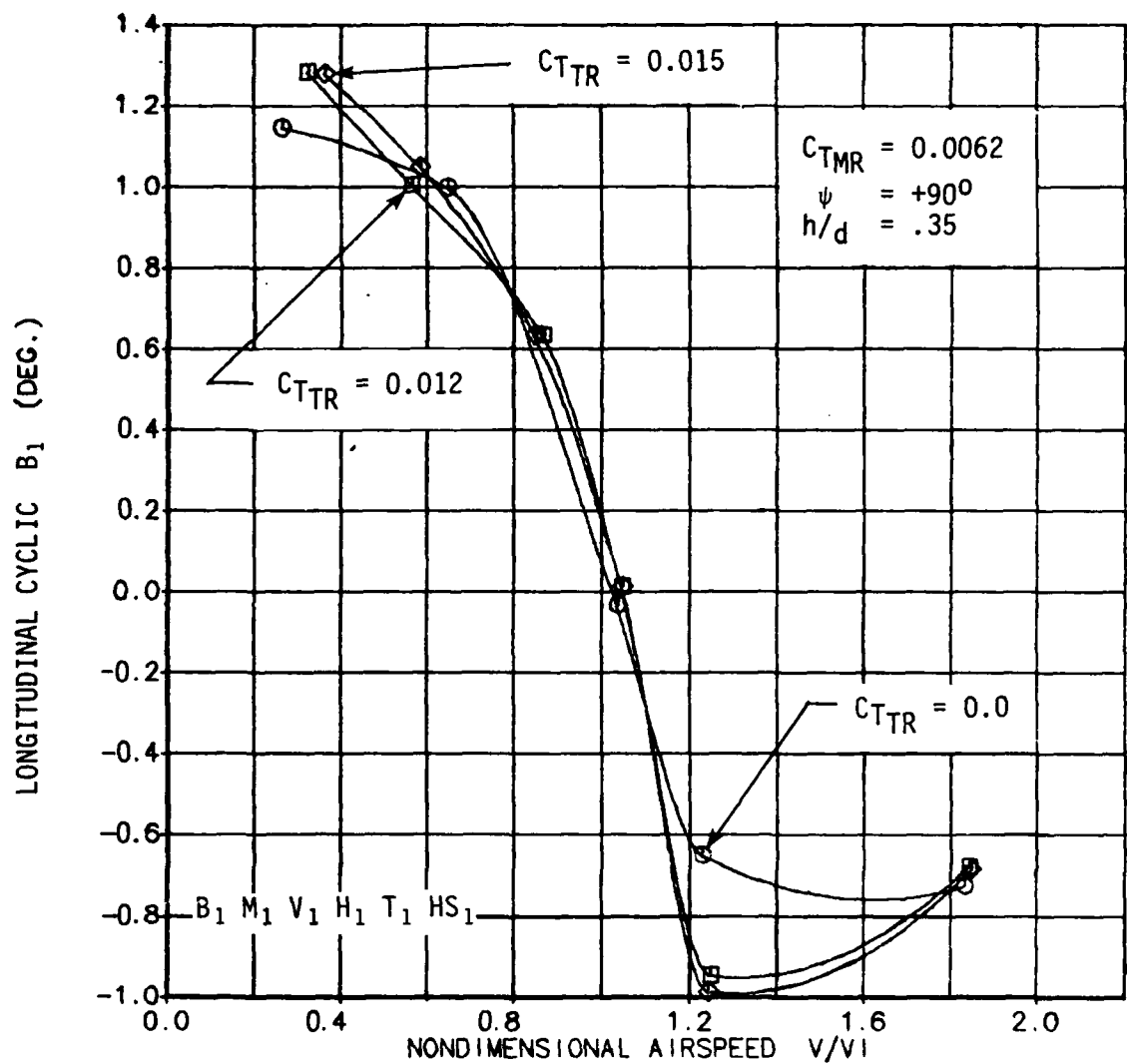


FIGURE 48. VARIATION OF LONGITUDINAL CYCLIC REQUIRED FOR ZERO HUB MOMENT AS A FUNCTION OF AIRSPEED AND TAIL ROTOR THRUST ($\psi = 90^\circ$).

This indicates that the tail rotor flow has a strong influence on the lateral flow distribution over the main rotor disk for sufficiently high airspeeds in left sideward flight.

Figure 49 is a plot of main rotor power coefficient against airspeed for the nominal main rotor and tail rotor thrust conditions. The variations in power for the four principal yaw conditions are included in this plot. As would be expected, the rearward flight condition experienced the highest main rotor power required for most of the flight speeds. Surprisingly, for nondimensional airspeeds greater than 1.0 the forward flight case shows a higher power required than sideward flight in either direction. For airspeeds lower than 1.0 the main rotor power for the left sideward flight increases significantly and must be influenced by the ground vortex in this condition.

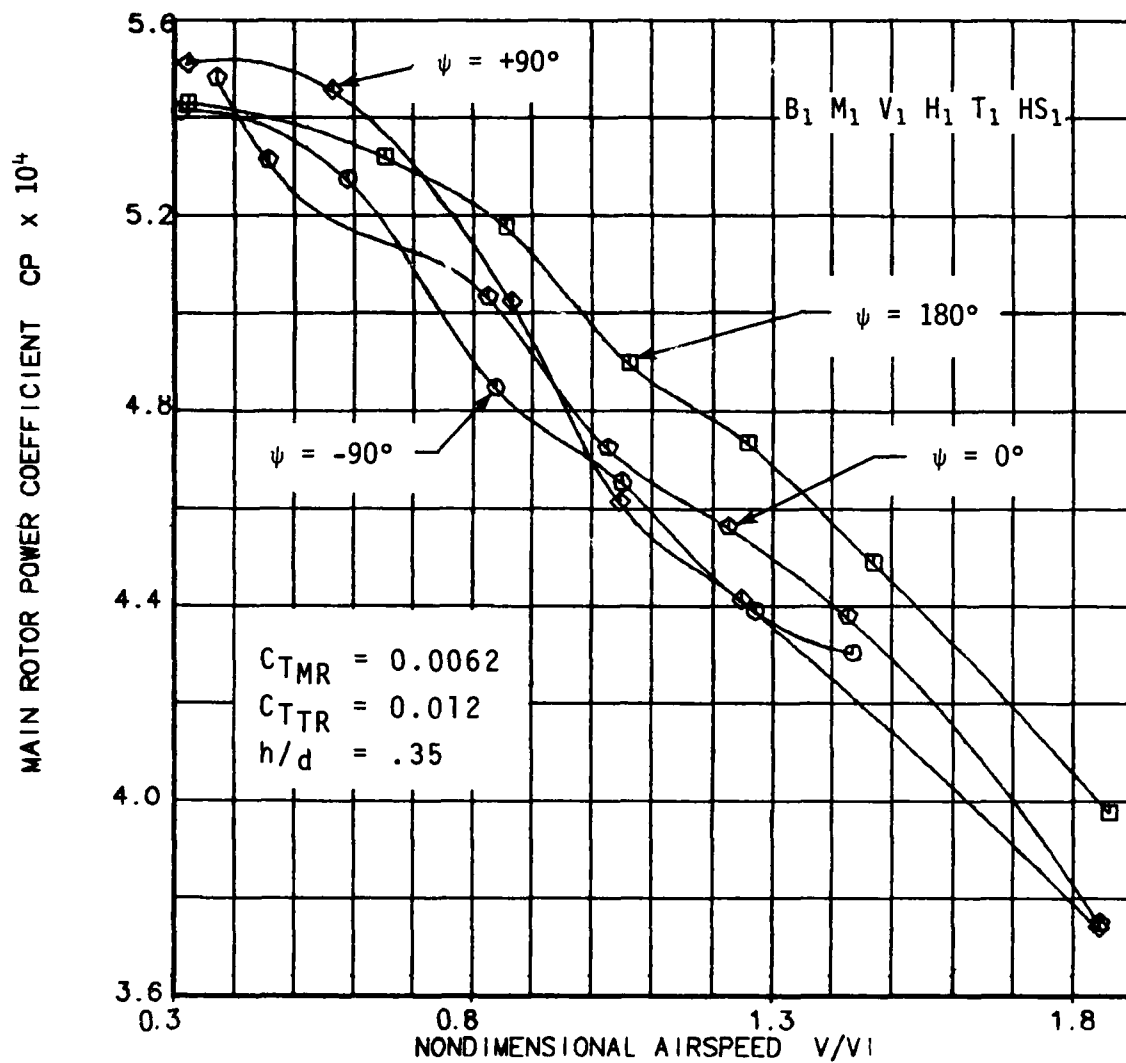


FIGURE 49. VARIATION OF MAIN ROTOR POWER COEFFICIENT AS A FUNCTION OF AIRSPEED AND WIND AZIMUTH.

TAIL ROTOR/FIN INTERACTIONS

The aerodynamic coupling of the tail rotor and fin is another aspect of interactional aerodynamics that requires a considerable amount of research to understand the flow mechanisms involved. Interposing the fin into the inflow-field of the pusher tail rotor results in adverse fin loads and increased tail rotor power. The adverse fin load is a function of tail rotor thrust as the flow on the side of the fin nearest to the tail rotor is drawn off by the inflow to the tail rotor. The resultant negative pressures at the fin generate a fin force that opposes the tail rotor thrust, thus reducing the net side force available for directional control. On the other hand, the presence of the fin on the inflow side of the tail rotor results in distortions of the flow distribution across the tail rotor disk, resulting in increased power required.

14
F

These two effects in combination have been called "blockage" and the ratio of swept fin area to tail rotor disk area has been called the blockage ratio. This ratio is used as the key design variable in the study of the adverse fin force as a function of tail rotor thrust. It is probably an oversimplification in that surface areas outside of the fin swept area have been observed to be washed by high velocity air. This results in additional adverse airloads. However, the fin force is the most significant element, and variations in fin size have a considerable effect on tail rotor/fin interactions.

The aerodynamic coupling of the tail rotor and fin is not restricted to the directional axis. Significant variations in the vertical lift force of the empennage resulted from changes in tail rotor thrust and fin size. Changes in the empennage lift force will have a strong effect on the longitudinal trim characteristics, thus resulting in cross axis coupling. It must be emphasized that the empennage balance measures the forces and moments on the model surfaces aft of the balance and does not include tail rotor loads (see Figure 11).

In the directional axis the fin force is the predominant side force. For the longitudinal axis the horizontal stabilizer vertical force is the predominant lift force. In both axes the tail boom has a small additional contribution to either side force or lift force. In the sections that follow, the nondimensional empennage vertical lift force is the sum of the horizontal stabilizer and the tail boom vertical forces normalized by the main rotor thrust. This quantity provides

a look at the interaxis coupling due to changes in fin configuration.

The baseline configuration for this test was a fin with a 35% blockage ratio. This is larger than the fin employed in previous tests reported in References 3 and 5 and is comparable to modern aircraft. A comprehensive investigation of tail rotor and fin interactions was conducted for this nominal fin configuration. Parametric sweeps of the fundamental parameters airspeed, azimuth, and tail rotor thrust were obtained at a height-to-diameter ratio of 0.35. A limited amount of supplemental data was acquired for two other fin configurations. The first was a 25% blockage fin and the other was a fin-off condition. The data pertaining to tail-rotor-on-fin and fin-on-tail-rotor interactions is presented in the subsections that follow.

TAIL-ROTOR-ON-FIN INTERACTIONS

Effects of Wind Azimuth and Tail Rotor Thrust

Figures 50, 52 and 53 show the effects of varying wind azimuth on the fin side force coefficient, boom side force coefficient and nondimensional empennage vertical lift. Data is plotted in these figures for two levels of tail rotor thrust. In Figure 50 a nonlinear variation in fin force is evident near plus and minus 50 degrees. This nonlinear character results from the main rotor tip vortices impinging on the vertical fin in a manner similar to the interactions with the tail rotor discussed in the previous section.

Without the flow anomalies associated with the main rotor wake, the variation in fin side force for the region from $\psi = 0$ degrees to $\psi = -90$ degrees should be equal and opposite to the variations from $\psi = 0$ degrees to $\psi = +90$ degrees with

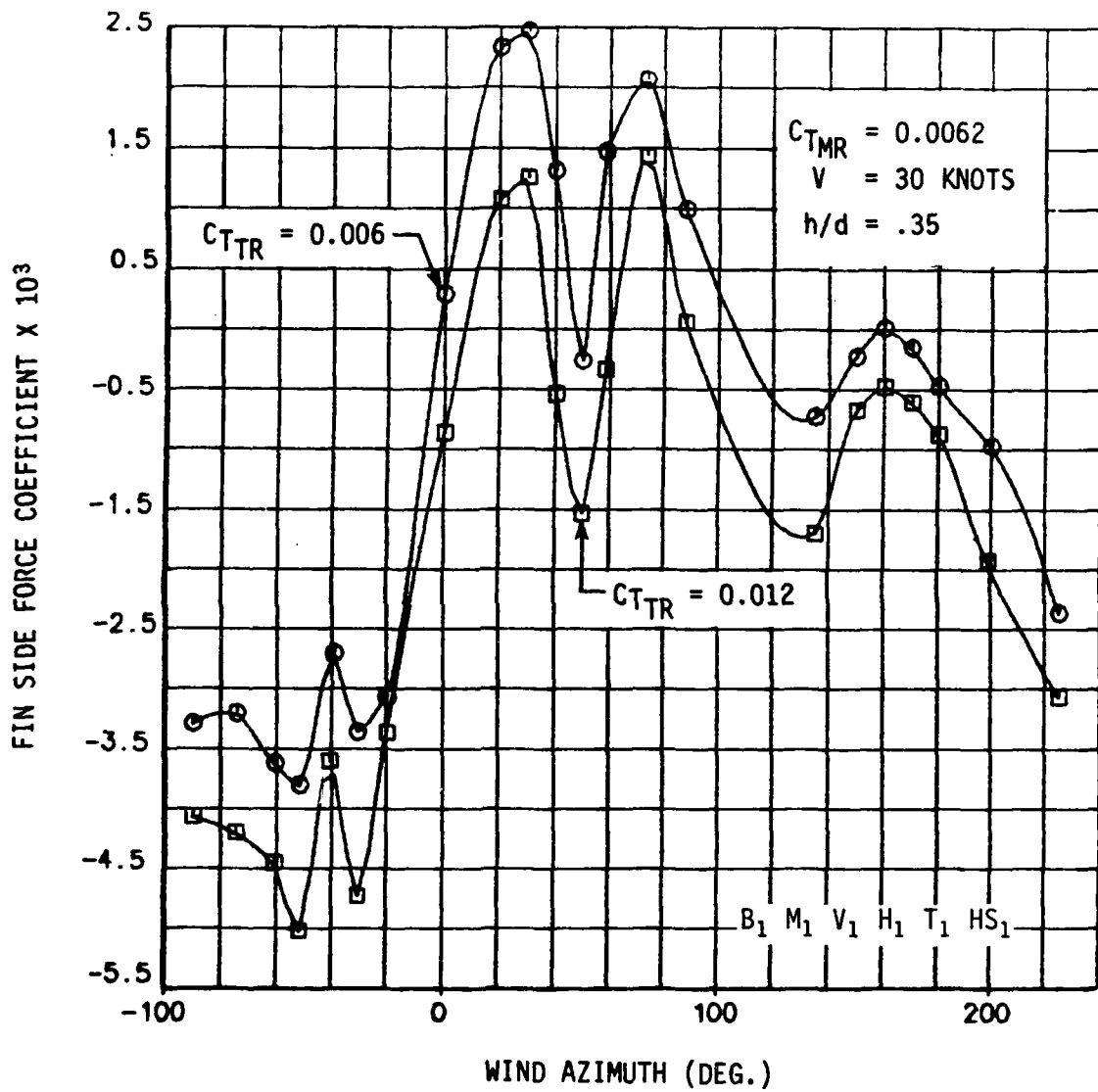
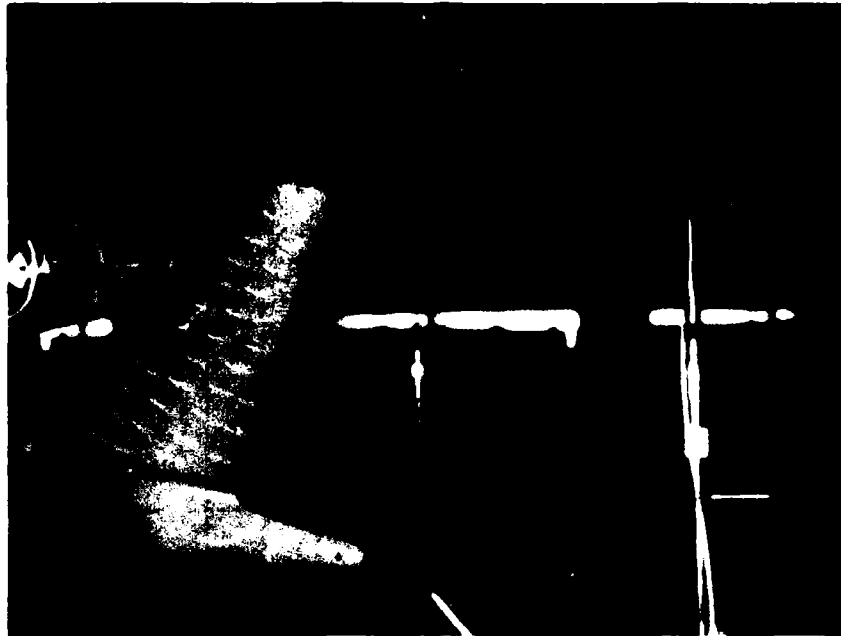
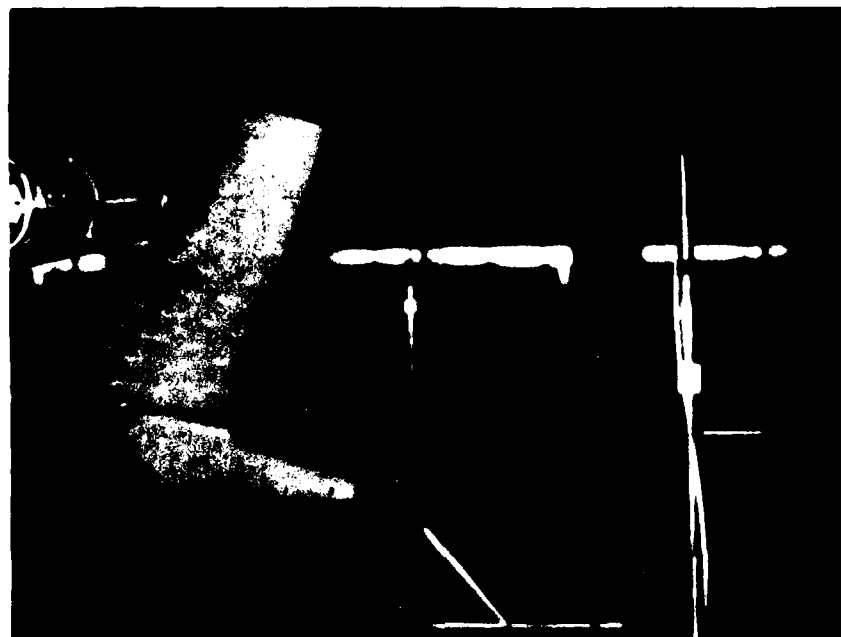


FIGURE 50. EFFECTS OF WIND AZIMUTH AND TAIL ROTOR THRUST ON FIN SIDE FORCE COEFFICIENT.



a. $C_{T_{MR}} = 0.0062$

$C_{T_{TR}} = 0.006$



b. $C_{T_{MR}} = 0.0062$

$C_{T_{TR}} = 0.012$

FIGURE 51. EFFECTS OF TAIL ROTOR THRUST ON FIN TUFT PATTERN AT
 $\psi = 40^\circ$, $V = 30$ KNOTS.

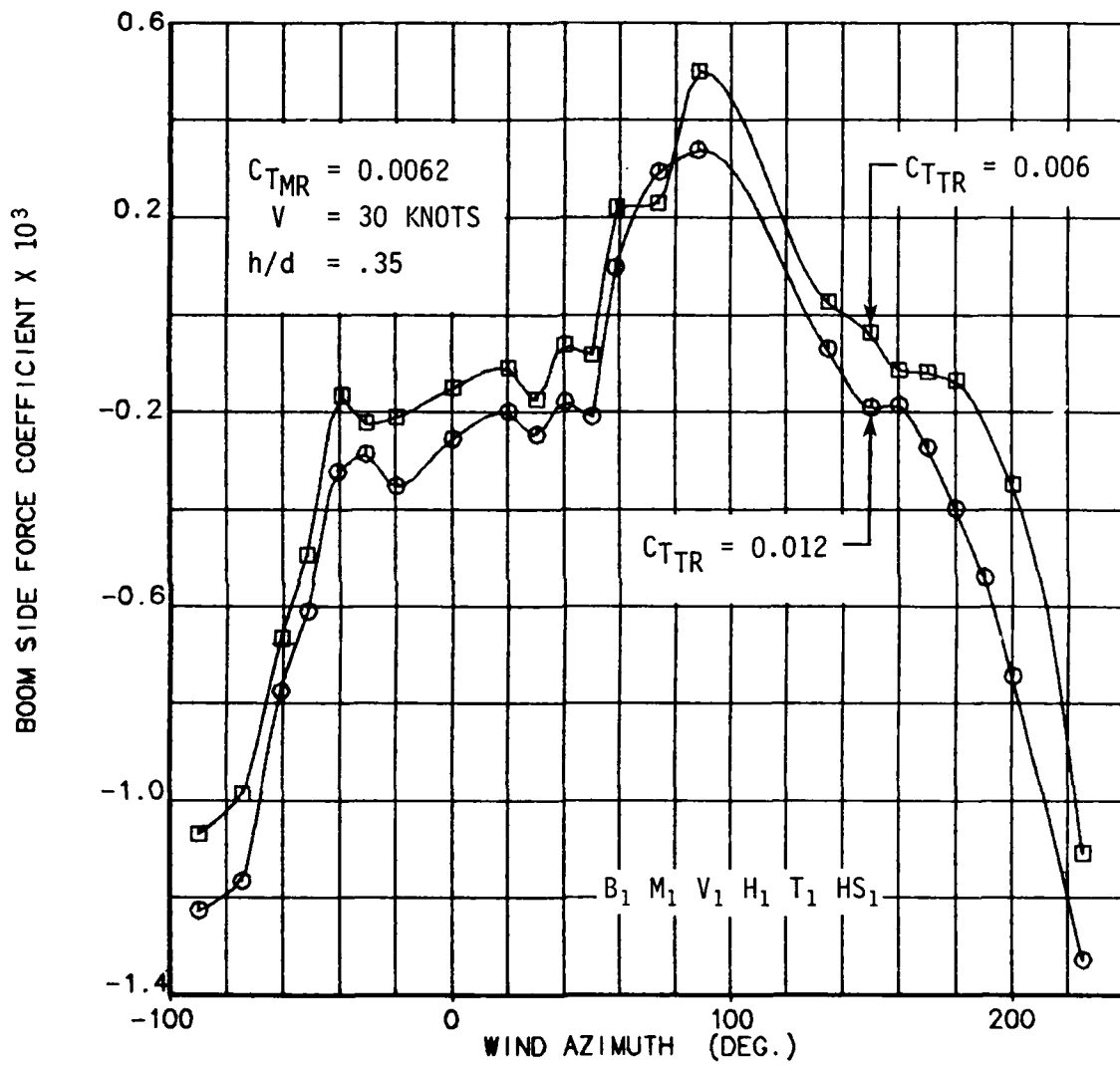


FIGURE 52. EFFECTS OF WIND AZIMUTH AND TAIL ROTOR THRUST ON BOOM SIDE FORCE COEFFICIENT.

the maximum fin force occurring at plus and minus 90 degrees. However, this is not the case, as seen in Figure 50. The fin force reaches its maximum adverse load at -50 degrees where the effect of the main rotor tip vortex is greatest. For a wind azimuth of +50 degrees a very large increase in adverse fin force is also evident, thus dramatically reducing the benefits of positive yaw angle.

Apparently, this nonlinear variation in fin force near +50 degrees is much more sensitive to variations in tail rotor thrust than the -50 degree case. Figure 51 is a photograph of the tuft patterns on the vertical fin for a wind azimuth condition of +40 degrees. The influence of the tail rotor thrust on the tufts is clearly indicated. Figure 51b shows the tufts raised off of the fin surface for the increased tail rotor thrust condition, indicating the negative pressurization on the fin. The corresponding variation in fin side force plotted in Figure 50 shows a very large increase in fin force for the increase in tail rotor thrust.

The variation in fin force for the wind azimuths extending from 140 through 200 degrees occurs within the flight regime of the ground vortex. The effects of the ground vortex are to alleviate the adverse fin load, with the maximum effect occurring at 160 degrees. The peak in the curve does not occur at 180 degrees because of the interactions of the tail rotor flow and the free stream inflow compounded by the presence of the ground vortex.

Figure 52 shows the variation in boom side force coefficient over the range of azimuths tested. In the region between ± 50 degrees the boom side force exhibits a flat variation with wind azimuth. At ± 50 degrees the boom breaks out of the main rotor wake and experiences a sharp increase in magnitude. This trend prevails out to ± 90 degrees. The essentially constant offset between the two curves indicates that the boom force is directly proportional to the tail rotor thrust. This is another indication that the tail rotor flow depressurizes the nearby surfaces of the fuselage, as was suggested in Reference 2.

Figure 53 shows the variation in empennage normal force for various yaw conditions. The empennage vertical force has been normalized by main rotor thrust. The empennage lift is positive for most wind azimuths due to the high incidence angle of 45 degrees set on the horizontal stabilizer. Figure 53 shows that significant variations in empennage loads also occur at ± 50 degrees due to the main rotor tip vortices. Finally, the effects of tail rotor thrust are significant only in the regime between ± 50 degrees. The tail rotor flow is apparently affecting the main rotor wake that impinges on the empennage in this flight regime.

Effects of Airspeed and Tail Rotor Thrust

The effects of flight speed and tail rotor thrust on the vertical fin side force and the empennage vertical lift are presented in this section. A comprehensive set of parametric variations was conducted at the four principal azimuths of 0, -90, 180 and +90 degrees.

$\psi = 0^\circ$: Figures 54 and 55 present the fin force coefficient and the nondimensional empennage vertical lift data for the forward flight case. Several aspects regarding the effects of main rotor wake as well as the effects of tail rotor thrust on empennage loads can be discerned from these figures. For example, the side force and lift data for all three levels of tail rotor thrust exhibit a flat variation with airspeed below a nondimensional speed of 1.0. Above this speed both side force and lift grow almost linearly with airspeed. From the results presented in the main rotor/tail rotor discussions, this variation in empennage loads must be associated with the passage of the ground vortex.

Below a nondimensional airspeed of 1.0, the data in Figures 54 and 55 indicate that there is little variation in either the lateral or vertical average velocity component of the main rotor wake in the vicinity of the empennage. Above this speed the main rotor wake blows back and under the model, as evidenced by the disappearance of the ground vortex, and the flow near the empennage is no longer insensitive to variations in airspeed.

The tail-rotor-off data in Figures 54 and 55 shows the effects of main rotor wake on empennage loads as a function of airspeed without the added flow complexity of the tail rotor. Both parameters have a residual positive value for low speeds (below $V/V_I = 1.0$). The positive fin force indicates that a lateral flow component, swirl, exists at the empennage; the positive lift force results from the horizontal stabilizer being set at an incidence angle of 45 degrees. For speeds above 1.0 the fin side force becomes increasingly positive,

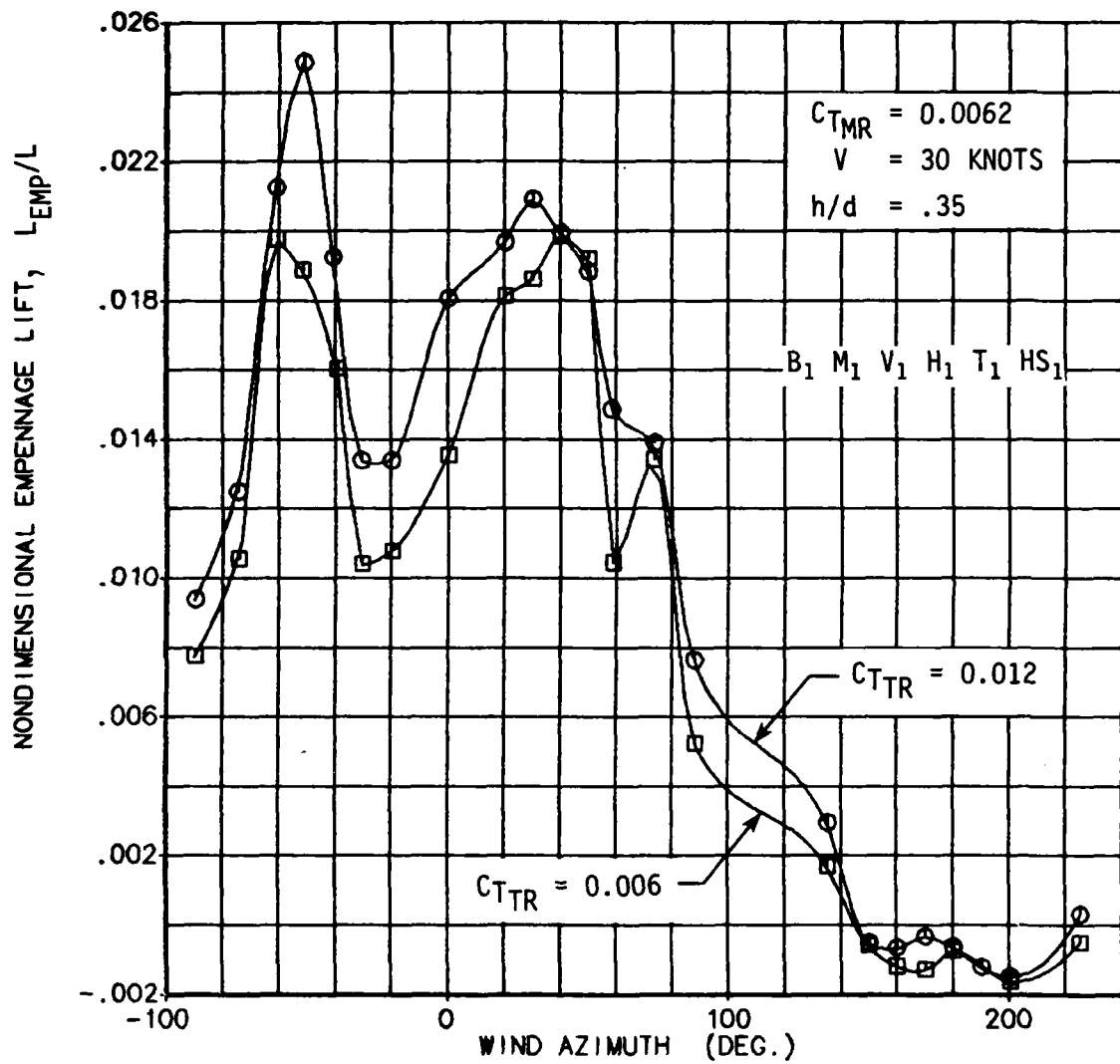


FIGURE 53. EFFECTS OF WIND AZIMUTH AND TAIL ROTOR THRUST ON NONDIMENSIONAL EMPENNAGE LIFT.

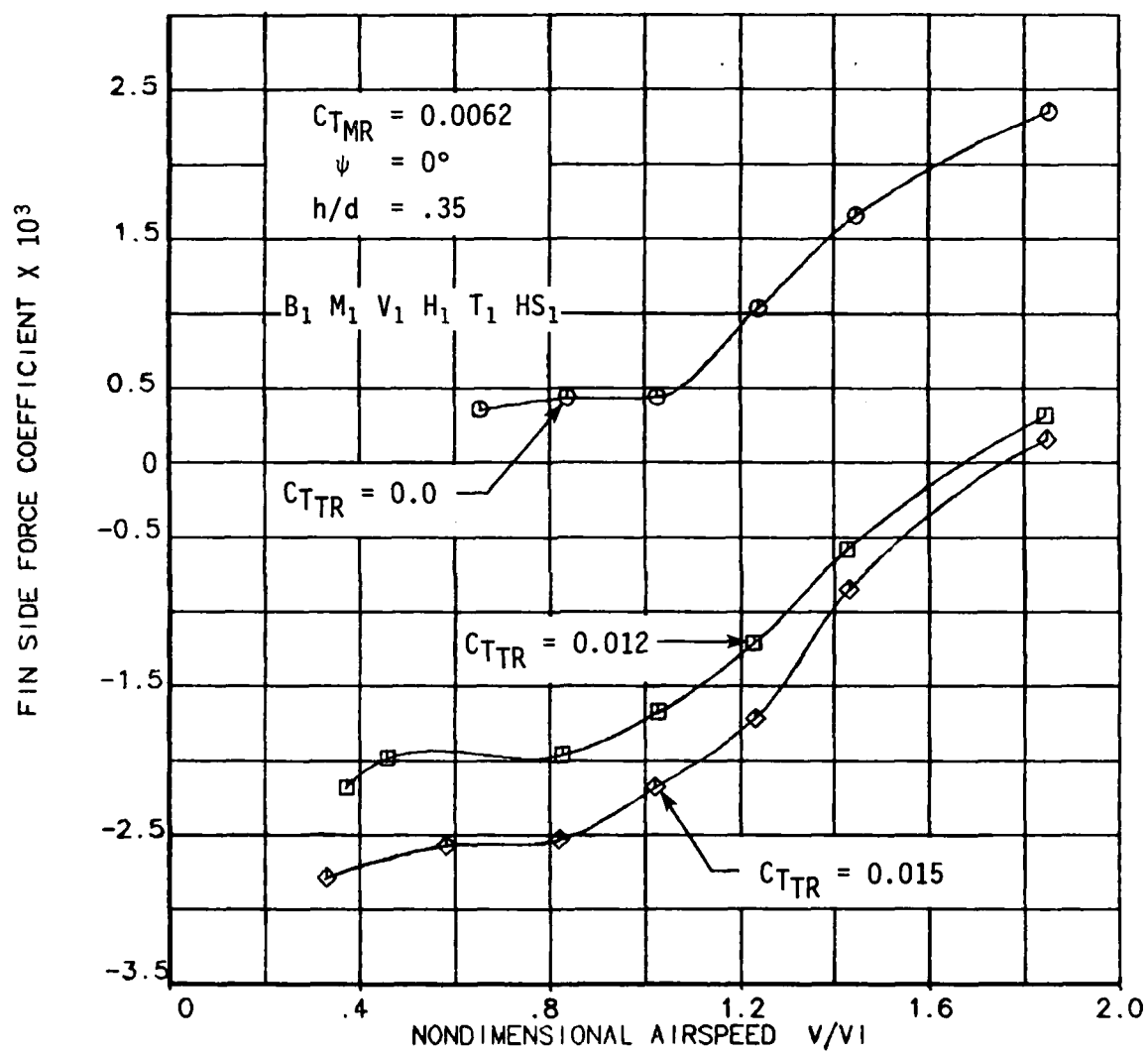


FIGURE 54. EFFECTS OF AIRSPEED AND TAIL ROTOR THRUST ON FIN SIDE FORCE COEFFICIENT FOR $\psi = 0^\circ$.

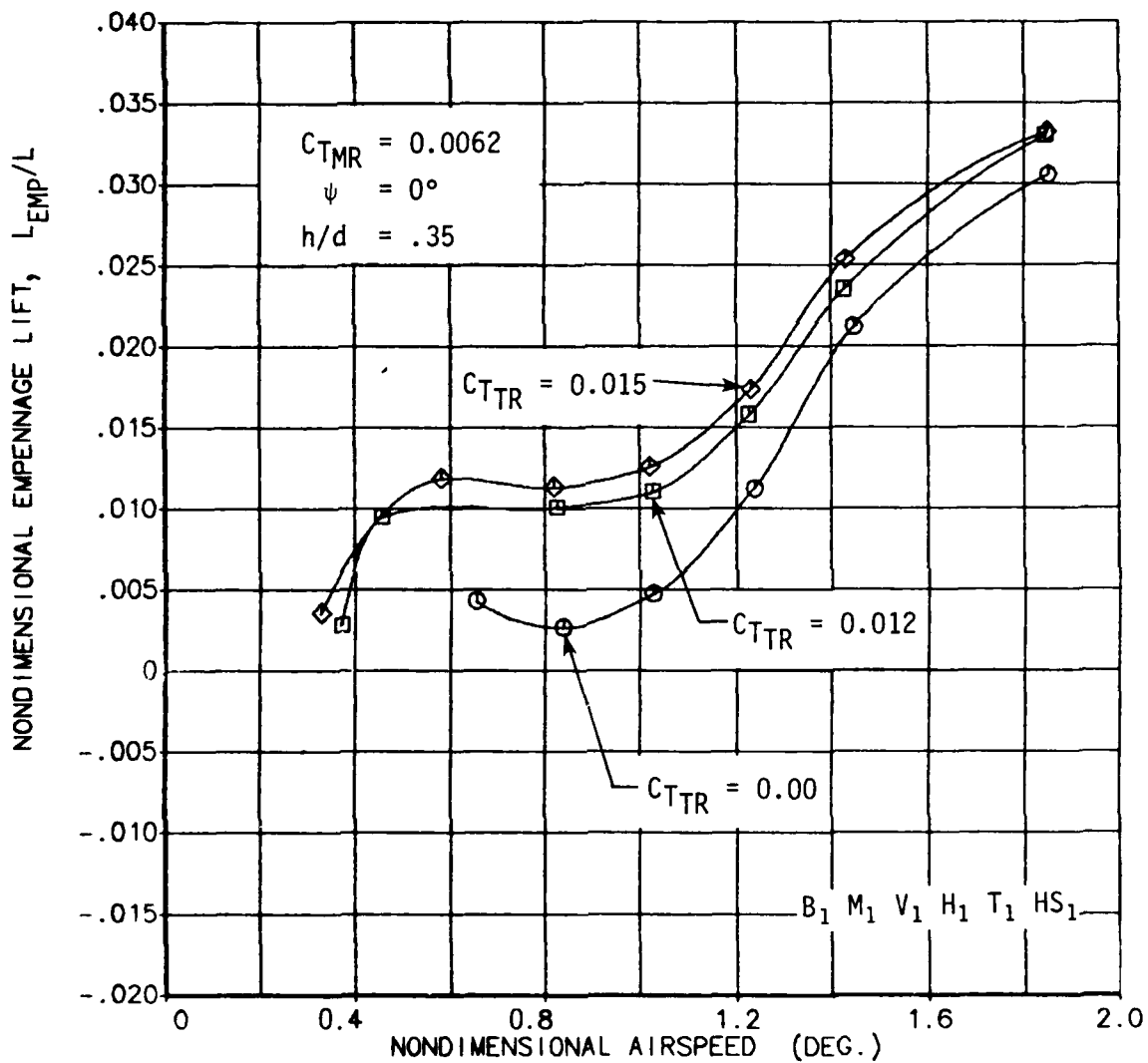


FIGURE 55. EFFECTS OF AIRSPEED AND TAIL ROTOR THRUST ON NONDIMENSIONAL EMPENNAGE LIFT AT $\psi = 0^\circ$.

indicating that the lateral flow component is increasing with airspeed. Similarly, the empennage lift grows with airspeed as the main rotor wake is blown back by the free stream flow.

By comparison, the tail-rotor-on condition results in a large adverse fin force at low speeds. Similarly, a slight increase in empennage lift ensues with tail rotor thrust increased from zero. However, the same variation with airspeed is exhibited for the tail-rotor-on case as for the tail-rotor-off condition. The result is a tendency for adverse fin force to diminish with increasing airspeed while empennage lift continues to increase with airspeed above 1.0. In summary, at any given speed the adverse fin force and empennage lift is approximately proportional to tail rotor thrust for the forward flight condition.

$\psi = -90^\circ$: The variations in fin side force and empennage lift with changes in right sideward velocity and tail rotor thrust are shown in Figures 56 and 57. Adverse fin force persists at all speeds and is aggravated by tail rotor thrust, as would be expected. The passage of the main rotor wake and the ground vortex is again evident by the variation in fin force for nondimensional airspeeds around 1.0. Similar variations in empennage lift coefficient are shown in Figure 57.

$\psi = 180^\circ$: The effects of airspeed and tail rotor thrust on empennage loads for rearward flight are given in Figures 58 and 59. The fin side force coefficient is very small for the tail-rotor-off condition over the full range of airspeeds tested. However, the curve does reverse signs at a nondimensional airspeed of 1.0 which, once again, is due to the ground vortex.

For the tail-rotor-on conditions the adverse fin force again grows proportionally with tail rotor thrust at any given airspeed. The effect of the ground vortex in this flight condition is to reduce the adverse fin force as airspeed is increased from hover. Apparently, the ground vortex significantly reduces the effects of tail rotor flow at a nondimensional airspeed of 0.9. For airspeeds greater than 1.2, the fin side force increases with airspeed but the magnitude of the adverse fin force is much reduced compared to the low speed condition.

Figure 59 presents the corresponding empennage lift data for rearward flight. Below a nondimensional airspeed of 1.2, the empennage lift appears to increase proportionally with tail rotor thrust at a given airspeed. Above an airspeed of 1.2, though, the effects of tail rotor thrust are nonexistent. Evidently, at sufficiently high airspeeds the free stream

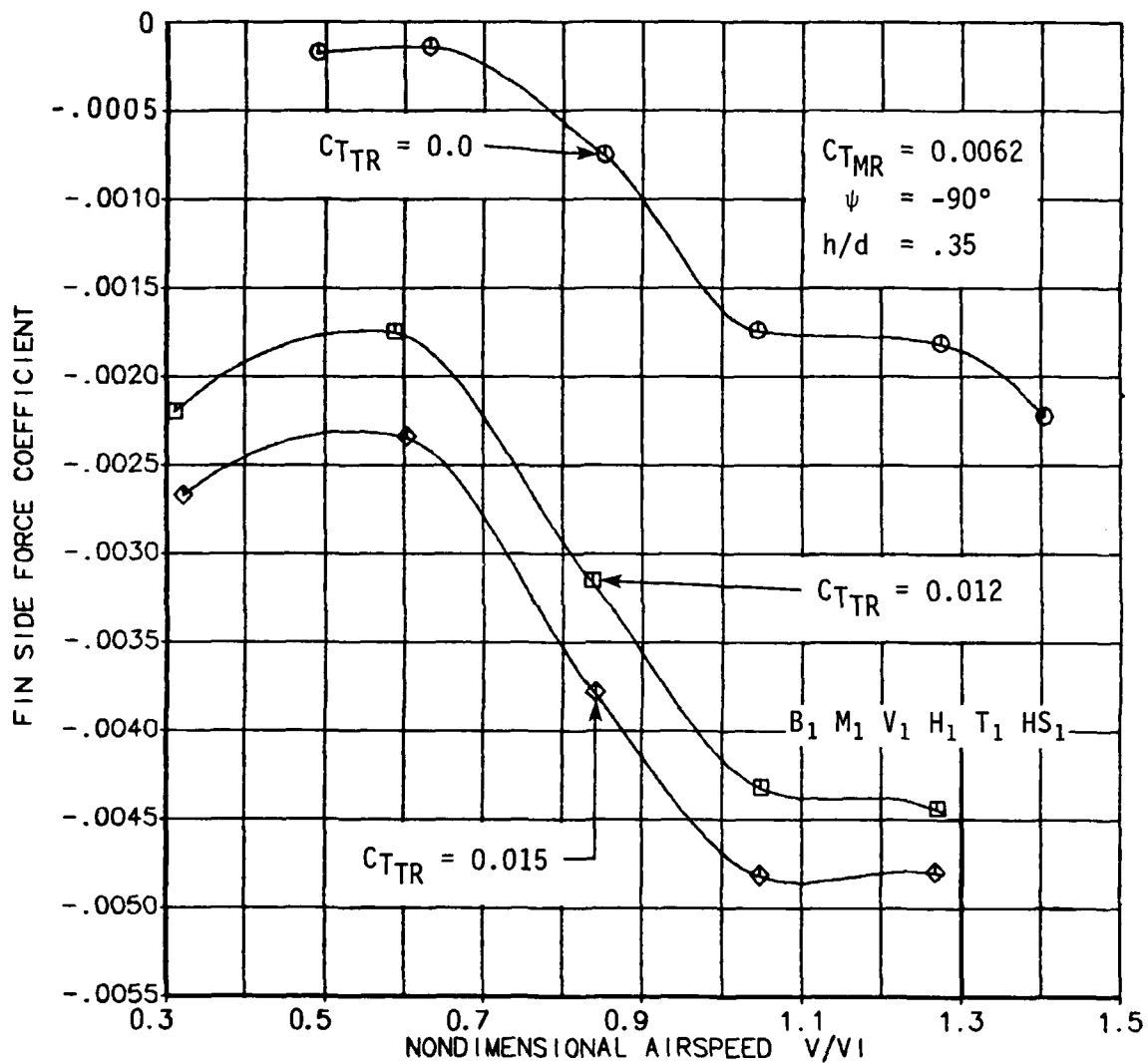


FIGURE 56. EFFECTS OF AIRSPEED AND TAIL ROTOR THRUST ON FIN SIDE FORCE COEFFICIENT FOR $\psi = -90^\circ$.

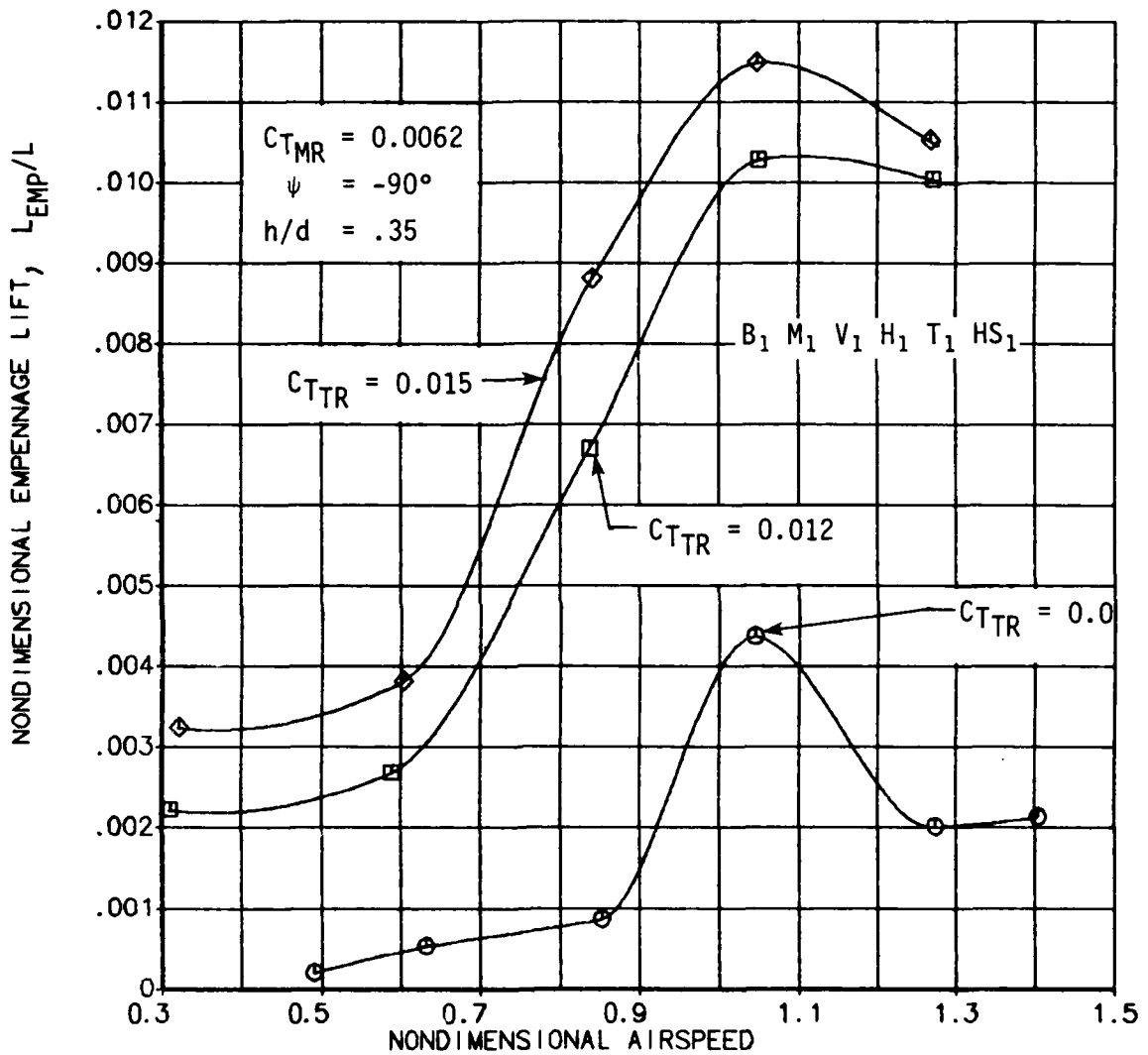


FIGURE 57. EFFECTS OF AIRSPEED AND TAIL ROTOR THRUST ON NONDIMENSIONAL EMPENNAGE LIFT AT $\psi = -90^\circ$.

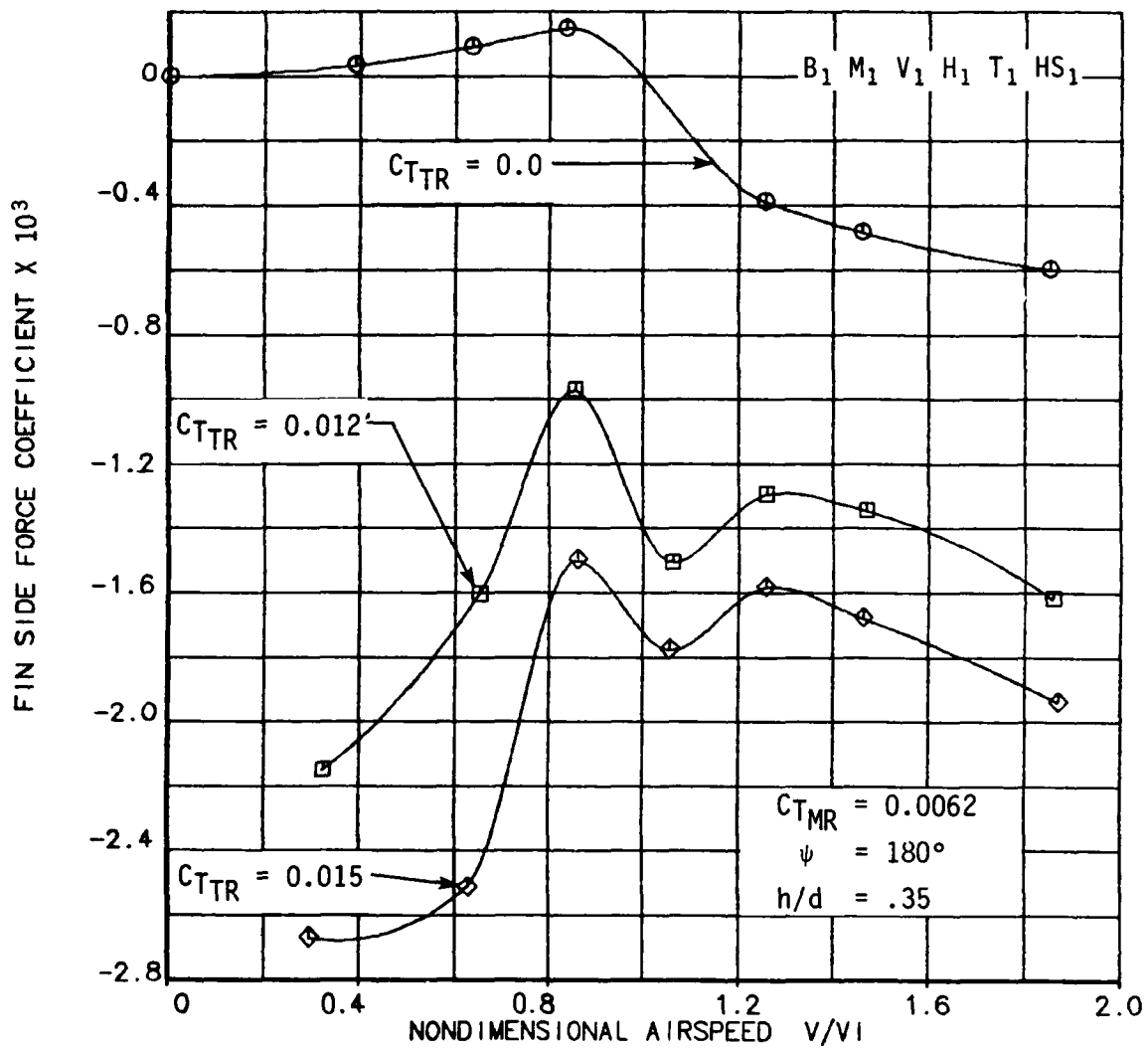


FIGURE 58. EFFECTS OF AIRSPEED AND TAIL ROTOR THRUST ON FIN SIDE FORCE COEFFICIENT FOR $\psi = 180^\circ$.

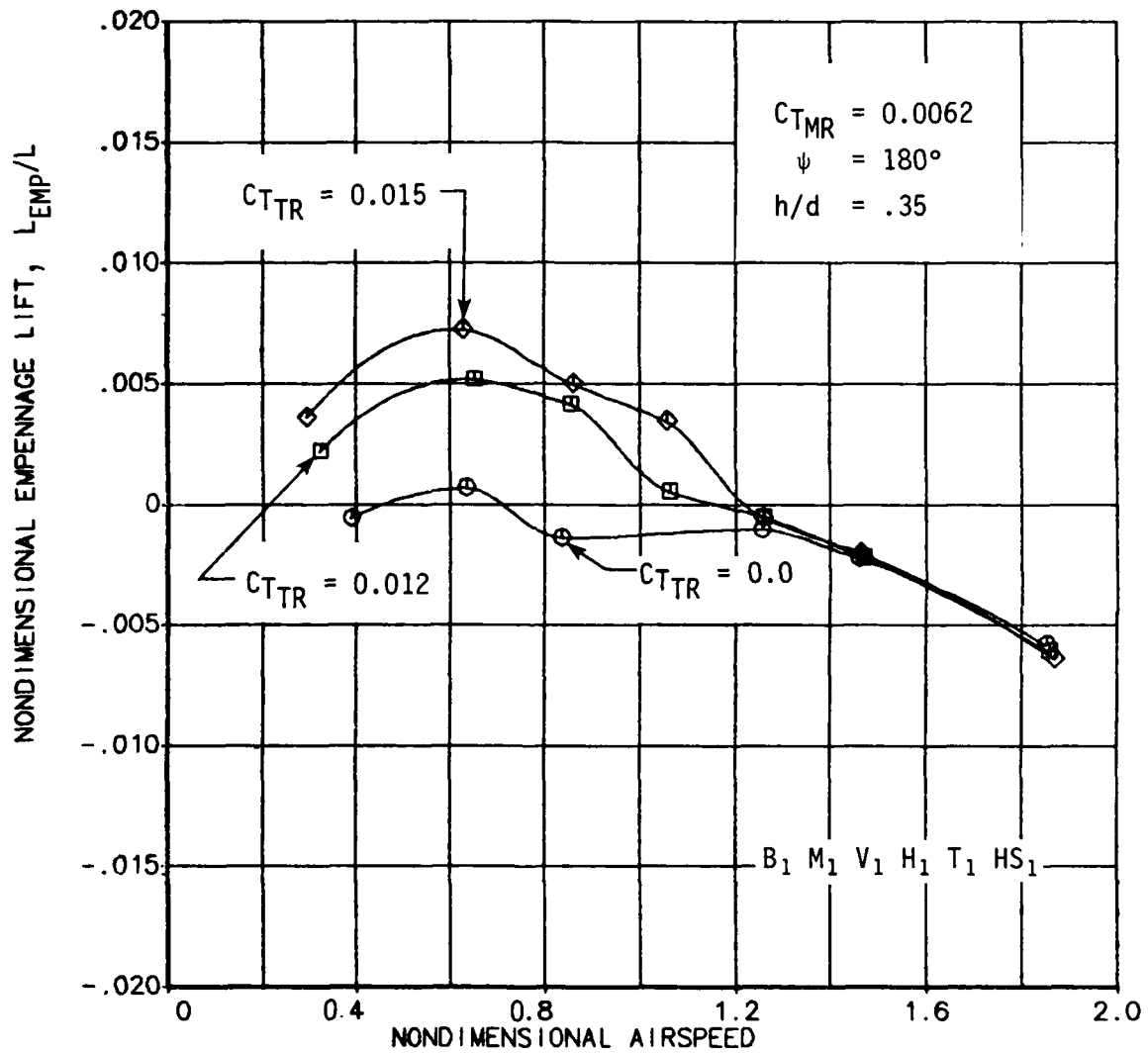


FIGURE 59. EFFECTS OF AIRSPEED AND TAIL ROTOR THRUST ON NONDIMENSIONAL EMPENNAGE LIFT AT $\psi = 180^\circ$.

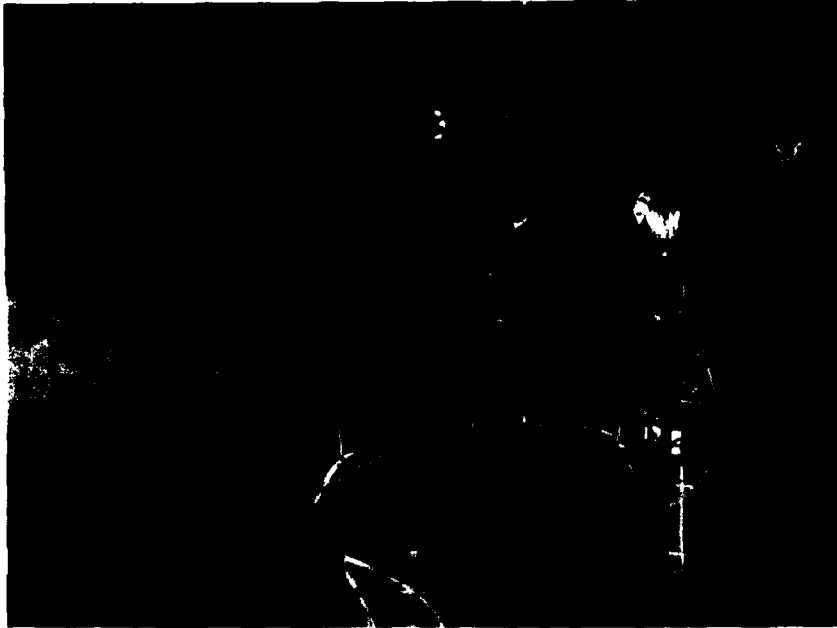
flow dominates the tail rotor flow near the horizontal stabilizer, which clearly is the component that produces the most lift for the empennage in any flight condition. The fact that the empennage lift coefficient is negative beyond an airspeed of 1.2 confirms that the main rotor wake has moved away from the empennage and the empennage is now in "clean" air. Figure 60 shows the fin tuft formation for two tail rotor thrust loadings at a wind azimuth of 170 degrees. The flight speed is 30 knots or $V/VI=1.23$ and the photographs show little variation in the fin tuft patterns for the two tail rotor loading conditions.

$\psi = 90^\circ$: The final condition for which the effects of airspeed and tail rotor thrust on empennage loads was studied is presented in Figures 61 and 62. For sideward flight to the left the ground vortex apparently has a significant effect on fin side force in the range of nondimensional airspeeds between 0.8 and 1.4. For low speeds the adverse fin force increases with tail rotor thrust. The onset of the ground vortex at an airspeed of 0.8 tends to reduce the adverse fin force.

At an airspeed of 1.2 the ground vortex has its maximum effect on reducing the adverse fin force. In addition, at this airspeed the sensitivity of fin force to changes in tail rotor thrust has been greatly diminished. The fin force for the tail-rotor-on condition approaches the value obtained for the tail-rotor-off condition at an airspeed of 1.2. This clearly indicates the dominance of the ground vortex over the tail rotor flow near the vertical fin.

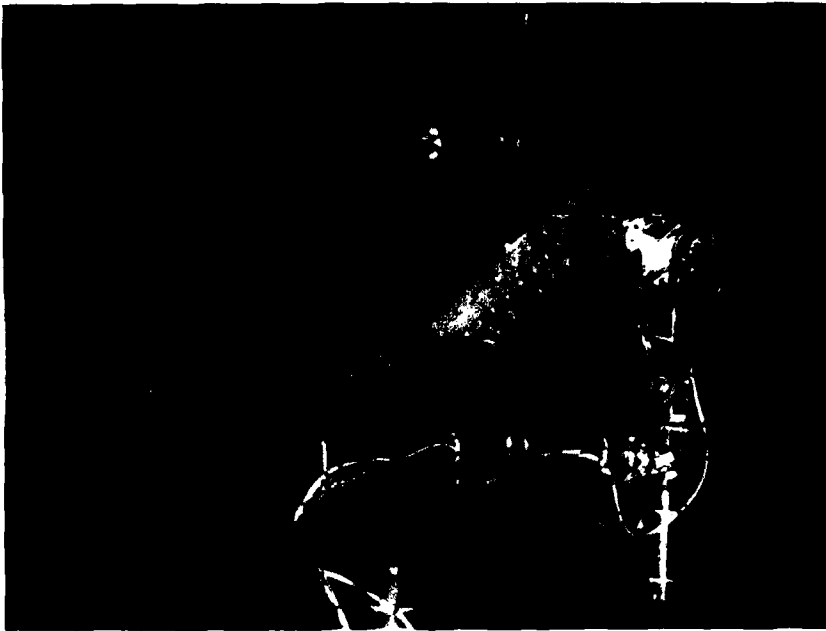
The variations in empennage lift force for sideward flight to the left are shown in Figure 62. For all three levels of tail rotor thrust the nondimensional empennage lift starts at a low positive value at low airspeeds. As airspeed is increased, the empennage vertical force also increases to its maximum near 1.2 nondimensional airspeed. For higher airspeeds the empennage lift force diminishes toward zero. The tail rotor thrust tends to increase the empennage lift in a positive sense at all airspeeds.

Figures 63 and 64 show the relative magnitude of the fin side force and empennage lift for the nominal tail rotor thrust condition at the four principal wind azimuths. At a nondimensional airspeed of 0.3 the four curves come together for both fin side force and empennage lift. At low speeds where the main rotor wake is nearly symmetrical around the azimuth, this result can be expected. However, the curves diverge very quickly as airspeed is increased. In Figure 63 the ground vortex has the most influence on fin force for the +90 and -90 degree yaw conditions. As expected, the greatest



a. $C_{TMR} = 0.0062$
 $C_{TR} = 0.006$

16
F



b. $C_{TMR} = 0.0062$
 $C_{TR} = 0.012$

FIGURE 60. FIN TUFT PATTERNS AT $\psi = 170^\circ$, $V = 30$ KNOTS.

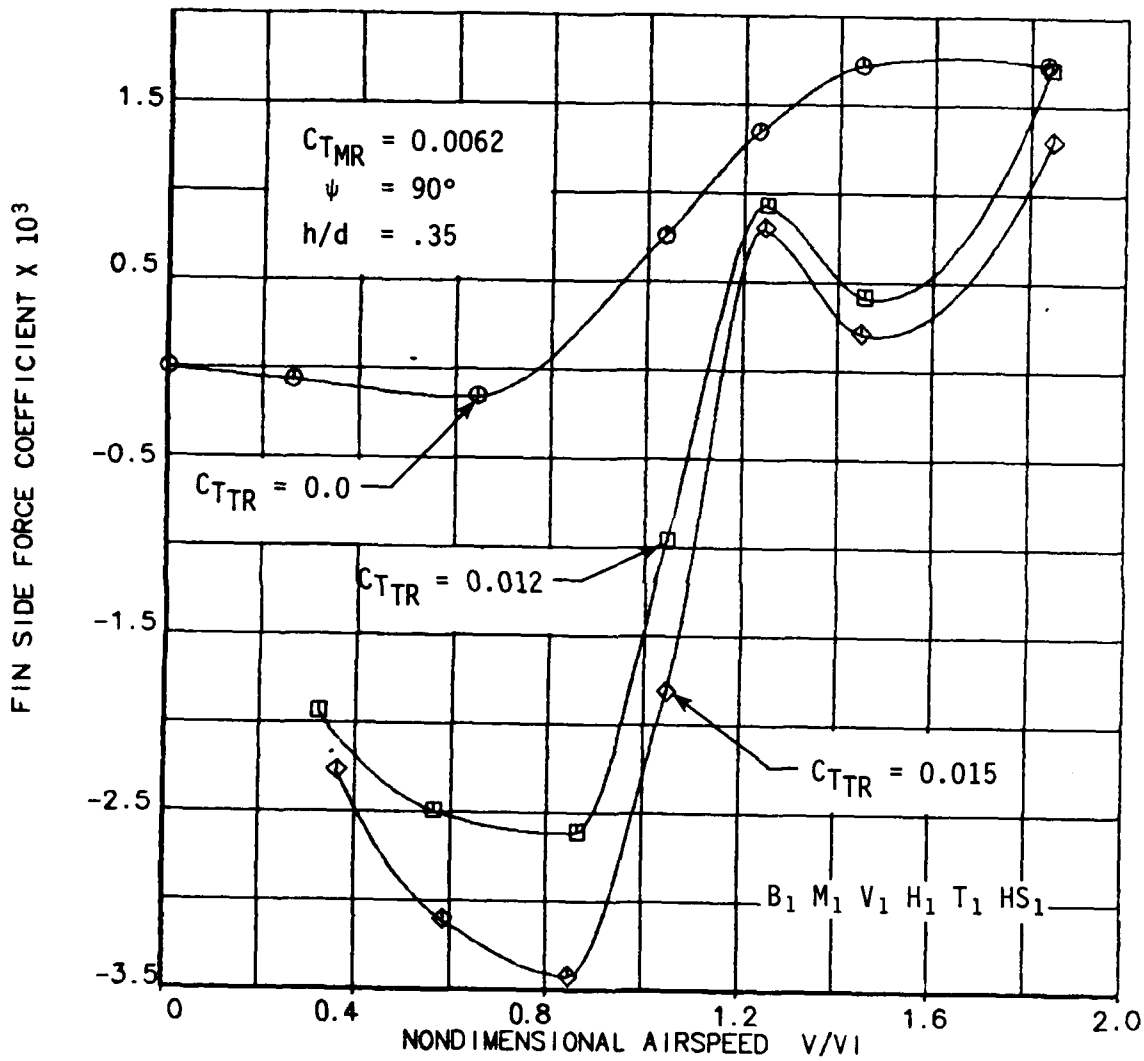


FIGURE 61. EFFECTS OF AIRSPEED AND TAIL ROTOR THRUST ON FIN SIDE FORCE COEFFICIENT FOR $\psi = 90^\circ$.

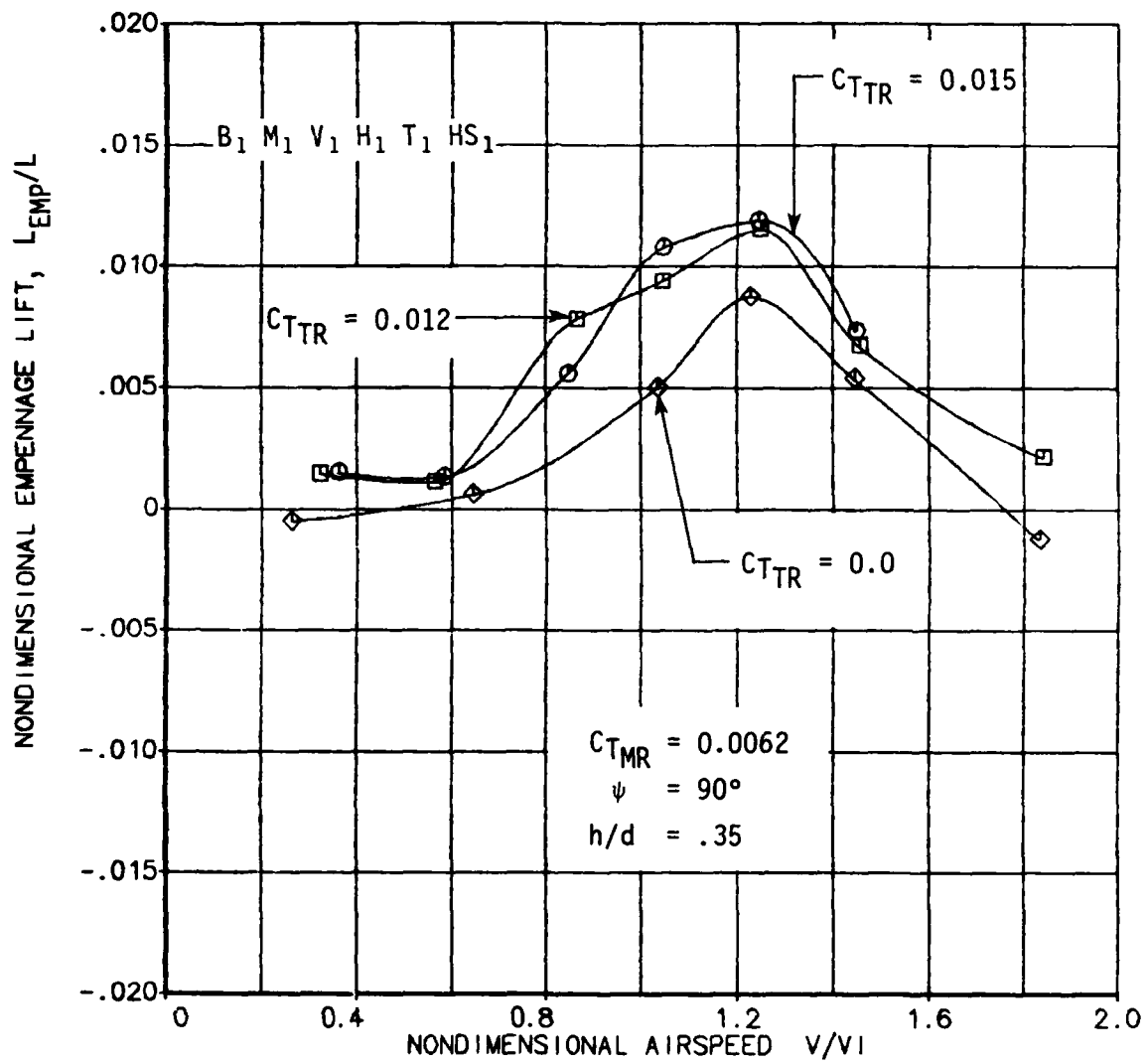


FIGURE 62. EFFECTS OF AIRSPEED AND TAIL ROTOR THRUST ON NONDIMENSIONAL EMPENNAGE LIFT AT $\psi = 90^\circ$.

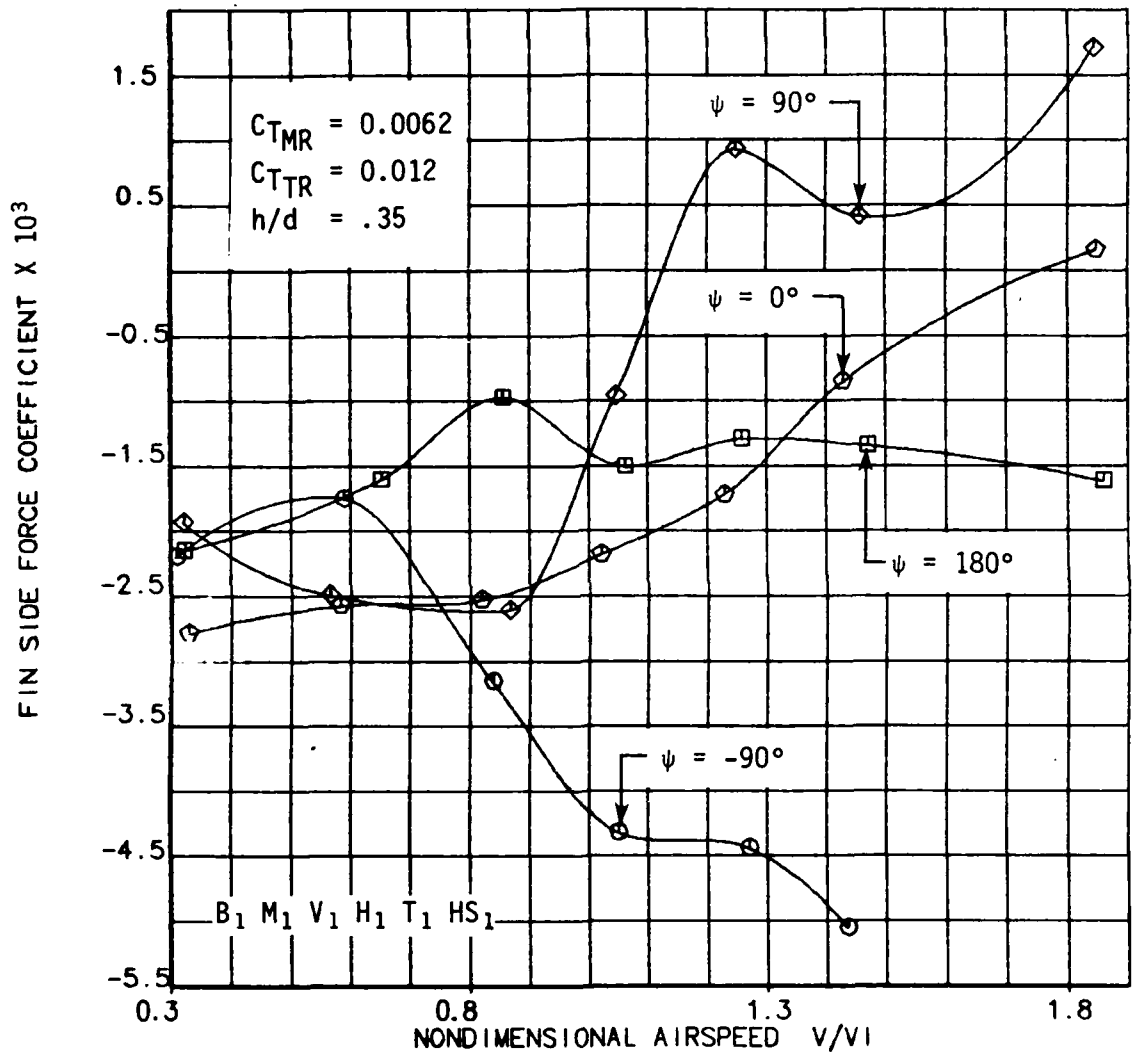


FIGURE 63. EFFECTS OF AIRSPEED AND WIND AZIMUTH ON FIN SIDE FORCE COEFFICIENT.

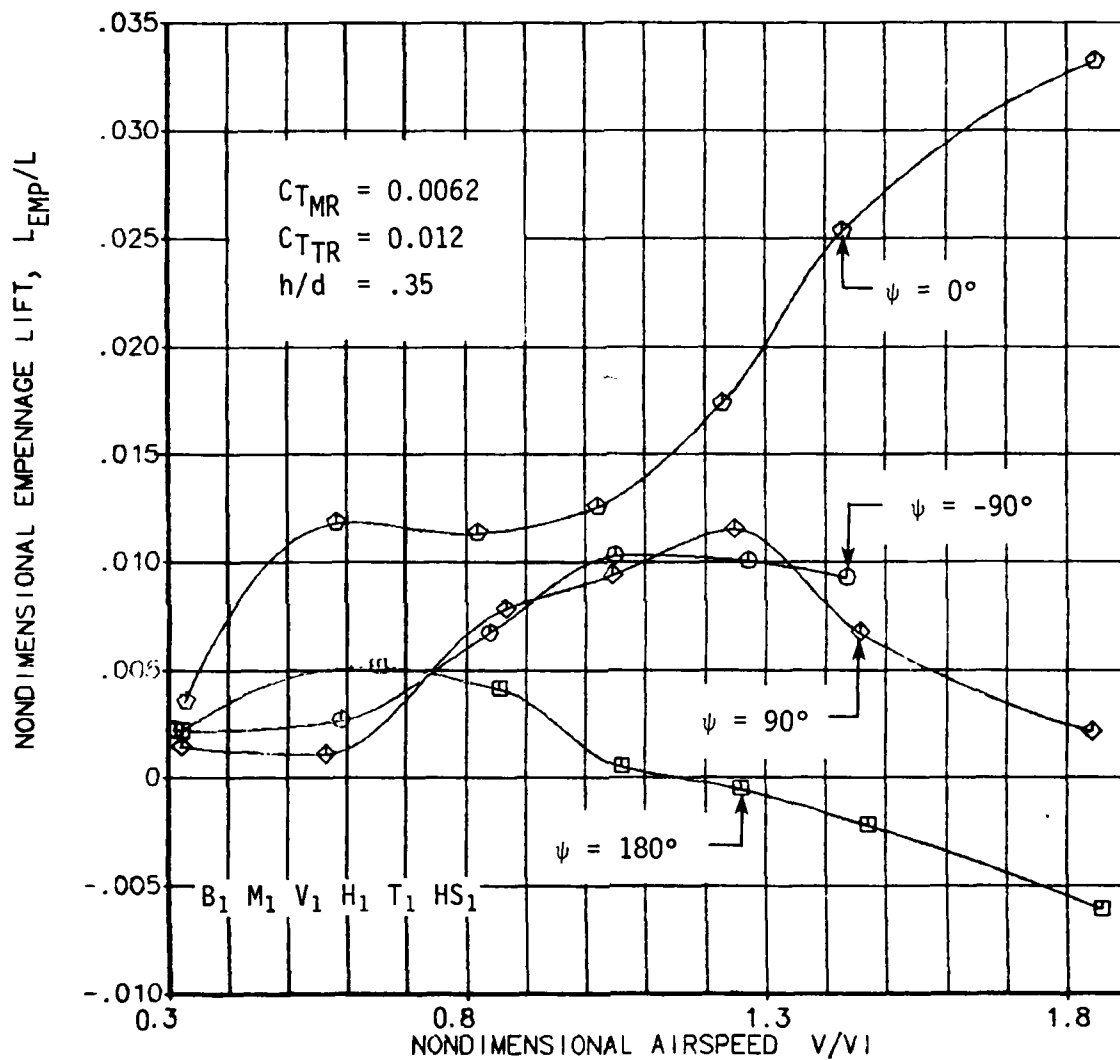


FIGURE 64. EFFECTS OF AIRSPEED AND WIND AZIMUTH ON NONDIMENSIONAL EMPENNAGE LIFT.

adverse fin force occurs in right sideward flight. On the other hand, the fin force becomes beneficial at higher speeds in left sideward flight and aids the tail rotor in maintaining directional trim.

Effects of Airspeed and Fin Size

Figures 65 and 66 show the effects of varying fin size on fin side force and empennage lift. The effects of fin size were not studied in References 2, 3 and 4. The flight condition represented in Figures 65 and 66 is right sideward flight ($\psi = -90^\circ$) at nominal main rotor ($C_{T_{MR}} = 0.0062$) and tail rotor ($C_{T_{TR}} = 0.012$) thrusts.

At all airspeeds the fin side force coefficient for the smaller fin is lower, as expected, and goes to zero for a fin-off configuration. The very low level of fin force registered in Figure 65 for the fin-removed case indicates the effects of airspeed on the exposed fin balance.

The variation in fin force with airspeed is very similar for both the 25% and 35% fins. The difference in these two curves at 0.6 nondimensional airspeed is uncertain due to the lack of a data point for the 25% fin configuration. However, the general character is the same for both curves. The effects of the ground vortex are diminished at an airspeed of 1.2 for both curves, indicating that the small variation in fin size studied does not have a significant effect on the main rotor/tail rotor/ground vortex interactions for $\psi = -90$ degrees.

Figure 66 shows the effect that fin size has on the vertical force generated by the empennage. Apparently the presence of the fin has a significant effect on the flow characteristics around the entire empennage. The precise mechanism through which the empennage force is influenced for different fin sizes is unknown.

Effects of Rotor Height Above the Ground

$\psi = 0^\circ$: Figure 67 shows the effects of ground proximity on fin side force coefficient in forward flight. Data for both tail-rotor-on ($C_{T_{TR}} = 0.012$) and tail-rotor-off ($C_{T_{TR}} = 0.0$) conditions is included in Figure 67. For both tail rotor thrusts the most striking feature is the different response to changes in airspeed for the two rotor heights that were tested. In the region where the low altitude data exhibited a flat variation with airspeed, the higher altitude case is varying almost linearly with airspeed. The variation has approximately the same slope as that displayed by the low

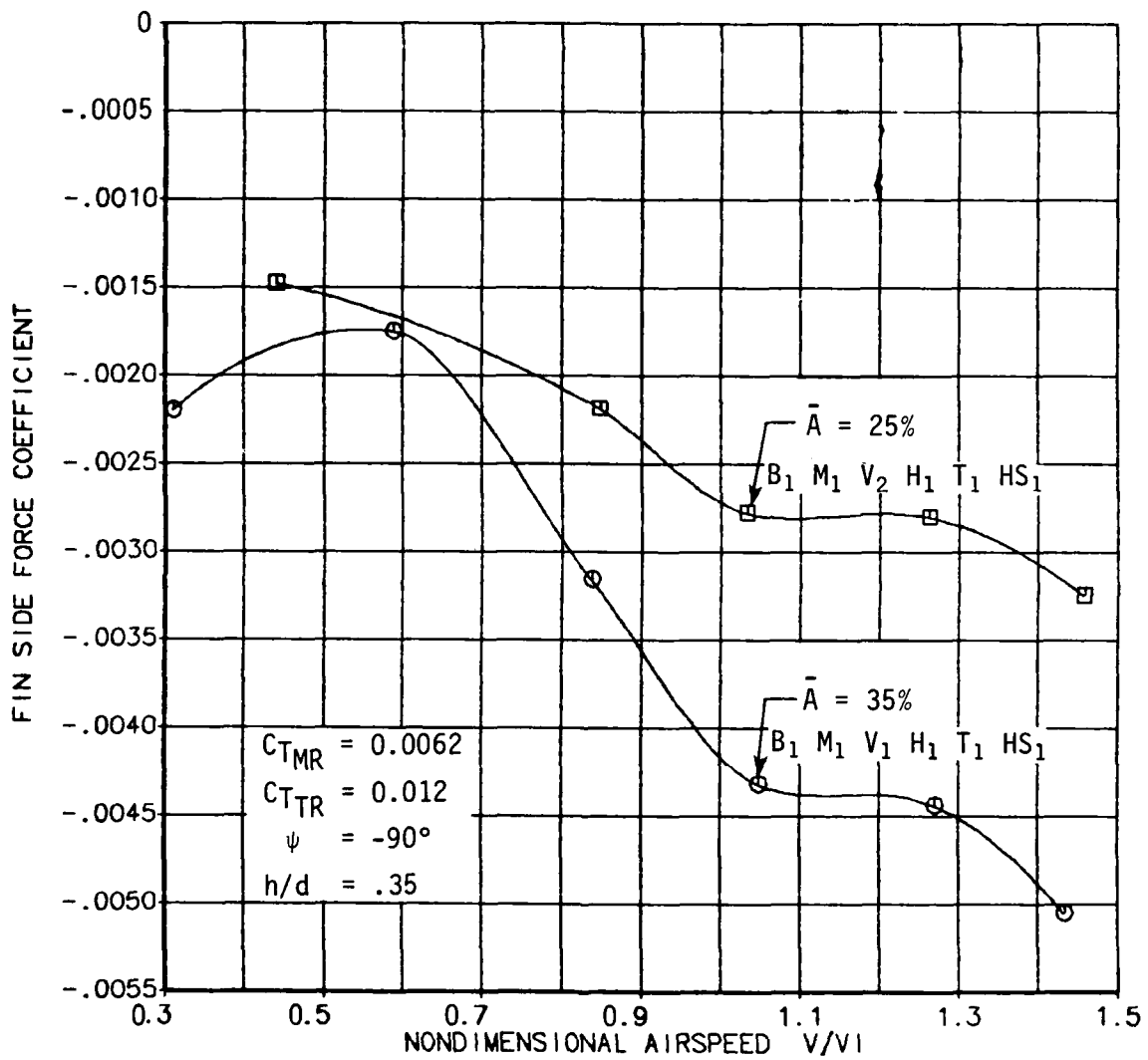


FIGURE 65. EFFECTS OF AIRSPEED AND FIN SIZE ON FIN SIDE FORCE COEFFICIENT FOR $\psi = -90^\circ$.

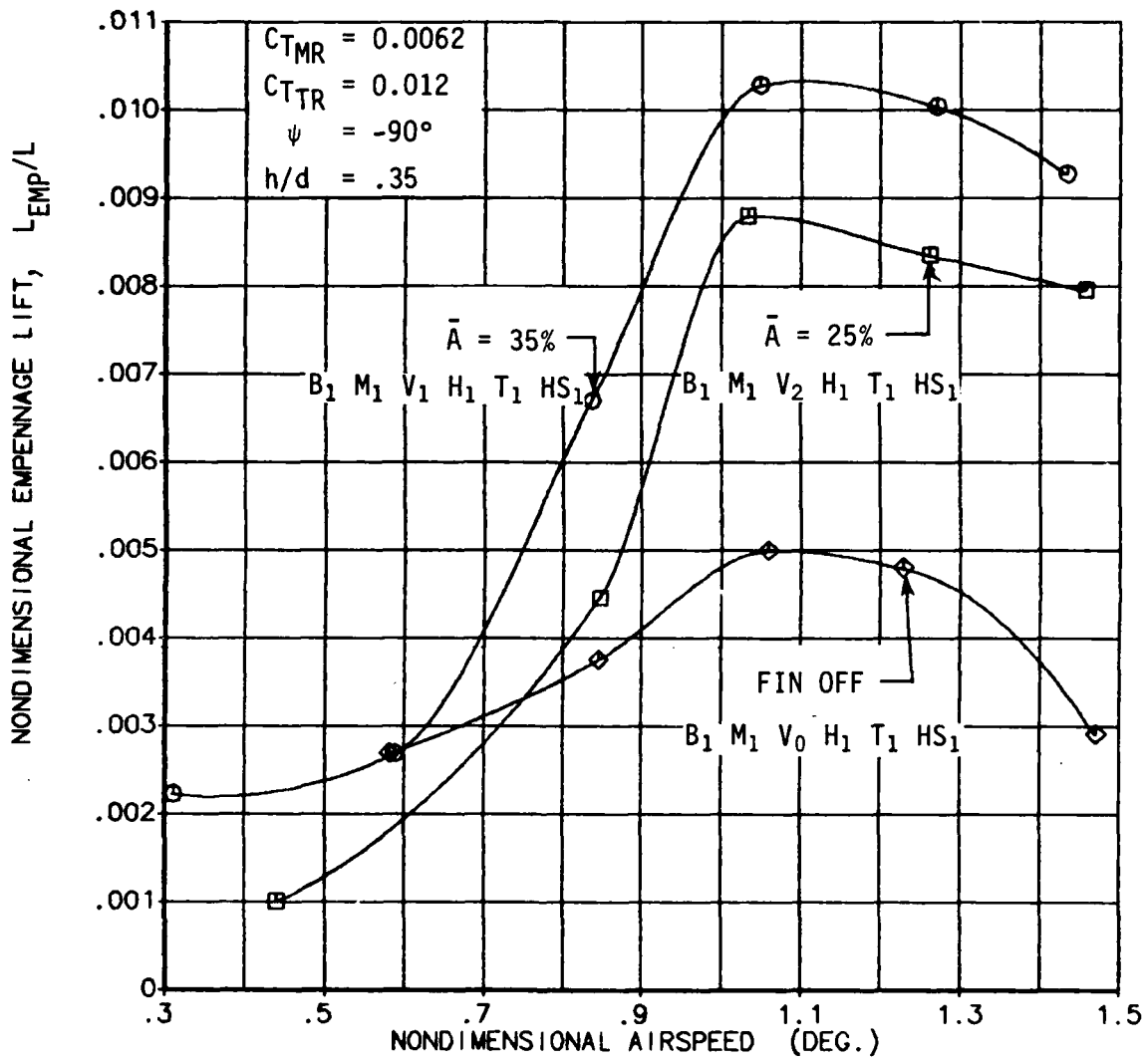


FIGURE 66. EFFECTS OF AIRSPEED AND FIN SIZE ON NONDIMENSIONAL EMPENNAGE LIFT FOR $\psi = -90^\circ$.

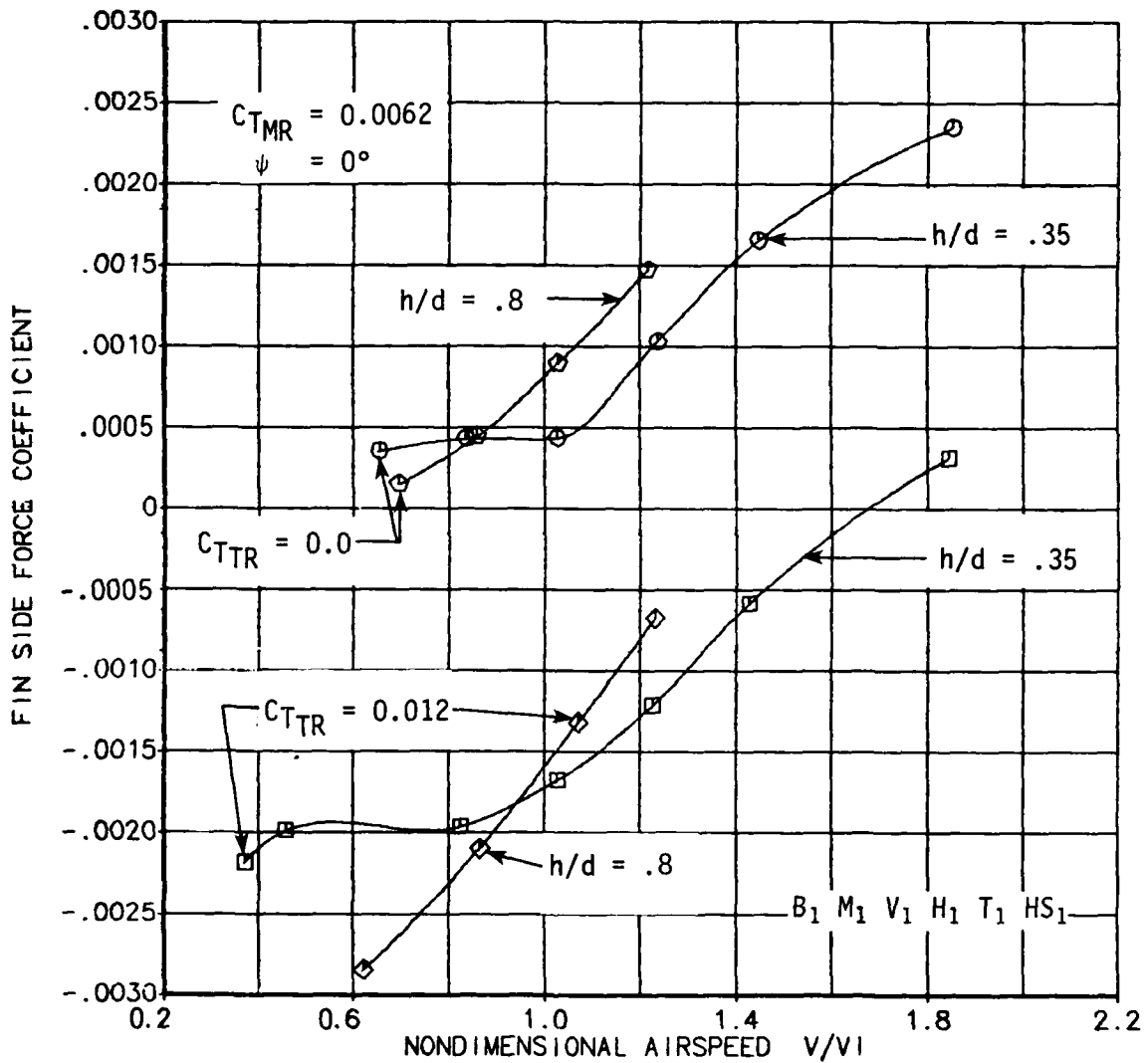


FIGURE 67. EFFECTS OF AIRSPEED AND HEIGHT ABOVE THE GROUND ON FIN SIDE FORCE COEFFICIENT FOR $\psi = 0^\circ$.

altitude configuration for nondimensional airspeeds greater than 1.0.

Apparently, for the higher altitude, the variation in airspeed has a significant effect on the lateral flow at the empennage due to the main rotor wake in the range of speeds dominated by the ground vortex flow at the lower altitude. The effects of the ground vortex on rotor loads were reported to diminish rapidly with increasing altitude in Reference 7. Figure 67 indicates that the wake effects on the empennage also change significantly as the model height is increased.

$\psi = -90^\circ$: Figure 68 is also a plot of fin side force coefficient for the two model heights tested but for a right sideward flight condition. Included in Figure 68 is data for tail-rotor-on and tail-rotor-off conditions at the nominal main rotor thrust condition. For the high altitude condition the adverse fin force builds up with airspeed in the same general way as it did for the baseline condition in Figure 67.

The curve of fin side force coefficient for tail-rotor-off at the higher altitude condition indicates that the main rotor wake, particularly the ground vortex, has its maximum effect at a nondimensional airspeed of 0.85 compared to the value of 1.0 for the low altitude condition. The passage of the ground vortex at lower airspeeds for higher rotor heights agrees with the experimental results presented in Reference 7. In Figure 68 this dependence on height above the ground results in a more rapid buildup of adverse fin force with airspeed for the $h/d = .8$ case at both levels of tail rotor thrust. Beyond a nondimensional airspeed of 1.2 the fin side force coefficient is coincident for the two model heights at the two tail rotor thrust conditions. For these speeds the main rotor wake is blown aft of the tail rotor and empennage system and only the effects of free stream flow are reflected in the fin loads.

Effects of Tail Rotor Placement

Tail rotor placement is a key design variable in the study of main rotor/tail rotor/fin interactions. The extent to which the fin can shield the tail rotor from the main rotor wake, particularly the rotor tip and ground vortices, in right side-

-
7. Curtiss, H.C., Sun, M., Putman, W.F., and Hanker, E. J., "Rotor Aerodynamics in Ground Effect at Low Advance Ratios", Paper presented at the 37th Annual Forum of the American Helicopter Society, New Orleans, La., May 1981.

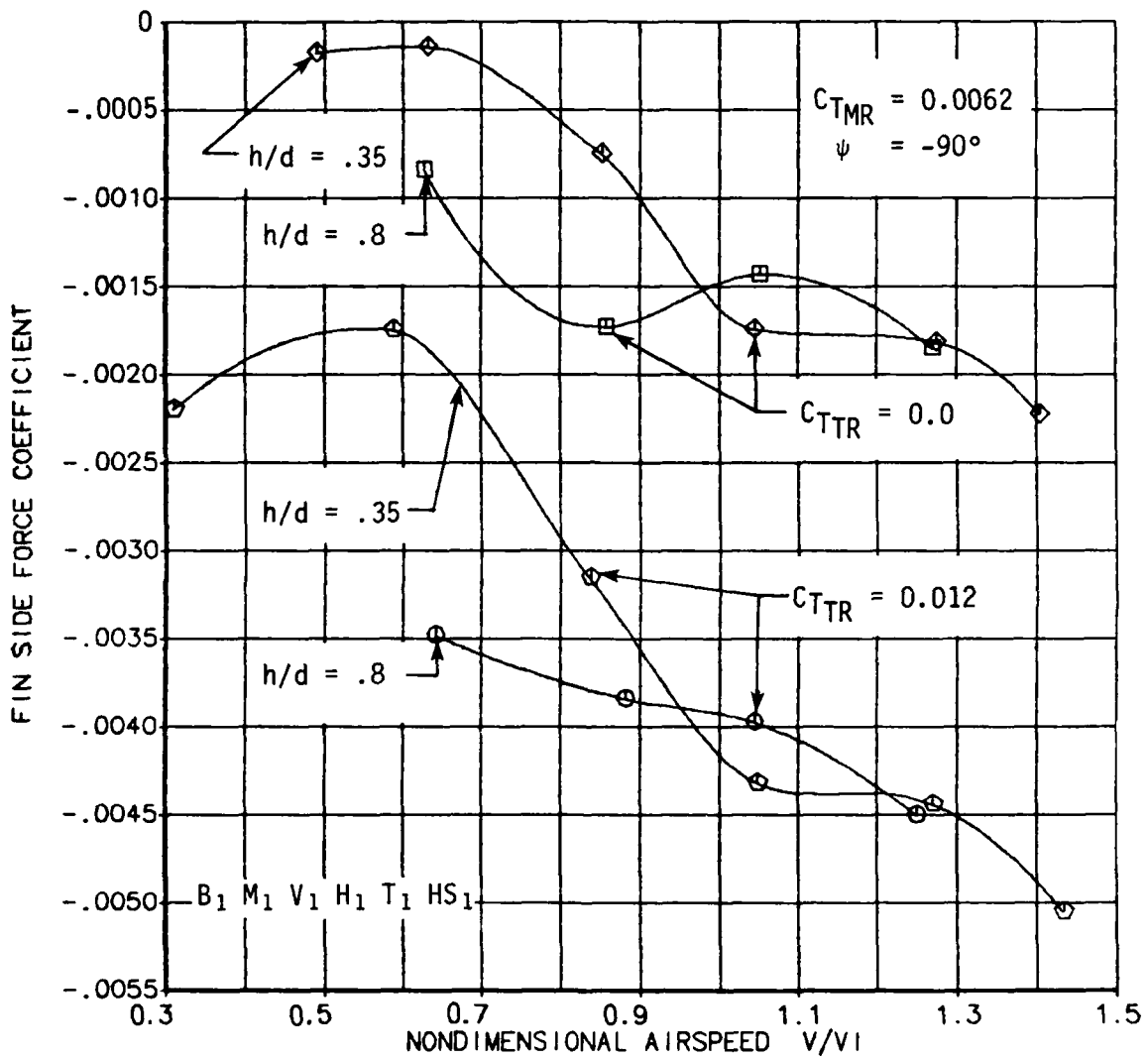


FIGURE 68. EFFECTS OF AIRSPEED AND HEIGHT ABOVE THE GROUND ON FIN SIDE FORCE COEFFICIENT FOR $\psi = -90^\circ$.

slip conditions is directly related to the configuration of the empennage. Moreover, the degree to which the fin blocks the inflow to the tail rotor in all flight conditions is also dependent on tail rotor placement. Finally, the generation of adverse fin side force is directly related to the position of the tail rotor relative to the fin.

For the pusher tail rotor configuration the inflow to the tail rotor causes a negative pressurization on the near side of the fin. This negative pressurization will be affected by the flow distribution across the tail rotor disk. Near the tips of the tail rotor the inflow will be greatest and the adverse pressurization will be high. Near the tail rotor centerline the inflow is negligible and the pressurization will be very low. So for conditions of equal blockage ratio the tail rotor position that exposes the fin to higher inflow velocities will generate a greater pressure differential across the fin, resulting in larger fin loads.

The effects of tail rotor position on the fin side force coefficient were studied for the 35-knot right sideward flight condition. Variations of the longitudinal, lateral and vertical placement of the tail rotor were investigated independently. For each location the tail rotor thrust was varied from zero to a maximum value of $C_{T_{TR}} = 0.018$. The airspeed was fixed at 35 knots to minimize effects of the ground vortex on the empennage.

Figure 69 is a plot of the fin side force coefficient for various tail rotor thrust levels with the tail rotor at its nominal position and at a location that is $.2r$ further aft, where r is the tail rotor radius. The data in Figure 69 shows that the aft tail rotor location results in a reduction in the adverse fin load due to the tail rotor flow. With all other parameters held constant both curves come together for the $C_{T_{TR}} = 0$ condition, as would be expected. As the tail rotor thrust is increased the fin load increases more rapidly for the nominal tail rotor position than for the aft position. The change in fin blockage ratio associated with this variation in tail rotor placement is a reduction from 35% to 32%. More importantly, the shift of the centerline in the aft direction moves the low velocity region of the tail rotor closer to the trailing edge of the fin. These two effects in combination resulted in the reduced fin load.

Figure 70 presents fin side force data for various tail rotor thrust conditions with the lateral position of the tail rotor being varied. With the lateral movement of the tail rotor, the fin blockage ratio does not change. However, the pressurization of the fin due to proximity to the tail rotor does

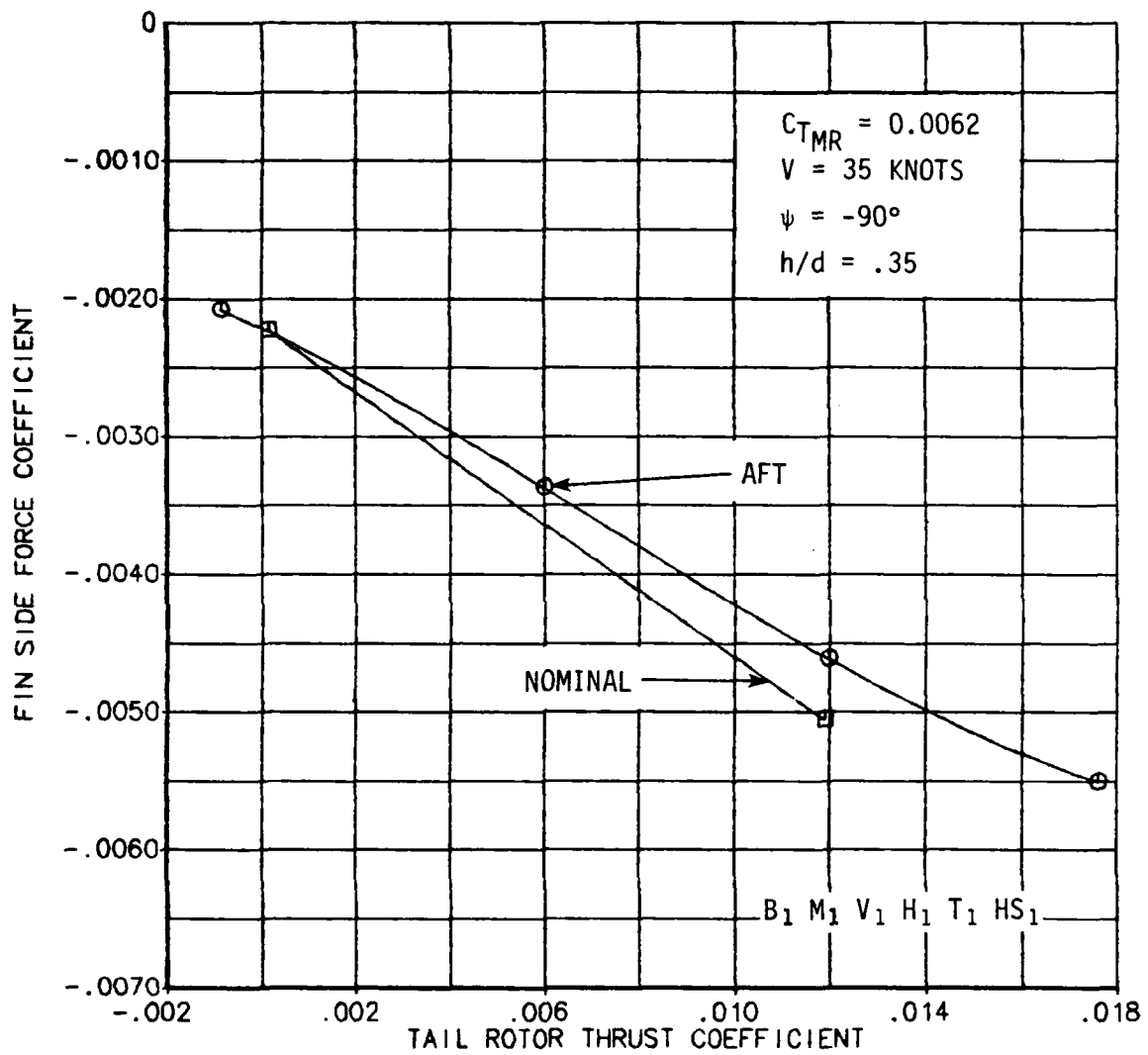


FIGURE 69. EFFECT OF TAIL ROTOR LONGITUDINAL PLACEMENT ON FIN SIDE FORCE COEFFICIENT IN RIGHT SIDEWARD FLIGHT.

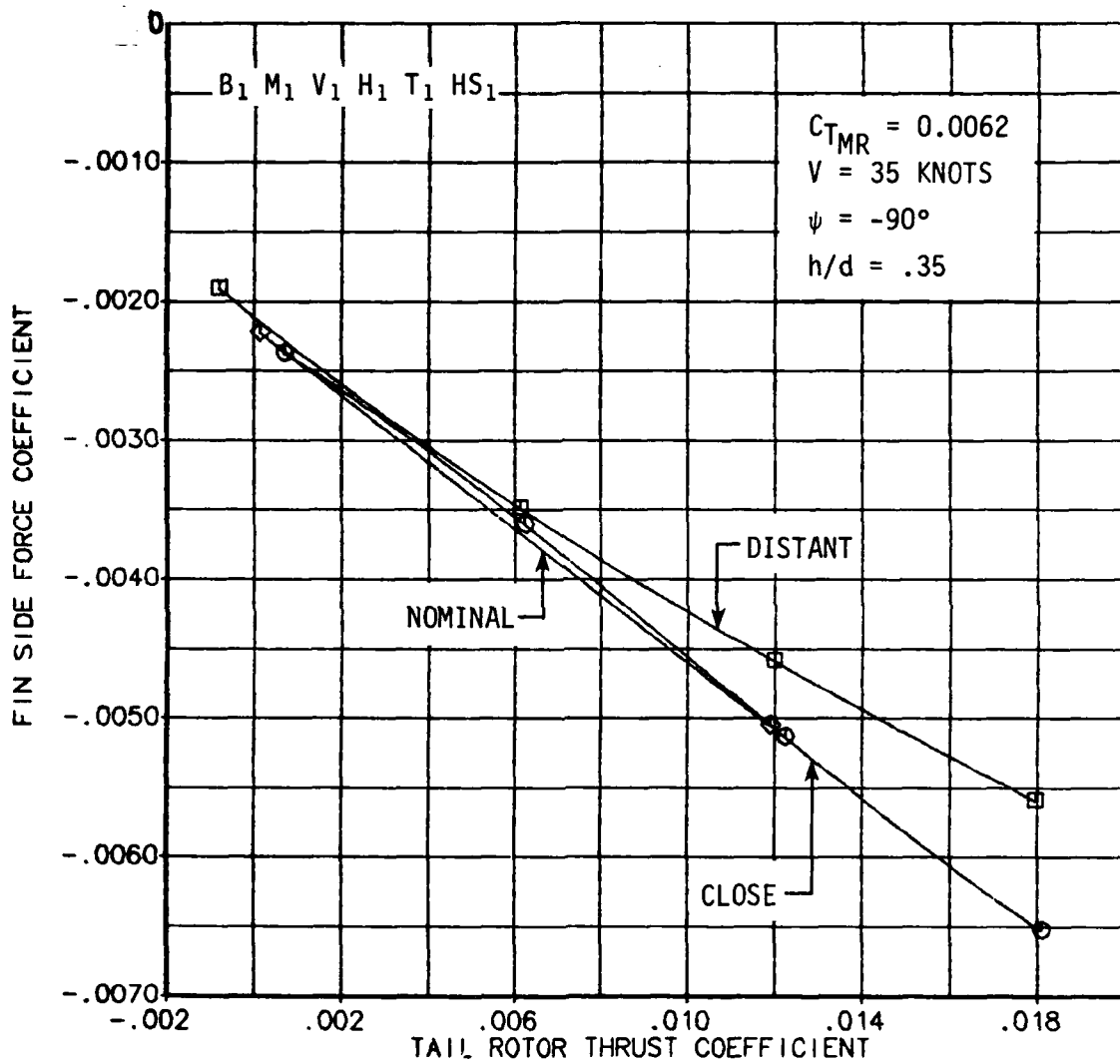


FIGURE 70. EFFECT OF TAIL ROTOR LATERAL PLACEMENT ON FIN SIDE FORCE COEFFICIENT IN RIGHT SIDEWARD FLIGHT.

change with lateral positioning. Figure 70 shows that the fin side force did not increase when the tail rotor was moved closer to the fin. On the other hand, the fin force did diminish as the tail rotor was pulled away from the tail plane. The lateral displacements from the nominal position that were studied represent $\pm 20\%$ of the tail rotor radius.

The third variation was the vertical position of the tail rotor relative to the fin. Figure 71 shows that the fin force was strongly affected by this change in tail rotor location. For the high tail rotor position (.4r above the nominal), the effective change in fin blockage ratio was 10% to the value of 25% blockage. In addition, the center of the tail rotor was placed at a height even with the top of the fin, thus reducing the flow velocities near the top portion of the fin. Again these two effects in combination resulted in lower adverse fin loads at a given tail rotor thrust for the high tail rotor position.

In contrast, the low tail rotor position (.4r below nominal) resulted in a significant rise in adverse fin loads. For this configuration the fin blockage ratio increased to 39% and the fin was exposed to higher flow velocities as the rotor centerline moved down. The variations in fin side force due to changes in tail rotor position are clearly dependent upon the proximity of the fin to high velocity inflow regions on the tail rotor inflow field. For example, at a tail rotor thrust of $C_{T_{TR}} = 0.012$ the variations in fin side force for the three tail rotor positions are not proportional to variations in fin blockage ratio alone.

During this study the subtle effects of varying the tail rotor flow relative to the free stream and main rotor flows were not considered. A more comprehensive testing of tail rotor placement effects, similar to that presented in Reference 3, but with a complete fuselage, is required to understand the subtle effects of tail rotor positioning.

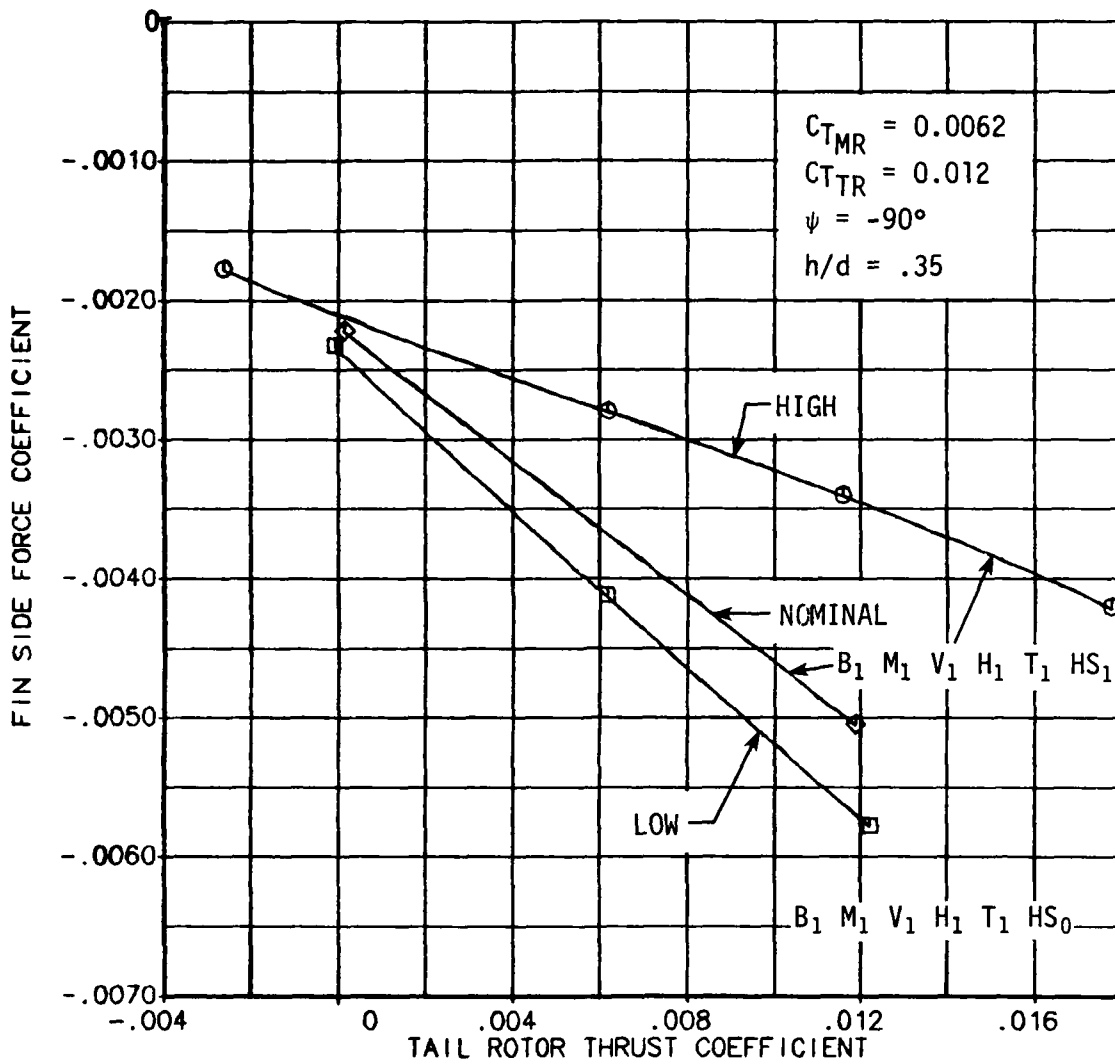


FIGURE 71. EFFECT OF TAIL ROTOR VERTICAL PLACEMENT ON FIN SIDE FORCE COEFFICIENT IN RIGHT SIDEWARD FLIGHT.

FIN-ON-TAIL-ROTOR INTERACTIONS

Effects of Airspeed and Fin Size

$\psi = -90^\circ$: The effect of fin size on tail rotor performance was investigated for the power critical condition of right sideward flight. Figure 72 presents the tail rotor power required at a constant value of tail rotor thrust for the three fin configurations tested. Airspeed sweeps were conducted for each fin configuration.

The variation in tail rotor power required for the fin-off configuration characterizes the effects of the main rotor wake on tail rotor inflow as a function of airspeed. The tail rotor power reaches a maximum at a nondimensional airspeed of 0.9 where the ground vortex dominates the aerodynamic environment of the helicopter. For airspeeds greater than this the effects of the ground vortex diminish and the tail rotor power decreases almost linearly with airspeed. This variation with velocity results from the increased inflow through the tail rotor due to the free stream flow.

In contrast, the power required for the 25% and the 35% blockage fins independently levels off to a constant value for airspeeds greater than 1.0 nondimensional. The most striking result shown in Figure 72 is the higher tail rotor power required for the smaller fin over the entire range of airspeeds compared to either the 35% fin or the fin-off configuration.

The exact cause of this variation in tail rotor power as a function of fin size is unknown. The observed variation in tail rotor power may be due to the change in inflow distribution associated with the change in fin size. Alternatively, the variation in fin size may change the main rotor wake effect on the empennage, resulting in the unexpected variations of tail rotor power. A more complete test matrix including variations of main rotor and tail rotor thrust for various fin sizes and shapes would verify the observed effects. To supplement the loads data, flow measurement studies very close to the tail rotor disk would provide a very rigorous method of investigating the effects of fin size on the tail rotor inflow distribution and the consequent changes in tail rotor power required.

Effects of Tail Rotor Placement

Variations in tail rotor power required as a function of tail rotor placement in the longitudinal, lateral and vertical directions are presented in Figures 73, 74 and 75 respectively. The flight condition is, once again, the power critical flight 35 knots to the right at a constant main rotor thrust.

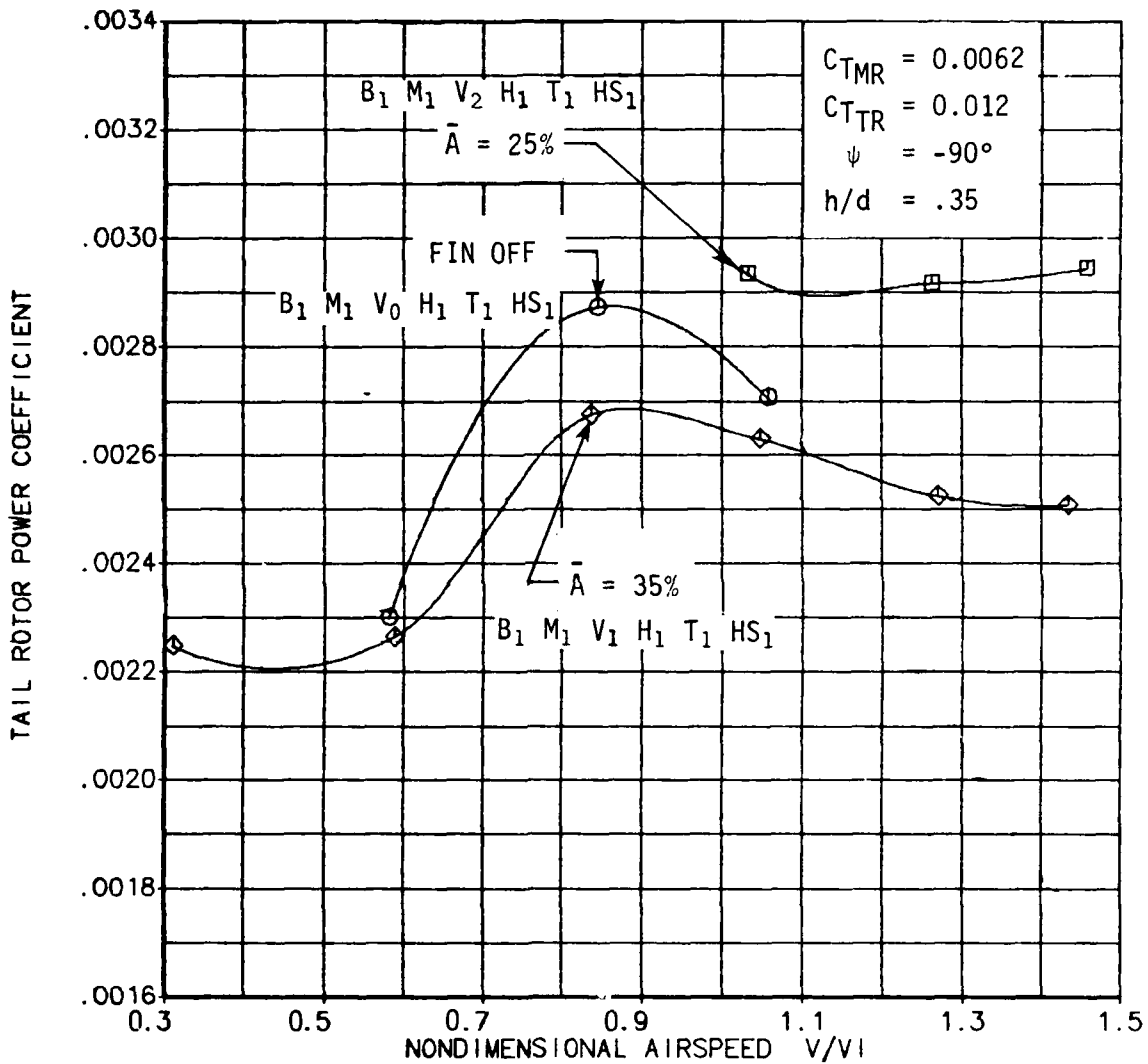


FIGURE 72. EFFECTS OF AIRSPEED AND FIN SIZE ON TAIL ROTOR POWER COEFFICIENT AT $\psi = -90^\circ$.

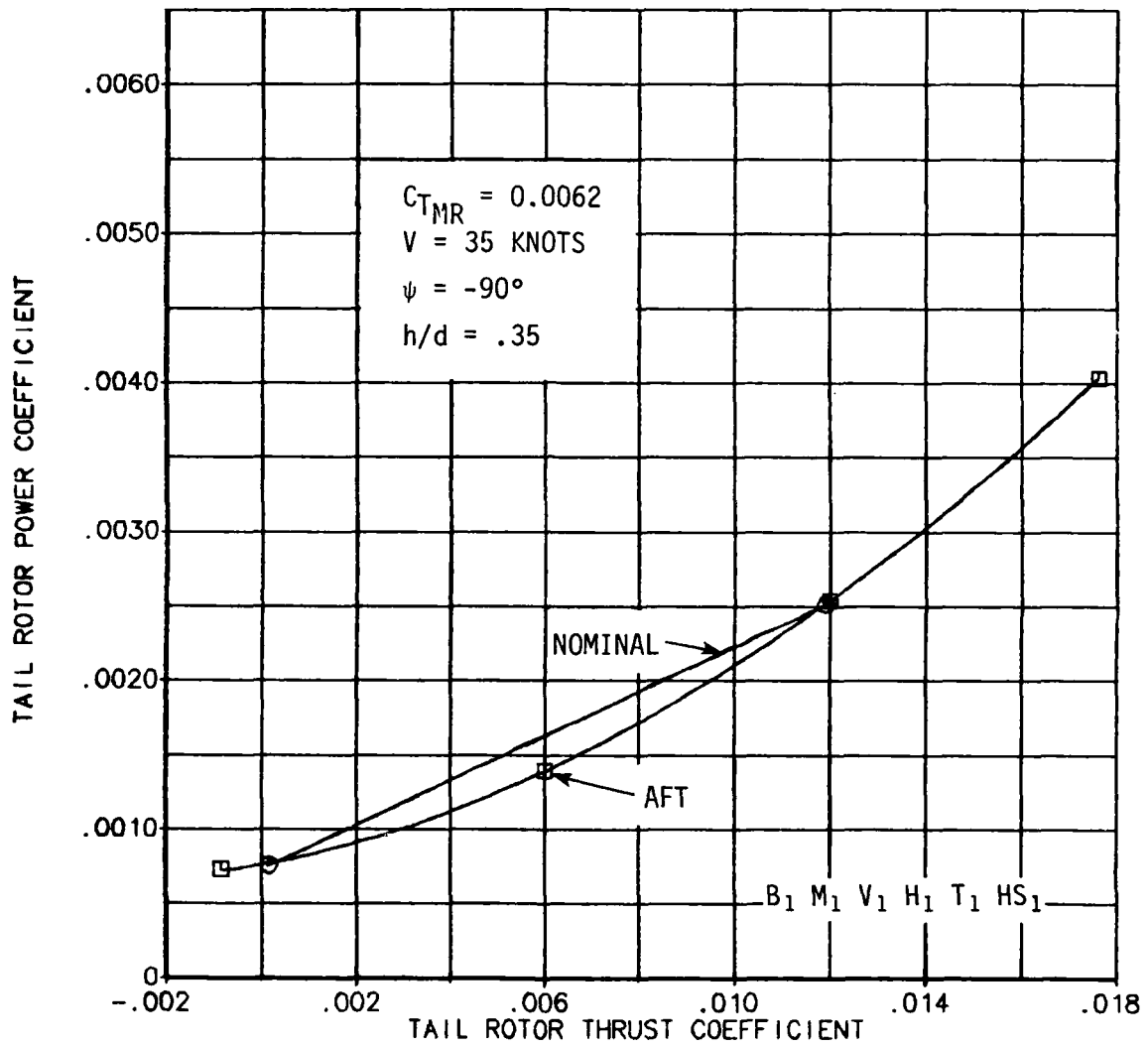


FIGURE 73. EFFECT OF TAIL ROTOR LONGITUDINAL PLACEMENT ON TAIL ROTOR POWER COEFFICIENT IN RIGHT SIDWARD FLIGHT.

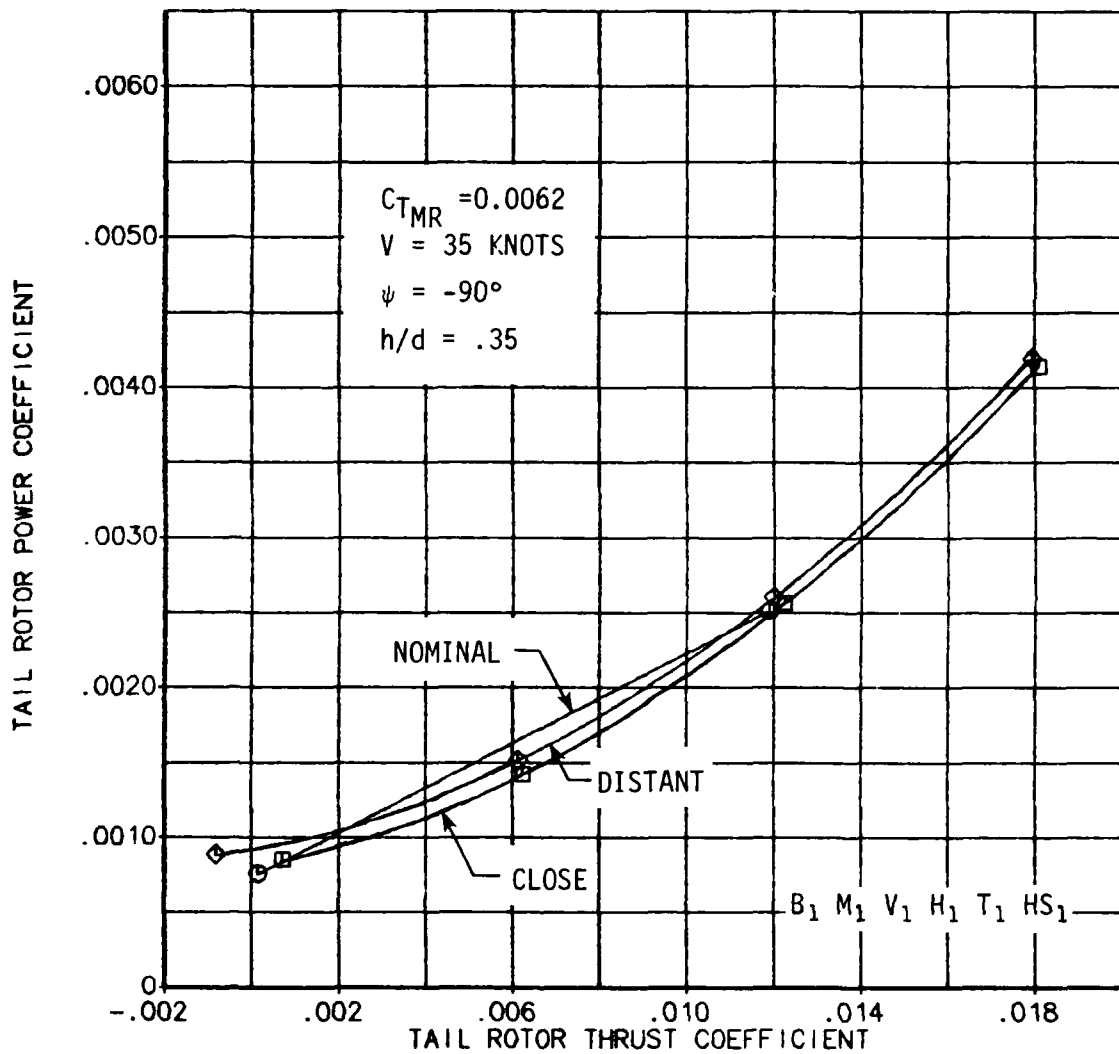


FIGURE 74. EFFECT OF TAIL ROTOR LATERAL PLACEMENT ON TAIL ROTOR POWER COEFFICIENT IN RIGHT SIDWARD FLIGHT.

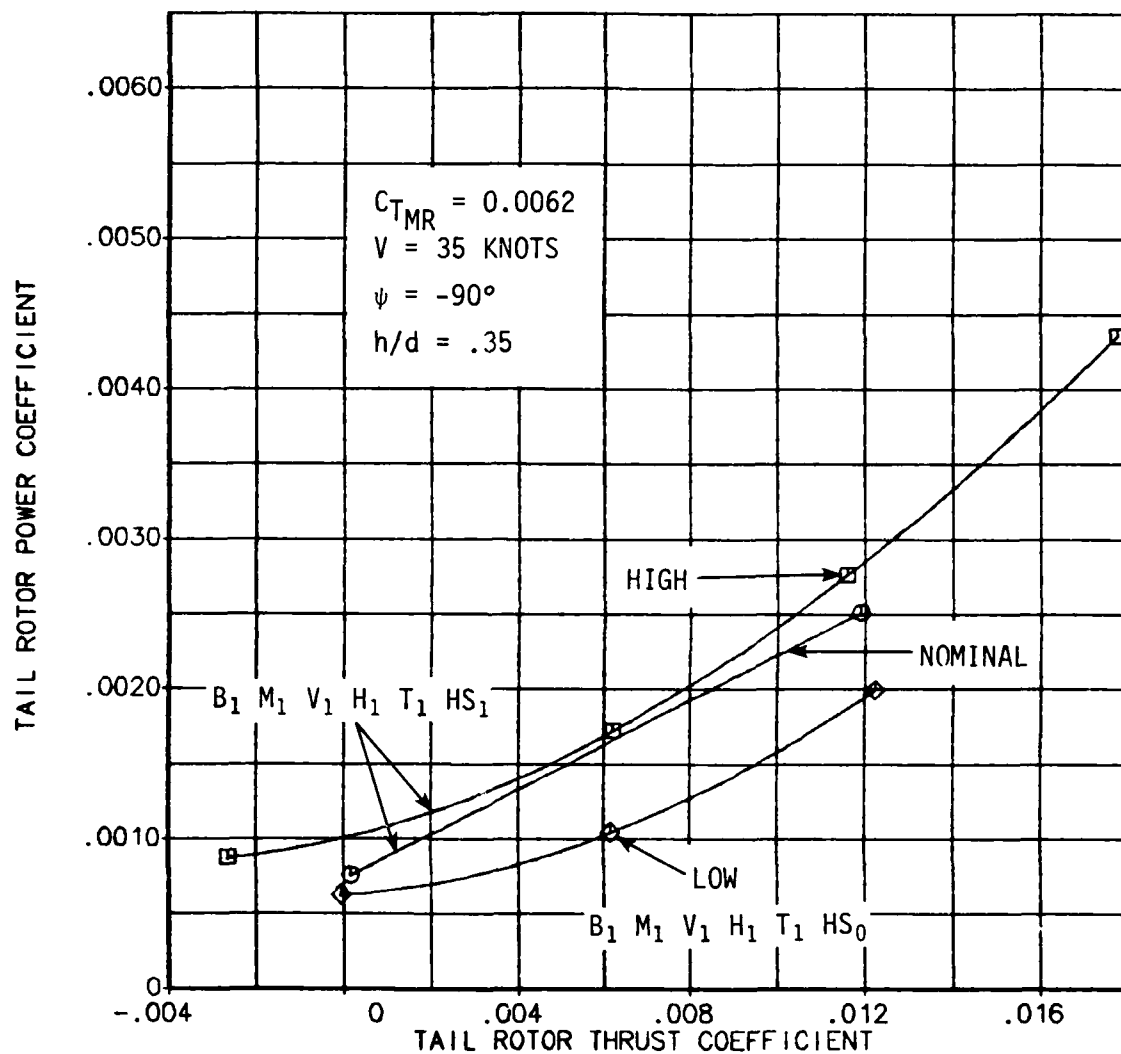


FIGURE 75. EFFECT OF TAIL ROTOR VERTICAL PLACEMENT ON TAIL ROTOR POWER COEFFICIENT IN RIGHT SIDEWARD FLIGHT.

Tail rotor thrust sweeps were conducted at each tail rotor position; see Table 7 for specific details.

Figures 73 and 74 show that the longitudinal and lateral changes in tail rotor location have a negligible influence on tail rotor power required. Vertical movement of the tail rotor relative to the fin, however, has a significant effect on tail rotor power (see Figure 75). For example, at the nominal tail rotor thrust condition, $C_{T_{TB}} = 0.12$, the total increase in tail rotor power required for the high compared to the low position is almost 40 percent. Furthermore, the results shown in Figure 75 agree with the trends shown in Figure 72. The high tail rotor position has a lower blockage ratio, yet the tail rotor power required is increased for this configuration. This variation with fin size was not expected. Much more analysis of the data is required before general conclusions about tail rotor/fin interactions can be proposed.

MAIN ROTOR/FIN INTERACTIONS

The contribution of the main rotor wake to fin side force is presented in this section. In addition, the effects of fin size on main rotor trim conditions for right sideward and rearward flight are addressed. The data is intended to supplement the previous discussion on some of the aspects of main rotor wake effects on fin load.

MAIN ROTOR ON FIN INTERACTIONS

Effects of Wind Azimuth and Main Rotor Thrust

Figure 76 is a plot of dimensional side force as a function of wind azimuth for two levels of main rotor thrust. The tail rotor was temporarily removed for these runs.

During the entire test program the model pitch attitude was fixed at +4 degrees, thus keeping the main rotor shaft perpendicular to the tunnel floor. In Figure 76 the curve of fin side force versus azimuth for the zero main rotor thrust condition represents the variation of fin force for various wind azimuths due to free stream effects alone. With the model pitch angle fixed at +4 degrees, some induced effects due to the fuselage will exist in forward flight. The most significant feature of this curve is the nonlinearity near minus 60 degrees of wind azimuth. This phenomenon possibly indicates the onset of fin stall for wind azimuths beyond 50 degrees. Stall may occur at such a high wind azimuth condition due to induced flow effects of the fuselage near the empennage for the forward quartering wind conditions. Insufficient data is available to identify a similar phenomenon near a wind azimuth of +50 degrees.

The plot of fin force with the main rotor operating at its nominal thrust condition ($C_{TMR} = 0.0062$) in Figure 76 shows a significant effect due to the main rotor wake at a wind azimuth of -30 degrees. The main rotor tip vortex impinges on the vertical fin in this condition, resulting in a large adverse fin load. The adverse load quickly decreases to the main-rotor-off level at wind azimuth of -40 degrees. Figure 77, however, shows the effects of increasing the main rotor thrust. The adverse fin force at -30 degrees is slightly larger for the high main rotor thrust condition. The most significant difference occurs at a wind azimuth of -50 degrees.

For the high thrust condition there is a dramatic reduction in adverse fin load between -30 and -50 degrees azimuth. Beyond -50 degrees the fin force once again continues to grow with increasing yaw angle. The exact flow mechanism by which

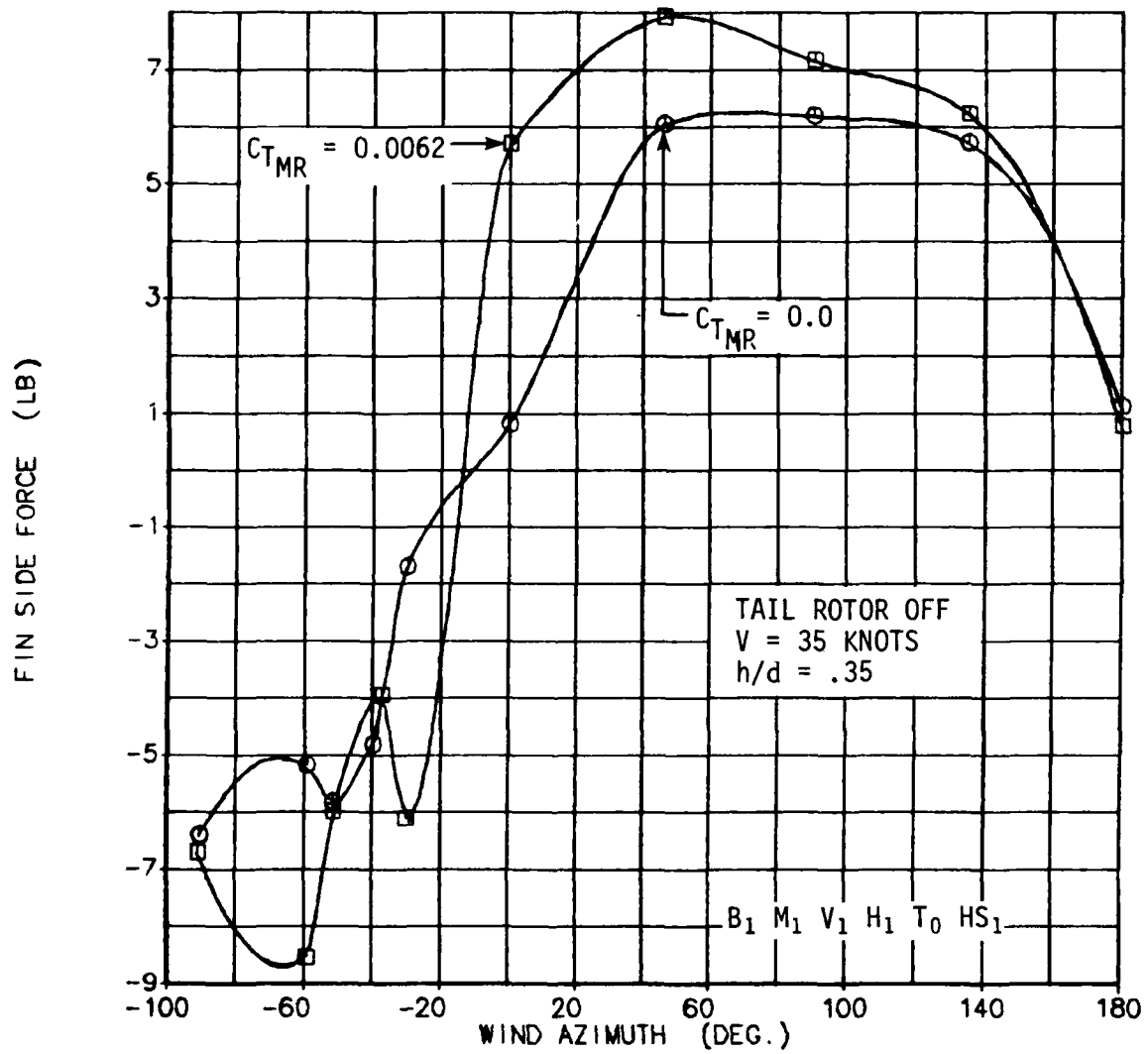


FIGURE 76. FIN SIDE FORCE AS A FUNCTION OF WIND AZIMUTH AND MAIN ROTOR THRUST.

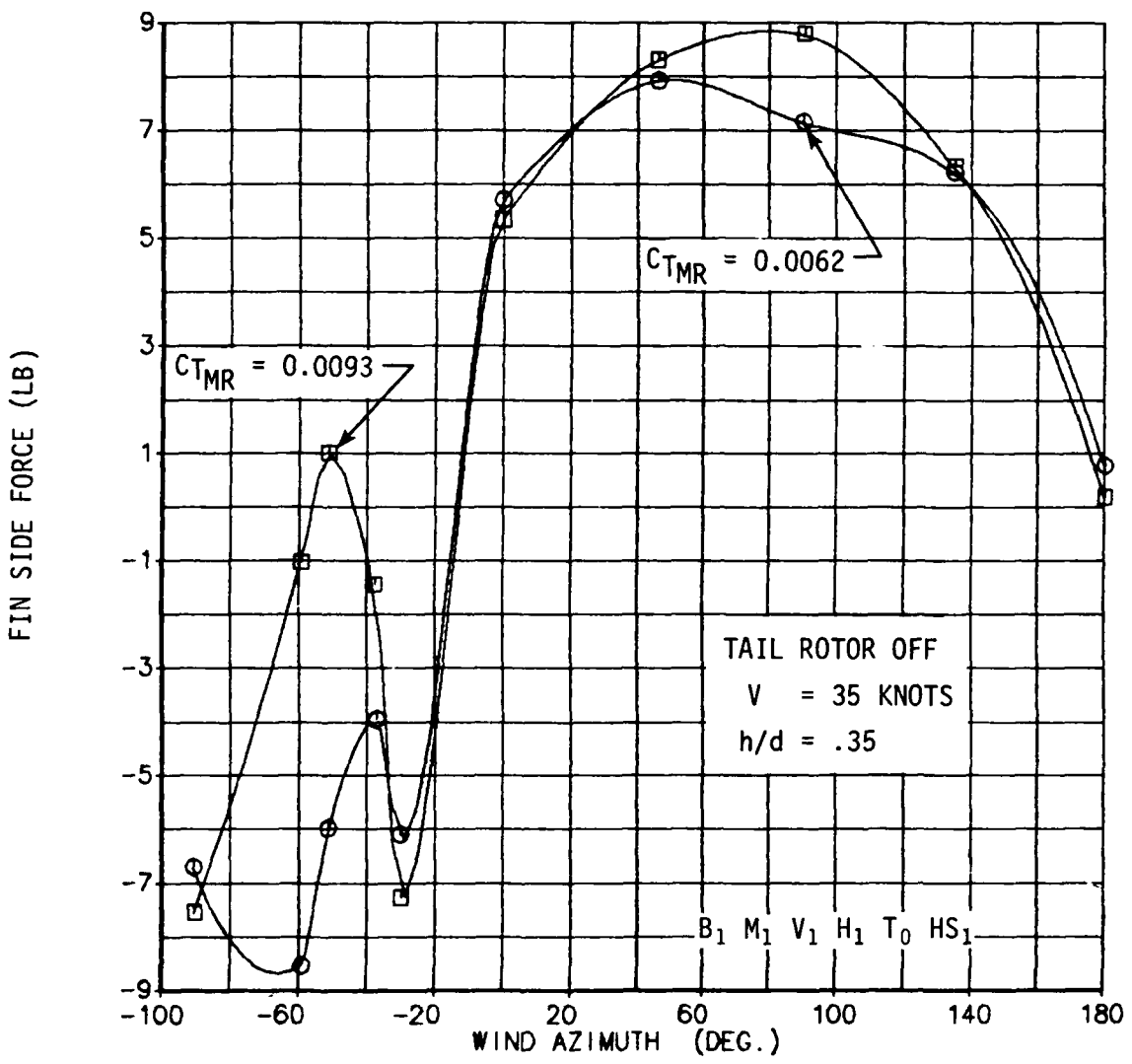


FIGURE 77. FIN SIDE FORCE AS A FUNCTION OF WIND AZIMUTH AND MAIN ROTOR THRUST.

the fin load varies so dramatically is uncertain. However, Figures 76 and 77 show that increasing main rotor thrust can have a significant effect on the directional control requirements due to resultant variations in fin side force.

The variation in fin side force due to changes in main rotor flow for the forward flight condition ($\psi=0^\circ$) shown in Figure 76 indicates that a significant swirl velocity exists near the empennage. In Figure 76 the fin force shows a very large increase for the main-rotor-on condition. The change is in a sense that adds to the tail rotor thrust. Figure 77 shows that the fin force is not sensitive to further increases in main rotor thrust at zero degrees wind azimuth.

Figure 78 shows a comparison of fin side force for the tail-rotor-on and the tail-rotor-off configurations at the nominal main rotor thrust condition. The tail-rotor-off data was taken from Figure 76 and the tail-rotor-on data from Figure 50. The airspeed for these two configurations does differ by 5 knots, and thus the curves are not directly comparable. However, Figure 78 does show the order of magnitude relationship between tail-rotor-on and -off conditions. For wind azimuths between -20 and -90 degrees the adverse fin force generated by the main rotor alone can be as much as 50% of the fin force generated with the tail operating.

Insufficient data exists for wind azimuths between 0 and 80 degrees to determine the effects of the main rotor tip vortex on fin loads for the tail-rotor-off condition. Figure 78 does show, however, that the tail rotor flow for all azimuths produces an adverse fin force that is larger in magnitude than the fin force due to main rotor flow alone.

Effects of Airspeed and Main Rotor Thrust

$\psi = -90^\circ$: The variation of fin side force as a function of airspeed for three levels of main rotor thrust is presented in Figure 79. The wind azimuth is -90 degrees and the tail rotor thrust was set to the nominal value $C_{T_{TR}} = 0.012$. Over the range of speeds tested, the adverse fin force is greater for the higher main rotor disk loadings. This trend can be attributed to the increased downwash velocities and the increased ground vortex strength associated with the increased main rotor thrust. In fact, the passage of the main rotor wake and ground vortex occurs in Figure 79 around a nondimensional airspeed of 1.0 for all three main rotor loadings.

Figure 80 shows the nondimensional empennage vertical lift for the right sideward flight condition. The empennage vertical lift force is normalized by the main rotor thrust and if it were proportional to main rotor thrust the three curves

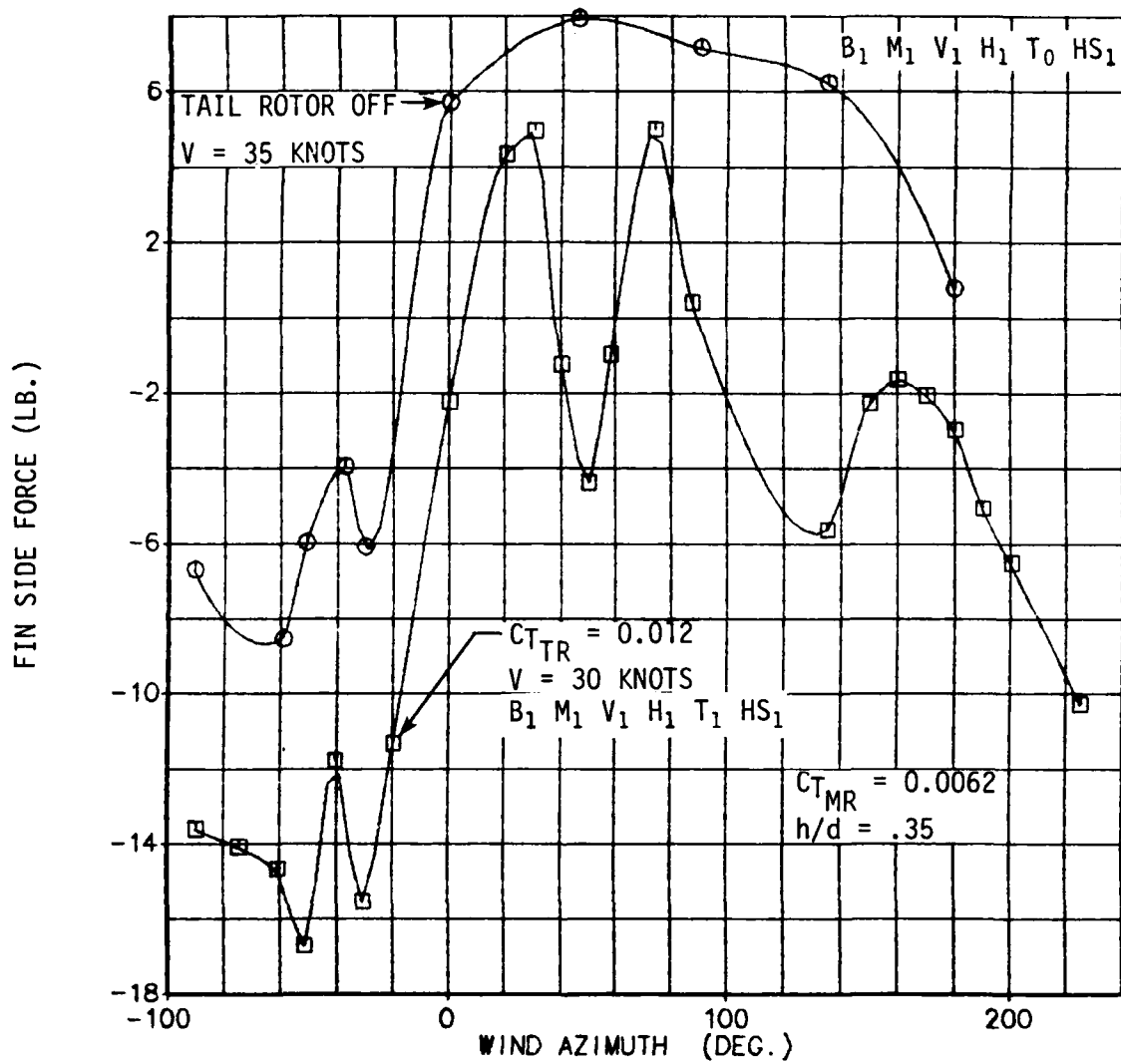


FIGURE 78. FIN SIDE FORCE AS A FUNCTION OF WIND AZIMUTH AND TAIL ROTOR THRUST.

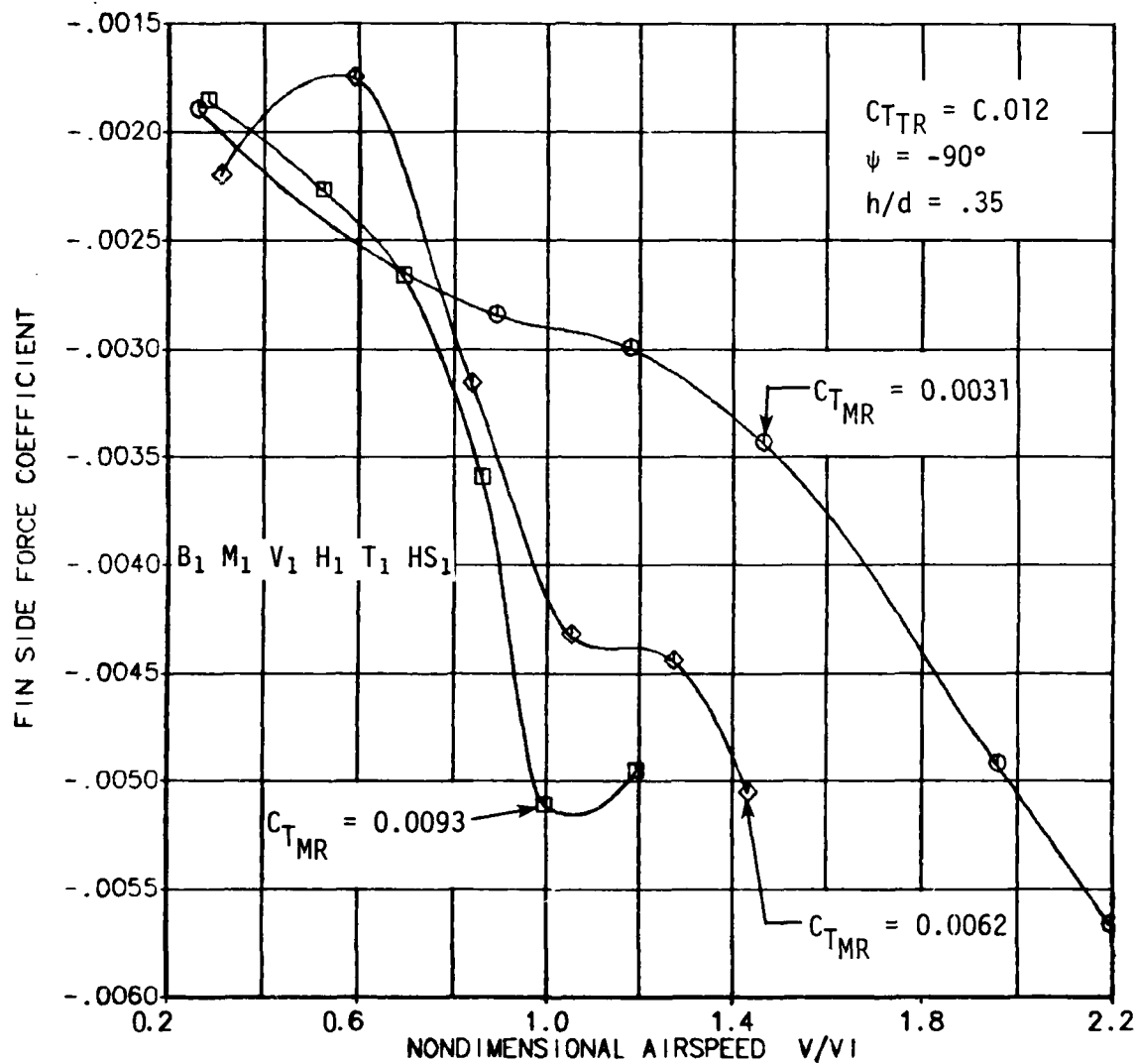


FIGURE 79. FIN SIDE FORCE COEFFICIENT AS A FUNCTION OF AIRSPEED AND MAIN ROTOR THRUST IN RIGHT SIDWARD FLIGHT.

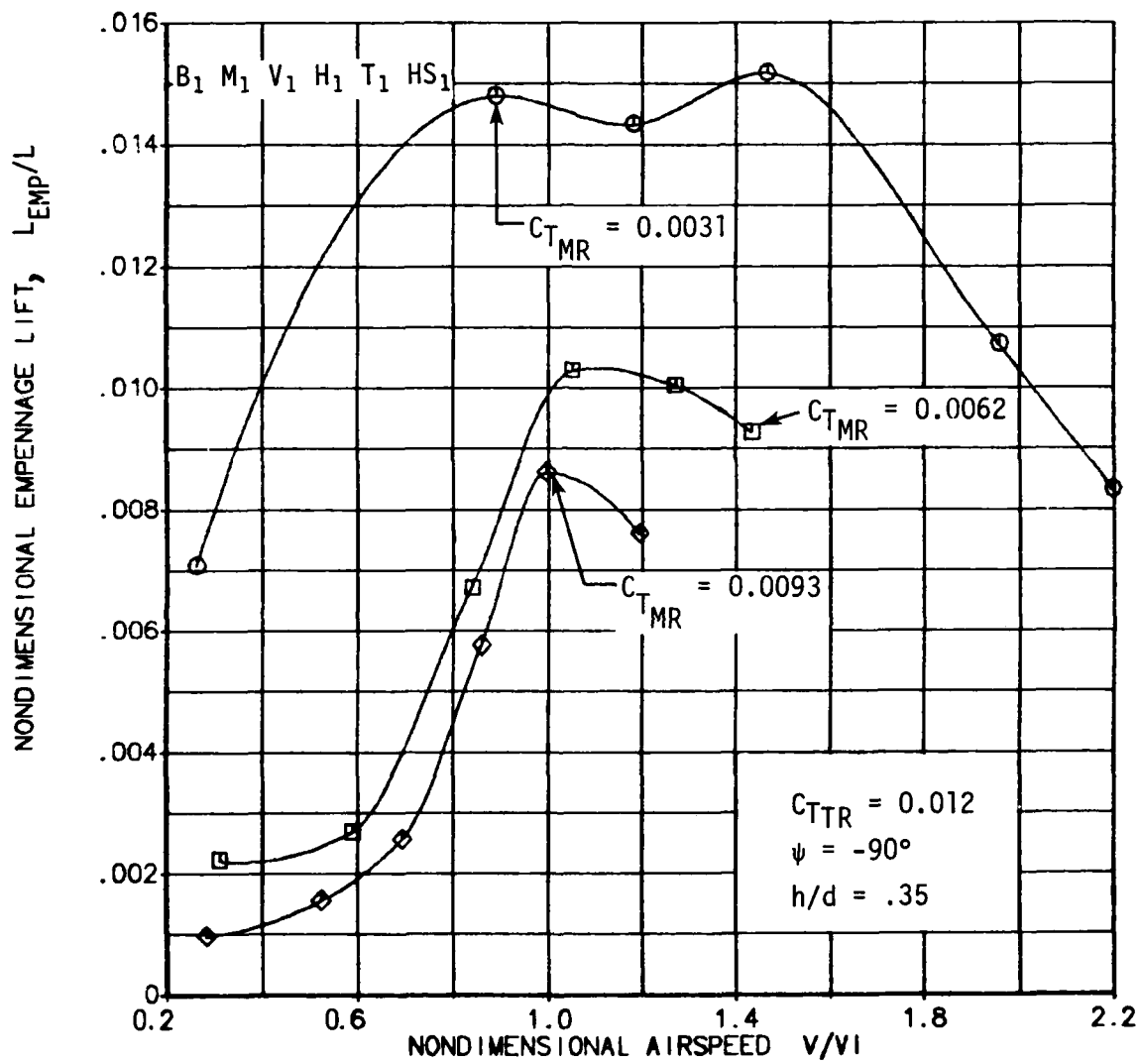


FIGURE 80. NONDIMENSIONAL EMPENNAGE LIFT AS A FUNCTION OF AIRSPEED AND MAIN ROTOR THRUST IN RIGHT SIDEWARD FLIGHT.

plotted in Figure 80 would be the same. However, Figure 80 shows three distinct curves, indicating that the increase in empennage lift is affected by both the increase in dynamic pressure of the main rotor wake and the change in flow characteristics associated with the wake skew angle and ground vortex phenomenon.

$\psi = 180^\circ$: For the rearward flight condition the fin side force coefficient and the nondimensional empennage vertical lift are plotted in Figures 81 and 82 respectively. The effects of increasing airspeed from hover through transition on fin side force are given in Figure 81. In general, adverse fin side force decreases significantly as airspeed is increased from hover. At a nondimensional airspeed of 0.9 the ground vortex begins to interact with the flow around the empennage, resulting in a slight increase in adverse fin force near 1.0 nondimensional airspeed.

Figure 82 shows the effects of airspeed on the nondimensional empennage vertical lift for various main rotor thrust conditions. Below a nondimensional airspeed of 1.0 the empennage lift is positive for all three curves. In this speed regime the influence of the main rotor wake is evident. The empennage lift decreases with increasing main rotor thrust except for the point at a nondimensional airspeed of 0.55. For airspeeds greater than 1.0 the three curves come together, similar to the results presented in Figure 59. This indicates that the ground vortex and the main rotor wake have been blown past the empennage and have little effect on the empennage vertical force.

FIN ON MAIN ROTOR INTERACTIONS

The effects of varying fin size on main rotor trim are described in this section. The location and the size of the vertical fin will affect the main rotor flow in two ways. First, the proximity of the fin to the main rotor will have some induced effects on the main rotor inflow directly, especially for winds from the left and right rear quadrants. Second, for the pusher configuration, interposing the fin on the inflow side of the tail rotor will result in distortions of the inflow distribution and corresponding variations in the tail rotor wake. This could have a significant impact on tail rotor/main rotor interactions for all wind azimuth conditions where the tail rotor wake interacts with the main rotor flow.

The fin size was varied in the right sideward and rearward flight conditions. Speed sweeps were conducted for each fin configuration at the nominal main rotor ($C_{TMR} = 0.0062$) and tail rotor ($C_{TTR} = 0.012$) thrust conditions. Variations in

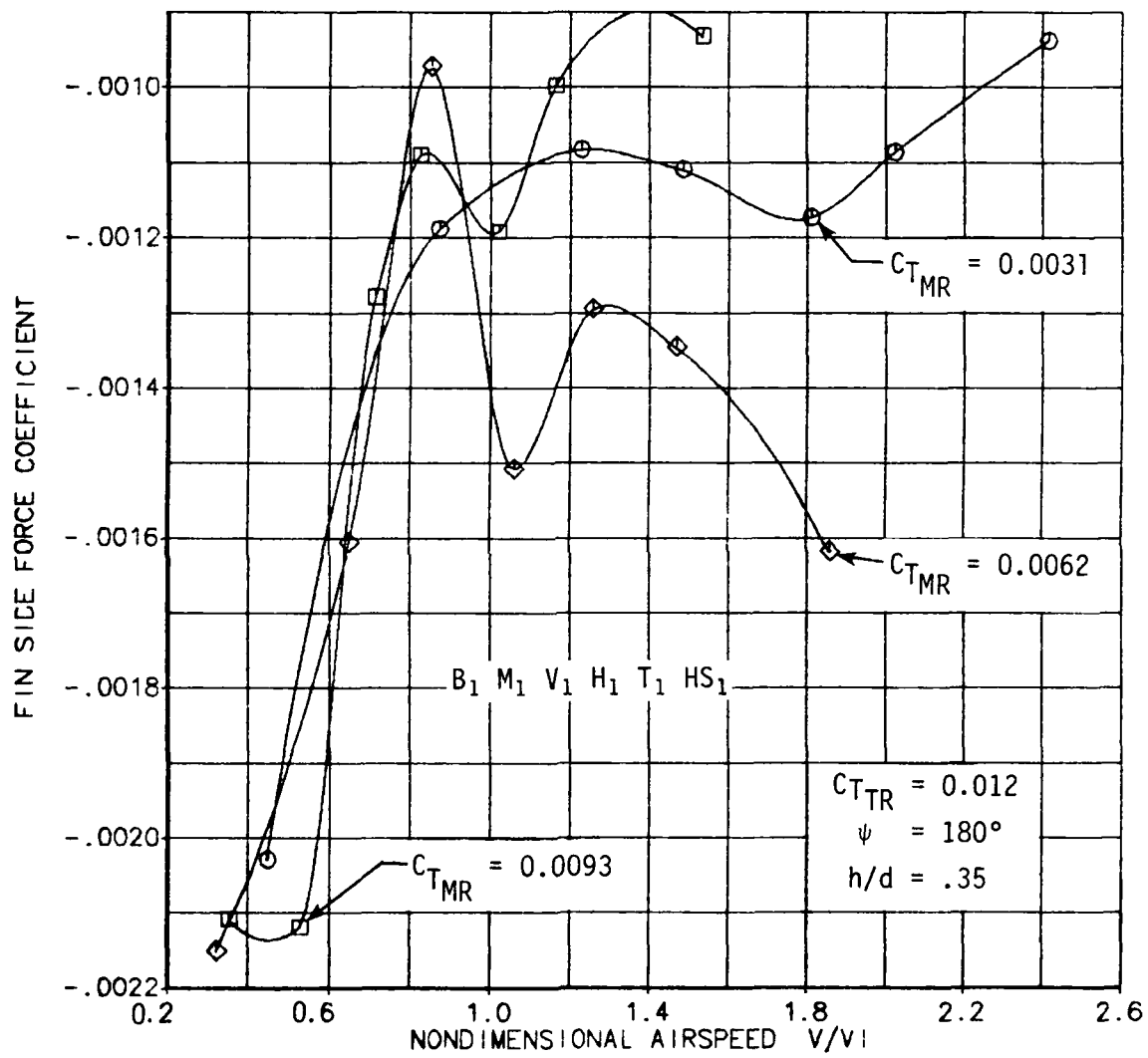


FIGURE 81. FIN FORCE COEFFICIENT AS A FUNCTION OF AIRSPEED AND MAIN ROTOR THRUST IN REARWARD FLIGHT.

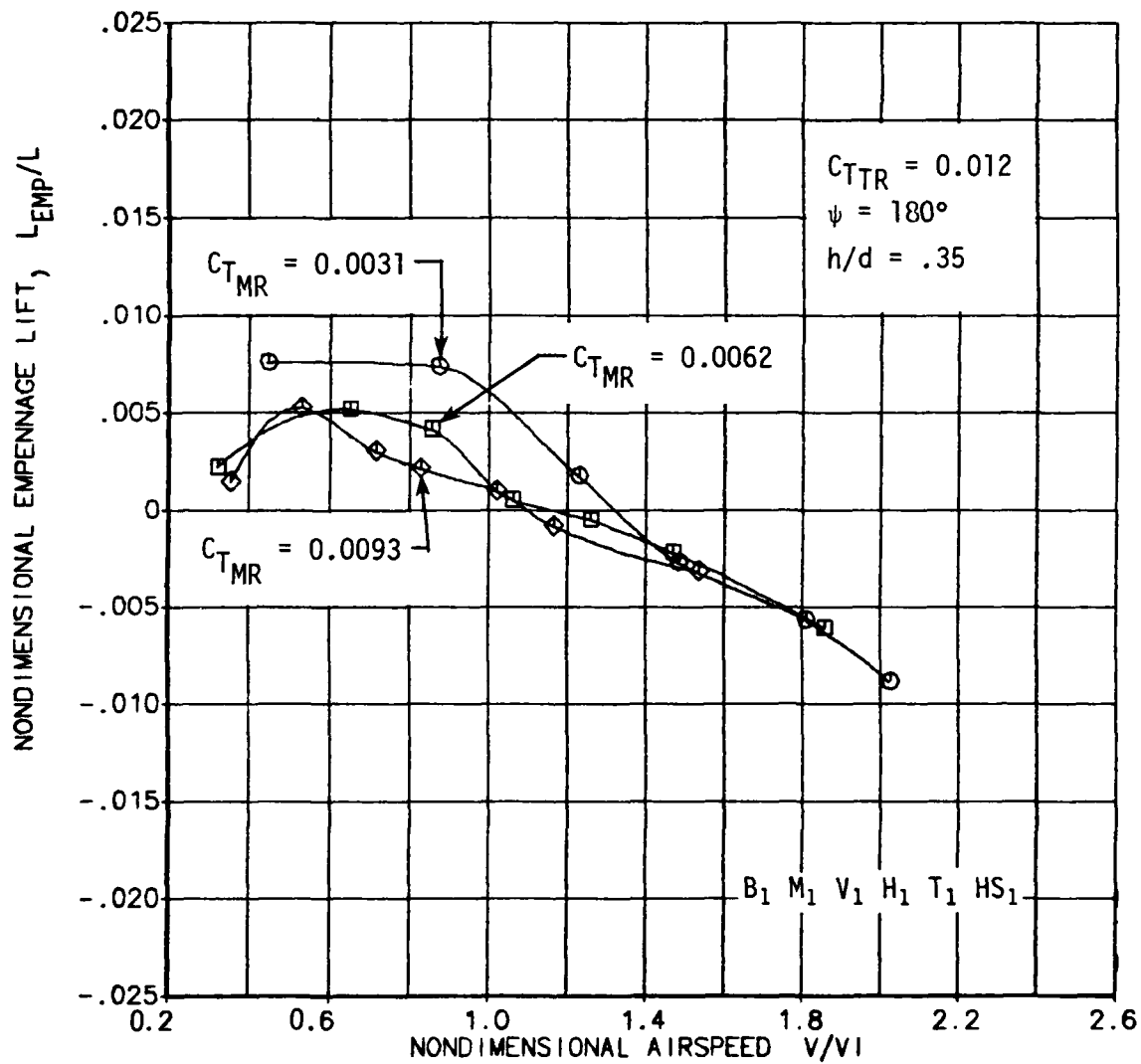


FIGURE 82. NONDIMENSIONAL EMPENNAGE LIFT AS A FUNCTION OF AIRSPEED AND MAIN ROTOR THRUST IN REARWARD FLIGHT.

main rotor power required at a constant thrust and longitudinal/lateral cyclics required for zero hub moments are presented as functions of airspeed.

$\psi = -90^\circ$: The main rotor trim data for the right sideward flight condition is shown in Figures 83, 84 and 85. Figure 83 shows the variation in main rotor power coefficient as a function of airspeed for the three fin configurations. For nondimensional airspeeds less than 1.3, the smaller fin ($A = 25\%$) resulted in a slightly higher main rotor power required than the larger 35% blockage fin. The fin-off data does not follow this trend below a nondimensional airspeed of 1.0. In fact, the largest variation in main rotor power required exhibited between the three fin configurations is only 3 percent and occurred at a nondimensional airspeed of 1.25. These slight variations in the main rotor power coefficient shown in Figure 83 indicate that the fin size has very little effect in right sideward flight.

Figure 84 shows the resultant lateral cyclic pitch angles required for zero hub moment. The flight condition is still right sideward flight. For this wind azimuth the lateral cyclic pitch variations will be indicative of changes in the longitudinal inflow distribution of the main rotor. Below a nondimensional airspeed of 1.0 the 35% blockage fin exhibited a requirement for more lateral cyclic pitch than the 25% blockage and the fin-off configurations which were virtually the same. Above a nondimensional airspeed of 1.0 all three curves come together, indicating that the aerodynamics of the empennage no longer influences the main rotor longitudinal inflow as the free stream flow blows the tail rotor wake downstream.

The longitudinal cyclic pitch angles required for zero hub moment in right sideward flight are presented in Figure 85. Contrary to the results shown in Figure 84, for a nondimensional airspeed greater than 1.0 the three curves do not converge. This result indicates that the fin size does have a slight effect on the lateral inflow distribution over the range of speeds investigated. Figure 85 also shows that the 25 percent blockage fin has less influence on the main rotor inflow than the larger 35 percent fin and the fin-off configurations at all speeds. Why the 25% fin exhibits less influence on main rotor inflow distribution than the fin-off configuration is uncertain. This result may be dependent on the placement of the fin relative to the tail rotor inflow.

$\psi = 180^\circ$: The main rotor trim data for rearward flight is presented in Figures 86 through 88. For this flight condition only the 35% and 25% blockage fins were investigated. No fin-off data was obtained. Figures 86, 87 and 88 reveal

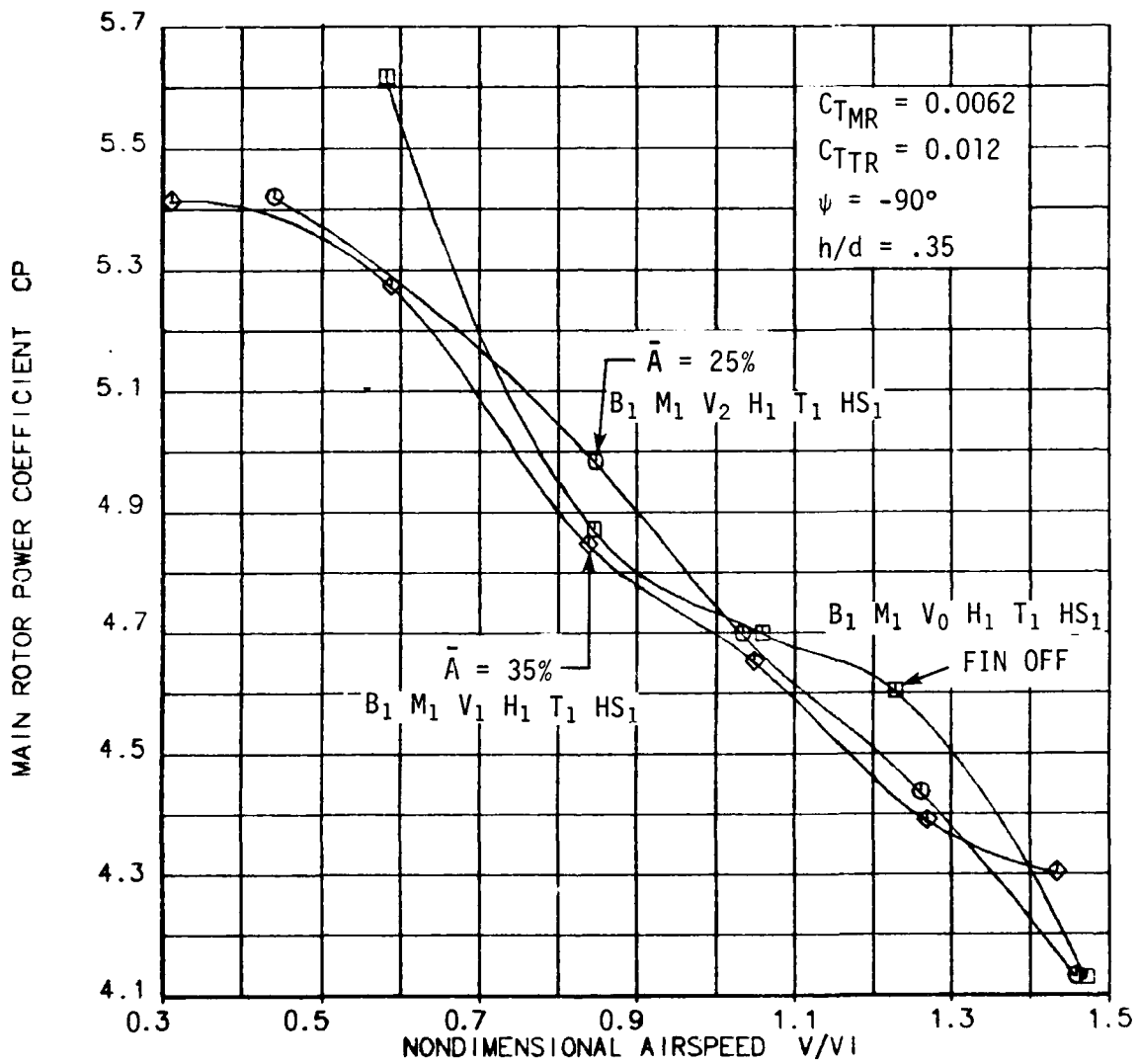


FIGURE 83. MAIN ROTOR POWER COEFFICIENT AS A FUNCTION OF AIRSPEED AND FIN SIZE IN RIGHT SIDEWARD FLIGHT.

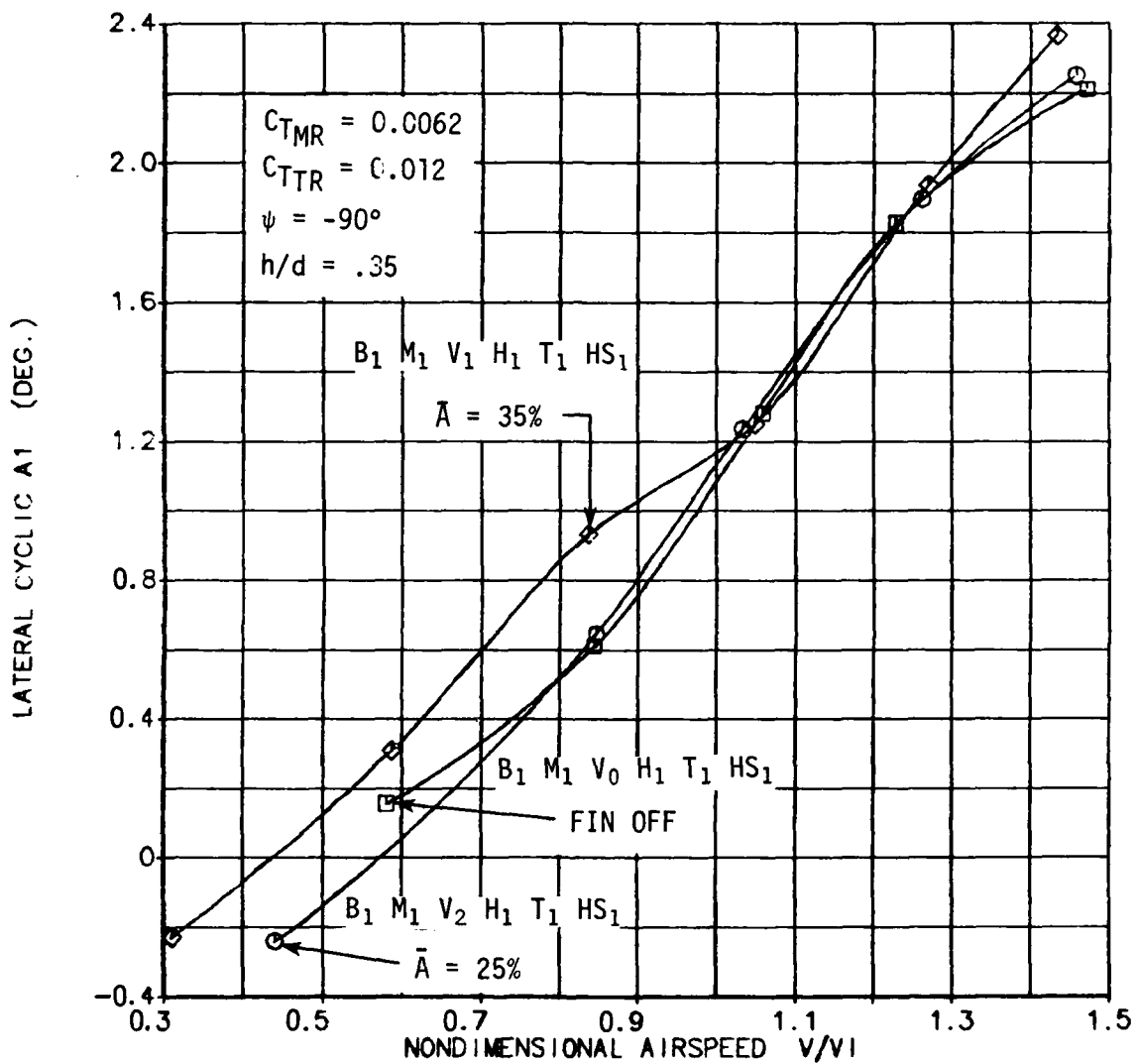


FIGURE 84. LATERAL CYCLIC REQUIRED FOR ZERO HUB MOMENT AS A FUNCTION OF AIRSPEED AND FIN SIZE IN RIGHT SIDEWARD FLIGHT.

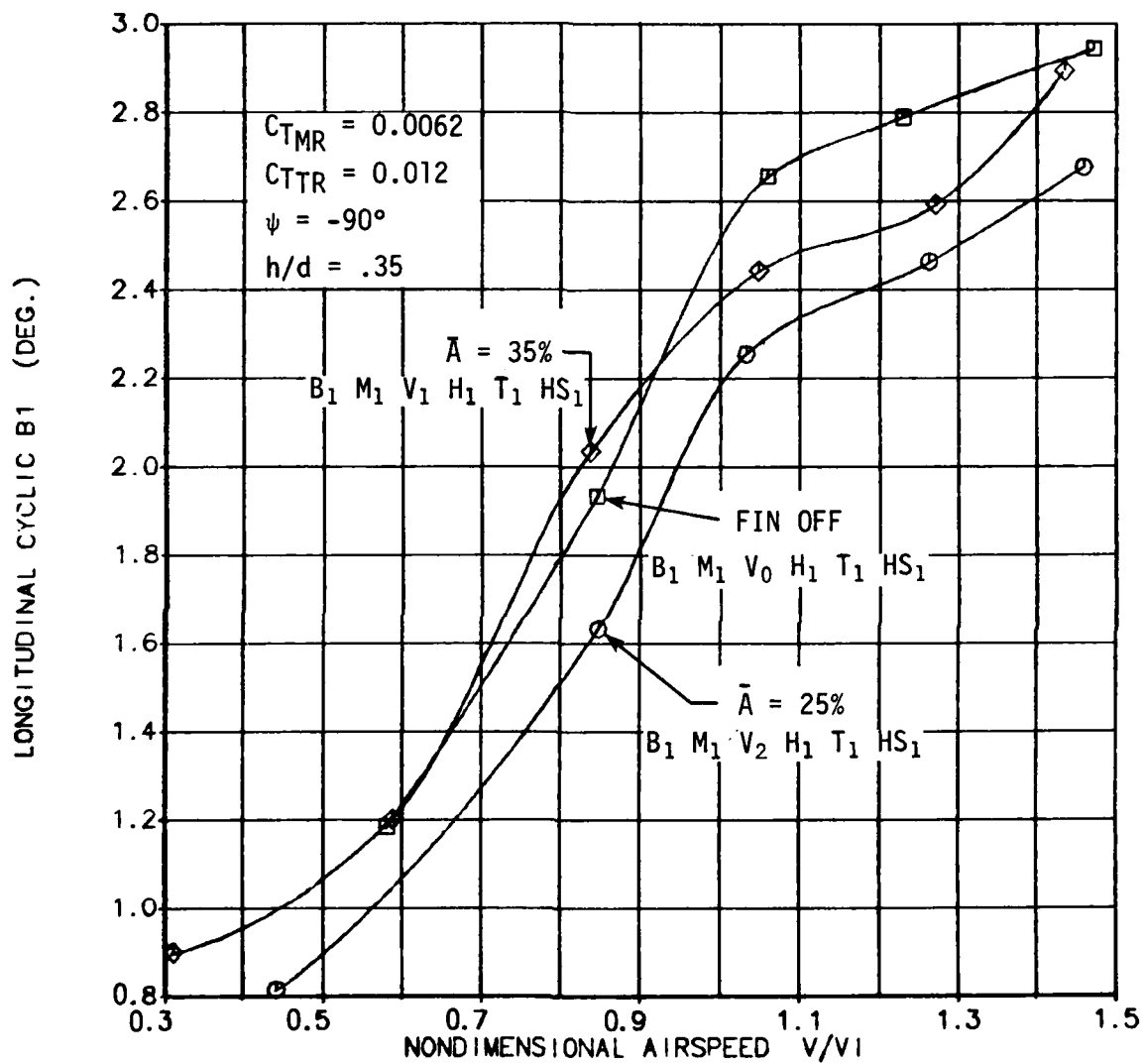


FIGURE 85. LONGITUDINAL CYCLIC REQUIRED FOR ZERO HUB MOMENT AS A FUNCTION OF AIRSPEED AND FIN SIZE IN RIGHT SIDWARD FLIGHT.

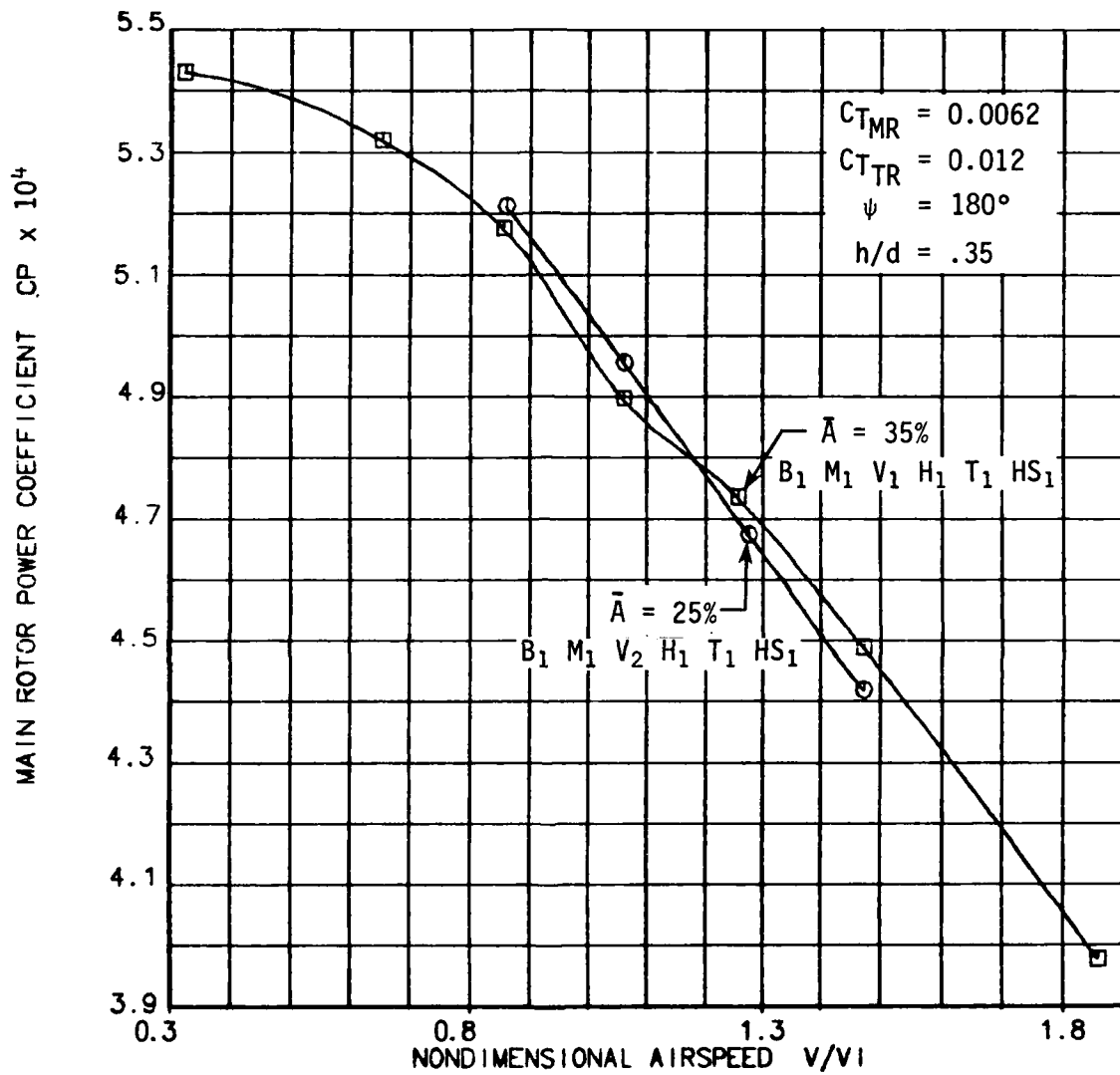


FIGURE 86. MAIN ROTOR POWER COEFFICIENT AS A FUNCTION OF AIRSPEED AND FIN SIZE IN REARWARD FLIGHT.

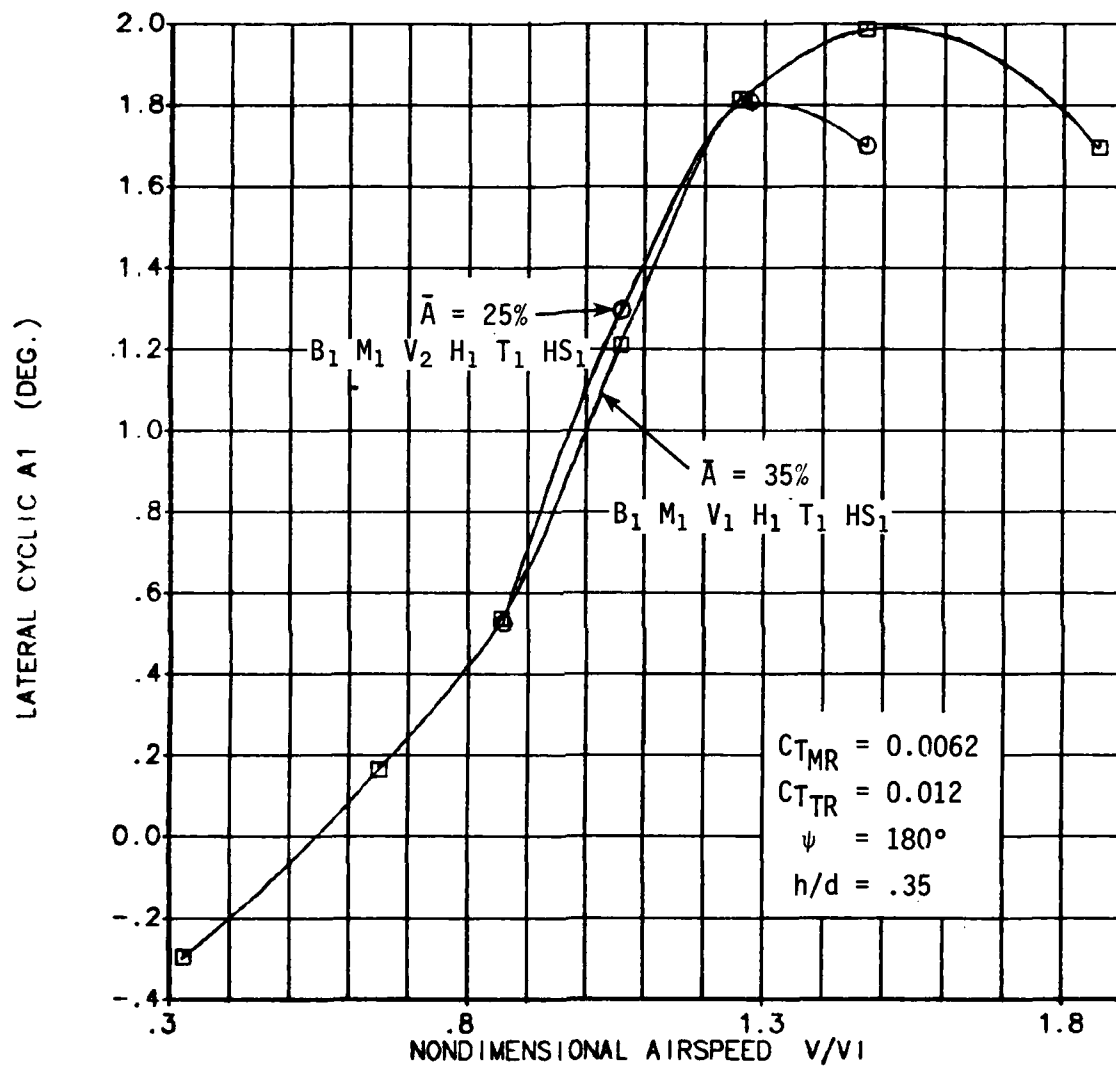


FIGURE 87. LATERAL CYCLIC REQUIRED FOR ZERO HUB MOMENT AS A FUNCTION OF AIRSPEED AND FIN SIZE IN REARWARD FLIGHT.

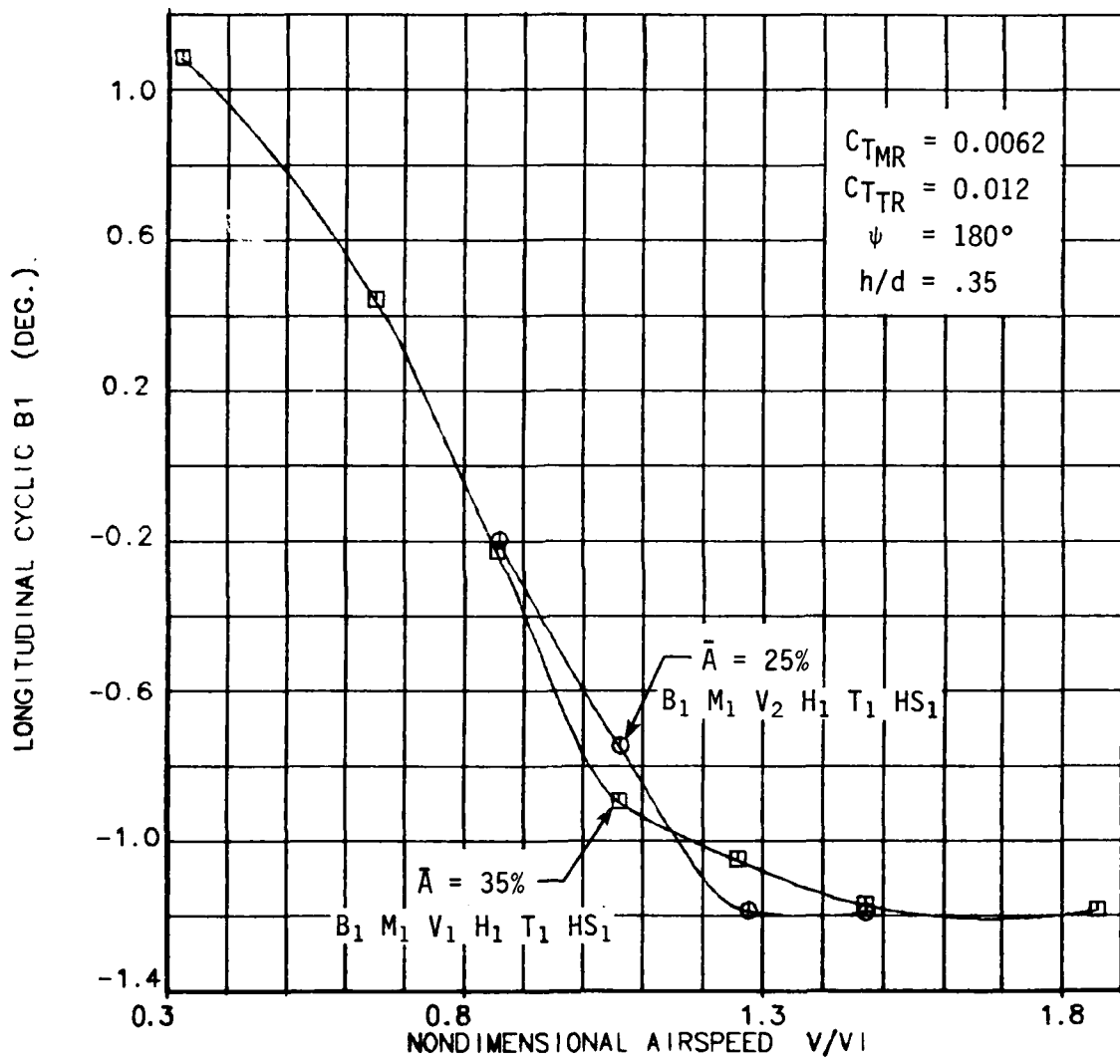


FIGURE 88. LONGITUDINAL CYCLIC REQUIRED FOR ZERO HUB MOMENT AS A FUNCTION OF AIRSPEED AND FIN SIZE IN REARWARD FLIGHT.

that the variation in fin size has little effect on main rotor power coefficient, or on longitudinal and lateral cyclic pitch angles. In rearward flight the flow around the fin has less effect on inflow to the tail rotor than rear quartering winds or sideward flight. Furthermore, the adverse fin loads are much greater for the $\psi = -90^\circ$ condition compared to the $\psi = 180^\circ$ case, as was seen in Figure 63. This clearly indicates that the interactive flows that impinge on the fin are more severe in right sideward flight. In return, the influence of the fin on these interactive flows must be greater in sideward flight to the right.

CONCLUSIONS

1. The main rotor tip vortex has a significant effect on tail rotor performance and adverse fin side force for an airspeed of 30 knots and a wind azimuth of minus 50 degrees. Hot film data quantified the strength of the tip vortex for this yaw condition at the nominal main and tail rotor thrust conditions.
2. Flow visualization records and hot film measurements verified that the ground vortex affects tail rotor performance and vertical fin loads out to wind azimuths of ± 90 degrees for an airspeed of 25 knots and nominal main/tail rotor loadings.
3. The maximum main rotor power required due to interaction with the tail rotor flow occurred at winds from the rear, as expected. However, the influence of the tail rotor resulted in a maximum increase of main rotor power of only 4 percent compared to variations on the order of 20 percent reported in Reference 3.
4. A limited amount of test data was obtained to study the effects of varying fin size on tail rotor performance in right sideward flight. The increased tail rotor power for the smaller blockage (25%) fin compared to both the nominal fin size with 35% blockage and the fin-off configurations was not expected. Further testing is required to understand this effect more fully.
5. Limited investigations of the effects of tail rotor placement on tail rotor performance in right sideward flight were conducted for the 35-percent blockage fin. For the 35-knot sideward flight condition, tail rotor power required was most sensitive to vertical placement of the tail rotor centerline and relatively insensitive to lateral and longitudinal placement.
6. A comprehensive data base of fin side force coefficient as a function of airspeed at the four principal azimuths (0, +90, 180, -90 degrees) was presented for different levels of tail rotor thrust. The data shows that the fin force is proportional to tail rotor thrust at all speeds, indicating the effects of tail rotor depressurization on the vertical fin. However, due to the tail rotor thrust limitation there is no evidence of fin stall for the range of tail rotor thrusts investigated during this test.

RECOMMENDATIONS

1. A sufficient data base exists to facilitate the development of simplified mathematical models. At first, these models should be made simple to predict the trends in fin side force and the effects on main rotor/tail rotor interactions for various geometric configurations. These models should avoid the complication of sophisticated wake models and begin with simple actuator disk theory for both the main and tail rotors in proximity to each other and the fin.
2. Although this test was comprehensive in nature and was successful in exercising many of the fundamental parameters that are significant in the study of interactional aerodynamics, no test can possibly cover all of the possible conditions. Future work to supplement the data presented herein should address the effects of aircraft angle of attack, rates of climb and descent, fuselage aerodynamics and empennage configuration.
3. Due to the flap-lag instability of the flex-strap tail rotor employed in this test, tail rotor thrusts of sufficient magnitude to result in fin stall as well as tail rotor stall were not obtained. Further research in this unsteady aerodynamic regime is required to quantify the effects of turbulent flows on empennage loads.
4. The effects of fin size and tail rotor placement on tail rotor performance presented in this report were not expected. More detailed analysis of the influence of fin size, shape and location on tail rotor/fin interactions is required to verify the trends in tail rotor power associated with changes in blockage ratio discussed in this report.
5. The mutual interactions of main rotor and tail rotor flows for many conditions of airspeed, wind azimuth and disk loadings were presented for the steady-state flight regime. Future tests should be conducted to quantify dynamic effects such as rate of change of tail rotor collective on tail rotor performance in maneuvers or the unsteady effects of main rotor tip vortices on tail rotor blade loadings. The former would require in-flight testing with a complete instrumentation package; the latter could be studied in the wind tunnel with the use of a dynamically scaled model.

REFERENCES

1. Sheridan, Philip, F., and Smith, Robert P., "Internactional Aerodynamics - A New Challenge to Helicopter Technology", Presented at the 35th Annual National Forum of the American Helicopter Society, Washington, D.C., May 1979.
2. Sheridan, Philip F., "Interactional Aerodynamics of the Single Rotor Helicopter Configuration, Volume I, Final Report", USARTL Technical Report 78-23A, Applied Technology Laboratory, U.S. Army Research and Technology Laboratories (AVRADCOM), Fort Eustis, Virginia, September 1978, ADA060389.
3. Wiesner, W., and Kohler, Gary, "Tail Rotor Design Guide", Boeing Vertol Company; USAAMRDL Technical Report 73-99, Eustis Directorate, U.S. Army Air Mobility Research and Development Laboratory, Fort Eustis, Virginia, January 1974, AD775391.
4. Huston, Robert J., and Morris, Charles E.K., Jr., "A Wind Tunnel Investigation of Helicopter Directional Control in Rearward Flight in Ground Effect", NASA Technical Note D-6118, National Aeronautics and Space Administration, Langley Research Center, Hampton, Virginia, March 1971.
5. Yeager, William T., Jr., Young, Warren H., Jr., and Mantay, Wayne R., "A Wind Tunnel Investigation of Parameters Affecting Helicopter Directional Control at Low Speeds in Ground Effect", NASA Technical Note D-7694, Langley Directorate, U.S. Army Air Mobility Research and Development Laboratory, Langley Research Center, Hampton, Virginia, November 1974.
6. Sheridan, Philip F., Hanker, Edward J., Jr., and Blake, Bruce B., "A Study of the Aerodynamic Interactions of the Tail Rotor and Fin", ARO, June 1983.
7. Curtiss, H.C., Sun, M., Putman, W.F., and Hanker, E. J., "Rotor Aerodynamics in Ground Effect at Low Advance Ratios", Paper presented at the 37th Annual Forum of the American Helicopter Society, New Orleans, La., May 1981.

LIST OF SYMBOLS

Symbols

A	Rotor Disk Area - Square Feet
A_1	Main Rotor Lateral Cyclic Pitch - Degrees
\bar{A}	Tail Rotor Blockage Ratio - S/A
B_1	Main Rotor Longitudinal Cyclic Pitch - Degrees
B.L.	Butt Line - Model Inches
C_{fin}	Fin Side Force Coefficient $SF/\rho A_{TR} V_{TTR}^2$
C_P	Power Coefficient $Q/\rho A V_T^2 R$
C_T	Thrust Coefficient $T/\rho A V_T^2$
C_P/C_T	Tail Rotor Power to Thrust Ratio
h/d	Rotor Height-to-Diameter Ratio
i	Vertical Fin Incidence Angle - Degrees
L_{EMP}/L	Ratio of Empennage Vertical Lift Force and Main Rotor Thrust
M.S.	Model Station - Model Inches
R	Main Rotor Radius - Feet
S	Tail Rotor Area Blocked by Fin - Square Feet
V	Airspeed - Knots
V/VI	Nondimensional Airspeed Ratio - $\mu / C_T/2$
V_T	Rotor Tip Speed - Feet Per Second
W.L.	Water Line - Model Inches
β	Sideslip Angle - Positive Wind on Right Cheek - Degrees
μ	Advance Ratio V/V_{TMR}
$\theta_{.75}$	Collective Pitch @ .75 Radius - Degrees
ψ	Wind Azimuth - Positive Nose Right - Degrees

Subscripts

EMP	Empennage
f	Fuselage
I	Induced
IGE	In Ground Effect
MR	Main Rotor
NF	Normal Force
SF	Side Force
SRH	Single Rotor Helicopter Test Stand
TR	Tail Rotor

END

FILMED

3-84

DTIC